UNIVERSITÀ
DEGLI STUDI
DI PADOVA

Sede Amministrativa: Università degli Studi di Padova

Centro Interdipartimentale Studi e Attività Spaziali (CISAS) “G.Colombo”

SCUOLA DI DOTTORATO DI RICERCA IN: SCIENZE TECNOLOGIE E MISURE SPAZIALI
INDIRIZZO: MISURE MECCANICHE PER L’INGEGNERIA E LO SPAZIO
CICLO XXV

NUMERICAL AND EXPERIMENTAL METHODS FOR DESIGN AND TEST OF UNITS AND DEVICES ON BEPICOLOMBO MISSION

Direttore della Scuola : Ch.mo Prof. Giampiero Naletto
Coordinatore d’indirizzo: Ch.mo Prof. Stefano Debei
Supervisore: Ch.mo Prof. Stefano Debei

Dottoranda: Francesca Cucciarrè

Abstract

In this thesis work several numerical and experimental methods for design and test of units and devices onboard BepiColombo Mission are studied, implemented and described.
BepiColombo Mission is the result of the joined efforts of European Space Agency and Japanese Space Agency: in 2015 two different orbiters (ESA Mercury Planetary Orbiter, MPO, which will support remote sensing and radio-science instrumentation, and JAXA Mercury Magnetospheric Orbiter, MMO) will be launched in the direction of Mercury to study the surface composition and morphology, the geology and the magnetosphere of the planet closest to the Sun. Italy plays an important role in the mission since it is involved in the design and development of the Spectrometer and Imagers for Mpo Bepicolombo Integrated Observatory SYStem (SIMBIO-SYS): this integrated package of instruments includes an imaging system with stereo (STC) and high spatial resolution (HRIC) capabilities along with a hyperspectral imager (VIHI) in the visible and near infrared range.
Due to the proximity to the Sun, MPO will face an extremely harsh environment from a thermal point of view, therefore the orbiter, and in particular instrumentation exposed to the thermal fluxes, shall be equipped with sophisticated thermal control devices, such as baffling systems for heat rejection. Starting from the deep knowledge of the thermal scenario in which units and baffles will operate, thanks to the results obtained from detailed thermal and mathematical models, different innovative test-beds have been conceived and designed in order to simulate the environmental thermal fluxes in laboratory.
At first, the Structural Thermal Models of SIMBIO-SYS baffles have been tested, subjecting the devices to the environmental infrared fluxes provided by infrared lamps and cold sources in vacuum conditions and assuring different temperature levels on the thermal interfaces of the units; after the test campaign, the thermal mathematical models of the baffles themselves have been validated thanks to the correlation with the experimental results, providing some useful information on the design of the Flight Models of the baffles. Afterwards an original set-up to test the Qualification Model of the Stavroudis baffle of HRIC unit has been designed: during tests, scheduled in January and February 2013, also solar fluxes will be simulated, thanks to CISAS solar simulator, with the aim to qualify the instrument reproducing in vacuum the maximum and minimum operative and non operative temperatures and the most critical heat fluxes (solar and infrared) in sequence.
In parallel to this activity, from the need to calibrate and qualify the units in space-like environment simulating the operative conditions, two thermal vacuum chambers have been designed: calibration will be performed for HRIC and STC-VIHI units separately, with and without baffles. The activity started from the comprehension of the instruments calibration requirements and proceeded with the conceptual design of the units, the detailed thermal, structural and electrical design and concluded with the procurement, the assembling and the test activity, which has been performed in order to verify the initial requirements.
Thanks to these activities, a series of methods, procedures and techniques, both numerical and experimental, have been developed and validated, with the aim to provide an original and useful contribution to the design and test of SIMBIO-SYS suite onboard BepiColombo mission.

Sommario

L'anno 2015 vedrà l'inizio della missione BepiColombo, promossa dall'Agenzia Spaziale Europea (ESA) in collaborazione con l'Agenzia Spaziale Giapponese (JAXA): la missione scientifica permetterà di approfondire la conoscenza di Mercurio, il pianeta più interno del Sistema Solare, studiandone la superficie, la composizione interna e il campo magnetico, consentendo inoltre di investigare sulle cause che hanno portato alla nascita dei pianeti e sulla loro evoluzione nel tempo. Il segmento di volo è costituito da 2 satelliti distinti: il Mercury Planet Orbiter (MPO), sotto la diretta responsabilità dell'ESA, che supporta la strumentazione per remote sensing e radioscienza, e il Mercury Magnetospheric Orbiter (MMO), che supporta la strumentazione per lo studio del campo magnetico e che è assegnato al controllo della JAXA. Mediante la missione Rosetta, l'ESA sta conducendo un programma che ha lo scopo di investigare sull'origine dei materiali presenti nella zona più esterna e fredda del Sistema Solare; lo studio di Mercurio rappresenta l'estremo opposto: la sua esplorazione permette di studiare la formazione planetaria nella parte più interna e calda della nebulosa proto ‑ solare. Il pianeta rappresenta un target interessante essendo caratterizzato da una sorprendente combinazione di proprietà differenti da quelle degli altri pianeti. Il rapporto 2/3 del periodo di rotazione rispetto al periodo di rivoluzione (risonanza 2:3), la natura e le dimensioni del nucleo, la topografia e la predominanza di terreni vulcanici lo rendono profondamente diverso dalla Luna e molto più simile a Marte; d'altra parte, la presenza di un esteso nucleo metallico e di un campo magnetico rappresenta un importante aspetto in comune con la Terra.
La sua vicinanza al Sole rende il pianeta un target difficile da studiare, sia da Terra (il pianeta è visibile solo per 2 ore al giorno) sia con missioni spaziali, dal momento che il flusso di radiazione solare (pari a 14490 W/m^2 al perielio, 6290 W/m^2 all'afelio), anche 10 volte maggiore rispetto a quello recepito a Terra, quello riflesso dal pianeta e quello emesso dal pianeta stesso nel campo della radiazione IR costituiscono degli input termici enormi e dei vincoli estremamente limitanti per satelliti in orbita attorno a Mercurio. Particolare rilevanza assumono quindi le procedure per controllare termicamente lo spacecraft e la strumentazione a bordo.
Su MPO, tra gli altri strumenti, sarà alloggiata la suite SIMBIO ‑ SYS (Spectrometer and Imagers for MPO Bepi Colombo ‑ Integrated Observatory SYStem), a cui sono affidate tutte le operazioni di imaging della missione e parte delle osservazioni spettroscopiche. La progettazione della suite è stata commissionata ad un team, gestito interamente dall'Agenzia Spaziale Italiana (ASI), comprendente membri appartenenti ad istituzioni internazionali, tra cui il CISAS di Padova. È costituita da 3 strumenti ottici dalle diverse funzioni, operanti su diversi canali, ma montati su un banco ottico comune:

- High Spatial Risolution Imaging Camera (HRIC);
- STereo Imaging Camera (STC);
- Visual and Infrared Hyper-spectral Imager (VIHI).

Punto cruciale nella progettazione della suite, dato lo scenario termico estremo in cui la strumentazione si troverà ad operare, è rappresentato dalla stabilità termo – strutturale, di cui ci si era già occupati durante l'attività di tesi specialistica (con la progettazione termica del baffle Stavroudis di HRIC), e che costituisce anche il campo di studio dell'attività di ricerca descritta. Ruolo fondamentale dal punto di vista della stabilità è rivestita dai sistemi di baffling dei 3 canali. In particolare:

- Il baffle Stavroudis di HRIC allo stesso tempo è un dispositivo per il controllo termico passivo (la sua geometria particolare, caratterizzata da una successione di ellissoidi e iperboloidi, permette di riflettere verso lo sky-background la quota di radiazione infrarossa

incidente sulla superficie interna del baffle, impedendole di raggiungere il filtro e i sensori del telescopio) e garantisce elevate prestazioni dal punto di vista ottico (respinge la radiazione visibile fuori asse);
- I baffles di STC e VIHI, essendo neri, non hanno funzione di controllo termico, ma, come per il caso di HRIC, garantiscono le prestazioni ottiche in condizioni operative, assorbendo la radiazione incidente di disturbo.

Risulta quindi di fondamentale importanza definire il profilo termico di tali componenti, in modo da poter verificare successivamente il conseguente stato tensionale e di deformazione, e che i valori ottenuti non impediscano di raggiungere le prestazioni desiderate.
Punto di partenza per l'attività è costituito da risultati numerici che definiscono il profilo termico derivante dai flussi incidenti sugli strumenti (telescopi e baffles) in orbita attorno a Mercurio.
All'attività di simulazione numerica è stata affiancata l'attività sperimentale in camera da termo – vuoto (TVC) per la verifica della strumentazione in condizioni operative. In particolare, le prove sperimentali in TVC sono state condotte al fine di:

- Validare, grazie ai risultati sperimentali, i risultati ottenuti precedentemente tramite simulazioni numeriche, per quanto riguarda lo Structural Thermal Model dei baffles di HRIC, STC e VIHI.
- Verificare le prestazioni del Qualification Model del baffle di HRIC, in seguito al test di qualifica e alla simulazione delle condizioni operative più gravose dal punto di vista termico in TVC.

Inizialmente sono state individuate e caratterizzate, in base ai modelli numerici già a disposizione, le condizioni di maggior criticità dal punto di vista termico per la strumentazione: in particolare è stata valutata, a partire dai modelli matematici e numerici, la variazione dei flussi termici incidenti sui baffles degli strumenti in funzione della posizione del satellite lungo l'orbita attorno a Mercurio e al variare della posizione di Mercurio attorno al Sole.

Individuate le condizioni di maggior interesse e criticità, che si verificano quando il pianeta si trova al Perielio, è stato ideato, progettato e realizzato un set – up sperimentale in TVC che permettesse di simulare l'ambiente termico radiativo in cui si trova ad operare la strumentazione in orbita. In questa fase, i test sono stati effettuati sugli Structural Thermal Models dei baffles di SIMBIO-SYS in condizioni di stazionarietà, con l'obiettivo principale di validare i modelli numerici precedentemente realizzati; una valutazione delle prestazioni ottiche dei baffles sarebbe stata prematura, dal momento che le superfici interne degli STMs (e in particolare quella del baffle Stavroudis di HRIC) non erano ancora rappresentative delle proprietà ottiche finali, che caratterizzeranno invece il Qualification Model. Di conseguenza è stato sufficiente sottoporre la strumentazione al flusso di radiazione infrarossa proveniente da una piastra calda opportunamente progettata e collocata all'interno della TVC, allo scopo di simulare il flusso massimo emesso dalla superficie calda di Mercurio; il flusso proveniente dalla superficie in ombra e fredda di Mercurio, invece, è stato simulato grazie ad un criostato interno alla TVC. Oltre alle temperature delle sorgenti radiative (piastra calda e criostato), è stato necessario controllare (mediante riscaldatori e trecce di rame connesse al criostato) le temperature delle interfacce interne alla scatola della strumentazione con cui si trovano a colloquiare termicamente i baffles.

I test sono stati effettuati nel mese di settembre 2010 sui componenti forniti da Selex ES, inizialmente sull'unità composta dai baffles di STC e VIHI, in un secondo momento sul baffle Stavroudis di HRIC. In seguito ai test, i componenti non sono risultati danneggiati e sono stati riconsegnati a Selex ES per l'integrazione finale dello STM di SIMBIO-SYS.

Successivamente, mediante il pacchetto di software per l'analisi termica ESATAN-TMS, il set-up sperimentale è stato simulato numericamente: dal confronto e dalla correlazione tra i risultati numerici e i risultati sperimentali, è stato possibile validare i Thermal Mathematical Models degli

STMs dei baffles, introducendo alcune modifiche che si sono rilevate utili nella modellazione numerica successiva dei FMs dei baffles.

In secondo luogo, la campagna di test è stata estesa al Qualification Model del baffle di HRIC, rappresentativo anche delle proprietà ottiche finali dello strumento. In particolare è stato progettato e realizzato un set-up sperimentale che rendesse possibile:

- La qualifica del baffle: tale test viene realizzato riproducendo le interfacce conduttive e radiative del baffle come specificato nell'Experiment Interface Document – part A, alla massima e alla minima temperatura operativa e non operativa.
- La simulazione in sequenza delle condizioni termiche operative più gravose (flusso solare e infrarosso): in questa fase il volume di controllo che supporta il baffle, interno alla TVC, è movimentato da un rotatore ad un grado di libertà, in modo da orientare alternativamente la superficie frontale esterna del baffle alle diverse sorgenti di radiazione, nelle condizioni orbitali più gravose (al Perielio). Oltre alla radiazione infrarossa proveniente dalle sorgenti interne alla camera e che simulano la superficie del pianeta, il baffle Stavroudis è sottoposto alla radiazione proveniente da un Simulatore Solare posto esternamente alla TVC e caratterizzato da una potenza specifica di 6-7 costanti solari.

La campagna di test avrà luogo presso il CISAS nei mesi di gennaio e febbraio 2013: in base alla temperatura misurata a valle del baffle, si rileveranno con tecniche numeriche eventuali variazioni delle performance dello strumento derivanti dall'imposizione, durante i test, dei carichi termici massimi attesi in orbita.

All'attività precedentemente descritta è stato affiancato il design di due TVCs che verranno utilizzate in fase di calibrazione e qualifica dei modelli da volo di STC, VIHI e HRIC, con e senza baffles.

A partire dall'analisi delle prestazioni degli strumenti e da una serie di requisiti meccanici, termici, elettrici, di vuoto, di cleanliness e contamination, è stato effettuato uno studio di fattibilità, a cui sono seguiti il design preliminare delle camere, una serie di analisi strutturali e termiche di dettaglio (per simulare in camera da vuoto le interfacce meccaniche e termiche degli strumenti), la progettazione elettrica, il procurement dei componenti e l'attività di test sui sistemi progettati, al fine di verificare i requisiti iniziali imposti.

Contents

List of the acronyms

ASI	Agenzia Spaziale Italiana
BOL	Beginning Of Life
CFRP	Carbon Fiber Reinforced Plastic
CHPS	Cold Heat Pipe Simulator
CMOS	Complementary Metal Oxide Semiconductor
CoG	Centre of Gravity
CPM	Chemical Propulsion Module
CTE	Coefficient of Thermal Expansion
DTM	Digital Terrain Model
EE	Encircled Energy
ESA	European Space Agency
FOV	Field Of View
FPA	Focal Plane Assembly
FWHM	Full Width Half Maximum
GMM	Geometrical Mathematical Model
HGA	High Gain Antenna
HP	Heat Pipe
HPS	Heat Pipe Simulator
HHPS	Hot Heat Pipe Simulator
HRIC	High Resolution Imaging Channel
HT	High Temperature
I/F	InterFace
IFE	Instrument Front End
IR	InfraRed
JAXA	Japanese Aerospace eXploration Agency
LEOP	Launch phase and the Early Orbit Phase
ME	Main Electronics
MCS	Mercury Composite Spacecraft
MMO	Mercury Magnetospheric Orbiter
MLI	Multi Layer Insulation
MPO	Mercury Planet Orbiter
MSC	Mercury Cruise Composite
MTF	Modulation Transfer Function
MTM	Mercury Transfer Module
N/A	Not Applicable
NECP	Near Earth Commisioning Phase
NIR	Near InfraRed
PE	Proximity Electronics
PEEK	PolyEther Ether Ketone
PSF	Point Spread Function
QE	Quantum Efficiency
QM	Qualification Model
REF	Radiative Exchange Factor
ROIC	ReadOut Intergrated Circuit
S/C	Spacecraft
S/N	Signal to Noise ratio

SC	Solar Constant
SCA	Sensor Chip Assembly
SpW	SpaceWire
SEPM	Solar Electric Propulsion Module
SGS	Science Ground Segment
SIMBIO-SYS	Spectrometer and Imagers for Mpo Bepicolombo Integrated Observatory SYStem
SPC	Science Program Committee
STM	Structural Thermal Model
STC	STereo imaging Channel
TBC	To Be Confirmed
TBD	To Be Defined
TEC	Thermo Electric Cooler
TIRD	Thermal Infrared Rejection Device
TMM	Thermal Mathematical Model
TRP	Temperature Reference Point
TVC	Thermal Vacuum Chamber
TVT	Thermal Vacuum Test
UV	UltraViolet
VF	View Factor
VIHI	Visual and Infrared Hyperspectral Imager
w.r.t.	With Respect To

Introduction

The main objective of planetary research is to understand and increase the knowledge of the mechanisms which led to the origin and the evolution of the Solar System and Universe: with BepiColombo Mission around Mercury, European Space Agency, together with the Japanese Space Agency, is involved in the challenging investigation on the hottest and innermost area of the Solar System. In 2015 two different orbiters (ESA Mercury Planetary Orbiter, MPO, and JAXA Mercury Magnetospheric Orbiter, MMO) will be launched around Mercury to study the surface composition and morphology, the geology and the magnetosphere of the planet. MPO will host the Spectrometer and Imagers for Mpo Bepicolombo Integrated Observatory SYStem (SIMBIO-SYS), which is an integrated package of instruments including a stereo imaging channel (STC), a high spatial resolution channel (HRIC) and a hyperspectral imager in the visible and near infrared range (VIHI).
Due to the proximity to the Sun, MPO will operate in an extremely aggressive environment: on Mercury, the surface temperature raises up to 690 K, the maximum direct solar radiation is about 10 times stronger than at Earth's distance (14490 W/m^2 at Perihelion, 6290 W/m^2 at Aphelion), and the heat flux is further increased above the dayside of the planet due to the albedo and infrared radiation. Therefore the orbiter, and in particular instrumentation exposed to the solar flux, shall be equipped with sophisticated passive thermal control devices, such as state-of-art heat rejection baffling systems, which have to be tested and qualified before launch due to their crucial function. As an example, SIMBIO-SYS High Resolution Imaging Channel (HRIC), with its large aperture (about 100 mm diameter) which would allow the entrance of the largest amount of heat towards the detector, is provided with a dedicated heat rejection system, composed of a Stavroudis highly reflective baffle and a heat rejection filter. In particular, the Stavroudis baffle consists in an alternated series of reflecting ellipsoid and hyperboloids with common foci located at the edge of the entrance aperture and guarantees incident light rejection towards the sky background after three reflections maximum.
The first three chapters of the thesis describe the Mission, the instrumentation and the operative thermal scenario, which constitutes the starting point to understand and assess which are the most crucial thermal and qualification levels to be reproduced and simulated in laboratory.
Chapter four describes the thermal test activity on the Structural Thermal Model of the baffles: in particular the goals and the design procedure of the test-bed are described, together with the test campaign operational sequence and the most relevant results. The proposed set-up guarantees the simulation in vacuum of the infrared orbital fluxes and assures different temperature levels on the thermal interfaces of the baffle, by means of infrared lamps and thermally controlled surfaces (heated and cooled plates).
Thanks to the correlation between the numerical and experimental results, obtained during the test campaign, the thermal mathematical and numerical models have been validated (for this purpose the software suite ESATAN-TMS has been used) and some original modifications and improvements have been introduced into the thermal model of the FM of the baffles. This activity is described in chapter five.
The test-bed used for the structural thermal model of the baffles has been then modified to test the qualification model of the Stavroudis baffle, which, being representative of the thermal optical properties of the final instrument, has to be subjected also to the solar flux. The new set-up has been designed with the aim to qualify the baffle (reproducing the conductive and radiative interfaces at the maximum and minimum operative and non-operative temperatures) and to simulate the most critical operative conditions in sequence (infrared fluxes, incoming from infrared lamps and heat sources, and solar flux, incoming from an innovative solar simulator, external to the thermal vacuum chamber) The design procedure of the test bed for the QM of the Stavroudis baffle is

described in chapter six. In January and February 2013 thermal tests will be performed: basing on the temperature detected behind the baffle, thanks to numerical analyses, eventual variations of the performance of the baffle, due to the thermal levels imposed during tests, will be detected.
At last, chapter seven describes the design activity of 2 thermal vacuum chambers (one for STC-VIHI unit, the second one for HRIC unit) which will be used for the calibration and the qualification of the whole SIMBIO-SYS suite, with and without baffles. Starting from the analysis of the performance of the instruments, a feasibility study has been performed, followed by the preliminary conceptual design of the chambers, the detailed thermal, structural and electrical design, the procurement and the test activity to verify the initial requirements.

1. BepiColombo Mission

1.1 Introduction

Mercury is one of the smallest planetary bodies in the inner Solar System and revolves around the Sun on a tilted and highly eccentric orbit. It is the closest planet to the Sun and, since its formation, it has been subjected to the highest temperatures and has experienced the largest diurnal temperature variation of any object in the Solar System.
Although its dimensions (the planet is bigger than the Moon, smaller than Mars), it has the highest uncompressed density of all planets: this aspect suggests the presence of an iron core and a large Fe/Si ratio, if compared with other terrestrial bodies. In addition, the planet is characterized by a weak magnetic field, which suggests the presence and the circulation of an iron-rich liquid core. As a consequence, since the magnetic field interacts with the solar wind, the magnetosphere of the planet is highly active; it lies directly on the surface of the planet, since the atmosphere is totally absent. Furthermore the absence of the atmosphere causes a variation in the diurnal surface temperature of about 500 K.
Solar tides have influenced the rotational state of the planet, causing the 3/2 spin-orbit resonance; in addition, the surface has been altered during the initial cooling phase and the chemical composition may have been modified by bombardment in the early history of the planet. Therefore Mercury plays a key role in constraining and testing dynamical and compositional theories of planetary formation.
The main objective of planetary research is to understand and increase the knowledge of the mechanisms which led to the origin and the evolution of the Solar System: thanks to Rosetta Mission, ESA is investigating on the origin of the materials which characterize the external and coldest area of the Solar System; on the contrary, the study and the exploration of Mercury, the planet closest to the Sun, allow to investigate on the planetary formation in the innermost and hottest part of the proto-solar nebula.
Due to the proximity to the Sun, the planet represents a critical target to study, both for ground-based observation and space missions: ground telescopes are unsatisfactory since, seen from Earth, Mercury is visible for just two hours preceding sunrise or following sunset and the maximum elongation from the Sun is only 28.3°. Therefore, Earth-based observations are normally performed in front of a strong sky background.
On the other side, inserting a spacecraft into orbit around Mercury represents a great challenge from a thermal point of view since the spacecraft and the instrumentation would face an extremely aggressive thermal environment: as previously stated, Mercury is the hottest planet of the Solar System, with surface temperature raising up to about 690 K; furthermore, the direct solar radiation is more than 10 times stronger than at Earth's distance and the heat flux is further increased above the dayside of the planet because of the albedo and infrared radiation, which cause enormous thermal constrains on any orbiter.
The American probe Mariner 10 at first returned data form Mercury: the spacecraft made 3 flybys in 1974-1975 (reaching a minimum distance of 327 km from the planet surface on 16th march 1975) and acquired images covering 45% of the surface of the planet at the average resolution of about 1 km/pixel. The main scientific objectives of the Mission were:

- Visible imaging, by means of twin narrow-angle cameras;
- IR radiometry;
- UV spectroscopy;
- Magnetic field detection;

- Solar Plasma investigation;
- Charged particles investigation.

Despite the great scientific interest for Mercury, there has been a lack of missions after Mariner 10. Only in recent years, a NASA discovery mission, Messenger, flew to Mercury: the probe has been launched on 3rd August 2004, with the aim to demonstrate how the knowledge of a planet evolution may change when good resolution data are available, since detailed identification of the surface characteristics is crucial to address key issues of the geological history of the planet, such as crustal differentiation and resurfacing, volcanism, tectonics and surface/atmosphere interaction. Messenger probe is the first spacecraft to orbit Mercury (it has been inserted into orbit on 18th march 2011) and it hosts the following experiments:

- Mercury Dual Imaging System;
- Gamma-Ray Spectrometer;
- Neutron Spectrometer;
- X-ray Spectrometer;
- Megnetometer;
- Mercury Laser Altimeter;
- Mercury Atmospheric and Surface Composition Spectrometer;
- Energetic Particle and Plasma Spectrometer;
- Radio Science.

The following figures represent the surface of Mercury as it appeared during the approach and the first flyby of Mariner 10 probe respectively: in the lower 2/3 of the first image the southern hemisphere is visible, the second one represents the northern hemisphere (2/3 down from the top of the image); the resolution on the ground is about 2 km.

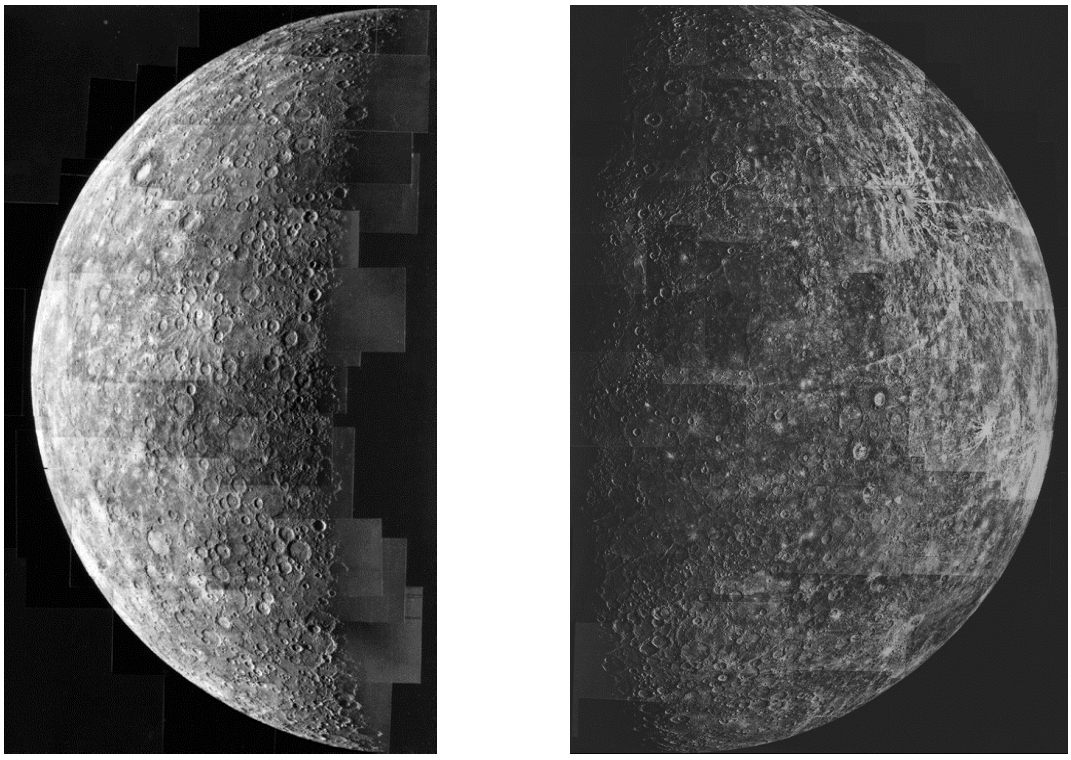

Fig. 1-1 Mapping of Mercury surface on the occasion of the Mariner 10 probe approach and the first fly-by respectively

An ESA cornerstone dedicated mission to Mercury is therefore critical for our understanding of planetary formation. In 1993 a group of ESA scientists proposed for the first time an interdisciplinary mission toward Mercury: in 1996 ESA planned the launch of the cornerstone mission BepiColombo, which is a an interdisciplinary mission to explore the planet Mercury

through a partnership between ESA and JAXA (Japan's Aerospace Exploration Agency). The instruments will be hosted on 2 different spacecrafts, which will be launched as the Mercury Composite Spacecraft (MCS) by means of a common launcher Ariane 5: the Mercury Planet Orbiter (MPO), led by ESA and carrying remote sensing and radio-science instrumentation for the study of the surface and the internal composition of the planet, and Mercury Magnetospheric Orbiter (MMO), led by JAXA and carrying fields and particles science instrumentation for the study of the magnetosphere. An additional dedicated Mercury Transfer Module (MTM) will complement the Mercury Cruise Composite (MSC) for the interplanetary cruise phase. The propulsion system has been designed in order to guarantee the necessary thrust to reach Mercury and the orbital insertion of the spacecraft into the relevant orbits: it combines ion propulsion with chemical propulsion, taking advantage of the gravity assist. The interplanetary transfer will be realized by means of the Solar Electric Propulsion Module (SEPM), the maneuvers for the orbital insertion will be performed thanks to the Chemical Propulsion Module (CPM).
The Mission which had been approved on 15th October 2000 by ESA's Science Program Committee (SPC) foresaw the launch of MPO and MMO by means of two separated launchers inside a common launch window, together with a third carrier rocket dedicated to the surface exploration (MSE). The latter was cancelled due to a severe reduction of the budget in 2001; subsequently the mission has been reviewed in order to optimize the scientific performances and the payload. As a consequence, the Committee decided to launch MPO and MMO by means of a single launcher, with higher carrying capacity, in order to reach a compromise between costs and flexibility. This choice caused an important reduction of the payload mass budget: therefore, after the analysis of the scientific objectives and the definition of the mission requirements, different instruments on board have been grouped together into suites, which are based on the sharing of functions and resources .
BepiColombo Mission has been fully approved on 6th November 2003 by SPC: thanks to this reviewed configuration, SPC assured that all the scientific goals of the mission will be fulfilled with the minimum amount of resources, assuring high performances as well.
On February 2007 the mission has been formally approved, JAXA and industries joined the program.
Nowadays the definition phase of the mission has been completed and key technologies have been developed by ESTEC (ESA's technical centre in the Netherlands), including a range of technologies designed to cope with the extreme thermal scenario (high temperature and intense solar radiation). Since 2007 the project has entered its implementation phase with Astrium-GmbH as Prime Contractor. The main partners in the Industrial Core Team include Astrium Ltd for the mechanical propulsion bus and Thales Alenia Space - Italy for the assembly, integration and test, the telemetry, tracking and command subsystem, the MPO thermal control and the electrical power subsystem and harness.

1.2 **Planet Mercury**

Mariner 10 images showed that the surfaces of the Moon and Mercury appear very similar: they are heavily cratered and present regions of smooth plains. However, the two bodies exhibit large differences in density, indicating that they must be different in internal composition. In addition their formation must have followed different paths. The knowledge of the geological and geophysical processes which involve the planet plays an important role on the comprehension of the evolution mechanisms of all the terrestrial planets of the Solar System. Similar processes cannot be understood basing on the exploration of other planets close to the central body of other solar systems, due to the technological limits in the observation science.
Many aspects of Mercury appear controversial at the moment, since the planet is characterized by a surprising combination of different properties if compared with those of the other planets: the 3/2 spin –orbit resonance (Mercury rotates 3 times every 2 revolutions around the Sun), the presence and the dimension of the core, the topography, the predominance of volcanic terrains and crustal

dynamics make the planet deeply different from the moon, much more similar to Mars. On the other side, the presence of an extended iron core represents an important aspect, as for Earth. Different evolutionary scenarios could explain the anomalous density (large Fe/Si ratio) if compared to other terrestrial bodies: the material contributing to Mercury formation was enriched in metallic iron; the basaltic crust might have been stripped away by impacts; a high-temperature phase in the Solar Nebula might have been volatilized the silicate crust and much of the mantle. Also the role of the volcanism on the planet is not still understood: volcanic deposits need high resolution images to be identified.

Mercury has no natural satellites and no substantial atmosphere; the surface temperature varies from 100 up to 700 K and reaches a maximum in correspondence of the sub-solar point; then the temperature steeply decreases moving toward the poles. The atmosphere/exosphere is so thin that the planet's surface forms the exo-base boundary. The polar caps have anomalously high radar reflectivity, that suggests the presence of surface or near-surface ices in permanently shadowed craters.

The magnetosphere is unique, since the planet is the sole known example of a magnetized body in the solar system without a significant ionosphere.

The following table summarizes the main physical properties of the planet, such as the mass, the dimension, the optical properties, the magnetic and gravitational properties.

General physical properties	Mercury
Mass [$\cdot 10^{24}$ kg]	0.3302
Volume [$\cdot 10^{10}$ km^3]	6.083
Mean density [kg/cm^3]	5427
Means radius R_h [km]	2439.7
Equatorial radius R_e [km]	2440
Ellipticity	0
Bond albedo[1]	0.119
Visual geometric albedo[2]	0.138
Surface temperature range [K]	100 – 688.5
Black body temperature (mean value) [K]	442.5
Equatorial surface gravity [m/s^2]	3.701
Escape velocity [km/s]	4.435
Gravity constant GM [$\cdot 10^6$ km^3/s^2]	0.02203
Dipole field strength [nT$\cdot R_h^3$]	330
Visual magnitude V(1,0)	-0.42
Solar irradiance @ Perihelion [W/m^2]	14490
Solar irradiance @ Aphelion [W/m^2]	6290
Moment of inertia (C/MR^2)	0.33
J_2 (10^{-6})	60

Table 1-1 Main physical properties of Mercury

[1] Fraction of the incident solar radiation which is reflected away toward the sky-background by a spherical body on the whole wavelength range.

[2] Fraction of the incident solar radiation which is reflected away toward the Sun.

In the following table the orbital parameters of Mercury are reported.

Orbital parameters	Value
Semi – major axis [$\cdot 10^6$ km]	57.909
Semi – minor axis [$\cdot 10^6$ km]	56.672
Perihelion [$\cdot 10^6$ km]	46.001
Apherlion [$\cdot 10^6$ km]	69.817
Eccentricity	0.20563
Inclination [°]	7.005
Orbital period (sideral) [yr]	0.2408467
Sideral rotation period [days]	58.646±0.0005
Length of Mercurian day [days]	175.94
Synodic period [days]	115.88
Mean orbital speed [km/s]	47.87
Maximum orbital speed [km/s]	58.98
Minimum orbital speed [km/s]	38.86
Obliquity to orbit [°]	0.01
Maximum angle from Earth – Sun line [°]	28
Maximum Earth - Mercury distance [$\cdot 10^6$ km]	221.6
Minimum Earth - Mercury distance [$\cdot 10^6$ km]	77.3

Table 1-2 Orbital parameters of planet Mercury in its orbit around the Sun

The distance between Mercury and the Sun as a function of the true anomaly (the value $\nu = 0°$ refers to Perihelion) and the orbital time (assumed zero at Perihelion) are shown in the following table.

***v* [°]**	***d* [10^6 km]**	***d* [AU]**	***t* [days]**
0	46.00	0.3075	0.00
20	46.48	0.3107	3.17
40	47.91	0.3203	6.48
60	50.29	0.3362	10.06
80	53.55	0.3580	14.06
100	57.52	0.3845	18.65
120	61.82	0.4132	23.95
140	65.83	0.4401	30.03
160	68.74	0.4595	36.80
180	69.82	0.4667	43.99

Table 1-3 Distance between Mercury and the Sun (units are km and AU) and orbital elapsed time (days) as a function of the true anomaly (degrees)

The revolution motion around the Sun and spin motion around the planet own axis are prograde (counter-clockwise when viewed from north pole of the ecliptic).
As stated before, an important aspect is the 3/2 spin-orbit resonance, which implies that the spin velocity is 1.5 times the orbital mean motion (which is the revolution velocity around the Sun on an circular orbit tangent to real elliptic orbit in 2 points); therefore the ratio between the spin period and the orbital period is equal to 2/3.
The following figure shows the orbit around the Sun and explains the 3/2 spin-orbit resonance.

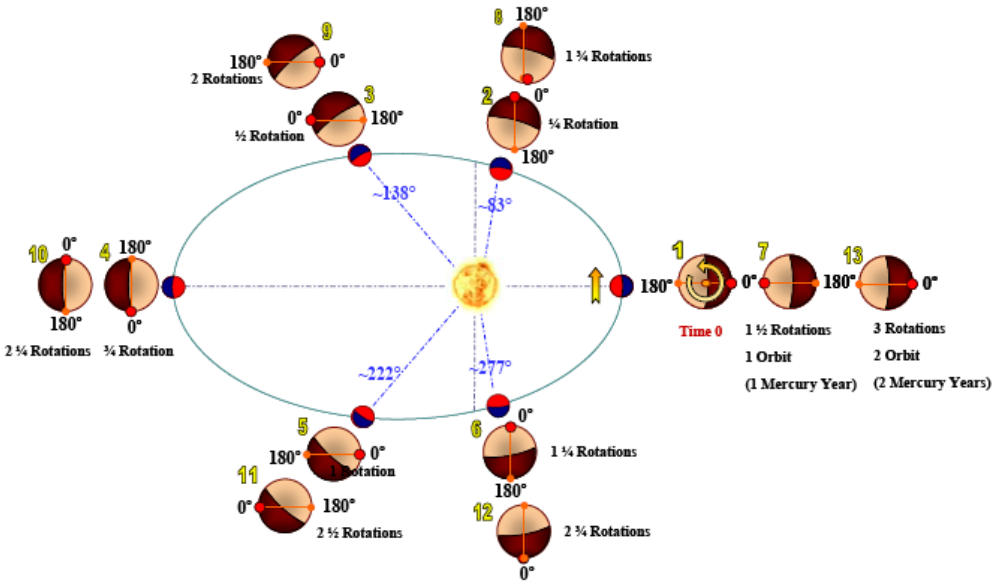

Fig. 1-2 Mercury orbit around the Sun and representation of the 3/2 spin-orbit resonance

In addition, it can be demonstrated that Mercury rotation period is almost exactly half of its synodic period with respect to the Earth. So, due to the 3/2 orbit-spin resonance, 54 Mercury's sidereal orbital periods correspond to 13.006 Earth years and the planet physical ephemeris - as viewed from Earth orbit - repeats itself once every 13 years.
In the following table the mean orbital parameters are listed, referring to J2000.

Mean orbital parameters	Value
Semi – major axis, a	0.387098 AU
Eccentricity, e	0.205632
Inclination, i	7.004986°
Longitude of the ascending node, Ω	48.3309°
Longitude of Perihelion, $\Omega+\omega$	77.4561°

Table 1-4 Mean orbital parameters, referring on J2000

1.3 Scientific Objectives

In 2000 the BepiColombo Science Advisory Group outlined the general scientific objectives, which can be summarized as follow:

- Exploration of Mercury unknown hemisphere;
- Investigation on the geological evolution of the planet;
- Understanding the origin of Mercury high density;
- Analysis of the planet internal structure and search for the possible existence of a liquid outer core;
- Investigation on the origin of Mercury magnetic field;
- Study of the planet magnetic field interaction with the solar wind;
- Characterization of the composition of the planet surface;
- Identification of the composition of the radar bright spots in the polar regions;
- Determination of the global surface temperature;
- Determination of the composition of Mercury vestigial atmosphere (exosphere);
- Determination of the source/sink processes of the exosphere;
- Determination of the exosphere and magnetosphere structures;

- Study of particle energisation mechanisms in Mercury environment;
- Fundamental physics: verification of Einstein's theory of gravity.

1.4 System description

1.4.1 System overview

As previously described, as a result of preliminary studies, BepiColombo mission will explore the planet Mercury and its environment by means of two different spacecraft, MPO (Mercury Planet Orbiter) and MMO (Mercury Magnetospheric Orbiter), in order to fulfill the scientific objectives in the most effective way. Every spacecraft which composes the space segment, has dedicated scientific tasks:

- The Mercury Planet Orbiter will support remote sensing and radio-science instrumentation;
- The Mercury Magnetospheric Orbiter will support fields and particles science instrumentation.

An additional transfer module, the Mercury Transfer Module (MTM), will be devoted to the interplanetary cruise phase. The propulsive system is composed of two different modules: the Solar Electric Propulsion Module (SEPM) and the Chemical Propulsion Module (CPM). MPO, MMO and MMT will be launched as the Mercury Composite Spacecraft in 2014 on an Ariane 5. The MCS will be launched on a geostationary transfer orbit, then it will be boosted to the phasing orbit using chemical propulsion. Thanks to the first flyby of the Moon, it will be set in its interplanetary trajectory; then, thanks to the gravity of the Earth, Venus and Mercury itself and by using solar electric propulsion, it will be able to compensate the gravity of the Sun, which increases getting closer to the star. Approaching to Mercury, the spacecraft will take advantage of the planet gravity and will use conventional rocket engines to insert itself into a polar orbit. At first, MMO will be released into its operational orbit; then the chemical propulsion module will bring MPO to its lower orbit. Approximately 6 years after launch, after a Moon, an Earth, two Venus and two Mercury flybys, the spacecraft will reach the target. The ground segment will be constituted of two elements: the Mission Control Centre at ESOC and the Science Ground Segment (SGS). From a procurement point of view, ESA will be in charge of control the launch, the operations of the MCS and the MPO spacecraft and operations, while JAXA will plan and control MMO operations. The following figure represents the Mercury Composite Spacecraft: from the bottom to the top, MTM, MPO, the removable sunshield and MMO are visible.

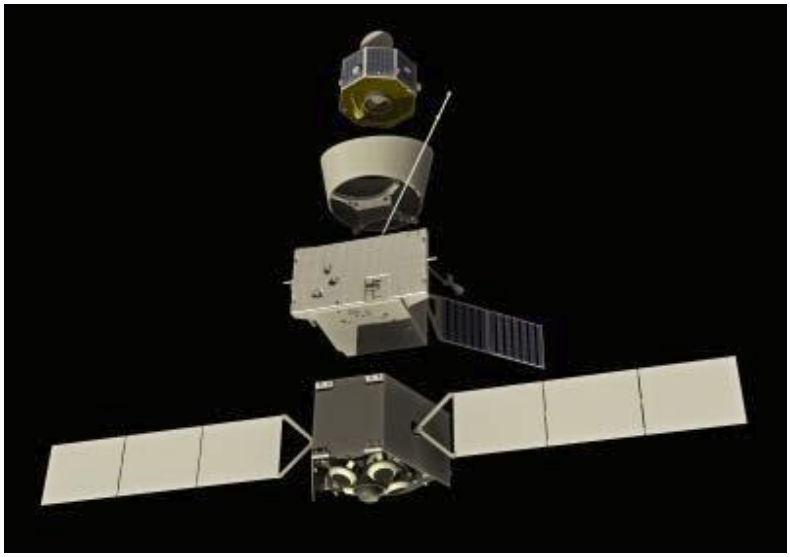

Fig. 1-3 View of the MCS: MTM, MPO, the sunshield and MMO are visible from the bottom to the top

With reference to the following figures, the MPO and MMO nominal orbital parameters are:

Orbital parameter	MPO	MMO
h_p [km]	400	400
h_a [km]	1508	11824
i [°]	90	90
Ω [°]	68	68
β [°]	0	0
ω [°]	0	0

Table 1-5 MPO and MMO nominal orbital parameter

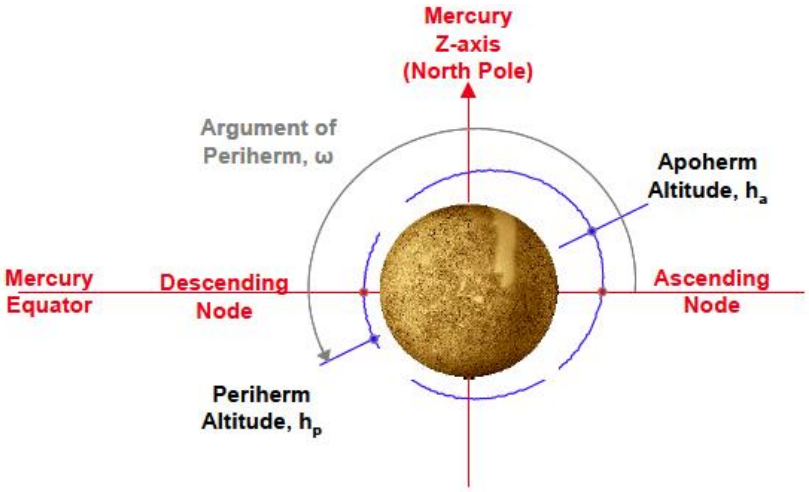

Fig. 1-4 Representation of the system Mercury – S/C with some characteristic orbital parameters

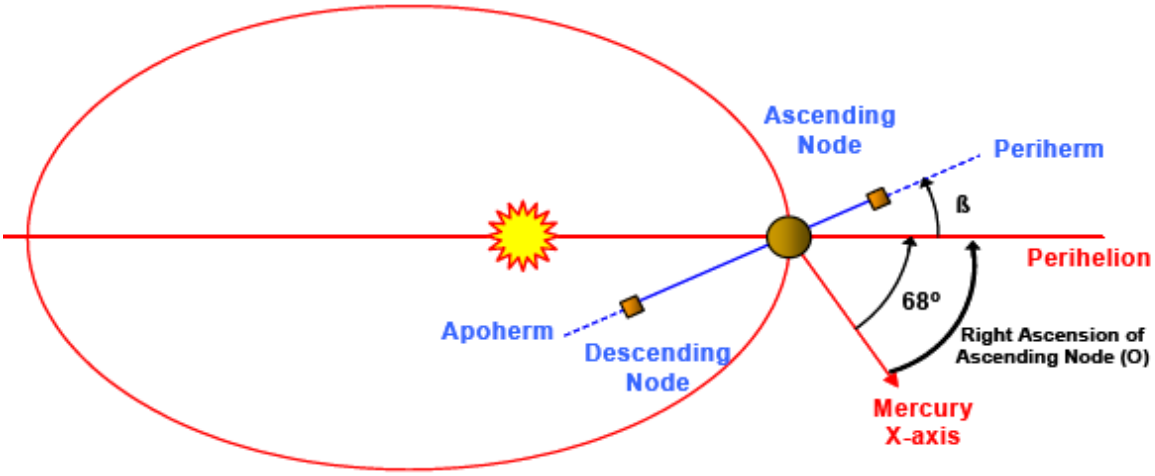

Fig. 1-5 Representation of the system Sun – Mercury – S/C with some characteristic orbital parameters

1.4.2 MPO payload

The MPO spacecraft is nadir pointing and three-axis stabilized, in order to assure a continue observation of the planet. The choice of a polar orbit facilitates the global mapping; in addition, the orbit is as low as possible in order to optimize spatial resolution. The minimum periapsis and apoapsis altitudes, 400 km and 1500 km respectively, are imposed by the thermal environment constraints.

The on-board instrumentation will be devoted to:

- Close range studies of the surface;
- Investigations of the interior structure of Mercury;
- Fundamental science;
- Magnetometry;
- Exospheric studies.

Imaging and spectral analyses will be performed in the infrared, visible and ultraviolet ranges, in the gamma – ray and X – ray as well. Furthermore neutron spectrometers will offer additional data about the elemental composition of the surface material. Also a laser altimeter will be available.
Radioscience experiments will be performed thanks to telemetry and telecommand up-and-downlink facility and to a high-precision accelerometer able to detect the effect of the Solar plasma on the wave propagation and the effect of the non-gravitational forces on the motion of the spacecraft.
The payload will be provided with the following instruments:

- Imaging instruments, combined into the camera suite SIMBIO-SYS, which is composed of:
    1. A High Resolution Imaging Camera (HRIC);
    2. A Stereo Camera (STC);
    3. A Visual and Infrared Hyper-Spectral Imager (VIHI).
- A Radiometer and IR Mapping Spectrum (MERTIS).
- A Laser Altimeter (BELA).
- An Ultraviolet Spectrometer (PHEBUS).
- A X- ray Spectrometer (MIXS – SIXS).
- A Gamma-ray & neutron spectrometer (MGNS).
- Radio Science Experiments (MORE, ISA).
- Magnetometer (excluding the boom) (MERMAG).
- Particle Suite:
    1. Neutral Particle Analyzer ELENA/Strofio.
    2. Ion Spectrometers MIPA/PICAM.

The next picture shows MPO payload.

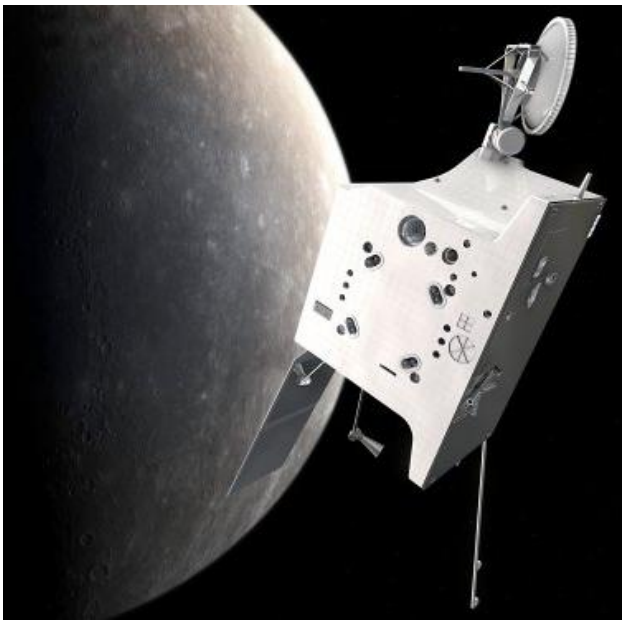

Fig. 1-6 Artist’s view of the MPO payload

1.4.3 MMO payload

MMO payload will host most of the instrumentation devoted to the study of the magnetic field, waves and particles present in the planet environment. MMO spacecraft is spin stabilized at 15 rpm in order to allow the azimuthal scan of the particles detectors and the deployment of 2 pairs of wire electric antennas. The orbit will be polar and highly ecliptic, in order to permit a global exploration of the magnetosphere from 400 to about 11800 km from the planet, by means of a 3-axis magnetometer.
On MMO the following experiments will be accommodated:

- Mercury Electron Analyzer (MEA);
- Mass Spectrum Analyzer (MSA);
- Mercury Ion Analyzer (MIA);
- High Energy Particle Analyzer for Electrons (HEP-ele);
- High Energy Particle Analyzer for Ion (HEP-ion);
- Energetic Neutral Atom Analyzer (ENA);
- Magnetic Field Sensor (MGF);
- Plasma Wave Investigation (PWI);
- Mercury Dust Monitor (MDM);
- Mercury Sodium Atmosphere Spectral Imager (MSASI).

The figure below shows the MMO payload.

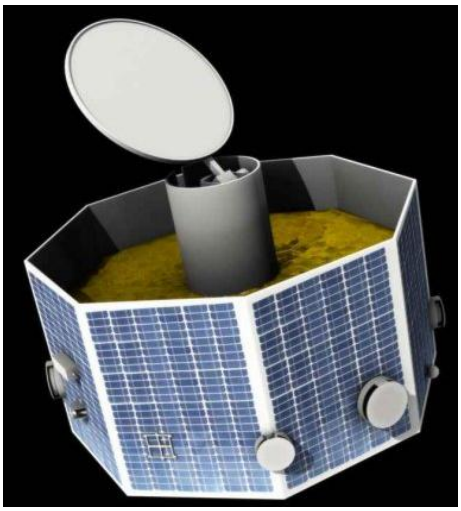

Fig. 1-7 MMO payload

1.4.4 The Solar Electric Propulsion Module (SEPM)

The SEPM will be used during the cruising phase: it will be able to carry a higher mass payload in a few time, if compared with a standard chemical propulsion module. This module shall be able to:

- Guarantee the necessary thrust during the cruise phase, by means of high-efficiency solar electric thrusters.
- Supply the necessary power to all the modules during the cruise phase, with the S/C sun illuminated.
- Provide the mechanical interface with the launcher.
- Provide the thermal control system for its proper units.

Despite of the low available thrust, SEPM provides a high exhaust velocity, 5-10 times higher than the velocity which is guaranteed by a standard chemical propulsion system, that assures a high specific impulse (~4500 s).

1.4.5 The Chemical Propulsion Module (CPM)

After the separation from SEPM, the CPM will be used to reduce MCS velocity and allow the capture by Mercury.
At first MMO will be inserted in its proper operative orbit, then, by means of an additional maneuver, MPO will reach its operative orbit.
The Chemical Propulsion Module will be able to provide:

- the necessary thrust for the orbital insertion of MPO and MMO.
- the AOCS of the spacecraft during the orbit insertion maneuvers.
- the mechanical interface between MPO and SEPM.
- the thermal control system for CPM sub-units and the propellant.

The CPM consists in a bi-propellant chemical propulsion system which combines N_2H_4 and N_2O_2. Since SEPM and CPM will not be able to send and receive commands, these functions will be provided by MPO, which will provide the power supply to CPM as well.

1.5 Mission phases

BepiColombo Mission can be divided into 5 different phases, 4 non-operative phases, 1 operative phase:

- Launch phase and Early Orbit Phase;
- Near Earth Commissioning Phase;
- Interplanetary Cruise Phase;
- Mercury Approach Phase;
- Mercury Orbital Phase.

The following figure represents the MCS in its flight towards Mercury: MMO is blue and it is covered by a sunshield (yellow in the picture); MPO is green with solar panel, MMT is grey with two solar wings.

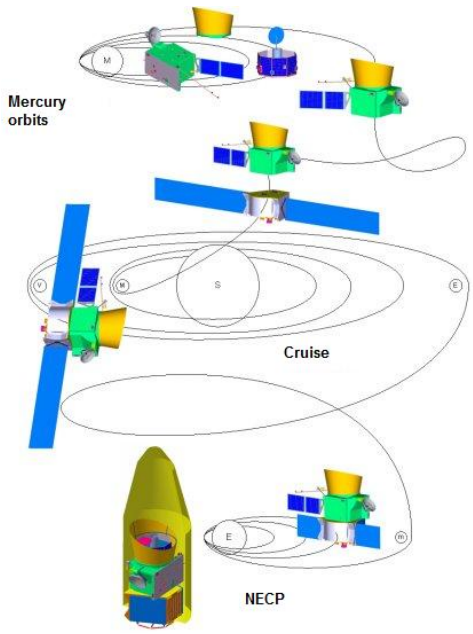

Fig. 1-8 Schematic of the mission deployment

1.5.1 Non-operative phases

From the previous figure different phases are recognizable:

- The Launch phase and the Early Orbit Phase (LEOP), which lasts from the removal of the vehicle umbilical connector until the achievement of a stable S/C configuration. This phase

includes the deployment of the solar arrays and all appendages, the initial attitude operations and the injection error correction maneuvers. During this phase the spacecraft is in a minimum power mode and the power is supplied from batteries until solar array deployment.

- The Near Earth Commisioning Phase (NECP), which extends from the LEOP until the end of the commissioning, also beyond the Moon fly-by.
- The Interplanetary Cruise Phase, which extends from the NECP until the beginning of the Mercury Approach Phase, about 3 month before the Mercury Capture Maneuver; the duration of this phase will be approximately 6years. MPO and MMO payloads will be nominally switched off, but regular check-outs will be planned. During this phase several gravity assists are foreseen, together with intermediate propulsion arcs provided by the Mercury Transfer Module.
- Mercury Approach Phase starts after completion of the Interplanetary Cruise Phase and lasts until the beginning of the MPO commissioning in its operational orbit; it includes the orbit insertion, the correction maneuvers and the delivery of MPO and MMO into their dedicated orbits with all the separation maneuvers.

1.5.2 MPO operative phase

After MPO orbital insertion, an engineering commissioning phase and a scientific performance verification phase will take place. The effective operative phase (Routine Operation Phase) starts after the completion of the MPO payload commissioning and lasts nominally one Earth year with a possible extension of another year.
Due to the orbital inertial properties and the radiators position, the spacecraft will perform two 180°-angle rotations every revolution around the nadir direction. After this operations, the instruments which point towards the progress direction will point towards the opposite direction, whereas the nadir-pointing instrumentation will not be affected by the 180°-angle rotation maneuver.
The following figure explains MPO attitude variations in its orbit around Mercury.

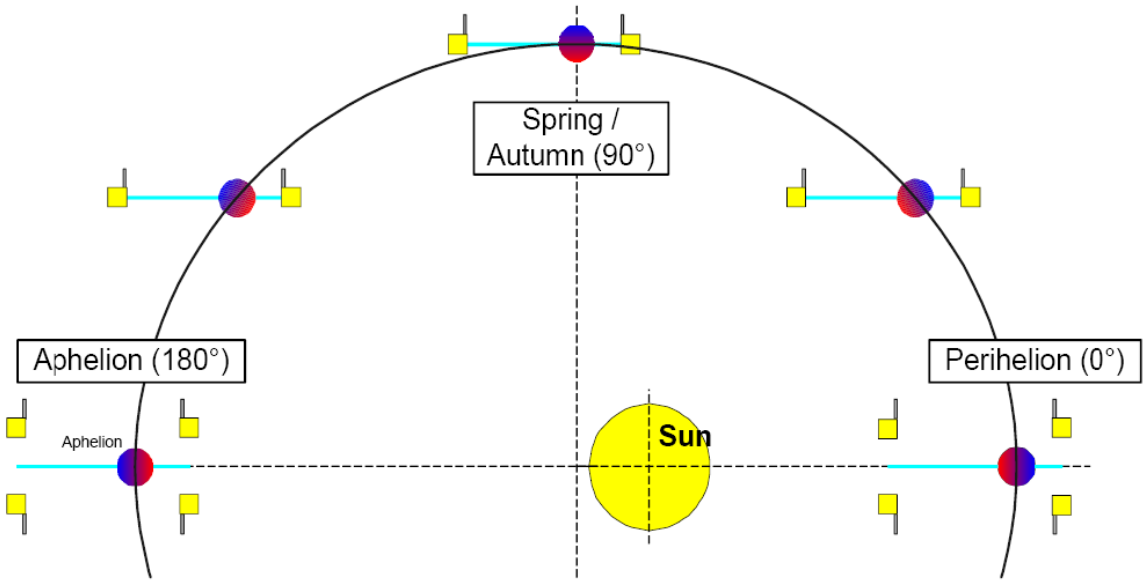

Fig. 1-9 MPO attitude maneuvers during its orbital phase

Thanks to geometrical considerations, the minimum solar incidence angle has been obtained as a function of Mercury's seasons, as showed in the plot below: black and red lines refer to STC forward and backward channels respectively (we have to consider that STC channels are 20° tilted

with respect to the nadir direction), blue line to HRIC and VIHI (nadir-pointing instrumentation) channels.
The minimum Sun incidence occurs for:

- Nadir-pointing instrumentation entering/exiting into/from the eclipse, at the beginning of Apoherm eclipse season;
- Instruments pointing off-nadir in the orbit plane at aphelion.

Instruments pointing in the direction above 28° off-nadir will see the sun directly: therefore shutters might have to be considered.

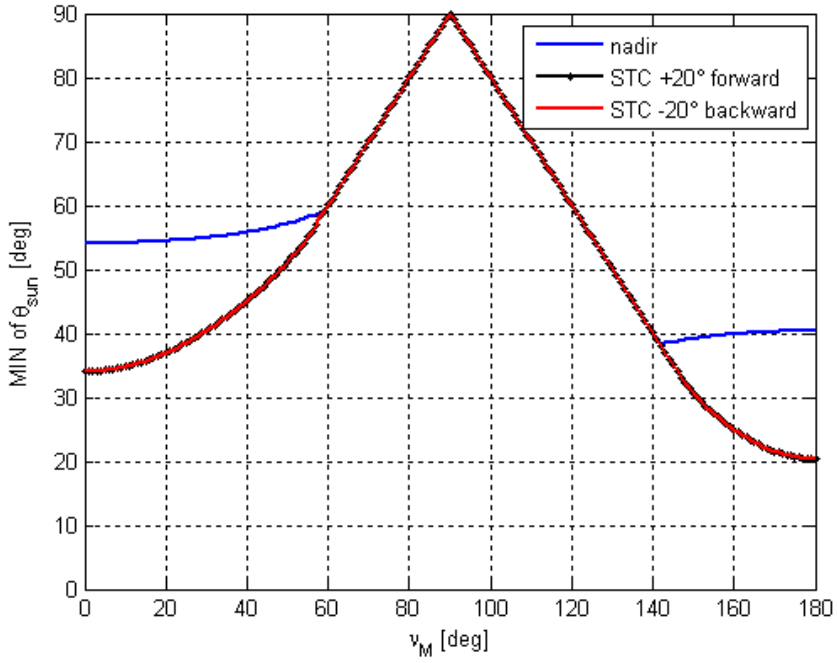

Fig. 1-10 Minimum incidence angle as a function of Mercury's season among half orbit around the Sun

In the next figure MPO nadir-pointing attitude is shown: *x*-axis points towards the S/C motion direction, *z*-axis is nadir-pointing, *y*-axis is perpendicular to the orbit and completes the right-handed triad. Roll, pitch and yaw Euler parameters represent the rotation angles around *x*, *y*, *z* directions respectively.

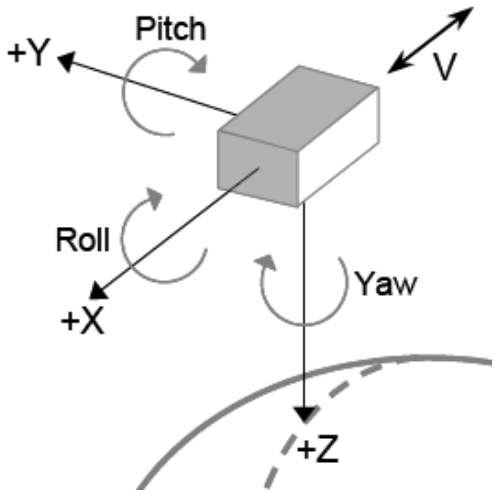

Fig. 1-11 Representation of the nadir-pointing attitude of MPO

The orbital parameters, such as Periherm and Apoherm altitude, have been defined in order to reach the scientific objectives (e.g. the spatial resolution, global mapping and the detection of the materials on the planet surface) optimizing the performances. Therefore the spacecraft will be inserted in a low polar orbit. Furthermore instruments will be operative once the spacecraft will

orbit over Mercury illuminated surface with the planet at Aphelion. Thanks to the ellipticity of the orbit, the energy necessary for the orbit insertion around Mercury – in term of ΔV – will be reduced as much as possible.
The following table summarizes MPO orbital parameters at beginning of life (BOL).

Parameter	Symbol	Unit	Value
Periherm altitude	h_p	km	400 ± 20
Apoherm altitude	h_a	km	1508 ± 20
Inclination	i	°	90 ± 2
Longitude of the ascending node	Ω	°	67.7
Argument of Periherm	ω	°	16
Period	T	hr	2.32
Eclipse duration	t_e	min	< 42

Table 1-6 Main MPO orbital parameters @ BOL

Due to the 3/2 spin-orbit resonance, since MPO orbital plane is fixed in an inertial frame, payload nadir-pointing instrumentation will view each illuminated meridian at with 3 different illumination angles, which will repeat every 2 Mercury years, as illustrated in the graph below (where $\beta = 0$, see Fig. 1-5).

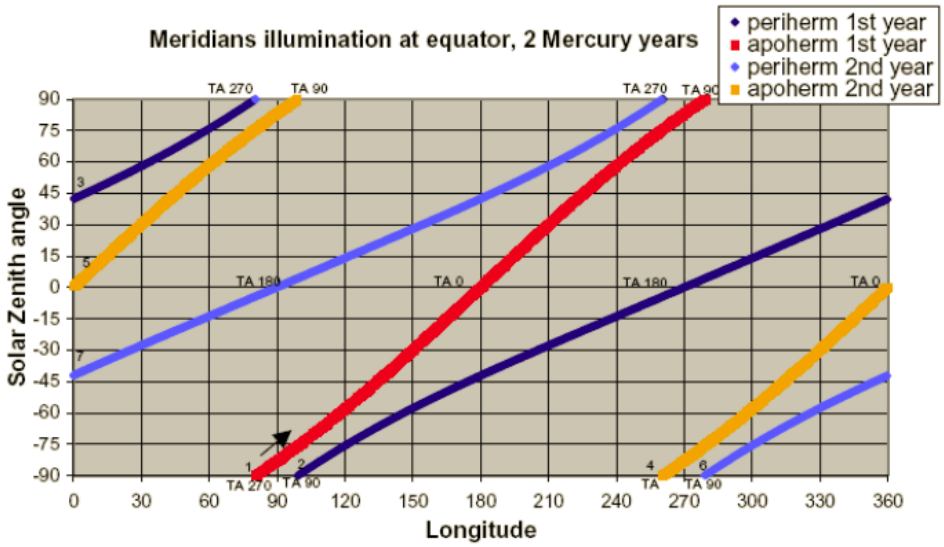

Fig. 1-12 Mercury Sun Illumination angles of Mercury meridians over the equator

Orbital parameters will continuously change during the mission as a function of the actual value of the J_2 – term of Mercury gravity field. This variation represents a crucial aspect since the thermal environment is strictly related to the variations of the orbital parameters, such as the argument of Periherm ω and the Periherm altitude h_p. The variation of these parameters as a function of J_2 is summarized in the table below, at the beginning of life, one year and two years later respectively.

Parameter	$J_2 = 40 \cdot 10^{-6}$			$J_2 = 60 \cdot 10^{-6}$			$J_2 = 80 \cdot 10^{-6}$		
	BOL	1 YR	2 YR	BOL	1 YR	2 YR	BOL	1 YR	2 YR
h_p [km]	400	392	407	400	400	427	400	406	434
ω [°]	16	-4	-23	16	-16	-48	16	-26	-73

Table 1-7 Values of the argument of periherm and the altitude of periherm as a function of J_2- term of Mercury gravity field

1.6 **Communication**

MCS and MPO will be controlled by ESOC (Germany), via its Ground Station in Cebreros (Spain); MPO will provide up-link via X-band and down-link via X/Ka-band communication with the ground segment. The down-link data volume for MPO experiments over the nominal mission life will be higher than 1550 Gb. Data rate will not exceed the link capability of the HGA and might vary during the operative life due to possible seasonal variations, such as the variation of Earth-MPO distance. In average the up – link data rate (telecommands) will be less than 4 kbits/s, the down.-link data rate (telemetry) will vary in the 30-675 kbits/s range.
MPO will provide all necessary on-board functions in order to allow the ground segment to perform tracking and navigation during MPO mission phases.
The following plot shows the data rate variation as a function of the elapsed time.

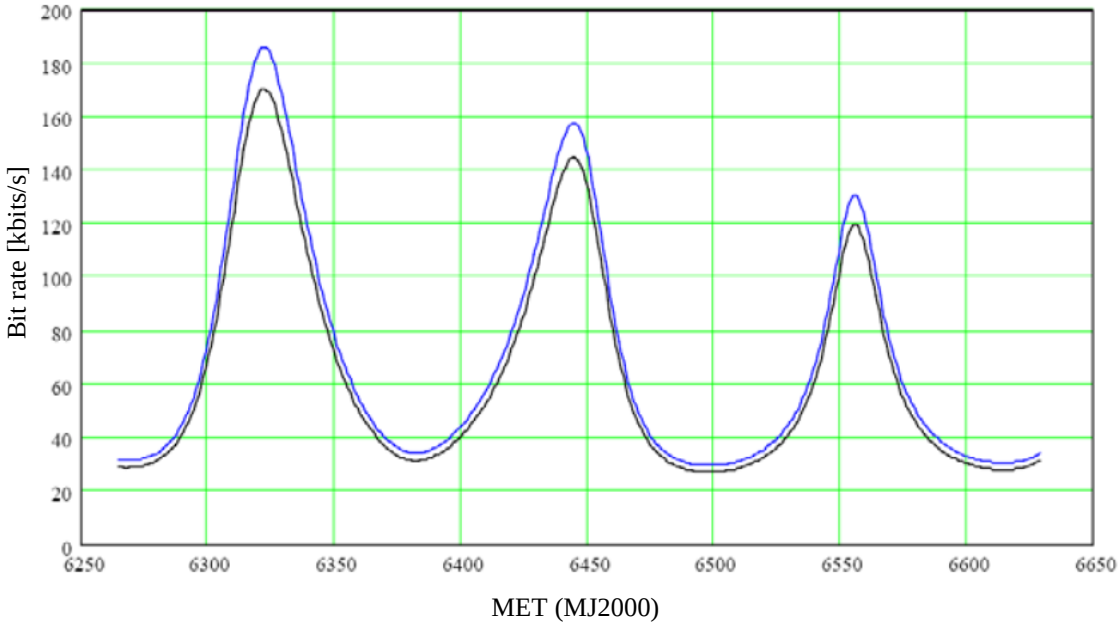

Fig. 1-13 Data rate as a function of time. Blue line represents down-link in Ka-band, black line represents down-link in X-band. The computation of the data rate has been performed at the reference distance of 1 AU, then propagating the result assuming the (1/distance^2) law.

During its operative life, MMO will be controlled by ISAS/JAXA ground station in Usuda (Japan). On the other hand, all communication during the cruise phase, both up-link and down-link, will be routed from MMO though MPO to ground via a military standard 1553 link.
The following sketch summarizes the communication chain.

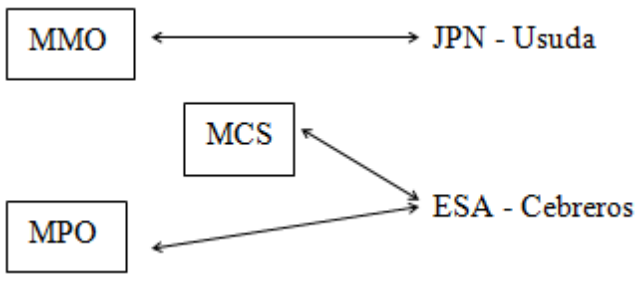

Fig. 1-14 Sketch which summarizes the communication chain

2. The SIMBIO-SYS suite

2.1 **Overall description**

2.1.1 Introduction

The suite SIMBIO – SYS (Spectrometer and Imagers for MPO BepiColombo Integrated Observatory SYStem), which is accommodated on MPO spacecraft, has been designed as an integrated package of instruments with different functions and operating on different channels, but mounted on a common optical bench, which represents the mechanical, thermal and electric interface with the spacecraft. It includes imaging system with stereo (STC) and high spatial resolution (HRIC) capabilities along with a hyperspectral imager (VIHI) in the visible-near infrared range. SIMBIO – SYS will provide a global view of Mercury and local high resolution images in order to reconstruct the overall evolution of the planet: it will provide an integrated picture of the planet combining information on the surface geology, topography and composition. Comparing with Messenger mission, SIMBIO-SYS will have higher image spatial resolution and stereo capabilities, larger imaging coverage and better spatial and spectral resolution for NIR acquisitions.
The instrument development is based on the joint efforts of Italy and France, with Selex ES S.p.A as industrial partner. The Structural Thermal Model of the suite has been developed and successfully tested in 2009; the Flight Model of the SIMBIO-SYS is currently under development and almost ready. The design of the suite is based on the maximum instrument's integration: power supply, data handling and software operations are shared, in order to optimize the scientific results during each phase of the mission. As previously explained the suite is composed of 3 different instruments: High spatial Resolution Imaging Channel (HRIC), Stereo Imaging Channel (STC), Visual and Infrared Hyper-spectral Imager (VIHI). The following figure shows the instruments suite as it seems in a recent Structural Thermal Model configuration.

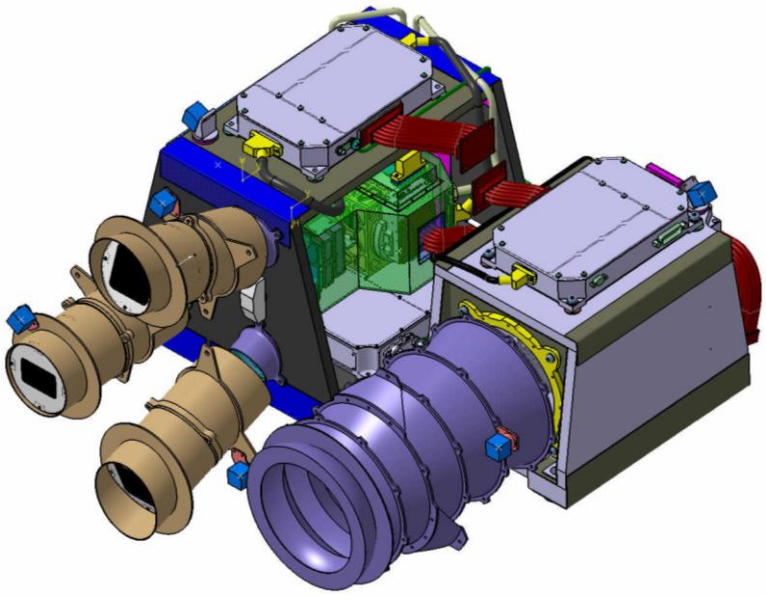

Fig. 2-1 Representation of SIMBIO-SYS Structural Thermal Model

The integration approach will allow to:

- Optimize the structural requirements, such as stiffness and vibrational performances;
- Minimize the mass;
- Guarantee the alignment stability for each channel, that is essential for the operations' coordination and the data transfer;
- Share the power supply system and main electronic functionalities, such as data elaboration and compression, control of the instruments, telemetry and telecommand;
- Simplify the passive thermal control system of the optical channels.

The optical channels have been designed in order to accomplish the following scientific objectives:

- Global mapping with stereo imaging with 50-110 m spatial resolution and 8.4 m vertical accuracy at Periherm over the equator.
- Color mapping of selected regions in 4 broad band filters in the range off from 410 to 930 nm.
- Global mapping with spectroscopy in the spectral range from 400 to 2000 nm with a spatial resolution better than 500 m.
- High spatial resolution (5-10 m) imaging of selected areas summing up to at least 20% of planet surface in a panchromatic filter and in 3 different broad band filters, in the range from 200 to 900 nm.
- Hyperspectral imaging of selected areas in the spectral range from 400 to 2000 nm with a spatial sampling down to 100 m.

2.1.2 General Scientific Objectives

In this paragraph the general scientific objectives are listed, referring on the different fields of interest, such as the study of Mercury surface, its composition and its geophysics.

1. The surface geology results from the thermal history of the planet and the alteration effects due to exogenic processes. Therefore, analyzing and mapping the surface of Mercury is fundamental to understand the upper crust evolution and the acting processes which formed and modified the planet's crust. SIMBIO-SYS shall provide global and local mapping of the surface with moderate and higher ground resolution respectively, as well as 3-dimensional information of the surface, in order to analyze the geological characteristics of the planet's surface. In particular, the SIMBIO-SYS instruments will:
    - Map the whole surface with a pixel scale lower than 110 m;
    - Characterize the main features of the surface, indentify craters, scarps, troughs, lava flows at a pixel size of 5 m at Periherm;
    - Correlate the observed morphology with surface composition with 100 m resolution and spectral sampling of 6.25 nm;
    - Generate the global Digital Terrain Model, in order to map the global height distribution of the surface assuring a vertical accuracy of about 80 m at the periherm on the equator.
2. Surface composition study allows to understand the alteration processes acting on the superficial layer of the planet.
   The suite shall provide global mapping of the mineralogical and elemental composition of the surface, in order to investigate its chemical composition. In particular, the SIMBIO-SYS instruments will:
    - Map the entire surface and correlate surface composition and surface features to a scale better than 500 m;
    - Measure global abundances of key minerals with an accuracy better than 10%;
    - Identify the spatial distribution of mineral species on the surface of Mercury at high spatial and high spectral resolution;

- Identify different mineralogical species and their abundances with a spectral sampling better than 10 nm and an accuracy better than 10%;
- Search and identify signatures of unexpected species with a confidence level better than 10%.

3. The SIMBIO-SYS instruments will provide data to measure and determine the orbital parameters such as the obliquity and the amplitude of libration, in order to investigate the structure of Mercury's interior.

2.1.3 Instrument Scientific Performances

The SIMBIO-SYS instruments shall be able to meet the following performance requirements:

Imaging:

1. Pixel scales:
    - Global mapping: 50 m at Periherm, 200 m at Apoherm;
    - High resolution imaging: 5 m at Periherm, 19 m at Apoherm;
    - Hyperspectral imaging global mapping: 100 m at Periherm, 400 m at Apoherm.
2. FOV:
    - Global mapping: 5.3° × 4.5° (cross and along track);
    - High resolution imaging: 4.7°;
    - Hyperspectral imaging global mapping: 3.7°.
3. S/N ratio:
    - Global mapping: > 150 at 600 nm;
    - High resolution imaging: 150 typical observations conditions in the panchromatic filter;
    - Hyperspectral Global Mapping: > 100 in all nominal operating conditions.
4. Coverage:
    - The low resolution global coverage will be completed within 6 celestial month.

Surface composition:

1. Broad band imaging:
    - Spectral range for the low resolution imaging: 410-930 nm. Filters: panchromatic (700 nm central wavelength, 200 nm bandwidth), band pass (410/20, 550/20, 750/20, 920/20).
    - Spectral range for the high resolution imaging: 400-900 nm. Filters: panchromatic (650 nm central wavelength, 500 nm bandwidth), band pass (550/40, 750/40, 880/40).
2. Visible-NIR Hyperspectral Imaging:
    - Spectral range: 400-2000 nm. Spectral sampling: 6.25 nm.
    - Imaging sampling capability: 100 m.
    - Global Mineralogical Mapping with < 500 m spatial resolution.
3. S/N: Hyperspectral Global Mapping:
    - Hyperspectral Global Mapping > 100 in all nominal operating conditions;
    - High Spatial Resolution: > 100 in nominal operation conditions.
4. Coverage:
    - The global mapping with < 500 m spatial resolution will be completed within 6 celestial months.

The measurement principle is based on coordinated operations of the 3 channels that constitutes the SIMBIO-SYS suite. This has to be selected in order to maximize the scientific return in each phase of the mission by suitably sharing the allowable resources in terms of power and data rate.
The operations sequence starts with the global mapping performed by STC (low resolution stereo-imaging) and VIHI (spectroscopy) during the early 6 terrestrial month of the operating life: during this phase, each point on the planet's surface will be visible just one time with the same angular and altitude conditions. For the following 6 month STC will perform specific measurements in order to ultimate the global coverage, whereas HRIC and VIHI will acquire specific targets with the highest spatial and spectral resolution, in order to cover the 20% of the overall surface.
In order to guarantee best performances, the channels will acquire images just orbiting on the illuminated surface of the planet: in these way the presence of shady areas is minimized and the colour contrast is as high as possible.

2.1.4 Instrument hardware description

As previously described, the SIMBIO-SYS instrument architecture is based on 3 different channels with a common Main Electronics (ME) and power supply. The 3 channels, which constitute an Instrument Front End (IFE), are listed below:

- High Resolution Imaging Channel (HRIC);
- Stereo imaging Channel (STC);
- Visual and Infrared Hyperspectral Imager channel (VIHI).

Each channel is formed by its own optics, detector (Focal Plane Assembly), thermal hardware, proximity electronics and electric interface for power supply, telecommand/telemetry link.
Main electronics and power supply at suite level are common for all the IFE channels: each channel is connected to the main electronics by means of a SpaceWire bidirectional link for both telecommands and telemetry. The proximity electronics is controlled by a FPGA, which handles commands from the main electronics and implements the required detector configuration when an acquisition is requested. The following sketch represents the IFE and the overall suite architecture from the hardware point of view.

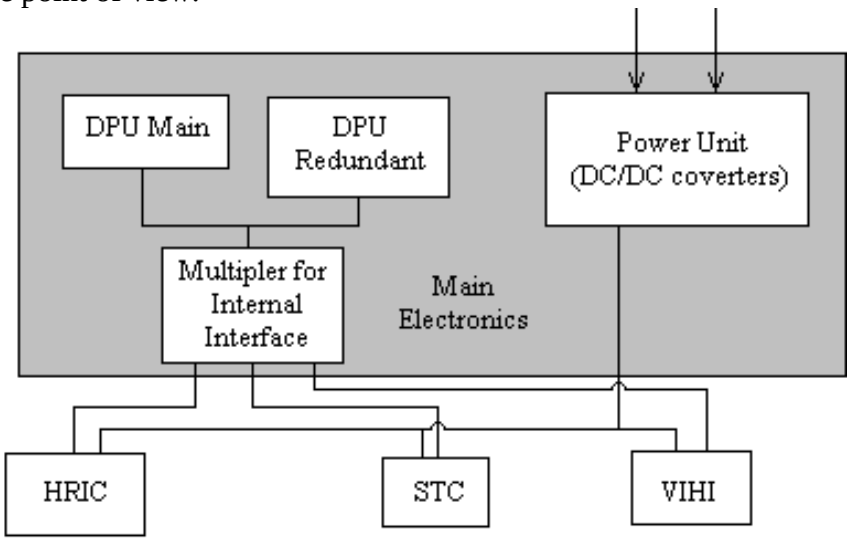

Fig. 2-2 Overall scheme of the SIMBIO-SYS suite architecture showing the main subsystem. DPU is the Digital Processing Unit

Since SIMBIO-SYS will operate in a very harsh environment, mainly from the thermal point of view and the presence of high-energy particles, dedicated state-of-art baffles and filters will be designed ad hoc, produced, tested and integrated. The qualification of these devices will be performed by means of innovative test beds able to reproduce operating environmental conditions, such as solar and infrared fluxes, as described in the latter.

From an electrical point of view, the followed approach allows the sharing of two main functions among the suite, which are implemented at suite level to avoid duplication and are incorporated in the ME:

1. Data processing electronics function, which is mainly devoted to data management and compression, instrument control and telemetry/telecommand handling to/from the spacecraft interface.
2. Power supply, which is devoted to supply all the subsystems with the required power, providing a common set of required voltages.

The proposed approach is sketched in the following figure.

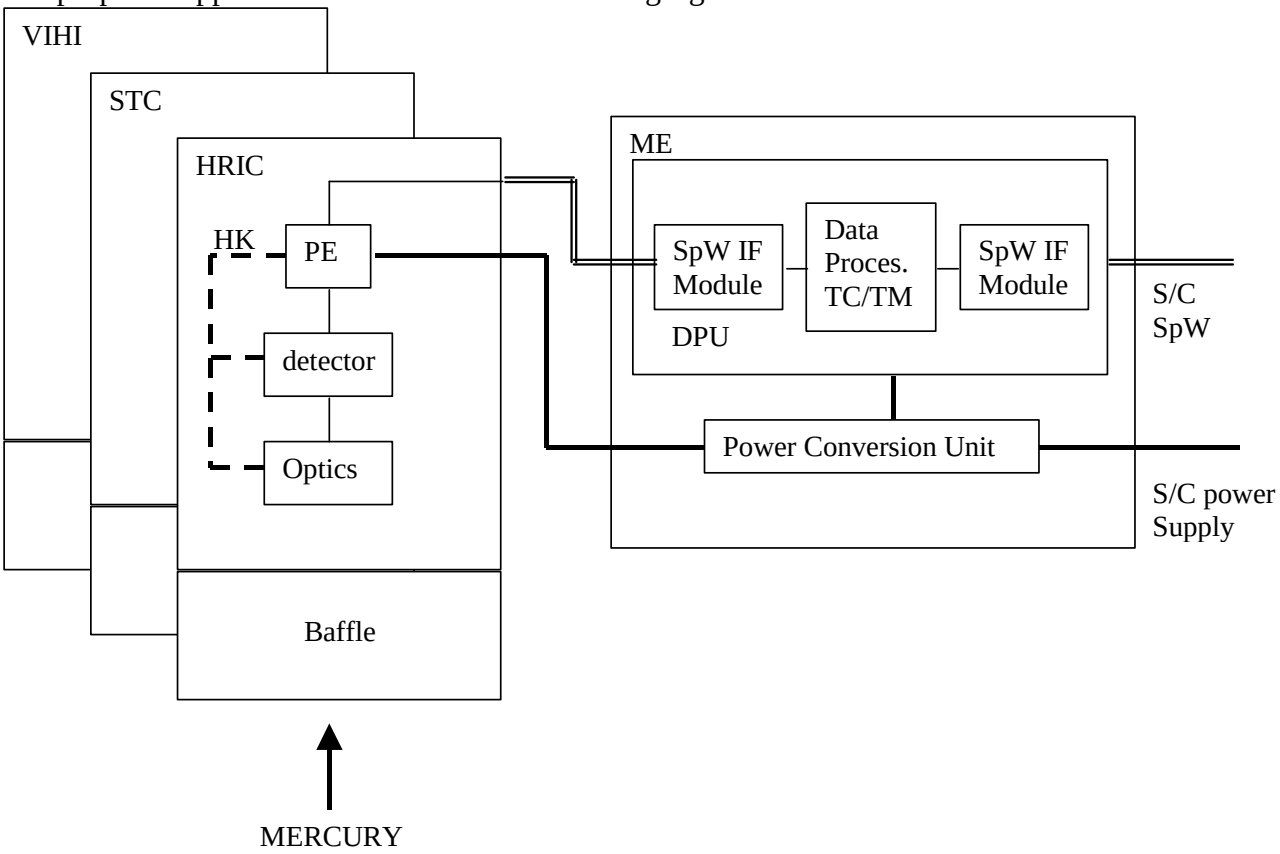

Fig. 2-3 Functional Block Diagram

The supporting structure guarantees fine pointing and stability during the operational life in order to meet the few arc-second precision requirement of the libration experiment.
Electronics components have been carefully chosen and detectors have been very accurately designed, in order to cope with total radiation dose and single events upset requirements.

2.1.5 Instrumentation lifetime

In this section the lifetime requirements, which affect the instrumentation design and regard all the instruments parts, are listed:

- The shelf life time shall be compatible with a launch time of 2 years from the nominal launch date. Therefore ground environmental influence has to be taken into account during the design.
- The overall instrument life time shall be compatible with the increased cruise time resulting from the worst-case single failure of the electrical propulsion system during the cruise phase. Therefore space environmental influence has to be taken into account in the instrumentation design.

- The nominal instrument operational life time shall be major than one Earth year in Mercury orbit environment (space environmental influence and use conditions).
- An extended orbiter operational life time of > 1 Earth year beyond the nominal mission life is desirable.
- For items which degrade with usage, the life time shall be 2 times the nominal operational life time.

The following table summarizes the lifetime requirements for all instrumentation components.

Time	Cause	Ground/space influence
5 years	Nominal ground lifetime from 2009 to Launch	Ground
+ 2 years	Launch delay	Ground
+ 6.32 years	Cruise	Space
+ 1 year	Nominal Mission	Space & use
(+ 1 year)	Optional Extended Mission	Space & use

Table 2-1 Summary of lifetime requirements

2.1.6 Mass budget

In the following table the mass budget of SIMBIO-SYS suite is detailed.

Parameter	Units	Value	Remarks
Mass, total	[kg]	11.487	Contingency: 11.8%
Mass, channels	[kg]	6.126	Optical channels + PE
Mass, baffles	[kg]	0.871	Stavroudis + STC&VIHI baffles
Mass, electronics	[kg]	3.168	ME cold redundancy with PCU
Thermal straps	[kg]	0.846	
Internal harness	[kg]	0.476	
Dimension	[mm^3]	470 × 490 × 325	W × L × H

Table 2-2 Mass budget and dimensions of the suite

2.2 **Mechanical Interfaces**

The suite is composed of 6 units:

1. HRIC, which is integrated on the S/C optical bench; the unit hosts on its top surface HRIC Proximity Electronics.
2. STC and VIHI unit, which is integrated on the S/C optical bench. The unit hosts on its bottom surface the Proximity Electronics of VIHI, on its top surface the Proximity Electronics of STC.
3. Main Electronics, which is integrated on the S/C.
4. HRIC baffle, based on Stavroudis geometrical design properties, is integrated on the S/C bracket.
5. Two STC baffles, which are integrated on the S/C bracket.
6. VIHI baffle, which is integrated on the S/C bracket.

Since the instruments operate in different bandwidth (STC and HRIC get images in the visible bandwidth range, VIHI in the spectral range from 400 to 2100 nm), the requested temperature environments are different: STC and HRIC require cold temperatures just for calibration purposes

and perform their duty with detector sensitive area at 0°C, whereas VIHI detector sensitive area is requested to be at about 223 K to properly perform. Therefore, since an active thermal control system is required, TEC elements are present in each camera detector, in order to control the sensitive area temperature within the assigned temperature range: TEC removes heat from sensitive area and reject it towards a heat pipe by means of a thermal strap, linked to each camera detector on its hot side, to the heat pipe on its colder side; at last the heat pipe performs a high efficiency joint between camera and radiator.
Cameras are structurally fixed to the optical bench which does not behave as a heat sink: therefore it provides the mechanical support with negligible heat flux exchanges. By means of decoupling structural and thermal function of the optical bench and isolating the cameras, incoming parasitic heat is highly reduced and the heat load on the detector cold sensitive area and TEC power demand are minimized. The baffles will be conductively decoupled from the cameras and conductively coupled to the satellite bracket.
The following figure shows the components listed before:

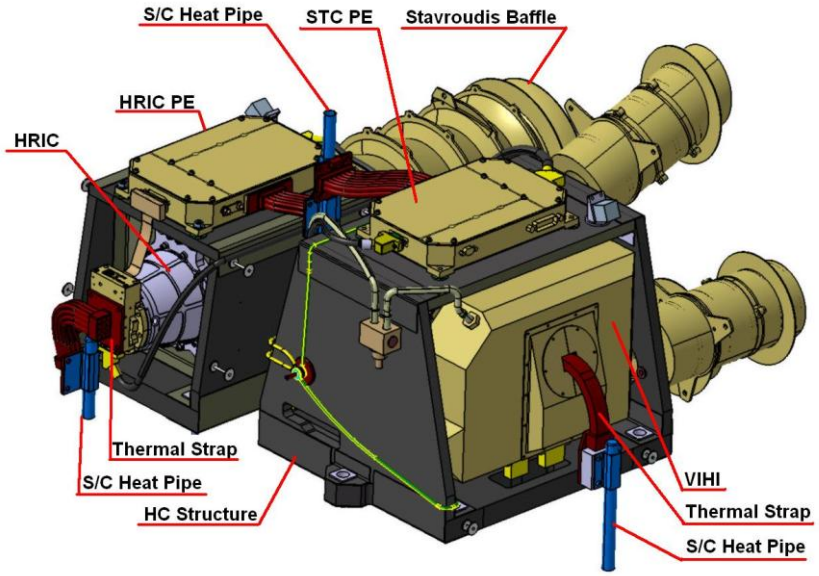

Fig. 2-4 Isometric view of SIMBIO-SYS Instrument

STC and VIHI share the same structure while HRIC has a dedicated one: these structures interface with the spacecraft bench and are made in AA honeycomb aluminum core panels with CFRP skins, show high stiffness over weight ratio while having a poor thermal conductivity. Furthermore they presents the same CTE as the optical bench, minimizing the thermo-elastic interface forces with respect to higher CTE materials interfaces. Inserts are introduced in these structures in order to supply the fixing interfaces. The panels which form the structures are stiffened together by means of angular CFRP components. The following figure shows the sandwich panels structure of STC-VIHI and HRIC.

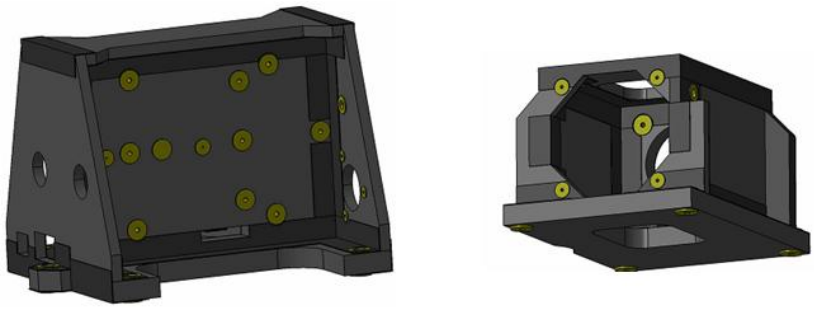

Fig. 2-5 Sandwich panels structure for STC-VIHI (on the left) and HRIC (on the right)

In the following table the mass budget for each unit is reported, referring to the nominal values and the allowable margin.

Description	Mass [kg] with contingency
HRIC channel	2.27
STC-VIHI channels	3.28
HRIC Stavroudis baffle	0.431
STC - VIHI Baffles	0.365
Thermal hardware	0.841
Cabling	0.347
Main Electronics	3.09
Total	**10.63**

Fig. 2-6 SIMBIO-SYS mass budget

Assuming an Unit Reference Frame with the *X*-*Y* plane coinciding with the mounting plane, the *Y* axis parallel to HRIC optical axis and *Z* axis normal to the mounting plane, the suite's main dimensions are:

- 532 mm in *Y*-direction;
- 480 mm in *X*-direction;
- 240 mm in *Z*-direction.

The following figures show the suite's main dimensions (figures refer to the STM configuration):

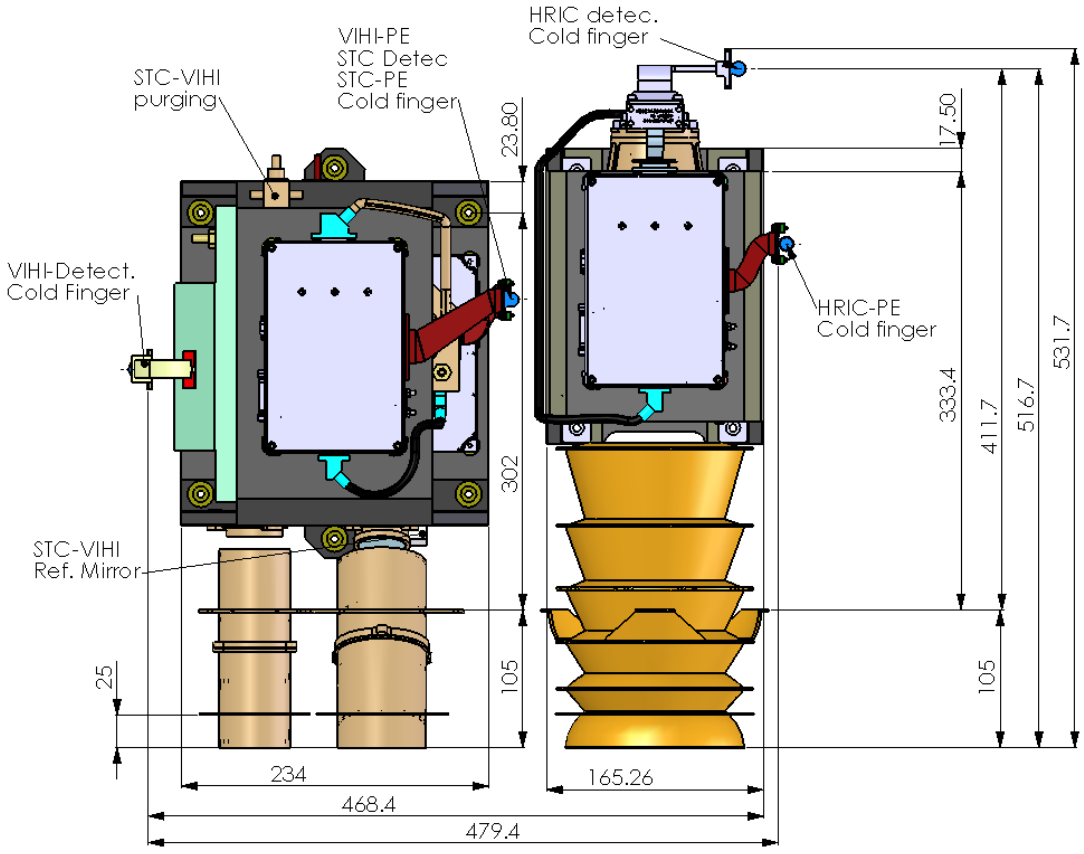

Fig. 2-7 SIMBIO-SYS main dimension (upper view)

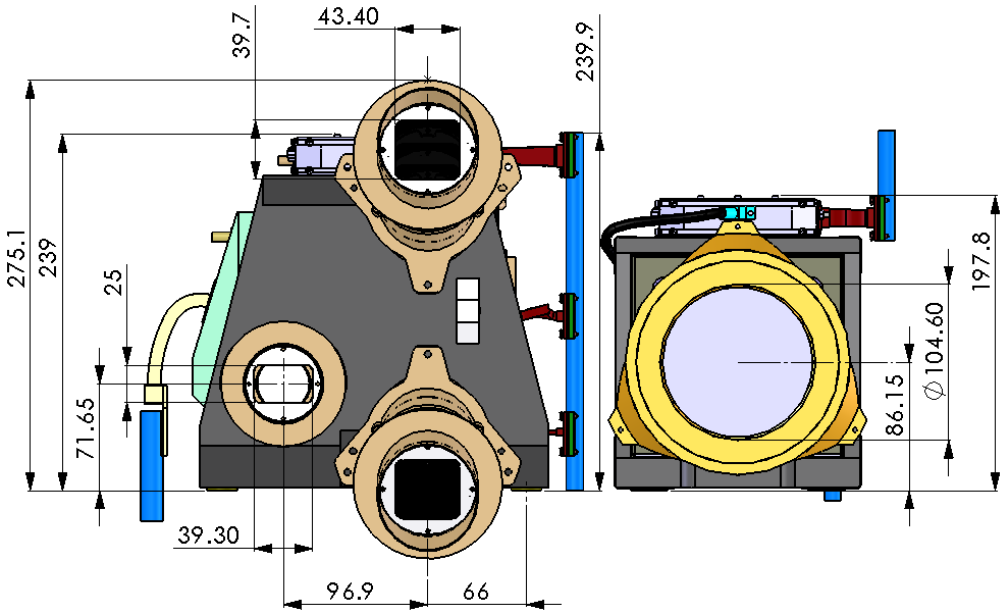

Fig. 2-8 SIMBIO-SYS main dimensions (front view)

2.3 Thermal interfaces

In this paragraph the guidelines for the thermal design are described. As stated in the previous section, the structural and thermal aspects are decoupled: each unit interfaces with a heat pipe cold finger provided by the S/C and the S/C bench does not act as a heat sink, providing only structural support with negligible heat exchange. The suite units of interest and the thermal interfaces with the spacecraft for each unit are here detailed:

- Main Electronics: it is conductively linked to the S/C main structure and the passive thermal control is provided by the conductive link through 6 pads and the ledge with metallic bottom surface.
- HRIC: the structure hosts HRIC PE on the top and is joined to the S/C optical bench by means of 4 mounding pads. A Thermal IR rejection device is interposed between HRIC Baffle and the camera telescope and sustained by the honeycomb structure. The active thermal control is performed by means of 2 dedicated cold fingers, the first one connected to the PE, the second one to HRIC detector.
- HRIC Stavroudis baffle: it is connected to the S/C baffle bracket by means of 3 pads; the thermal contact between these 2 components is very poor. In addition, it is thermally decoupled from the camera. The Stavroudis baffle is internally reflective and based on a series of highly reflective hyperbolas and elliptical surfaces: thanks to this particular geometrical concepts, it rejects towards the sky-background the incoming radiation misaligned with respect to the optical axis (after 2 reflections maximum), constituting a passive thermal control system.
- STC and VIHI: the honeycomb structure which supports the aluminum made cameras is joined to the S/C optical bench by means of 6 pads. As for HRIC, the heat flux exchange with the optical bench is negligible and IR filters are interposed between baffles and cameras. The IR filters are composed by a IR reflecting treatment deposed on a substrate IR opaque for STC, opaque to IR radiation higher than 2.4 μm for VIHI. A system of cold fingers provide the thermal control, one per unit: the first one, placed on STC side, removes the heat generated by the TEC controlling the STC detector temperature and by STC-VIHI PE; the second one removes the heat generated by the TEC controlling the VIHI infrared detector temperature and the radiative heat incoming from the environment.

- STC and VIHI Baffles have smaller aperture respect to Stavroudis baffle and black inner surfaces, therefore they reject the external radiative absorbed heat to space. The baffles are connected to the S/C baffle bracket panel by means of 6 pads for STC (3 per channel), 3 for VIHI.

The following figure shows TRPs and relevant heat loads.

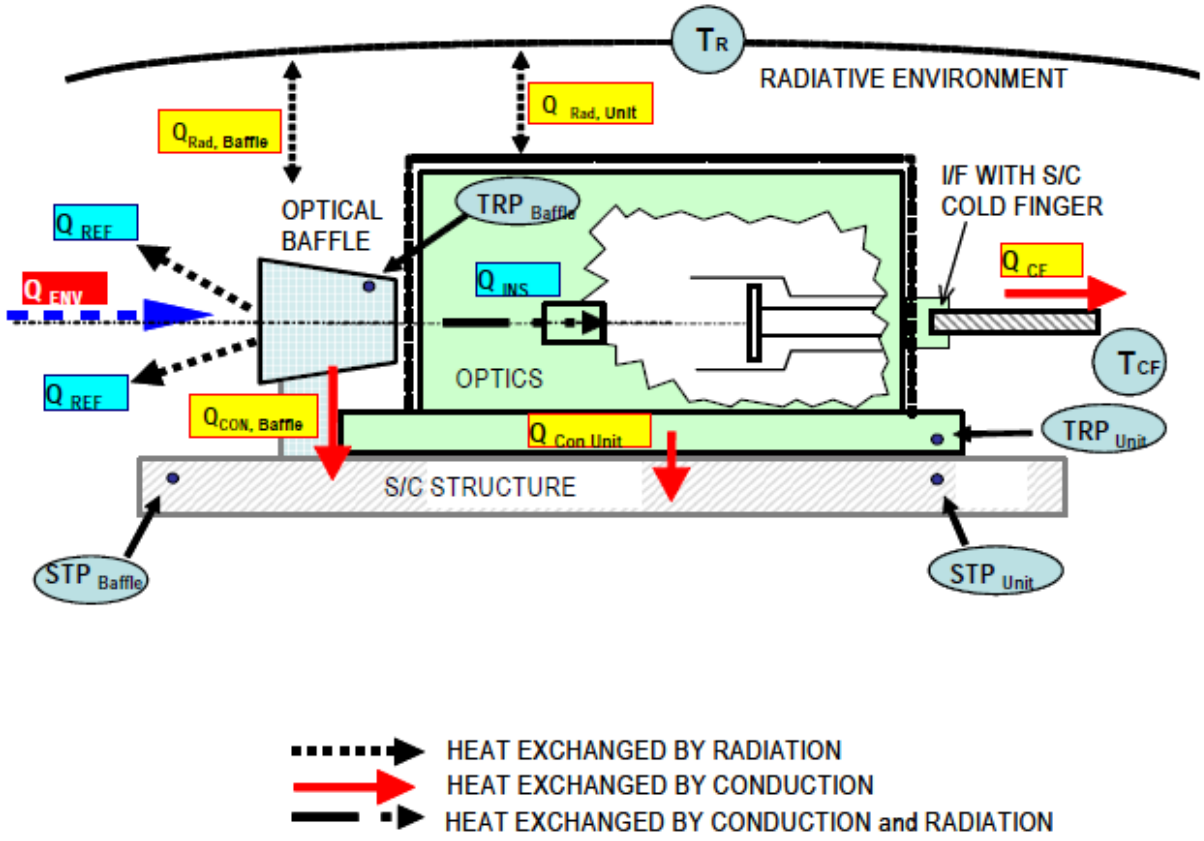

Fig. 2-9 TRPs and heat load definitions

The parameters reported in the figure below are described in the following list:

- Q_{ENV} is the environmental thermal inputs, mainly dependent of the aperture size of the baffle and the actual environment.
- Q_{REF} is the heat flux rejected by the baffles to space, given by the sum of the reflected flux and the re-emitted flux.
- $Q_{RAD,Baffle}$ and $Q_{CON\ Baffle}$ are the environmental heat load entering the baffle aperture and not reflected back: part of this flux is absorbed by the baffle and either radiated into the S/C body, part is conducted into the S/C structure which supports the baffles.
- Q_{INS} is the environmental heat load entering the instrument aperture (such as lenses) either directly or by baffle induced effects.
- Q_{ELC} is the electrical heat dissipation of the electronic unit.
- $Q_{RAD\ Unit}$ and $Q_{CON\ Unit}$ are the total heat derived from the sources above partly absorbed by the unit structure and either radiated into the S/C body or conducted via the unit mounting into the S/C structure.
- Q_{CF} is the heat load dumped into the S/C via the cold finger.

The following equations can be deduced:

$$Q_{ENV} = Q_{REF} + Q_{RAD,Baffle} + Q_{CON\ Baffle} + Q_{INS}$$

$$Q_{INS} + Q_{ELC} = Q_{RAD\ Unit} + Q_{CON\ Unit} + Q_{CF}$$

Solving the second equation and introducing it in the first one by saying that sum of all heat loads introduced in the S/C by the baffle is $Q_{ABS\ Baffle}$ (= $Q_{RAD,Baffle}$ + $Q_{CON\ Baffle}$) and that introduced by the unit is $Q_{ABS\ Unit}$, it results:

$$Q_{ENV} - Q_{REF} + Q_{ELC} = Q_{ABS\ Baffle} + Q_{ABS\ Unit} + Q_{CF}$$

The following table summarizes the maximum allowable heat flux to S/C for SIMBIO-SYS.

Unit	$Q_{abs\ Baffle}$ [W]	$Q_{abs\ Unit}$ [W]	Q_{CF} [W]	Cold Finger I/F temp.	Notes
VIHI, STC, HRIC baffles	15.0	N/A	N/A		
Main Electronics	N/A	17.0	N/A		
PE and HRIC housing	N/A	0.0	12	@ 14°C	+14°C at HP I/F
HRIC detector	N/A	0.0		@ 14°C	+14°C at HP I/F
STC – VIHI unit	N/A	0.0		@ 14°C	+14°C at HP I/F
VIHI detector	N/A	0.0	4.5	@ -16.5°C	

Table 2-3 Maximum heat fluxes

The following table shows the temperature requirements at cold finger interfaces.

Unit/subsystem	Operating temperature [°C]		Non-operating temperature [°C]		Switch-on Temperature [°C]		Temp. stability	At max heat load
	Min	Max	Min	Max	Min	Max		
HRIC FPA	-10	+14	-40	+55	-15	+14	2 °C/orbit	12 W
STC FPA PEs	-10	+14	-40	+55	-15	+14	2 °C/orbit	
VIHI FPA	-60	-16.5	-63	+40	-63	-16.5	2 °C/orbit	4.5 W

Table 2-4 Temperature requirements at cold finger interfaces

These temperature values have been taken into account during the thermal test campaign, increased (maximum value) or decreased (minimum value) by a 10°C qualification margin. The required stability during tests is 1°C/hour.

The baffles face with the camera on the inner side, with the space environment on the external side. The suite instrumentation is thermally insulated with respect to the external thermal environment by means of a double Multi Layer Insulation composed of high temperature MLI as external blanket, standard MLI as internal blanket, which have to be kept at a minimum distance of 20 mm.

- The high temperature blanket is composed of 20 layers, with white fabric as outmost layers (Nextel), with an expected thickness in orbit of 25 mm. The thickness can be locally reduced by means of additional sewing threads, with negative effect on the insulation performance.
- The standard blanket is a 20 layers MLI with external layers built form VDA Kapton, in order to minimize the heat exchange between high temperature MLI and standard MLI.

The cavity between the 2 blanket is assumed to be black with a sink temperature between -80°C, during eclipse and earth escape phases, and 250°C at perihelion.

The sequence of blanket can be summarized as follow:

- 25 mm HT-MLI allocated volume, filled by either 17 mm thick MLI type A-1 or 7 mm type A (both under 1 g condition). Emissivity and absorptivity coefficient of the external foil (Nextel) are 0.87 and 0.23 (value at BOL) respectively, emissivity coefficient of the inner foil is 0.04.
- 20 mm gap for the micro-meterorite protection.
- 20 mm standard MLI allocated volume, filled by 5 mm thick standard MLI (under 1 g condition). The emissivity coefficient of the outer and the inner foils of the standard MLI is 0.04 (Kapton)
- 20 mm MPO bottom panel, supporting MLI.
- 20 mm gap between the bottom panel and the baffle support panel.
- Baffle support panel.

The allocated volume for HT and standard MLI is overestimate since all blankets will expand under 0 g and in vacuum. The thickness of the HT MLI will be constrained by means of a grid of sewing lines. The proposed blanket layout is shown in the following figures, first for HT-MLI type A-1, then for HT-MLI type A-2.

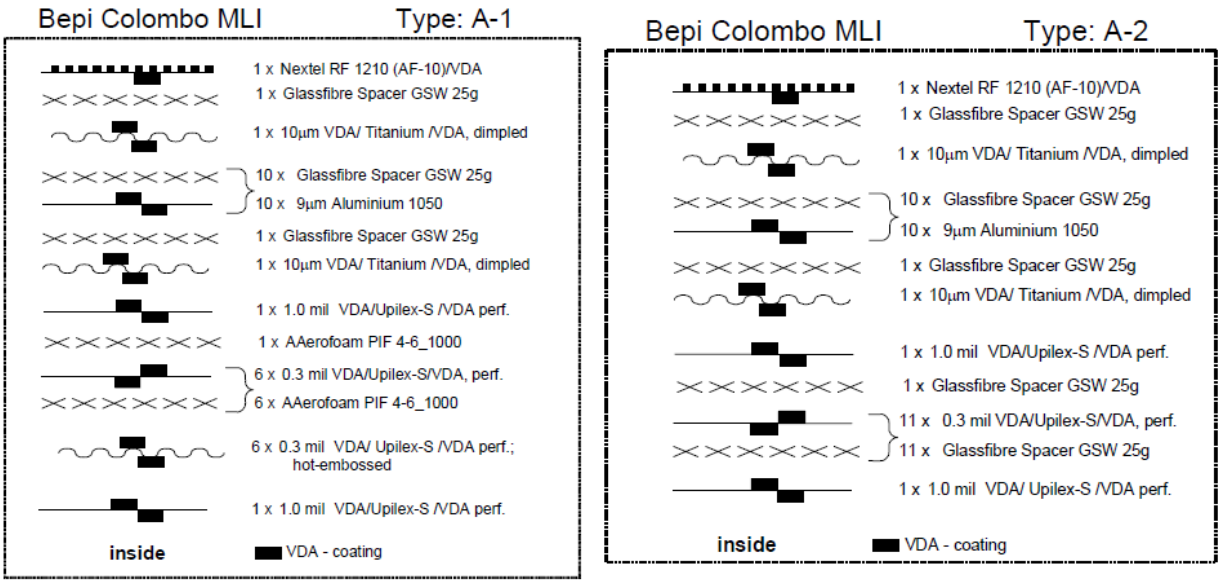

Fig. 2-10 High Temperature MLI type A-1 (on the left) and A-2 (on the right)

HT-MLI and standard MLI are both mounted on the bottom panel; around instrument apertures an additional HT-MLI blanket might be necessary for manufacturing and integration reasons, as shown in the following figure.

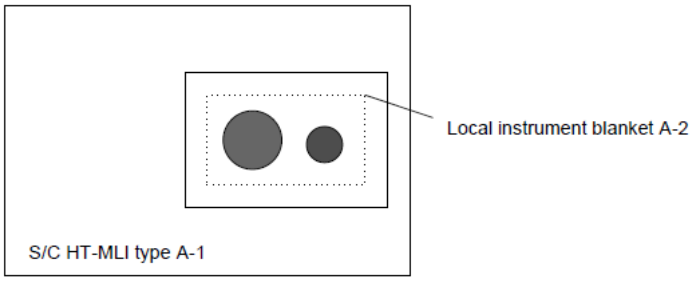

Fig. 2-11 Principle of local instrument blanket

The following pictures represent the blanket sequence and the baffle MLI interface concept for HRIC and STC-VIHI baffles (a single dedicated blanket is provided for all 3 baffles).

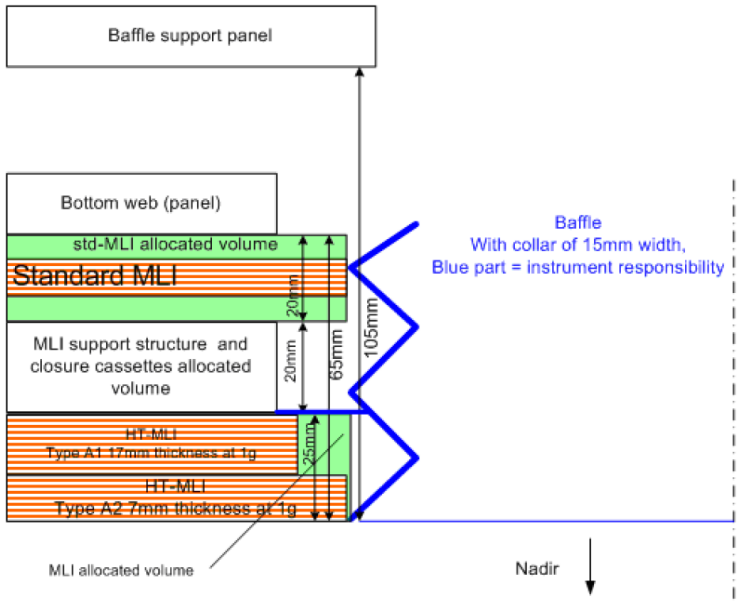

Fig. 2-12 HRIC baffle MLI interface concept

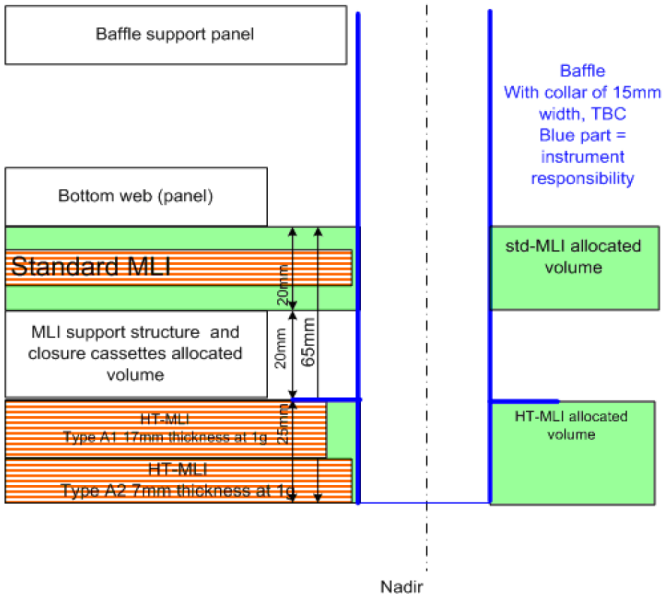

Fig. 2-13 VIHI and STC baffles MLI concept

2.4 HRIC: High spatial Resolution Imaging Camera

2.4.1 Overall description

The HRIC channel has been designed in order to satisfy the requirement of high spatial resolution imaging over the covered field of view in a panchromatic filter and in 3 band-pass filters centred at 550, 750 and 880 nm. It will be able to provide images at 5 m/pixels scale from periherm in order to identify key surface features, such as craters, scarps, lava flows and plains. The optical design has been optimized in order to satisfy not only scientific requirements and nominal optical performance but also dimensional requirements and mechanics constraints of compactness and low mass. Therefore a catadioptric Ritchey – Chretien configuration equipped with a dedicated refractive corrector camera has been chosen.
The main objectives are hereafter summarized:

- Providing images at ground pixel size of 5 m/pixel at 400 km;
- Providing high spatial resolution images of selected regions, 20% of planet surface at least;
- Providing high spatial resolution images in one panchromatic and 3 broad-band filters.

The following table shows the main resolution data.

Parameter	Unit	Value	Remarks
Spectral resolution	Nm	N/A	Filers width 40 nm, but for panchromatic (500 nm)
IFOV	μrad/pixel	12.5	
Ground pixel scale	m/pixel	5	@ 400 km
Dwell time at periherm	Ms	1.9	
Dwell time at apoherm	Ms	14	

Table 2-5 Resolution data

2.4.2 Optical design

The optical design is based on a catadioptric concept, with optimization of a Ritchey – Chretien configuration with a dedicated corrector of 3 refractive elements. It provides a resolution of 2.5''/pixel for a pixel size of 10 μm and high image quality over the whole field of view of 1.47°, covered by a hybrid SiPIN detector array of 2048 × 2048 pixels.
The channel has a focal length of 800 mm and dedicated refractive camera correct the FOV covered by the detector; the focal ratio is *f*/9.4 in order to be diffraction limited at 400 nm and to optimize radiometric flux and overall mechanical dimensions.
The combined reflective and refractive solution allows to reach a good balance between optical performances and optimization of resources, such as mass and volume.
The central obscuration, defined as the ratio between the secondary mirror diameter and the primary mirror diameter, is equal to 0.3: this low value guarantees to minimize the radiation losses due to the secondary mirror and to optimize the energy transfer from the telescope entrance pupil to the telescope exit pupil.
The refractive elements present a spherical curvature, in order to reduce the manufacturing costs; the diameter and the thickness has been minimized in order to reduce the light losses due to the absorption by the material. The distance between these elements has been determined by means of analysis with Zemax code, providing the optimization of the optical performance.
The following figure shows HRIC optical design.

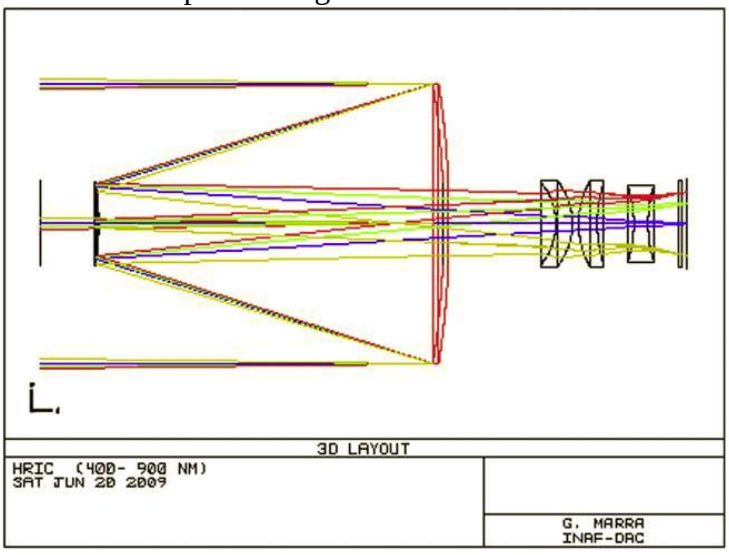

Fig. 2-14 HRIC optical layout with 3 lens corrector plus filter integrated onto the detector window

In order to evaluate the optical performances, the following parameters, represented in the graphs below, have been taken into account:

- Encircled Energy, which is the energy fraction enclosed in one pixel: maximum EE in the FOV is 68%.
- The image contrast, evaluated by means of the Modulation Transfer Function (MTF): minimum MTF in the FOV at Nyquist frequency is 33%.
- Aberration of the catadioptric systems, such as the field curvature and the distortion: at present, the maximum field curvature is 0.03 nm and the image maximum distortion is 0.16%.
- RMS spot radius on the image plane.

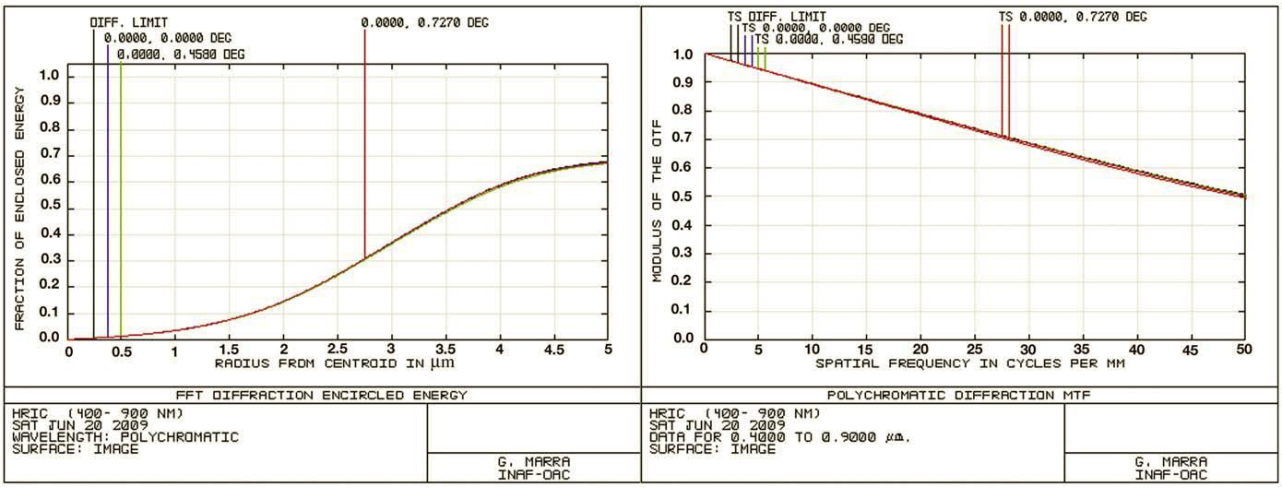

Fig. 2-15 Polychromatic diffraction EE curves (left) and diffraction MTF curves (right)

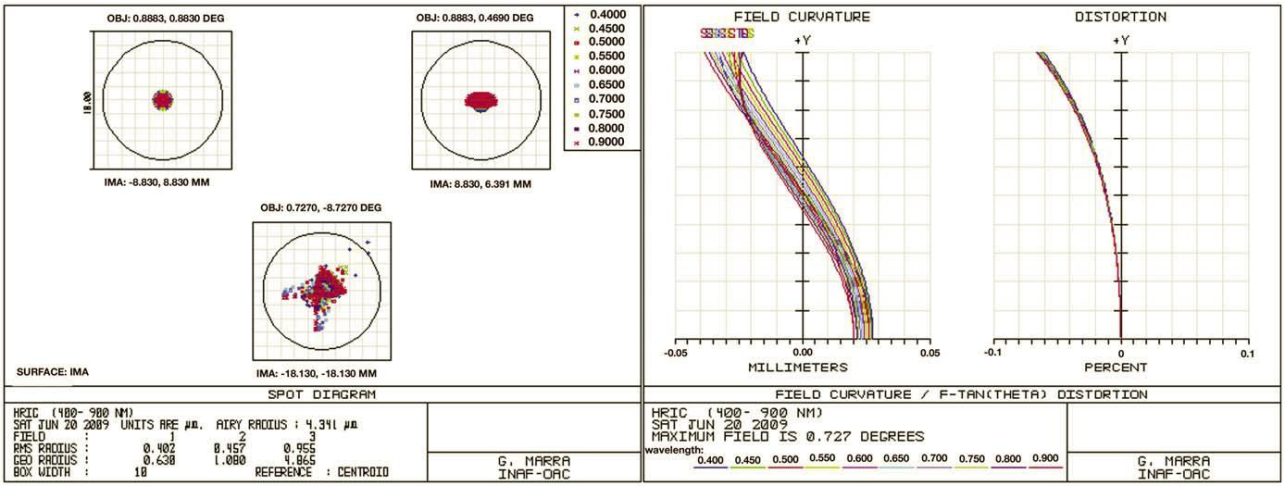

Fig. 2-16 Spot diagrams on the image plane (scale bar is 10 µm) on the left; field curvature and percent on the right

The following table summarizes the optical parameters.

Parameter	Unit	Value / Description	Remarks
Aperture	mm	85, diameter	130 including vanes
Focal length	mm	800	
Focal number		9.4	
λ for diffraction limit	nm	400	
Field of view	°	1.47	

Central obstruction	%	10	Area
Pixel IFOV	μrad	12.5	
Spectral range	nm	400 – 900	
Filter bandwidth	nm	40/50	For the 3 broad band/ panchromatic filter
Spectral channels	nm	Panchromatic 650; 550, 700, 880	Filters
Mirror material		Aluminum	Alternatives: SiC, zerodur
Diffraction EE in one pixel	%	68	worst case in the FOV
MTF @ Nyquist frequency	%	33 - 30	in field & out of field
Rms spot diameter	μm	1.6	edge of the FOV
Field curvature	nm	0.03	worst case in the FOV
Distortion	%	0.05	worst case in the FOV

Table 2-6 HRIC optical parameters

2.4.3 The sensor

The high pixel scale is performed by means of a 2048 × 2048 pixels SiPIN Complementary Metal Oxide Semiconductor (CMOS) sensor with a pixel size of 10 μm: this sensor is realized with 2 layers which are independently optimized and then stacked to form a single imager: the working principle of the SiPIN (Positive – Intrinsic – Negative) layer is based on the conversion of the incident light into electric charge; the CMOS layer is a multiplexer circuit able to measure the induced charge in each one of the photodiodes.
The following table shows the sensor characteristic data.

Parameter	**Unit**	**Value/description**
Sensor type	-	Si-PiN-Hybrid
Format	-	2048 × 2048
Pixel size	μm	10 × 10
Spectral range	nm	400 to 1000
QE × FF	%	> 42 for 400 to 800 nm > 24 for 800 to 900 nm > 10 for 900 to 950 nm
MTF	%	> 50 @ Nyquist freq.
Read noise @ 20°C	e^-	< 100
Dark signal @ 20°C	e^-/s	< 10000
DSNU	%	< 5 (rms)
Full well capacity	ke^-	120
PRNU	%	< 2 (rms)
Exposure time	ms	4
Read out	MPS	<5
Spurious charge	e^-/s	< 100
Non operating temperature	°C	-40 to 60

Operating temperature	°C	-5 to 20
Linearity	%	< ± 1
Power dissipation	W	< 0.1
FPN	mV	< 15
Defects	-	< 0.5%, no blemish of > 2 adjacent pixels
Radiation – total dose	-	70 krads(Si)
Radiation – SEE	MeV/mg/cm^2	SEL threshold > 70 SEU threshold > 70
CVF	µV/ e$^-$	~ 14
Photon flux	ph/pxl/s	- High flux case: 8·10^8 photons to 2·10^9 - Low flux case: 10^6 to 1·10^7

Table 2-7 Sensor data

2.4.4 Observation strategy

During the mission, HRIC will map about 20% of the planet's surface, operating on the illuminated side of Mercury. In order to maximize the ground pixel size, HRIC will acquire images at MPO orbit Periherm and in the second part of the mission, when almost all the global mapping will be performed. Data rate and data volume will change depending on the choice of targets and their size and position on the surface. Specific observations will be devoted to the calibration of the channel.

2.4.5 Performances

A radiometric model of HRIC has been developed in order to check the performances in the nominal operative conditions, taking into account both optical and sensor characteristic.
Signal-to-noise ratio trend is shown in the following figures as a function of the latitude: different curves have been obtained varying the albedo and the planet's orbital position around the Sun (Perihelion and Aphelion). The graph on the left refers on the S/N with the broad-band filter, the one on the right refers on the S/N with the panchromatic filter.

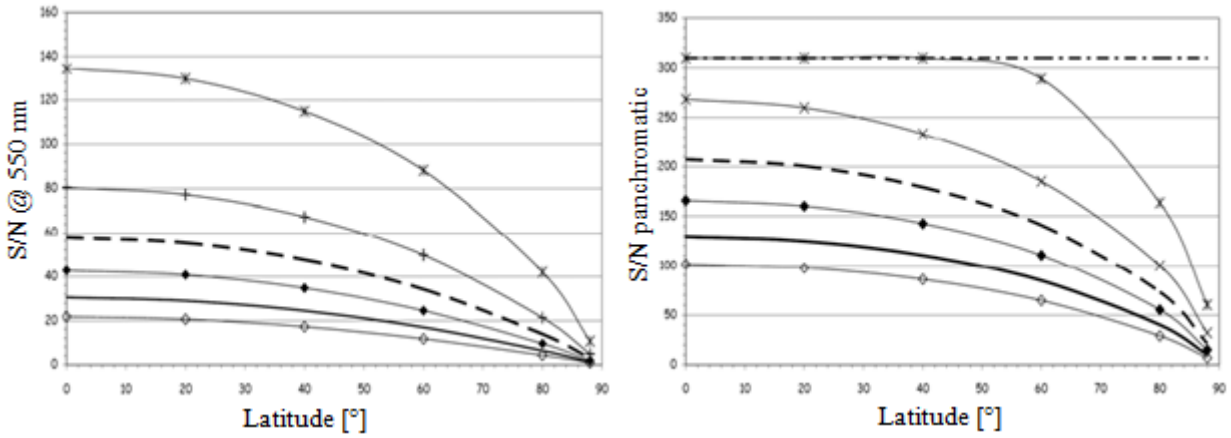

Fig. 2-17 Signal-to-noise ratio with 550/40 nm and panchromatic filter. Blank rhombi: albedo *A* = 0.08, Aphelion; black rhombi: albedo *A* = 0.08, Perihelion; crosses: albedo *A* = 0.45, Aphelion; stars: albedo *A* = 0.45, Perihelion; continuous line: *A* = 0.12, Aphelion; dotted line: *A* = 0.45, Perihelion; horizontal line: saturation level.

The coverage of the planet's surface is 100% with a ground pixel from 5 to 20 m at Apoherm; the coverage decreases to 97% with a ground pixel size from 5 to 11 m.

The graph below shows the spatial resolution (ground pixel size) trend as a function of the latitude, hence the altitude with respect to the planet's surface. The red curve refers to the Apoherm hemisphere, the blue one to the Periherm hemisphere. This plot, which has been obtained thanks to numerical simulations, is an useful instrument to select areas for the high spatial resolution imaging.

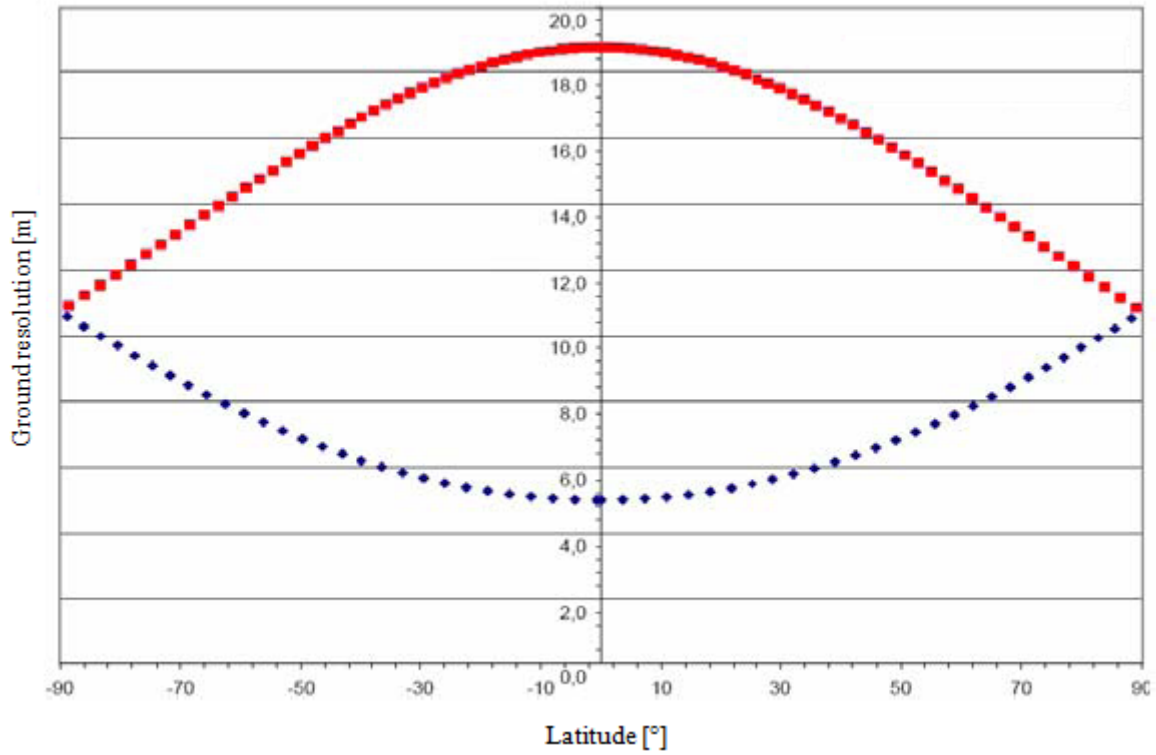

Fig. 2-18 Spatial resolution as a function of the latitude

2.5 STC: Stereo imaging Channel

2.5.1 Overall description

STC is a wide angle camera designed to image each portion of the Mercury surface from two different perspectives: it is composed by two channels with the orientation of +20° and -20° from the nadir direction and adopts a catadioptric optical design with common detector in order to save mass and power. STC provides panchromatic stereo image pairs in order to reconstruct the Digital Terrain Model (DTM) of the planet surface with 80 m vertical accuracy and colour images of selected areas. STC configuration takes into account 5 filters in 400-1000 nm spectral range: a broad-band filter for stereoscopic acquisition is centred at 700 nm with 250 nm FWHM; 4 filters for low-resolution spectral observations are centred at 420, 550, 700 and 920 nm.
The main objectives are hereafter summarized:

- Global and stereo mapping at moderate resolution and colour mapping of selected areas.
- Moderate resolution for stereo and colour imaging.

STC will allow to analyze key features of the planet surface, such as craters and volcanic edifices, and will provide the context for HRIC acquisitions.

The following figure explains the STC concept.

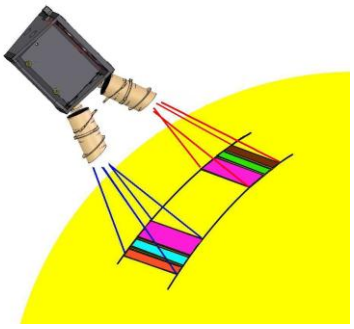

Fig. 2-19 STC concept

The following table shows the main resolution data.

Parameter	Unit	Value	Remarks
Spectral resolution	nm	N/A	Filers width 20 nm, but for panchromatic
Angular resolution	μrad/pixel	111	
Spatial resolution	m/pixel	50	@ 400km distance, @ 21.3° from nadir
Vertical accuracy	M	80	
Dwell time @ Periherm	Ms	20.3	
Dwell time @ Apoherm	Ms	166.2	

Table 2-8 Resolution data

2.5.2 Optical design

In order to reach a good balance between optical performances and optimization of resources, such as mass and volume, the camera is based on a catadioptric optical design in which the detector and most of the optical elements are shared by the 2 channels. The design has been chosen to satisfy the optical performance for all the filters in the whole FOV of each filter and it has been kept as short as possible, compatibly with the need of limiting the cross-talk and to cope with stray-light problems due to the common optical path.

The focal length of the system is 90 mm and allows to reach the 50 m/pixel scale factor at Periherm, adopting a 10 μm pixel size SiPIN CMOS as detector, useful in terms of radiation hardness and for the capability of snapshot image acquisition, allowing very short exposure times (~ 1 ms).

The global FOV of each channel is 5.3° × 4.5°, subdivided in 3 strips, one for each filter, covering 3 quasi-contiguous strip on Mercury surface: at Periherm on the equator each strip corresponds to an area of about 40 × 19 km^2 for the panchromatic filter, 40 × 3 km^2 for the colour ones.

The system consists on a modified Schmidt telescope preceded by a pairs of rhomboids prisms positioned in front of the objective: it redirects the ± 20° wide beams along direction much closer to the system optical axis (± 3.5°). The prisms can be made of either BK7G18 or Fused Silica radhard glasses. A correcting doublet is positioned after the prisms and replaces the classical Schmidt correcting plate, in order to reduce the telescope length by about a factor 2 respect to the classical configuration. This correcting doublet has a nearly null optical power: it mainly corrects the aberrations induced by the primary mirror.

The following picture shows the optical design layout, which has been simulated and optimized by means of the ray-tracing code Zemax.

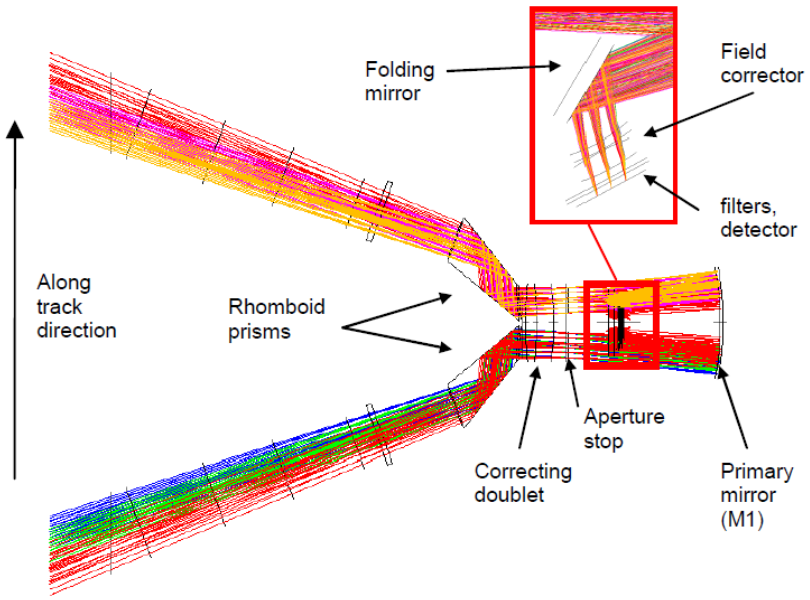

Fig. 2-20 STC optical design layout

The on-axis and lateral chromatic aberration affects the system, because of the extended wavelength range. The position of the aperture stop, which is placed in front of the focal plane of the primary mirror after the correcting doublet, has been chosen in order to obtain a good aberration balancing over the whole FOV and to guarantees the telecentricity of the design.
In order to compensate the field dependent aberrations, such as the field curvature and the lateral color, a two-lens field corrector in front of the detector has been designed.
In order to evaluate the optical performances, the following parameters, represented in the graphs below, have been taken into account:

- RMS spot radius on the image plane: the spots are within a 10 μm size square which represents the dimension of the pixel; a small lateral colour residual is present in one corner of the field, but it is less than 1/3 of a pixel, that is tolerable.
- Encircled Energy, which is of the order of 80% all over the FOV of each filter.
- The image contrast, evaluated by means of the Modulation Transfer Function (MTF): mean MTF in the FOV at Nyquist frequency of 50 cycle/mm is about 60-70%. Taking into account the sensor's MTF of 50-60%, the global MTF of the system is about 30%.
- Aberration of the catadioptric systems, such as the field curvature and the distortion: at present, thanks to the adopted Schmidt design, the image maximum distortion is 0.3% for all the filters.

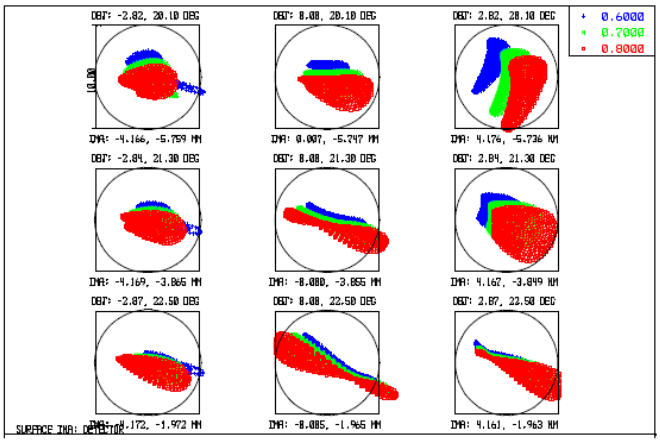

Fig. 2-21 Spot diagram for the panchromatic filter (on the left): spot at the center, corners and edges of the FOV are shown for 600, 700 and 800 nm wavelength in filter band (scale bar is 10 μm).

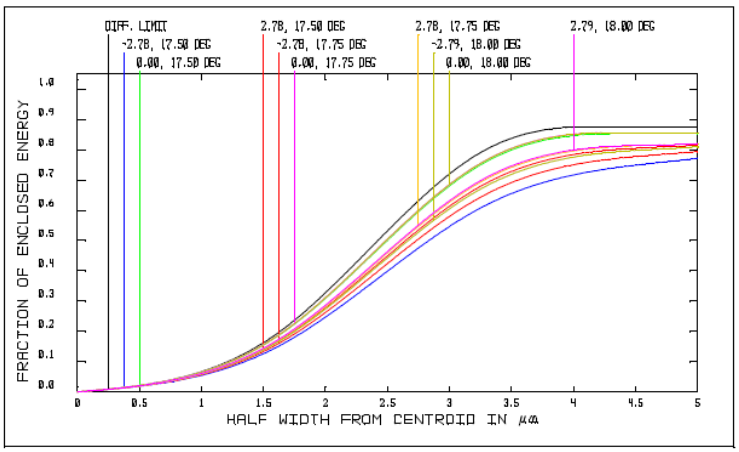

Fig. 2-22 EE for the panchromatic filter: different lines correspond to different points in the FOV (center, edges, corners).

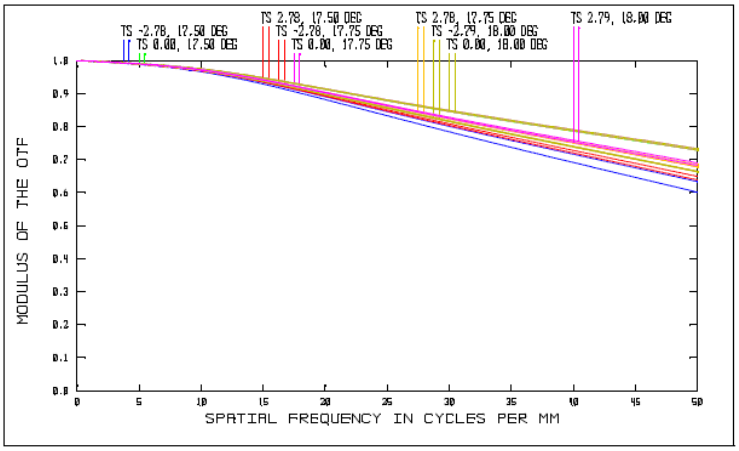

Fig. 2-23 MTF for the panchromatic filter: different lines correspond to different points in the FOV (center, edges, corners).

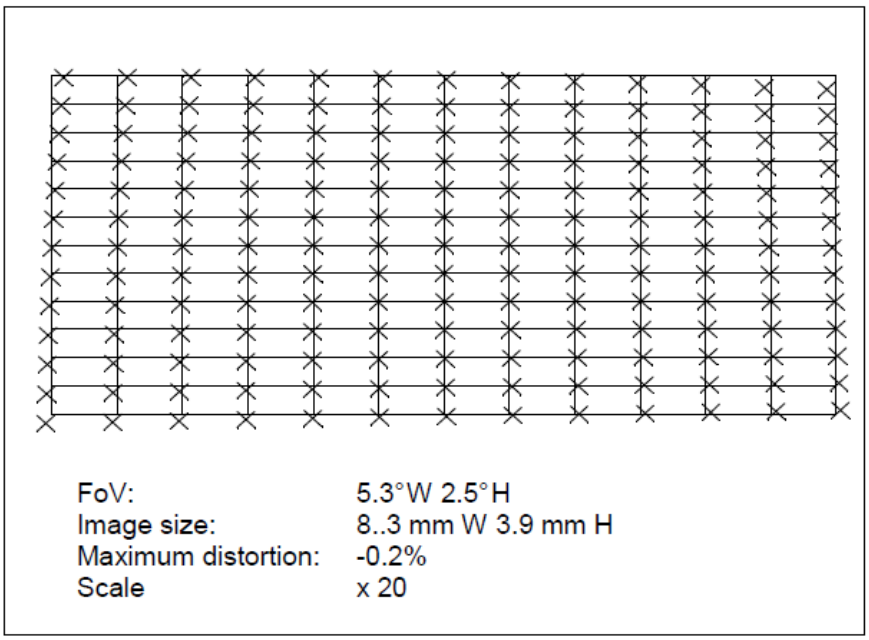

Fig. 2-24 Grid distortion for the panchromatic filter: the underlying grid is the predicted position of the chief rays, the crosses identify the position of the real chief rays; the difference in position has been multiplied by a factor 20.

The following table summarizes STC optical parameters.

Parameter	Unit	Value / Description	Remarks
Aperture	mm	24 × 24 mm	
Focal length	mm	90	
Focal number	-	6	
Field of view	°	5.3 × 4.5	
Pupil size	mm	15	
Central obstruction	%	0	
Pixel IFOV	μrad	111	
Spectral range	nm	410 – 930	
Filter bandwidth	nm	20/200	For the 3 broad band/ panchromatic filter
Spectral channels	nm	Panchromatic (700) + 420, 550, 750, 920	
Mirror material		BK7	
Mirror efficiency	%	> 80	
Mirror coating		Al + MgF_2	
Diffraction EE in one pixel	%	< 70	
MTF @ Nyquist frequency	%	> 60	
Distortion	%	< 1.6	Over all the FOV for each filter

Table 2-9 STC optical parameters

2.5.3 The sensor

As for HRIC, the detector is a 2048 × 2048 pixels SiPIN Complementary Metal Oxide Semiconductor (CMOS) sensor with a pixel size of 10 μm. The sensor's properties are those summarized in table Table 2-7.

2.5.4 Observation strategy

The main scientific objective of STC is to map the 100% of the surface for the generation of a global DTM; detailed stereo maps and colour images of selected targets will be then obtained.
The global stereo mapping will be completed in the first 6 month of the mission, eventually in the following 6 month: in this period the instrument will work continuously. During the following part of the mission it will work on predefined targets of interest.
In order to map in stereo mode the whole surface, STC shall work with both sub-channels. Since the sub-channels are independent, STC is extremely flexible as regards the operative scenarios: depending on the mission phase, STC will work with one or both sub-channels, using any filter combination, with different windows sizes on the filters areas and different compression ratios.
STC will be able to obtain colour mosaics of chosen regions with resolution better than VIHI and DTMs of interesting targets with a grid size of at least 2 pixels.

2.6 VIHI: Visual and Infrared Hyper-Spectral Imager

2.6.1 Overall description

VIHI will study Mercury surface's composition by sensing the photon flux reflected off the planet; it will work in the range of 400 to 2000 nm with a spectral resolution around few hundreds.
The detector is a single detector matrix (264 × 264 pixels) for both visible and infrared wavelengths. The spatial resolution will be better than 100 m at Periherm and the instrument FOV of 64 mrad cross-track allows to perform the global coverage of the planet surface within the first 6 month of the mission. The second half will be devoted to the detailed investigation of the selected locations at VIHI's maximum spatial and spectral resolution. The main objectives are hereafter summarized:

- To perform global hyperspectral imaging of the surface with a resolution better than 500 m in the spectral range 400 to 2100 nm and a spectral resolution of 6.65 nm/pixel.
- To perform 5 to 10% surface coverage with best spatial sampling capability (100 m) in the spectral range 400 to 2100 nm and a spectral resolution of 6.65 nm/pixel.

The following table shows the main resolution data.

Parameter	Unit	Value	Remarks
Spectral resolution	$\lambda/\Delta\lambda$	64 - 320	Filers width 20 nm, but for panchromatic
Angular resolution	μrad/pixel	250	
Spatial sampling	m/pixel	100/375	@ 400km and @ 1500 km
Dwell time @ Periherm	Sec	0.04	
Dwell time @ Apoherm	Sec	0.075	

Table 2-10 Resolution data

The channel design is based on a collecting telescope and a diffraction grating spectrometer ideally joined at the telescope focal plane, where the spectrometer slit is located. The image of the slit is dispersed by the grating on a 2-dimensional detector. In order to obtain a complete image, given by subsequent acquisitions, the S/C track speed has to be matched with the slit size projected on the ground (push broom mode): the final result is a 3 dimensional data set, which associate a spectrum to each pixel on ground.
The optical system (telescope and spectrometer) is placed in a single box interfaced to the STC channels, together with the calibration unit, the shutter (located at the spectrometer slit), the Focal Plane Assembly and the Proximity Electronics.
The shutter is constituted by a rotary solenoid holding a small metallic blade which covers the slit; it is essential to determine and remove the dark signal introduced by the detector and the background signal due to the spectrometer housing. Periodically, during acquisition of science data, it will be closed in order to perform a dark/background acquisition.
The internal calibration unit will be used to periodically verify degradations of the performances of the channel with respect to the absolute calibration performed on-ground.
The crucial part of the instrument is the Focal Plane Assembly, which contains the order sorting the filters on the closure window, the detector and a 2 stage thermo-electric cooler (Peltier cell), which will cool the detector to its operative temperature (< 220 K). The package shall be highly conductively linked to the spacecraft cold finger (210 to 260 K) in order to obtain the maximum heat dissipation; at the same time, it will be thermally decoupled with respect to the instrument structure (250 – 300 K), in order to minimize the parasitic heat to the Peltier.

2.6.2 Optical design

The instrument is based on a reflective telescope and a grating spectrometer in Littrow configuration; 2 dioptric doublets will correct the aberrations both in the telescope and spectrograph optical path. As for HRIC and STC, the design has been made as compact as possible in order to save mass and volume, without degrading the performance.
The telescope is based on a modified Schmidt design, with 25 mm aperture and 160 mm focal length. The following figure shows the optical layout.

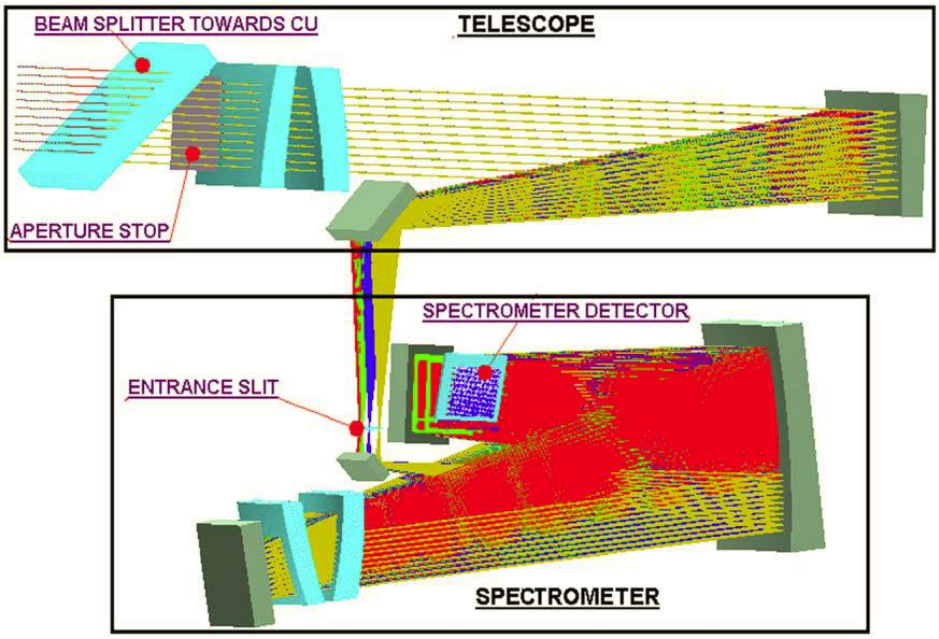

Fig. 2-25 VIHI optical layout: telescope and spectrometer

In all conditions, except at the extreme edge of the FOV and of the spectral range, the spot diagram is contained inside the pixel, as shown in the following figure.

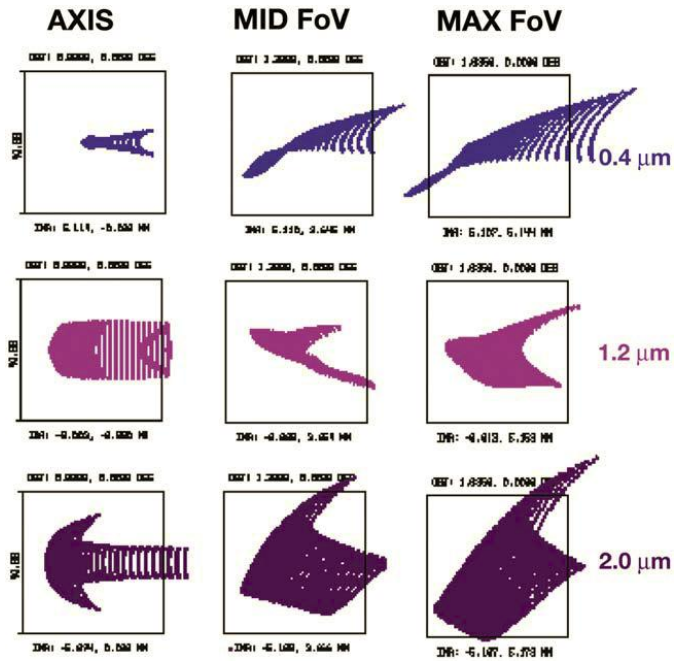

Fig. 2-26 Spot diagram of the VIHI spectrometer set for a point source at 3 wavelengths (0.4, 1.2, 2 µm) at the centre, middle and edge of field

The following table summarizes the optical properties:

Parameter	Unit	Value / Description	Remarks
Aperture	Mm	25	Diameter
Focal length	Mm	160	
Focal number	-	6.4	
Field of view	Mrad	64 × 0.25	
Central obstruction	%	0	
Pixel IFOV	Mrad	250	
Scale per pixel	m/pixel	100	@400 km
Spectral range	Nm	400 - 2000	
Spectral channels	-	256	
Spectral dispersion	Nm/pixel	6.25	

Table 2-11 VIHI optical parameters

2.6.3 The sensor

The Sensor Chip Assembly (SCA) is an array of 40 μm × 40 μm, 264 × 264 pixels SWIR HgCdTe photodiodes hybridized on a silicon ReadOut Intergrated Circuit (ROIC), which is a custom design of a standard CMOS process. The ROIC has the following characteristics:

- Low flux detection capability;
- Sequential readout of the pixels on one output;
- 3.3 V power supply;
- Linearity better than 0.4%;
- Storage charge around 2.3 Me^-;
- Operating temperature between 213 K and 273 K with testing capability up to ambient;
- Integration time from 115 μs to several minutes;
- Power consumption < 50 mW;
- 41 bits for programmable options, for adjusting biases current and testing capabilities.

SCA and Peltier cooler are hybridized inside an insulated package that contains an order sorting filter and a cold baffle. Hot side of the Peltier cooler is thermally connected to the spacecraft cold finger by means of a thermal strap.

Dimension of the detector package is around 50 × 10 × 30 mm^3 and the weight is about 150 g (without thermal strap). The module is shown in the following figure.

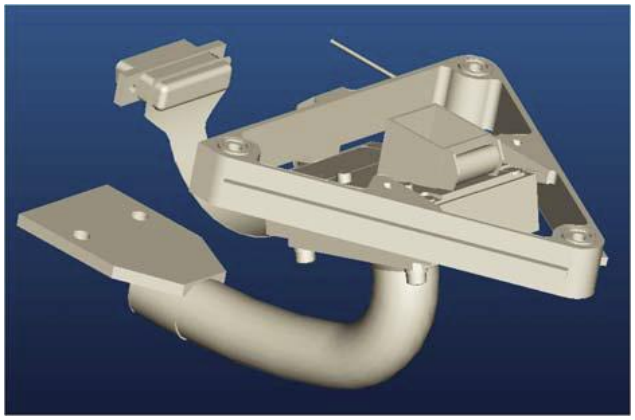

Fig. 2-27 SCA layout.

From the following graph, it can be seen that the quantum efficiency is higher than 70% over the useful band, from visible to short wave IR.

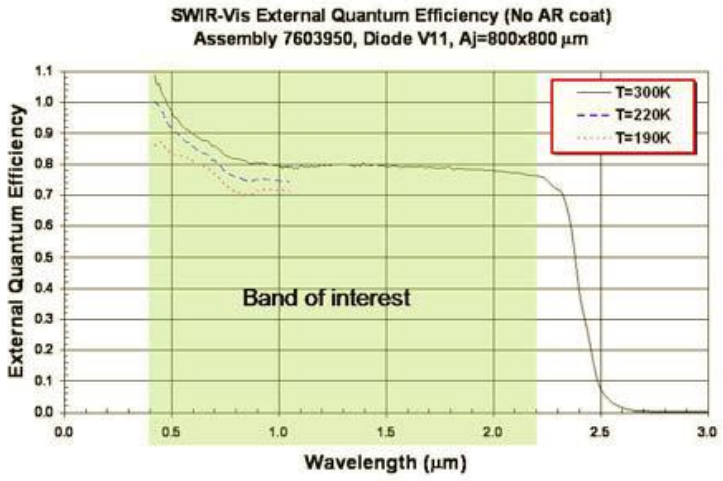

Fig. 2-28 QE of the detector as a function of the wavelength

Standard hybrid CMOS GgCd Te array detectors cannot guarantee the scientific objectives (spectral range of interest between 400 and 2000 nm) since they present a short-wave-cut-off at 800 nm, due to the CdZnTe substrate which becomes opaque to radiation below 800 nm. A special technique has been implemented in order to remove the substrate and substitute it with a transparent material, allowing to use a single detector to cover both visible and IR range.
The following graph summarizes the sensor performances.

Parameter	Unit	Value/Description	Remarks
Sensor type	-	Hybrid HgCdTe	HgCdTe on visible transparent substrate with TEC
Pixel lines	#	264	Only 256 × 256 are used for scientific coverage
Pixel per line	#	264	
Pixel pitch	µm	40	
Dark current	Me^-/s	10	
Wavelength range	µm	0.4 – 2.2	
Peak quantum efficiency	%	> 50	
Read noise	e^-	< 600	
Full well capacity	e^-	> 2×10^6	ROIC with CTIA input circuit, snapshot mode, Integrate While Read
Readout rate	Mpix/s	> 4	
Power dissipation	mW	< 100	
Operability	%	> 96	QE, dark current, read noise capacity and well capacity
Order suppression filters	#	yes	
Operating temperature	°C	≤ -50	
Exposure time	ms	10	Minimum value @ Periherm

Table 2-12 Sensor data

2.6.4 Observation strategy

During the global mapping phase, VIHI will operate continuously along the sunlight side of the orbit, changing operational parameters at given orbital positions according to the observing condition. The observation will be limited to an illumination angle of 45°, which coincides with the true anomaly (polar orbit), allowing a global coverage of the planet within 6 months.
During the following high resolution coverage of selected regions, the spectrometer will be used in flexible way, changing the measurements parameters according to the scientific objective and the chosen target.

2.7 The SIMBIO-SYS baffles

A crucial point in the performance optimization of the space telescopes consists in limiting the stray-light radiation, due to the reflection of the radiation incoming from the external environment by the surfaces which precede the detector and present a proper surface roughness.
Baffles systems allow to shield the detector, by absorbing or rejecting the disturbance radiation towards the sky background.
For instance, a simple radiometer is shown in the following figure, in which the radiometer is represented by a lens and a detector. The incoming radiation, if reflected by the internal surfaces, might reach the detector, saturating the sensor itself. In order to avoid the disturbance effect due to the undesirable stray radiation on the sensor, baffles vanes can be adopted in order to trap or reject the radiation.

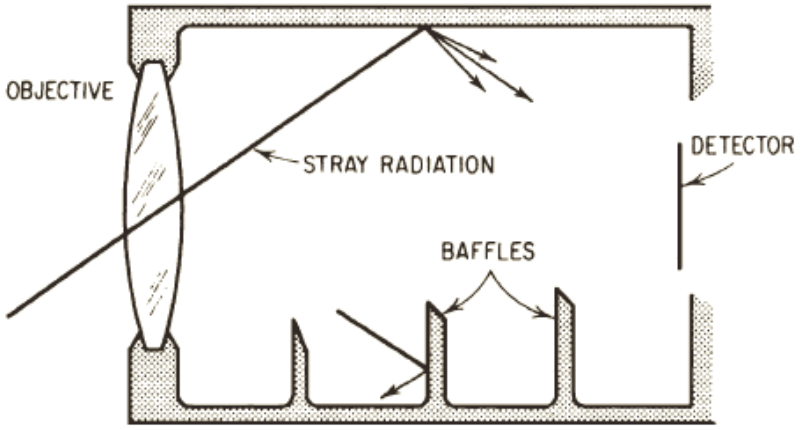

Fig. 2-29 In the upper part of the figure, the stray radiation incoming from a off-axis light source is reflected by the internal surface of the optical system and degrades the optical performance; in the bottom part, baffles vanes trap the radiation

SIMBIO-SYS suite is equipped with 4 baffles, one for each optical channel: these devices play a key role in the thermal-mechanical stability, considering the extremely harsh thermal environment. They are placed on a baffle bracket plate normal to the S/C optical bench and thermally decoupled with respect to the following cameras.

- HRIC baffle is based on the Stavroudis configuration, which consists in a series of highly internally reflective hyperbolas and elliptical surfaces. The foci of these conic surfaces are placed on the entrance section of the baffle and the surfaces are obtained by the revolution of the curves around the baffle's axis. The following figure shows the longitudinal section of a Stavroudis baffle.

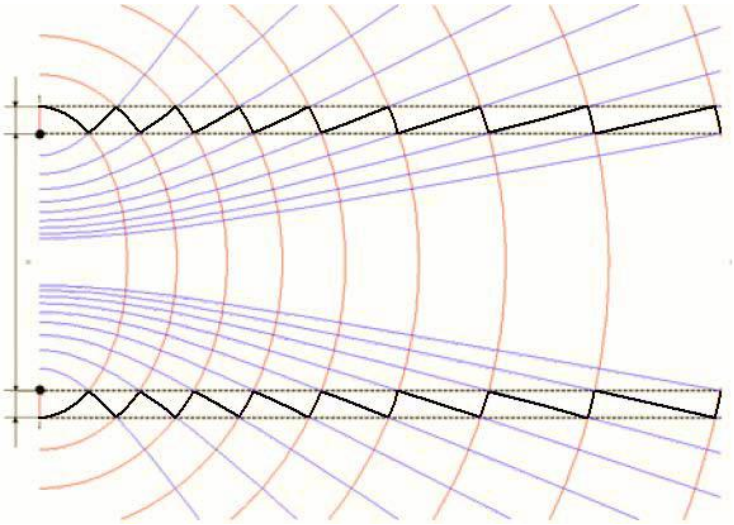

Fig. 2-30 Stavroudis baffle concept: red curves represent the ellipses, the blue curves the hyperbolas; the black outline is the baffle profile. On the left the foci, which are common to all the conics, are visible.

Thanks to the special design, the Stavroudis baffle can reject any incident off-axis ray by means of 2 reflections maximum, if the ray is contained in the meridian plane (which contains the baffle axis), 3 reflections with skew rays: any meridian ray which hits ellipsoid surfaces is rejected towards the entrance section, any ray which hits hyperbolas surface is then deviated towards the next ellipsoid surfaces, which redirect the radiation towards the entrance section.
The following figure represents the HRIC Stavroudis baffle, which is internally highly reflective: 6 ellipsoids and 5 hyperboloids are visible, together with a titanium external ring (thermally decoupled with respect the first conic surface) and 2 titanium shields which cover the external surfaces of the baffle. An additional ring before the first conic surface and connected to the first ellipsoid is present, but not visible in the figure.

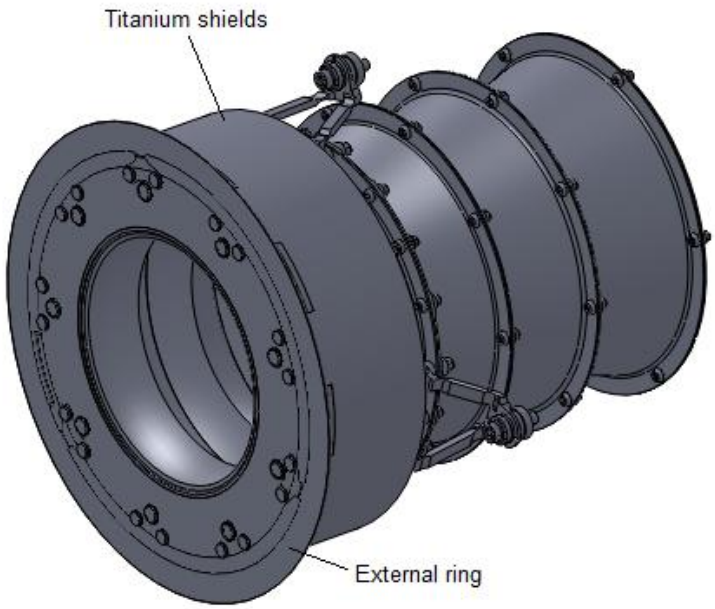

Fig. 2-31 HRIC Stavroudis baffle

Stavroudis baffle represents a passive thermal control system, since it reflects the incident IR radiation misaligned with respect to the optical axis towards the sky-background, preventing it to reach the filter and the sensor. At the same time, since it rejects the off-axis

solar radiation, it allows to reach high optical performance. The thermal contact between the baffle and the baffle bracket is very poor.

- STC and VIHI baffles are internally black and equipped with a series of internal vanes. They guarantee high optical performances, since they absorb the incident disturbance radiation, avoiding it to reach the following cameras.
  The figure below represents STC (on the left) and VIHI (on the right) baffles.

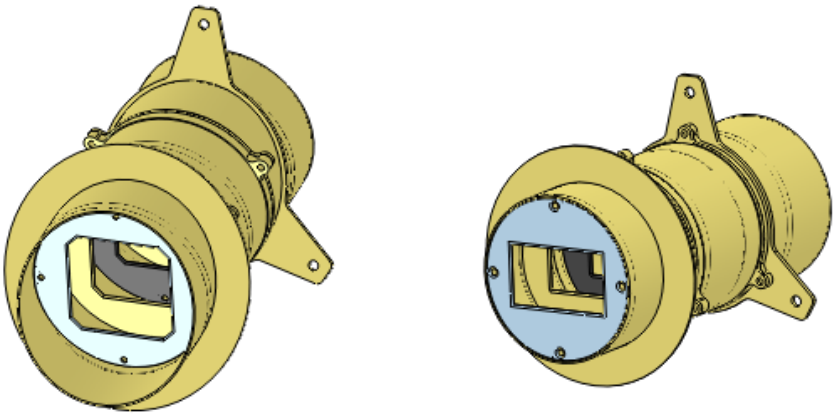

Fig. 2-32 STC (left) and VIHI (right) baffles

3. The thermal scenario

3.1 Heat exchanges in space

The main thermal balance analytical equations are explained in this section, in order to introduce the issues which have been experienced before and during the thermal tests campaign on SIMBIO-SYS baffles. These relations can be applied to any object orbiting around a celestial body of the Solar System and are implemented by any numerical thermal code used for the prevision of orbiting systems thermal behavior and subsequent thermal tests and verification.
The possible thermal interactions and modes of heat transfer which take place in orbital environment are hereafter summarized:

- Thermal exchange by conduction: it takes place when either a temperature gradient appears inside a body or at least two bodies at different temperature are in physical contact, without fluid motion. For instance, the conduction laws are used to calculate the thermal resistance (or the conductance) between real components or between consecutive nodes inside thermal models.
- Thermal exchange by radiation, which takes place also in vacuum environment, since it is based on the spontaneous energy emission which characterizes all bodies. The intensity of such energy flux depends on the temperature of the body and the nature of its surface. Since the energy is strictly related to the temperature, the heat transfer by radiation can be predominant at high temperatures, if compared with the heat transfer by conduction. In orbital environment, the radiation laws are applied in order to determine the thermal flux incoming from the Sun and the planet (planetary IR flux and albedo flux) onto the spacecraft and the thermal flux which the spacecraft dissipates towards the sky back-ground at 4 K – temperature. Basing on the calculated incident fluxes on the spacecraft, different experimental test-beds have been designed and developed in order to simulate the thermal environment in which SIMBIO-SYS suite will operate.

The thermal exchange by convection is absent in space-like environment, therefore it has been neglected, since it takes place when two bodies at different temperature are in physical contact and at least one of them is fluid (liquid, gaseous or bi-phase).

3.1.1 Heat transfer by conduction

As previously stated, conduction takes place when a thermal gradient between two areas is present inside a solid, liquid or gaseous body, in absence of fluid motion. Isothermal surfaces can be identified inside the body and can be defined as the locus of points at the same temperature: these surfaces never intersect each other and are time-variant.
The conduction mathematical model is applied on continuous, homogenous, isotropic and steady state (the chemical and physical properties are stable in time) bodies and derives from simple empiric observations: considering two points lying on 2 different and infinitely close isothermal surfaces, the heat transfer by conduction increases with the thermal gradient and the contact area, decreases with the distance between the two points.
The conduction mathematical model is based on the Fourier's law, which is shown below:

$$dq_n = -\lambda dA \frac{dT}{dn} \tag{3.1}$$

where:

- dq_n is the thermal flux along the direction normal to the isothermal surfaces;

- λ is the thermal conductivity and has the dimensions W/(mK);
- *dA* è is the infinitesimal contact area;
- *dT* is the infinitesimal thermal difference;
- *dn* is the infinitesimal distance between the 2 points.

Fourier's law can be verified applying the first law of the thermodynamics on a infinitesimal volume inside the considered body.

$$\sum dQ = dU_T + dL \tag{3.2}$$

where dQ is the exchanged heat, dU_T the total energy and dL the infinitesimal work, which is negligible since the particles of the body are fixed.
Some useful assumptions and hypothesis are reported below:

- The total energy can be written as the sum of the internal energy dU_i and internally-generated energy dU_g (related to the processes which generate internally-generated heat, such as chemical, nuclear and electrical reactions).

$$dU_T = dU_i + dU_g \tag{3.3}$$

- The internal energy is defined as:

$$dU_i = dm \cdot dT \cdot c \tag{3.4}$$

  where *dm* is the mass of the infinitesimal volume and *dT* is the difference in temperature, *c* is the specific heat (constant volume).
- dU_g is considered negligible.
- Temperature is stable and doesn't change as a function of the time; furthermore its distribution is mono-dimensional.

The final relation provides the conduction thermal flux exchanged between two bidimensional surfaces at different temperature T_A e T_B, at *s* distance.

$$q = \frac{\lambda A}{s}(T_A - T_B) \tag{3.5}$$

The quantity $\frac{\lambda A}{s}$ is the thermal conductance (also called *GL* in the chapters which follow) and the reciprocal is the thermal resistivity.
Given a number *i* of adjacent two-dimensional layers with different thermal resistance, the total thermal resistance is obtained as the sum of the layers' thermal resistance.

$$q = \frac{T_n - T_1}{\sum_{i=1}^{n} \frac{s_i}{\lambda_i A_i}} \tag{3.6}$$

3.1.2 Heat transfer by thermal radiation

All bodies constantly emit and absorb energy by a process of electromagnetic radiation. The intensity of the radiation depends on the temperature of the body and the optical properties of the surface. The electromagnetic radiation is characterized by the wavelength λ, which is related to the frequency *f* by the following relation:

$$c = \lambda \cdot f \tag{3.7}$$

where c is the speed of the radiation inside a mean with refraction index n (which is a function of the wavelength). In vacuum the speed of the radiation c_0 is not a function of the wavelength and it is equal to:

$$c_0 = 2.9979 \cdot 10^8 \quad m/s \tag{3.8}$$

The ratio between the speed of the radiation in vacuum and inside a dielectric body with refraction index n is given by the following relation:

$$c = \frac{c_0}{n} \tag{3.9}$$

Supposing that a radiant heat flux falls upon a surface, a fraction α of the total incident energy , called the absorptance, is absorbed by the body; a fraction ρ, called the reflectance, is reflected by the surface, and a fraction τ, called the transmittance, passes through. q_I, q_R, q_A e q_T are the incident, reflected, absorbed and transmitted heat fluxes respectively.

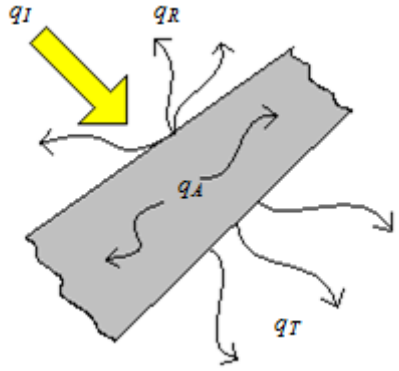

Fig. 3-1 Possible interaction between an incident radiation and a body

α, τ and ρ are defined in the following relations and are a function of the wavelength λ and the incident angle φ:

$$\rho_{\lambda\varphi} = \frac{q_R}{q_I} \tag{3.10}$$

$$\tau_{\lambda\varphi} = \frac{q_T}{q_I} \tag{3.11}$$

$$\alpha_{\lambda\varphi} = \frac{q_A}{q_I} \tag{3.12}$$

These coefficients vary between 0 and 1 and the following relation is verified:

$$\alpha_{\lambda\varphi} + \rho_{\lambda\varphi} + \tau_{\lambda\varphi} = 1 \tag{3.13}$$

The model for the perfect thermal radiator is so-called black body: it absorbs all energy that reaches it and reflects nothing. Therefore, black bodies present the following coefficients:

$$\rho_{\lambda\varphi} = 0, \quad \tau_{\lambda\varphi} = 0, \quad \alpha_{\lambda\varphi} = 1, \quad \forall \lambda, \varphi \tag{3.14}$$

Thus the radiation irradiated by a real body can always been expressed as a fraction of the radiation irradiated by a black body (Kirchhoff law).
The flux of energy radiating from a body is commonly called *e(T)* [W/m^2]. The symbol $e_\lambda(\lambda,T)$ is the distribution function of radiative flux in λ, or the monochromatic emissive power:

$$e_\lambda(\lambda,T) = \frac{de(\lambda,T)}{d\lambda} \Rightarrow e(\lambda,T) = \int_0^\lambda e_\lambda(\lambda,T)d\lambda \tag{3.15}$$

$$e(T) = E(\infty,T) = \int_0^\infty e_\lambda(\lambda,T)d\lambda \tag{3.16}$$

It can be demonstrated that the flux of energy radiating from a black body is given by the Stefan-Boltzmann law:

$$e(T) = \sigma T^4 \tag{3.17}$$

where the Stefan-Boltzmann constant σ is 5.67 × 10^{-8} W/(m^{2}K^4) and *T* is the absolute temperature.
At a given temperature, a body will emit a unique distribution of energy in wavelength; the energy spectrum of the black body has been accurately measured: the results is reported in the following figure, where the locus of maxima of the curves is also plotted, obeying the Wien's law.

$$(\lambda T)_{e_{\lambda=\max}} = 2898 \ \mu\text{m}\cdot\text{K} \tag{3.18}$$

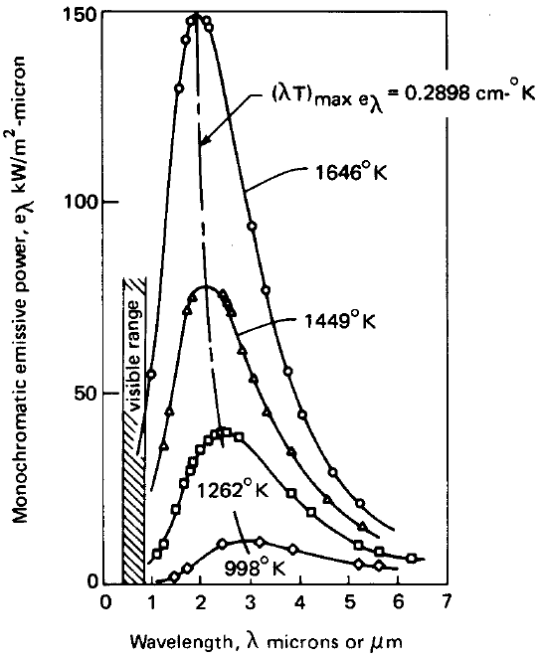

Fig. 3-2 Monochromatic emissive power of a black body at several temperatures – predicted and observed

It can been experienced that the monochromatic emissive power of a black body with a radiation at constant wavelength increases with the temperature. Furthermore, the locus of maxima leans toward lower wavelength values at higher temperatures.
The mathematical model of the black body behavior (shown in the plot above) has been predicted by Max Planck. Planck's law is shown below:

$$e_{\lambda_b} = \frac{2\pi h c_0}{\lambda^5 \left(e^{\frac{h c_0}{k_B T \lambda}} - 1 \right)} \tag{3.19}$$

where c_0 is the speed of the light, h is Planck's constant ($6.626 \cdot 10^{-34}$ J·s) and k_B is Boltzmann's constant ($1.38 \cdot 10^{-23}$ J/K).
As previously stated, the radiation irradiated by a real body can always been expressed as a fraction of the radiation irradiated by a black body (Kirchhoff law): the ratio between the monochromatic emissive power of a real body and the monochromatic emissive power of the black body at the same temperature is the so called emissivity.

$$\varepsilon_{\lambda\varphi} = \left[\frac{e_\lambda}{(e_\lambda)_b} \right]_T \tag{3.20}$$

It can be demonstrated that the emissivity coincides with the absorptance coefficient.

$$\varepsilon_{\lambda\varphi} = \alpha_{\lambda\varphi} \tag{3.21}$$

Finally, considering the monochromatic emissive power definition and the Stefan – Boltzmann's law, the thermal flux q which is emitted by a black surface A at temperature T_1 and absorbed by a black surface B at temperature T_2 is:

$$q = \sigma A \left(T_1^4 - T_2^4 \right) F_{A \to B} \tag{3.22}$$

$F_{A \to B}$ is the so called view factor and represents the fraction of energy emitted by the object A that is intercepted by the object B. It can be demonstrated that $A_A \cdot F_{A \to B}$ is equal to $A_B \cdot F_{B \to A}$, where A_A and A_B the areas of the considered surfaces.
Considering two lambertian surfaces,

$$F_{A \to B} = \frac{1}{\pi A_A} \int_A \int_B \frac{\cos\varphi_1 \cos\varphi_2}{d^2} dA_A dA_B \tag{3.23}$$

where φ_1 and φ_2 are the angles between the direction normal to the surfaces and the propagation direction, d is the distance between the surfaces.
Considering two real lambertian surfaces, in other words introducing the emissivity, the heat flux becomes:

$$q = \sigma \varepsilon A \left(T_1^4 - T_2^4 \right) F_{A \to B} \tag{3.24}$$

3.2 Orbital thermal scenario

In this paragraph the thermal scenario for a spacecraft around Mercury is described and the relations which define the thermal fluxes which are absorbed and emitted by the spacecraft are reported.
The exchanged thermal flux are listed and described below:

- Thermal input due to the solar radiation, highly dependent on the cyclic solar activity and on the position of the body with respect to the sun.

- Thermal input due to the albedo radiation, which is the fraction of the solar radiation that is reflected by the planet's surface and is highly dependent on the surface's optical properties.
- Thermal input due to the planetary radiation, which depends on the temperature of the planet's surface and the mutual position of the spacecraft and the planet.
- Thermal output towards the sky – background at 3-4 K temperature.

The temperature of the spacecraft results from a balance between thermal inputs (which cause an increase of the temperature) and thermal outputs (which cause a drop of the temperature). The thermal balance in steady state conditions is given by the following relation, which contains the terms described above:

$$q_{SUN} + q_{ALBEDO} + q_{PLANET} + q_{SKY} = 0 \tag{3.25}$$

Modern thermal analysis softwares, such ESATAN – TMS, after the geometry realization and meshing and the orbital parameters definition, apply this relation to each element and give as an output the exchanged thermal fluxes and the nodal temperatures (in steady state conditions).
The relation above represents the thermal balance in steady state condition, taking into account the only contribution due to the radiation. In fact the thermal regime is determined also by the conductive link between adjacent components or elements: supposing to mesh a component into infinitesimal elements, the heat exchanged between two adjacent elements *i* and *j*, due to the conduction, is given by the following relation:

$$dq_{cond,i} = -\lambda \cdot dA_i \frac{T_i - T_j}{s} \tag{3.26}$$

where λ is the thermal conductivity of the material, s is the distance between the element centers of mass, T_i and T_j are the temperature of the adjacent nodes, dA_i is the contact area between elements.
The thermal balance in steady state condition which takes into account both radiative and conductive contribution is:

$$q_{SUN} + q_{ALBEDO} + q_{PLANET} + q_{SKY} + \sum_i dq_{cond,i} = 0 \tag{3.27}$$

Finally, transient analysis is performed considering an additional term, which represents the internal energy variation as a function of time. The thermal balance equation in transient condition is:

$$q_{SUN} + q_{ALBEDO} + q_{PLANET} + q_{SKY} + \sum_i dq_{cond,i} = m \cdot c \cdot \frac{dT}{d\tau} \tag{3.28}$$

The term on the right represents the variation of the internal energy due to the thermal evolution: m is the mass of the system, c is the specific heat, $d\tau$ is the time lapse and dT the temperature variation in the elapsed time.

3.2.1 Solar radiation

The electromagnetic radiation incoming from the Sun is a function of the solar activity. The Sun photosphere is the region from which energy is radiated to space, whereas the chromospheres, which extends for a few thousand km above the photosphere and the corona, emit electromagnetic radiation in the UV, EUV and X – ray spectral ranges.

The direct solar flux, also called solar irradiance, is inversely proportional to the square of the distance to the Sun. The integrated irradiance over all wavelengths at 1 AU distance is called solar constant (SC) and its mean value is:

$$SC = 1366.1 \quad W \cdot m^{-2} \tag{3.29}$$

The standard deviation of this mean value is 425 ppm, with a 0.37% minimum-maximum range (1363-1368 W·m^{-2}).
Thermal analysis of terrestrial orbiting spacecraft are computed assuming a maximum value for the solar constant of 1370 W·m^{-2}, in order to take into account the maximum solar activity and to obtain the worst hot case. For a spacecraft orbiting around Mercury, considering the variation of the Mercury-to-Sun distance and the mean value of the solar constant, the irradiance goes from a minimum of 6272 W·m^{-2} (minimum solar irradiance at Aphelion) to a maximum of 14448 W·m^{-2} (maximum solar irradiance at Perihelion).
The following figure shows the solar irradiance variation at 1AU: it can be noticed that the trend is cyclic and depends on the solar activity.

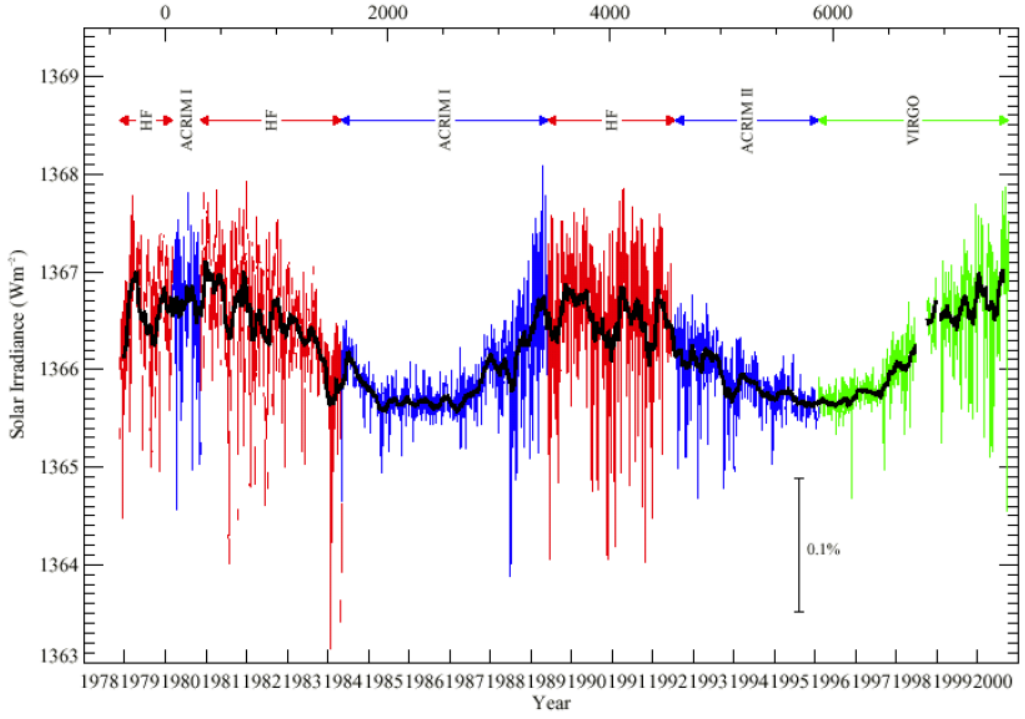

Fig. 3-3 Solar irradiance variation at 1 AU

Since the solar rays at Mercury are not parallel, the solar disc subtended angle at Mercury varies from 1.14 ° at Aphelion to 1.73° at Perihelion. Therefore, because of the finite size of the Sun, surfaces aligned with the direction of the Sun receive a non-zero heat input, which varies form13.5 W·m^{-2} at Aphelion to 47 W·m^{-2} at Perihelion.
The following table shows the maximum solar irradiance, computed basing on a solar irradiance of 1370 W·m^{-2} at 1 AU, as a function of the planet's orbital position (true anomaly).

v **[°]**	***d*** **[AU]**	**Irradiance [W·m^{-2}]**	**t [days]**
0	0.3075	14489	0.00
10	0.3083	14414	1.58
20	0.3107	14192	3.17
30	0.3147	13833	4.80

40	0.3203	13354	6.48
50	0.3275	12773	8.23
60	0.3362	12121	10.06
70	0.3464	11417	12.00
80	0.3580	10689	14.06
90	0.3707	9970	16.28
100	0.3845	9267	18.65
110	0.3988	8614	21.21
120	0.4132	8024	23.95
130	0.4272	7507	26.90
140	0.4401	7073	30.03
150	0.4511	6732	33.34
160	0.4595	6489	36.80
170	0.4649	6339	40.37
180	0.4667	6290	43.99

Table 3-1 Computed solar irradiance as a function of Mercury's true anomaly

The average solar irradiance is equal to 9342 $W \cdot m^{-2}$.
The solar spectrum can be approximated by a black body emission curve, according to the Planck's curve, with a characteristic black-body temperature of 5776 K.
The following figure shows the solar irradiance spectrum between 0.2 and 2.4 μm wavelength (blue line); the grey line represents the black – body spectrum at 5776 K. It can be noticed that the solar electromagnetic radiation includes infrared, visible, ultraviolet and soft X – ray radiation, with most of energy falling within the visible part of the spectrum.

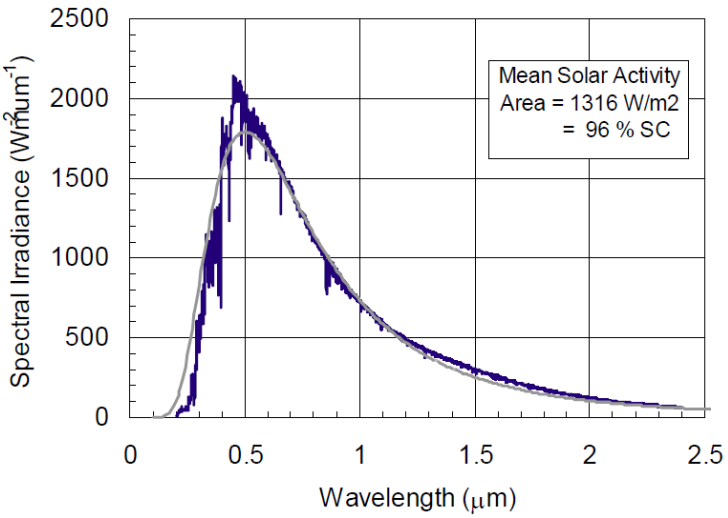

Fig. 3-4 Solar irradiance spectrum between 0.2 and 2.4 μm wavelength

As previously stated, the spacecraft's surfaces receive a highly variable solar radiation. The first reason is the cyclic variation of the solar activity; furthermore the solar aspect angle, which is the angle between the solar radiation and the perpendicular direction to the surfaces of the spacecraft, changes continuously, causing a variation of the view factor. Supposing to subdivide the spacecraft into *n* surface elements, in order to compute the solar flux incident on each surface, the view factors have to be determined with the following relation:

$$F_{i\to SUN} = \frac{1}{\pi A_i} \int_A \int_B \frac{\cos\varphi_i \cos\varphi_{SUN}}{d^2} dA_i dA_{SUN} \tag{3.30}$$

The following figure shows the parameters which are used in the previous relation: A_i is the area of the surface element i, A_{SUN} represents the solar surface.

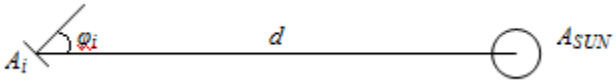

Fig. 3-5 Representation of an element *i* belonging to the spacecraft surface, of the Sun and of all parameters which are necessary for the view factor computation

Considering the Sun as a black body (hence a lambertian body), the solar surface can be replaced with the solar disc normal to the element-to-Sun direction. Furthermore, supposing that the Sun and the body are far enough, the angle φ_i is equal to zero.
Thanks to these simplifying assumptions, the view factor can be analytically determined. The method which is implemented by commercial softwares (such as ESATAN – TMS) for the computation of the view factors is based on ray-tracing techniques.
The solar input q_{SUN} can be finally calculated with the following equation:

$$q_{SUN} = \sigma A_i \left(T_{SUN}^4 - T_i^4\right) F_{i \to SUN} \cdot \alpha_{0.5\mu m} \tag{3.31}$$

$\alpha_{0.5\mu m}$ is the absorptance coefficient of the spacecraft surfaces at 0.5 μm wavelength. Usually the temperature of the Sun T_{SUN} is assumed to be equal to 5600 K. Since q_{SUN} along the orbit is known, the temperature of each surface element T_i can be immediately determined.
The following figure shows the solar incident flux on MPO nadir surface, which host SIMBIO-SYS instrumentation, when the planet is at Perihelion. The different curves refer to the fluxes computed on the nominal orbit, one year after and 2 years after, assuming a median value of the J_2-term. The radiation peaks occur entering and exiting into and from the eclipses respectively; in addition the peaks intensity decreases after one and two years from the beginning of the operations, because of the argument of Periherm's drift.

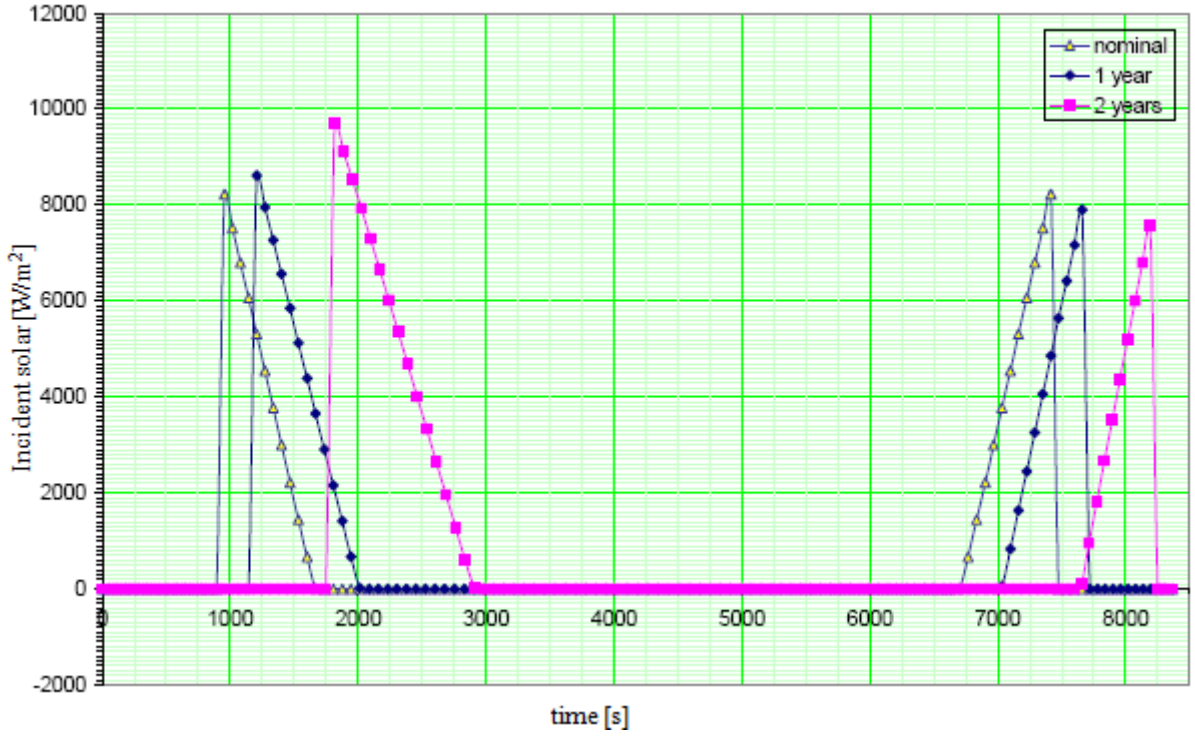

Fig. 3-6 Incident solar fluxes on the nadir surface orbiting the MPO orbit at Mercury Perihelion; time zero corresponds to the Periherm.

3.2.2 Planet albedo radiation

The bond albedo is the fraction of incident solar energy which is reflected back into space by a spherical body. Part of this reflected radiation arrives on the spacecraft surfaces and constitutes a thermal input. To a first approximation, the planet can be considered a lambertian body: therefore the radiation is reflected back into space in all directions.
The albedo radiation can be assumed to have the same spectrum as the solar radiation, therefore the maximum of the spectrum corresponds to 0.5 μm (visible wavelengths); in fact, the actual albedo radiation spectrum can change depending on the properties of the surface, since different materials can lead to absorption in certain wavelength bands.
The fraction of the solar radiation which is reflected is:

$$q_{refl} = \rho_{0.5\mu m} A_{S,PLANET} \cdot q_{SUN} \tag{3.32}$$

Where $\rho_{0.5\mu m}$ (or a) is the bond albedo coefficient at 0.5 μm and $A_{S,PLANET}$ is the planet's illuminated surface.
As for the solar flux, the fraction of the radiation which is effectively intercepted by the spacecraft's surfaces requires the view factors' computation to be determined: these parameters can be calculated either analytically (meshing the planet's and the spacecraft's surfaces) or by means of ray-tracing methods. Finally, the albedo flux q_{ALBEDO} is:

$$q_{ALBEDO} = q_{rifl} \cdot F_{S,PLANET \to i} \cdot \alpha_{0.5\mu m} = \rho_{0.5\mu m} A_{S,PLANET} \cdot q_{SUN} \cdot F_{S,PLANET \to i} \cdot \alpha_{0.5\mu m} \tag{3.33}$$

$$q_{ALBEDO} = \rho_{0.5\mu m} A_i \cdot q_{SUN} \cdot F_{i \to S,PLANET} \cdot \alpha_{0.5\mu m} \tag{3.34}$$

Usually, for thermal analyses of orbiting elements around Mercury, a nominal albedo coefficient of 0.12 can be assumed.

3.2.3 Planet Infrared Radiation

The fraction of the solar radiation which is not reflected by the planet's surface is absorbed by the planet itself and then re-emitted as infrared radiation. Usually, for fast rotating planets, assuming a negligible heat flux coming from the planet interior, the thermal inertia of the planet opposes to fast temperature variations. Therefore the equivalent black – body temperature can be computed, assuming that it is in thermal equilibrium with the environment.

$$T_{eq} = \sqrt[4]{\frac{SC}{r_{AU}^2} \frac{F_{A \to B}}{4\varepsilon\sigma}} \tag{3.35}$$

SC is the Solar Constant, r_{AU} the planet-to-Sun distance (AU), $F_{A \to B}$ the planet-to-Sun view factor, ε the planet's surface emissivity, σ the Stefan – Boltzmann constant, equal to $5.67 \cdot 10^{-8}$ $W \cdot m^{-2} \cdot K^{-4}$.
Assuming a mean albedo coefficient of 0.12, an emissivity equal to 1 and considering the maximum value of the Solar Constant, the following values of the black-body temperature for the planet's surface are obtained:

- 487 K at Perihelion;
- 434 K at average distance between the planet and the Sun;
- 395 K at Aphelion.

However, since the rotation of Mercury is very slow, the surface of the side of the planet facing the Sun is in equilibrium with the solar flux while its dark side is much colder. The surface's temperature goes from 725 K at the equator, near the sub - solar point at Perihelion to 90 K at the equator, near the local midnight.
In order to compute the infrared radiation incident on a orbiting surface, a temperature distribution over the planet has to be assumed; a simplified planet black-body temperature distribution is defined as follow:

$$T(\varphi) = T_{\max}\left[\cos(\varphi)\right]^{\frac{1}{4}} \tag{3.36}$$

where φ is the angular distance between the normal to the point of interest on the planet and the sub - solar point direction, and $T_{\max}$ is the maximum black – body temperature.
The previous relation is valid until the minimum temperature (100 K) is reached. Obtained the angle φ_0 which verifies the relation $T(\varphi_0)$ = 100 K, all the points on the surfaces with $\varphi > \varphi_0$ are characterized by a constant temperature equal to 100 K.

$$T(\varphi) = T_{\max}\left[\cos(\varphi)\right]^{\frac{1}{4}} \quad , \quad 0 \le \varphi \le \varphi_0 \tag{3.37}$$

$$T(\varphi) = T_{\min} = 100 \quad K \quad , \quad \varphi_0 \le \varphi \le \pi \tag{3.38}$$

Assuming an albedo coefficient of 0.12 and a Solar Constant of 1370 $W \cdot m^{-2}$, the following sub – solar temperatures can be obtained:

- $T_{\max}$ = 688.6 K at Perihelion;
- $T_{\max}$ = 559.0 K at Aphelion.

A MatLab code has been implemented in order to obtain the temperature distribution on the surface of Mercury. The following figure shows the result obtained, together with the MPO orbit representation. The same code has been used to calculate the incident heat fluxes on the external surfaces of the S/C (equations reported in this chapter have been implemented), as a function of the position of the S/C around Mercury and of Mercury true anomaly.

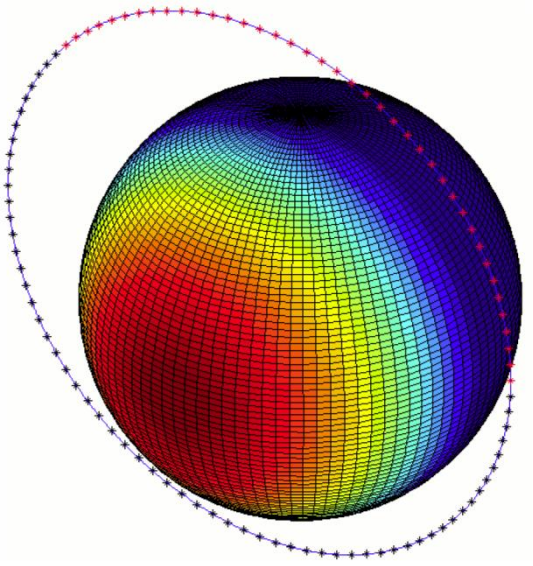

Fig. 3-7 Thermal distribution on Mercury surface and MPO orbit representation

The variation of the temperature $T_{\max}$ as a function of Mercury's true anomaly is given by the following relation.

$$\frac{T_{\max}(\nu)}{T_{\max}(0)} = \sqrt{\frac{r(0)}{r(\nu)}} = \sqrt{\frac{1+e\cdot\cos\nu}{1+e}} \tag{3.39}$$

where $T_{\max}(0)$ is the maximum temperature at Mercury Perihelion and e is the orbital eccentricity. All relations reported below are valid in the black-body hypothesis, since they are obtained assuming a unity emissivity. If the actual temperature needs to be assessed, a total hemispherical emissivity of the surface ε_{surf} can be assumed equal to 0.82 ± 0.06. The actual terrain temperature is related to the black – body temperature by the following equation:

$$T_{surf} = \sqrt[4]{\frac{T_{blackbody}^4}{\varepsilon_{surf}}} \tag{3.40}$$

Due to the Mercury orbital resonance, a certain orbital geometrical configuration is repeated every two-revolution periods. At Mercury's equator, the longitudes 0° and 180° are sub-solar points near alternate perihelion passages and are called hot poles. Similarly, equatorial longitudes 90° and 270° are sub-solar points near alternate aphelion passages and are called warm poles, because they receive less solar energy per day than the hot poles. The highest planet surface temperatures always occur at the hot poles.

Once locally determined the temperature of the planet's surface, the planetary IR radiation spectrum can be traced out: it can be approximated by the radiation of a black-body at the same temperature of the surface. At 724 K temperature, which is the highest temperature reached at Perihelion and associated with the hot poles locations, considering a surface emissivity of 0.82, peak emission occurs at 4.0 μm wavelengths.

In order to compute the IR planetary heat flux q_{PLANET}, the spacecraft's and the planet's surfaces have to meshed and the view factors have to be obtained, finally a temperature is assigned to each *j*-element on the planet's surface. The IR planetary flux is:

$$q_{PLANET} = \sigma A_i \left(T_{j,PLANET}^4 - T_i^4\right) F_{i\to j} \cdot \alpha_{4\mu m} \tag{3.41}$$

where $\alpha_{4\ \mu m}$ is the absorptance coefficient of the spacecraft surfaces at 4 μm wavelength (since the peak of the radiation spectrum is at 4 μm).

Orbiting spacecraft will receive highly variable IR emitted radiation due to the temperature distribution over the planet and due to variable altitude. Detailed thermal analyses require planetary fluxes to be computed by ray-tracing programs that are able to handle planets with non-uniform temperature distribution. The following graphs show the fluxes on single-sided surfaces orbiting the MPO nominal orbit.

The surfaces are oriented as in the following:

- Surface 1: parallel to nadir, perpendicular to roll axis;
- Surface 2: parallel to nadir, perpendicular to pitch axis;
- Surface 3: perpendicular to nadir and to yaw axis.

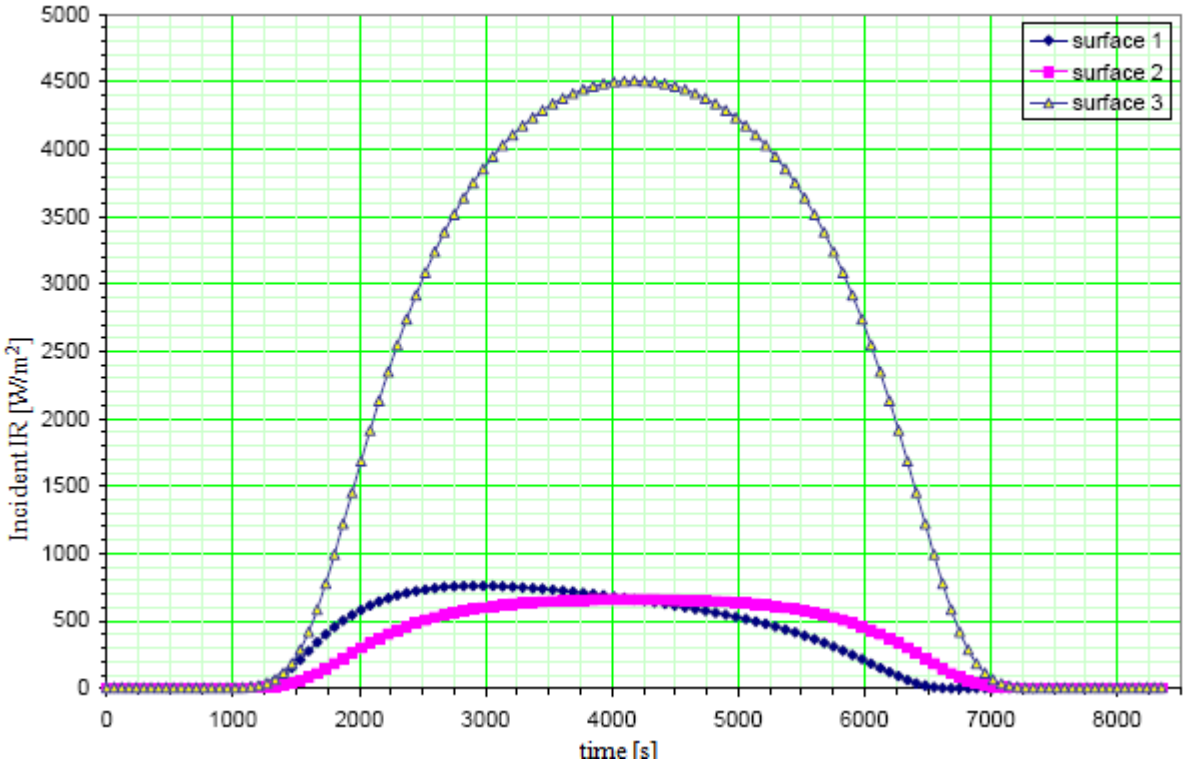

Fig. 3-8 Incident IR fluxes on 3 surfaces orbiting the MPO orbit at Mercury Perihelion. Time is counted from orbit Periherm

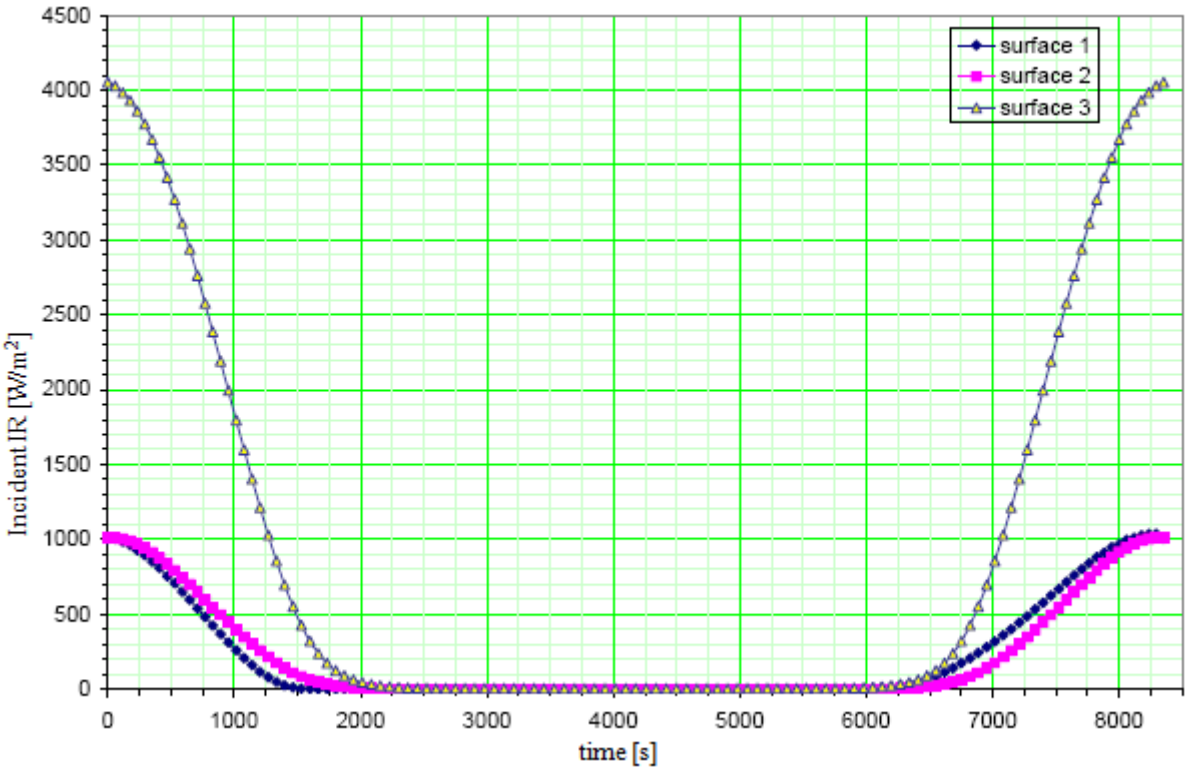

Fig. 3-9 Incident IR fluxes on 3 surfaces orbiting the MPO orbit at Mercury Aphelion. Time is counted from orbit Periherm

Some variations in the fluxes computation have to be taken into account, due to:

- The effect of the directional emissivity, which induces slightly higher incident IR fluxes, since the emissivity is related to the emission angle φ (angular distance between the normal to the surface and the emission direction) from the following equation:

$$\varepsilon(\varphi) = 0.90(\cos\varphi)^n \tag{3.42}$$

The parameter n is obtained by experimental observations and varies within the 0.19 ± 0.07 range. The largest variations occur for nadir pointing surfaces at Mercury Perihelion for the largest value of the exponent n ($n = 0.26$): the increase is equal to 1% at Mercury Perihelion, 0.05% at Mercury Aphelion.

- The effect of drifting of MPO orbit. The most important variation to be considered is the evolution of the argument of Periherm, ω. The drift rate goes from 22°/year to 44°/year depending on the value of the J_2- term of the gravitational field. The following plot shows the IR incident planetary flux on a MPO nadir surface at Mercury Perihelion, taking into account the non-directional emissivity and the average value of the J_2-term. The 3 curves refer to 3 different values of the argument of Periherm: ω = 16° (nominal orbit), ω = -16° (one year of operations) and ω = -48° (2 years of operations).

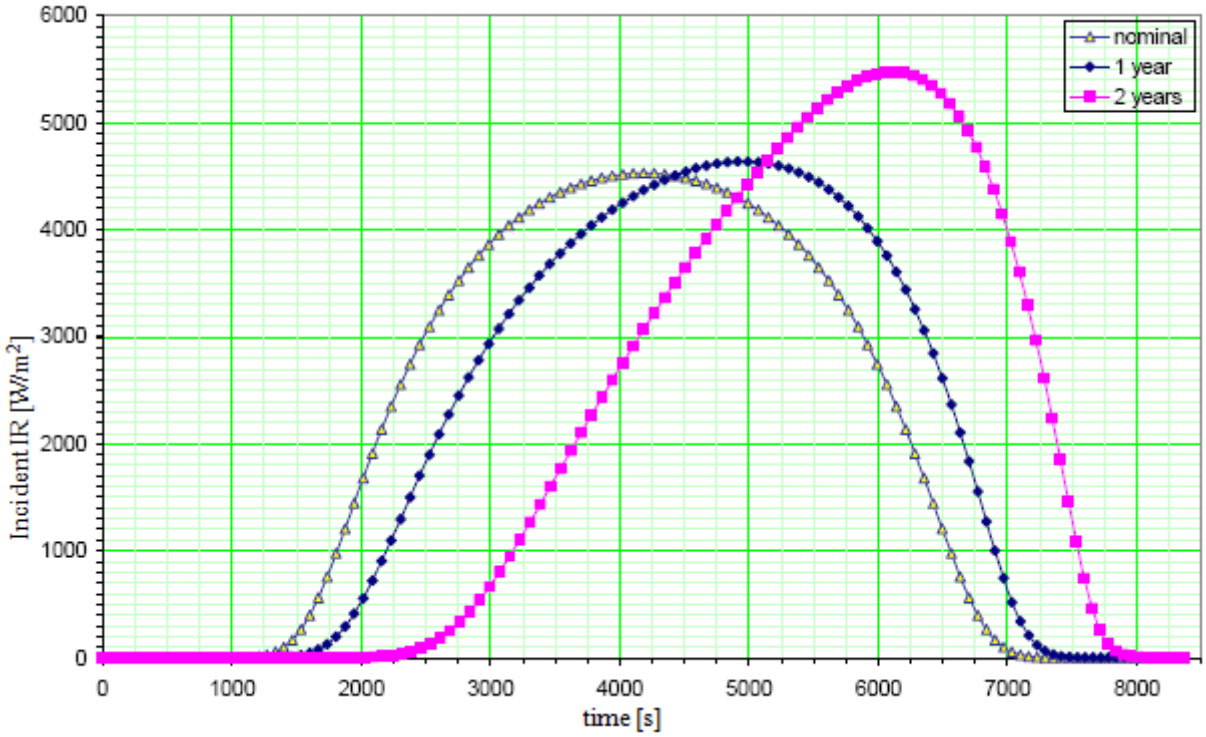

Fig. 3-10 Incident IR fluxes on a nadir pointing surface orbiting the MPO orbit at Mercury Perihelion. Time is counted from Periherm

3.2.4 Heat exchange with the sky – background

The spacecraft emits toward the sky – background, which is at a mean temperature T_{SKY} of 3-4 K and is assumed to behave like a black – body.
The heat flux q_{SKY} exchanged between the element i of the spacecraft's surface and the sky – background is given by the following relation:

$$q_{SKY} = \sigma A_i \left(T_{SKY}^4 - T_i^4\right) F_{i\to SKY} \cdot \alpha_{4\mu m} \tag{3.43}$$

By the knowledge of all other view factors (previously calculated), the view factor $F_{i\to SKY}$ is computed as follow:

$$F_{i\to SKY} = 1 - \sum_{i} F_{i\to j} \tag{3.44}$$

4. Thermal test activity on the STMs of SIMBIO-SYS baffles

4.1 Introduction

One of the most critical issues in space mission design is the thermal control, provided with active or passive systems, in order to maintain the components within the temperature operating range and consequently guarantee the scientific performances of the instruments.
During the preliminary phases of the design, thanks to numerical thermal analyses, the thermal behavior of orbiting systems can be foreseen. In addition, before the delivery of the instrumentation, at least one thermal experimental test is performed on the system in vacuum conditions (TVT).
In this chapter the test campaign on the Structural Thermal Model of the SIMBIO – SYS baffles is described: the first section is devoted to the description of test – bed design phase and to the test procedure; in the following section main experimental results are reported.
During thermal tests, the prototype or flight components are placed into a thermally controlled environment, which reproduces the operative thermal environment. Tests are performed in order to demonstrate the performance and the operation of units and subsystems in thermal environments that are realistic simulations of flight conditions.
The figure below sketches the temperature margins that are applicable during thermal test activity.

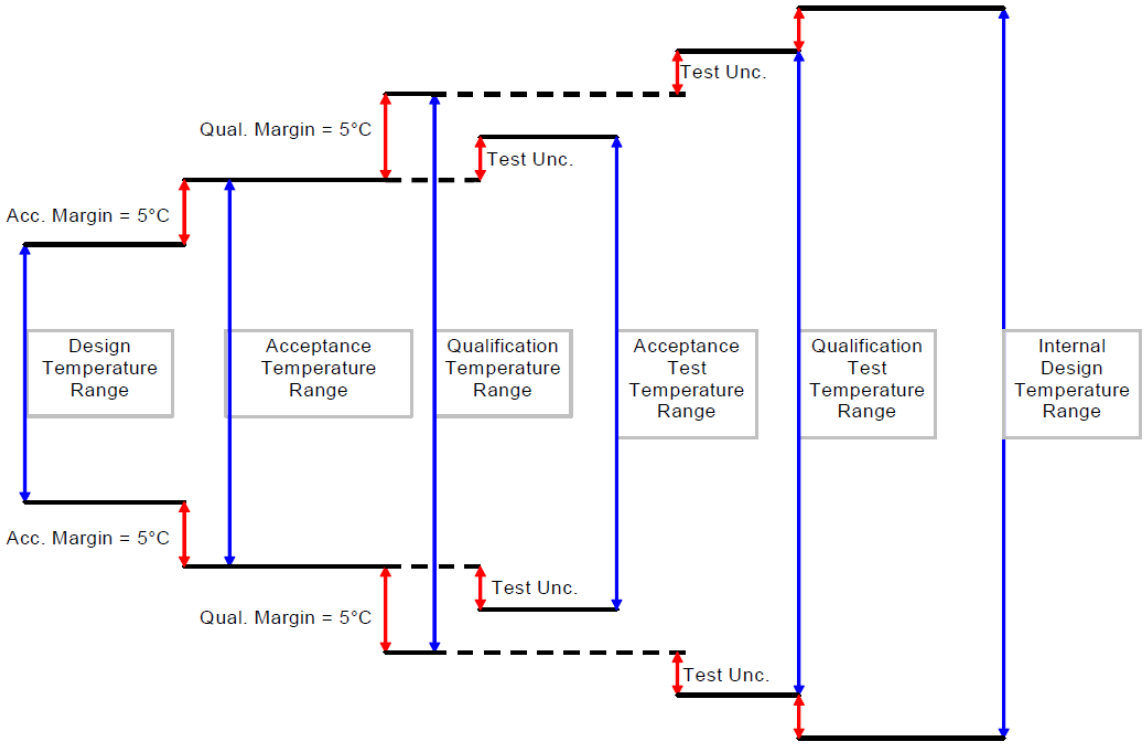

Fig. 4-1 Required TRP test margin logic.

The terms which are shown in the figure are explained below:

- Design temperature range: it is the maximum range of temperature experienced by a unit on ground and during the mission.
- Acceptance temperature range: it is an extension of the design temperature range by the acceptance margin at both ends. No deviation from the performance requirements are allowed within unit acceptance margins.
- Qualification Temperature Range: it is an extension of the acceptance temperature range by the qualification margin at both ends. Partial deviation from the performance requirements may be accepted within unit qualification margins.
- Acceptance test temperature range: this is the extreme temperature range at which all flight units shall be tested prior to delivery to the spacecraft. It is an extension of the acceptance range by the test uncertainties.
- Qualification test temperature range: it is the extreme test temperature range at which a unit shall be tested to qualify its design. It is an extension of the qualification range by the test uncertainties.
- Internal design temperature range: this is the extreme temperature against which unit internal components shall be designed.
- Temperature Reference Point (TRP): it is a physical point located on the unit. It provides a simplified representation of the unit thermal behavior.

Test activity (design, manufacture of the test facility, test operations) is highly expensive; in addition, it is quite hard to simulate all the operative conditions. Therefore numerical thermal analyses play a key role in the prevision of the thermal behavior of the system, not only during the earlier stages of the design; the experimental tests, on the other side, allow to verify the accuracy of the numerical thermal models: thanks to the correlation and the comparison between numerical results and experimental results, obtained in controlled conditions, thermal models can be refined, validated and re-implemented in order to increase the knowledge of the thermal behavior of the systems. This approach, which is based on the interconnection and on the correlation between numerical and experimental methods, allows to reduce costs and time.
The thermal vacuum tests on the STMs of HRIC, VIHI and STC baffles are mainly aimed to validate baffles thermal models: the results obtained during the test campaign on the SIMBIO-SYS baffles STMs have been compared with the results obtained with a numerical thermal analysis on the mathematical model of whole the set – up, including both thermal I/Fs and the baffles themselves (chapter 5 reports the outcome of the correlation between the experimental and the numerical results). All the objectives of the thermal vacuum tests described in this chapter are hereafter listed:

- To simulate the baffles thermal interfaces and relevant thermal fluxes inside the Thermal Vacuum Chamber (TVC).
- To validate the Thermal Mathematical Model as follows:
    - Comparing measured temperatures with predicted ones using boundary condition representative of the thermal vacuum set-up;
    - Tuning the Thermal Mathematical Models to fit measurements (experimental correlation);
    - Issuing a series of new thermal analyses, running correlated Thermal Mathematical Models with the in flight boundary conditions.

4.2 **Test-bed description**

4.2.1 Test objects

The thermal vacuum tests have been performed separately for Stavroudis HRIC baffle and for STC&VIHI baffles. Test objects are shown in the following figure.

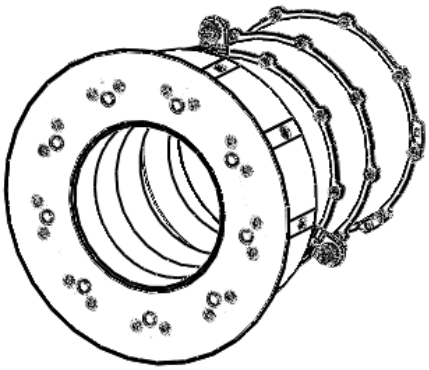

Fig. 4-2 STM of the HRIC baffle.

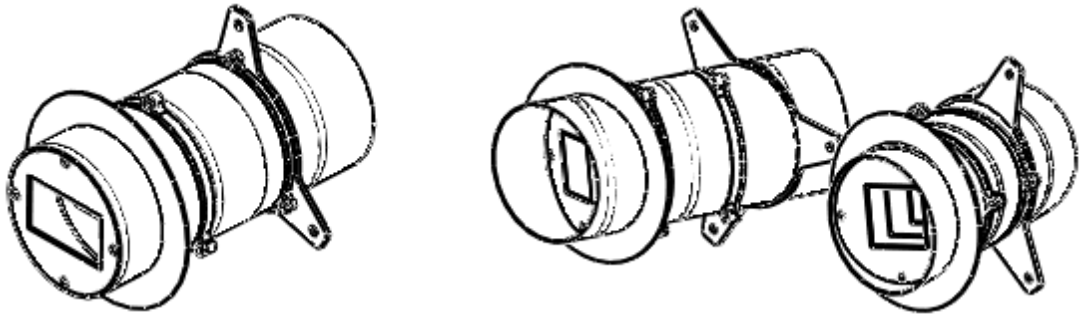

Fig. 4-3 STM of VIHI and STC baffles.

4.2.2 Test facility

Tests have been performed inside a Thermo Vacuum Chamber, which is essentially constituted by a cylindrical container in stainless steel (AISI 304) with a distributed series of flanges on the cylindrical surface, on the front and on the posterior part, in order to connect the pump group, the system for pressure measurements and the electrical cables. The chamber can operate in high vacuum thanks to the pump group, composed by one rotating pump, for the pre-vacuum, and one turbo-molecular pump. The system, managed from a controller, gives the possibility to fill with gaseous nitrogen the climatic chamber, before opening it to the atmosphere. A cylindrical cryostat, which is coaxial and thermally decoupled with respect to the chamber, allows the control of the temperature thanks to liquid Nitrogen (volume up to 1400 litres). The chamber (internal diameter equal to 1100 mm, length equal to 1130 mm) can reach a vacuum of 10^{-6} mbar; the cryostat can reach a minimum temperature of 90 K.
A HP34970A data – logger allows to manage up to 30 RTD PT 100 (class A), four wires measurements.

4.2.3 Set – up overview

As explained in Chapter 3, during flight, baffles are exposed to direct Sun illumination, albedo and infra-red radiation from the Planet, and are subjected to heat exchange with the sky background.
In order to simulate that thermal environment, a preliminary planning of the test campaign foresaw:

- An external beam generated by a Xenon lamp (up to 10 kW) to simulate the Sun;
- A black plate with active thermal control system (active heating and cooling) to simulate the hot Planet surface;
- A cylindrical cryostat to represent the cold Planet surface and the sky background.
- A rotary stage to rotate the test objects in order to face them to different heat sources.

A sketch of the proposed testbed is shown in the following figure.

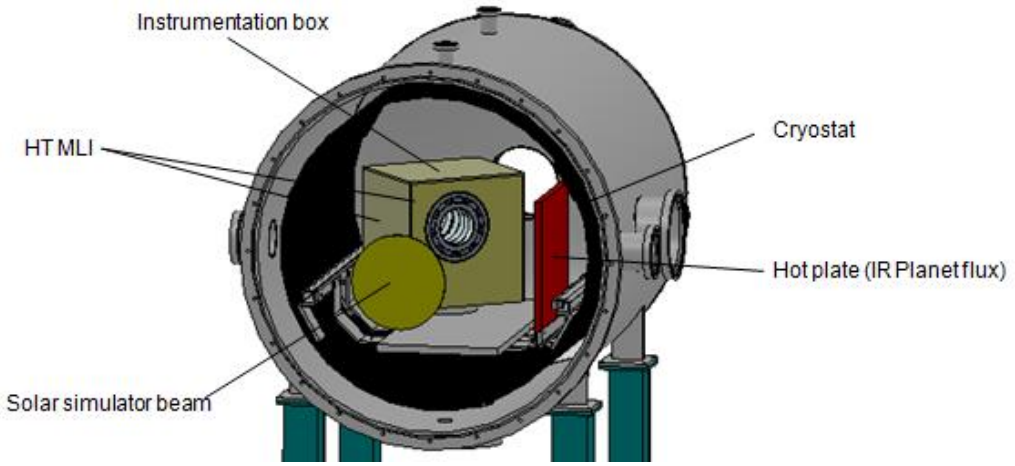

Fig. 4-4 Test-bed for the Stavroudis baffle STM: the red plate simulates the hot planet surface, the yellow circle represents the solar simulator beam, the black cylinder represents the internal cryostat

This solution has been rejected considering that STM tests have been performed at S/C level neglecting the actual environmental condition; in addition STMs of the baffles are not representative of the thermal-optical properties of the final flight instrumentation. Therefore, in order to minimize the time to perform tests and speed-up the delivery of sub – units, considering that the main goal of these tests was the validation of the thermal mathematical models, a back – up solution for STM baffles test-bed has been proposed, in which the solar simulator has been replaced by IR lamps. As previously stated, the STM baffles and, in particular, Stavroudis one are not fully representative of the optical properties so that the flux source can be simply reproduced heating the system by means of IR lamps (simulating the IR planetary flux) instead of solar flux. This proposal implies:

a. At a later stage, testing of the Qualification Models (QMs) of the baffles introducing the solar flux, thanks to the solar simulator;
b. Correlation between STM TMMs and QM ITMMs.

Since rotary stage was not available for the STM tests because of delay in delivery, hot case and cold case have not been simulated continuously in sequence inside the TVC: the hot heat source has been removed from the set-up at the end of the hot case simulation for each unit, before the simulation of the cold case. The hot heat source has been simulated by means of a black plate heated up by IR lamps; simulations for cold case have been performed by means of a rectangular cryostat positioned opposite to the frontal side of the instrumentation box.
STMs of the baffles have been placed inside a (367×364×290) mm^3 box, thermally insulated with respect to the surrounding environment by means of High Temperature MLI on the frontal and lateral sides, Standard MLI on the other sides. The bottom face of the instrumentation box has been thermally insulated with respect to the baffles, both conductively and radiatively (thanks to MLI coverage). Inside the control volume, baffles have been placed on a vertical aluminum plate (10 mm

thickness, normal to the bottom face of the instrumentation box), which has been provided with heating resistors and connected to the cryostat by means of copper braids in order to regulate the plate temperature: since tests on STMs referred to Perihelion case (hot case), temperature of this mechanical and thermal I/F has been imposed to be equal to baffle bracket temperature at Perihelion. The aluminum plate has been radiatively insulated thanks to MLI coverage from other internal components of instrumentation box. Each baffle has been connected to the aluminum panel by means of 3 screws (M5 for Stavroudis baffle, M4 for STC and VIHI baffles respectively). A black-painted aluminum box (2 mm thickness) has been located behind the aluminum plate, surrounding the rear part of the baffles, and provided with heaters and copper braids connected to the cryostat, in order to adjust the temperature of the walls. The box has been externally insulated by means of standard MLI. Aluminum plate and aluminum box have been fixed to the horizontal aluminum panel supporting the instrumentation box by means of four M8 stainless steel threaded bars, in order to reduce the heat exchange due to the conduction. Finally a light aluminum frame has been fixed to horizontal plate to support High Temperature and standard MLI. The following figure shows the layout of the test-bed: the instrumentation box with STC and VIHI baffles is placed inside the TVC in front of the heat source, represented as a red plate (IR lamps) for the hot case (figure on the left), with a blue plate (cryostat) for the cold case (figure on the right).

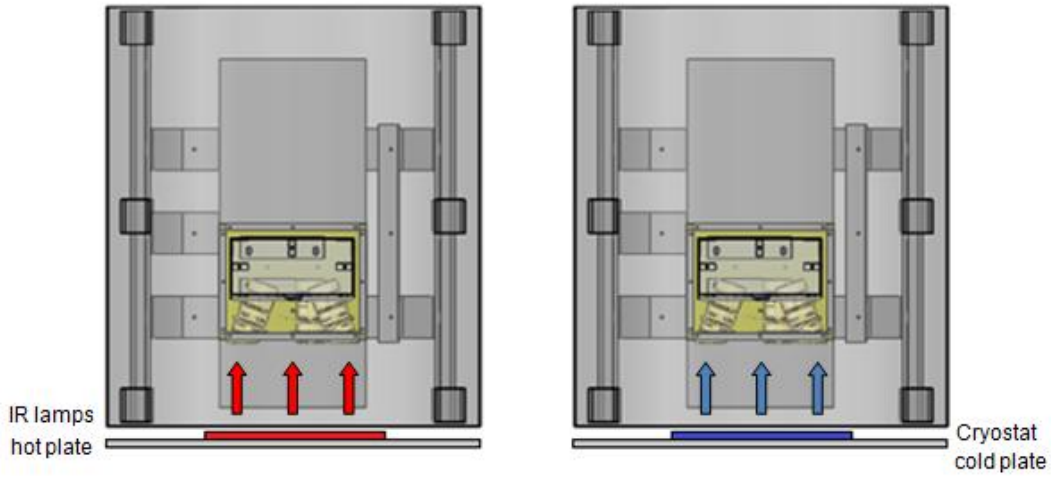

Fig. 4-5 Layout of the test-bed

HRIC baffle unit and STC-VIHI baffles unit are sketched below; external HT and standard MLI coverage is not shown.

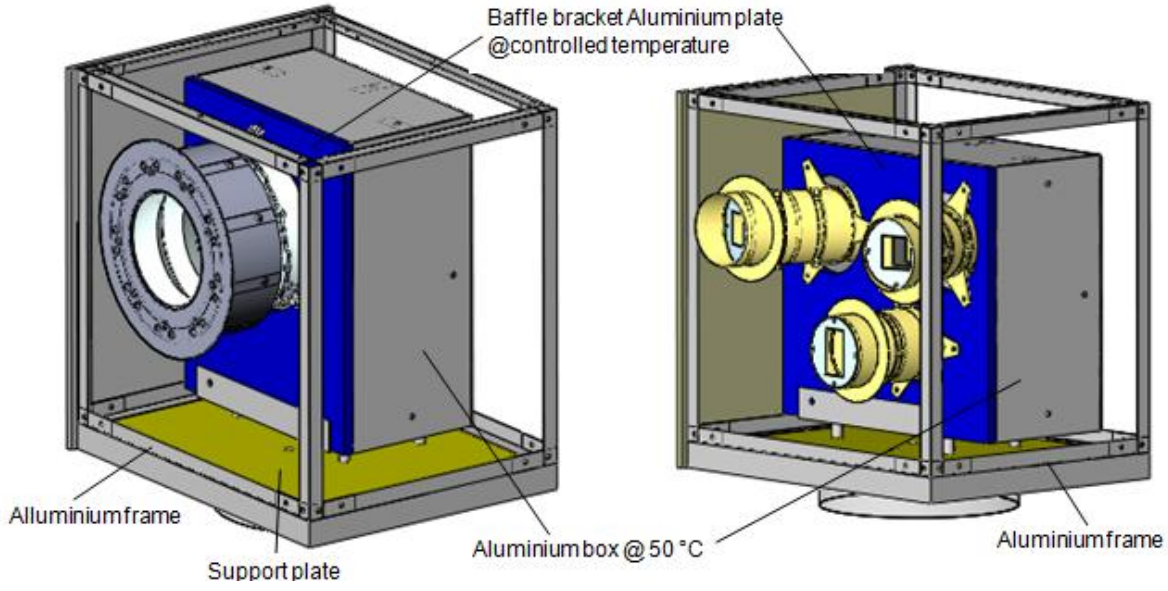

Fig. 4-6 Instrumentation box for HRIC baffle and STC – VIHI baffles

As previously explained, hot case and cold case have been simulated in different moments since TVC has been opened after the hot case, before the cold case, in order to remove the hot source and modify the set- up. In the following photos the two different configurations are represented: the first one shows the hot case configuration, with the hot black plate and the IR lamps behind it positioned on the frontal aperture of the TVC; in the second one only standard MLI which covers instrumentation box and cryostat plate is visible. Configurations are similar for STC – VIHI baffles unit and for HRIC baffle unit.

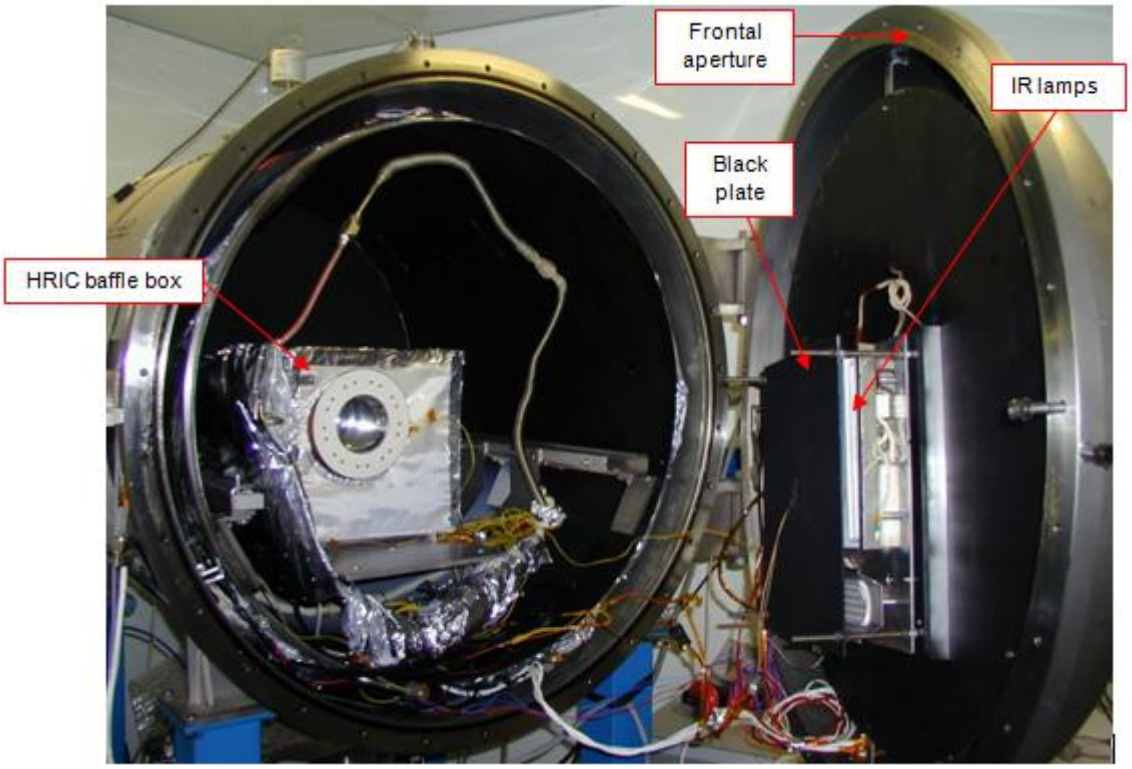

Fig. 4-7 HRIC baffle box inside the TVC before hot case simulations; the configuration employed for hot tests on STC-VIHI baffles unit is similar

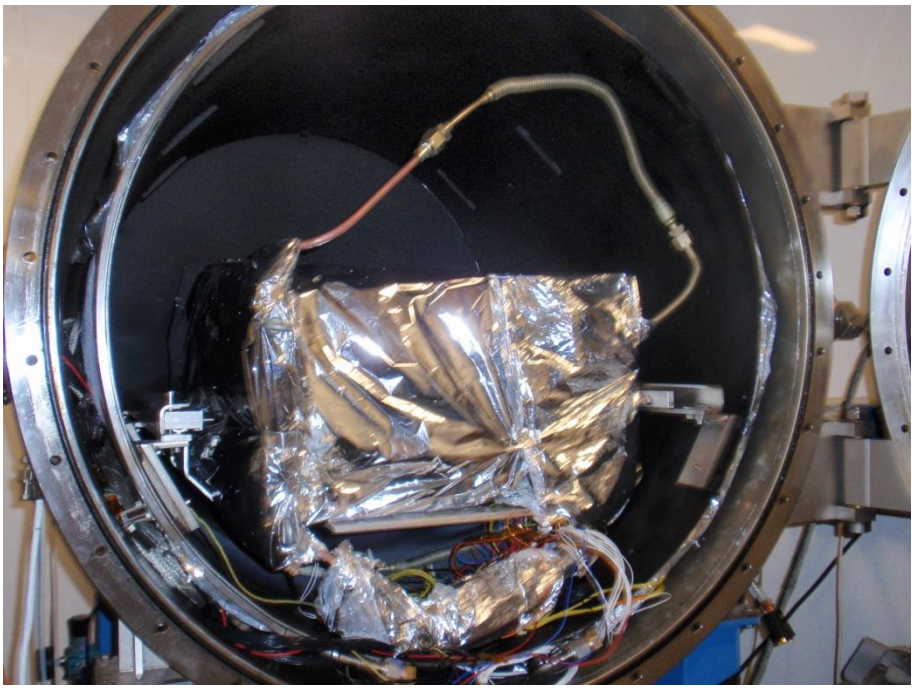

Fig. 4-8 Instrumentation box inside the TVC before cold case simulation; the configurations employed for cold tests on STC – VIHI baffles unit and HRIC baffle unit are similar

The following pictures show the STC – VIHI baffles unit and the Stavroudis baffle unit during assembling operations: baffles are fixed to the aluminum plate at controlled temperature (covered by standard MLI in the photo); the aluminum box behind represents the S/C thermal environment for STC – VIHI unit, HRIC filter for Stavroudis unit.

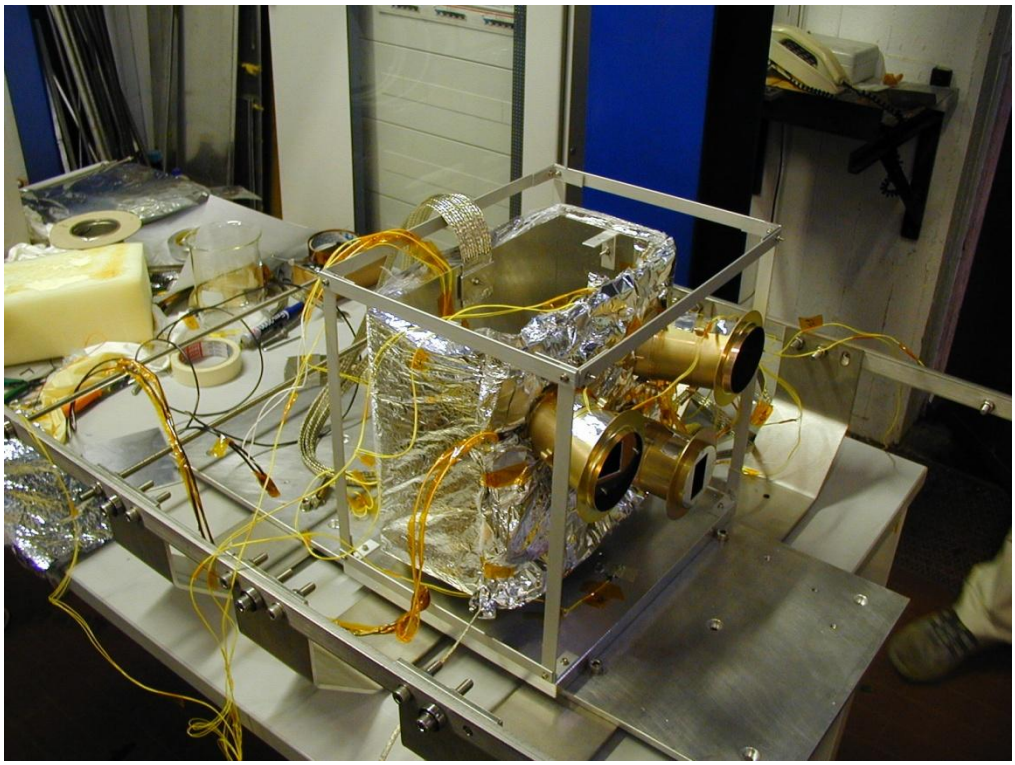

Fig. 4-9 STC – VIHI unit during assembling operations.

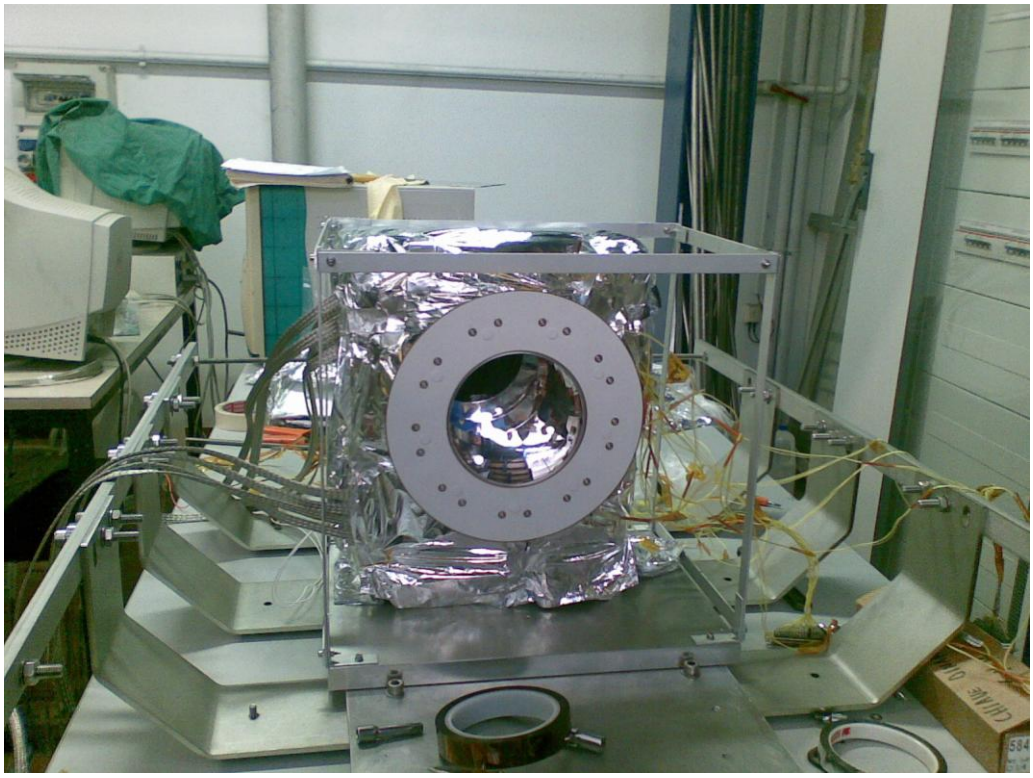

Fig. 4-10 HRIC baffle unit during assembling operations.

4.2.4 Sensors position

The following parameters have been monitored during the test campaign:

- internal chamber pressure;
- cryostat temperature;
- hot plate temperature;
- progressive time;
- temperature of aluminum plate and aluminum box inside the instrumentation box;
- temperature the baffle bracket plate, which supports the baffles;
- temperature of different points of interest on the baffles (e.g. temperature of external ring of Stavroudis baffle).

Temperature has been measured by means of class A four wires PT100. The collocation of the temperature sensors is reported below.

- N.1 sensor has been connected to the hot plate, which represents the hot illuminated surface of the planet;
- N.1 sensor has been placed on the aluminum plate which supports baffles, simulating the baffle bracket plate;
- N.1 sensor has been placed on the aluminum box inside the instrumentation box;
- N.1 sensor has been connected to the cryostat;
- N.1 sensor has been connected to the plate which supports the instrumentation box;
- N.10 sensors for STC – VIHI baffles and N. 11 sensors for Stavroudis baffle have been linked to the instrumentation (baffles), in different points of interest;
- N.2 sensors monitored the temperature of the liquid nitrogen which flows inside and outside the cryostat respectively;

Three PID controllers have been used in order to adjust the temperature of the 3 main thermal I/Fs (hot plate, baffle bracket plate supporting baffles and aluminum box simulating the S/C environment for STC-VIHI baffles or the filter for HRIC baffle) at a mean stable value. For this purpose, two additional PT100 sensors have been electrically connected to the PID controllers of the baffle bracket plate and the aluminum box, an integrated type K thermocouple has been used to thermally control IR lamps temperature. Points of interest for the measurement of the temperature are different depending on the instrument unit which has been tested. Temperature sensors and their position description are listed in the following tables: the first table refers on STC – VIHI baffles unit, the second one on Stavroudis baffle unit.

STC – VIHI baffles unit		
Temperature sensor	**Position**	**Notes**
PT100 1	Baffle bracket plate	Temperature control
PT100 2	Aluminum box	Temperature control
PT100 3	Baffle bracket plate	Data logging
PT100 4	Aluminum box	Data logging
PT100 5	STC 1 – 1st vane	Data logging
PT100 6	STC 1 – 2nd vane	Data logging
PT100 7	STC 1 – 3rd vane	Data logging
PT100 8	STC 2 – 1st vane	Data logging
PT100 9	STC 2 – 2nd vane	Data logging
PT100 10	STC 2 – 3rd vane	Data logging
PT100 11	VIHI – 1st vane	Data logging
PT100 12	VIHI – 2nd vane	Data logging
PT100 13	VIHI – 3rd vane	Data logging
PT100 14	HT MLI – internal surface	Data logging
PT100 15	Plate which supports instr.	Data logging
Thermocouple 16	IR lamps	Temperature control
PT100 17	Hot plate	Data logging

PT100 18	Cryostat	Data logging
PT100 19	Nitrogen circuit – IN	Data logging
PT100 20	Nitrogen circuit – OUT	Data logging

Table 4-1 Position of sensors employed during tests on STC and VIHI baffles

HRIC baffle unit		
Temperature sensor	**Position**	**Notes**
PT100 1	Baffle bracket plate	Temperature control
PT100 2	Aluminum box	Temperature control
PT100 3	Baffle bracket plate	Data logging
PT100 4	Aluminum box	Data logging
PT100 5	3rd ellipse	Data logging
PT100 6	Baffle bracket plate	Data logging
PT100 7	2nd ellipse	Data logging
PT100 8	4th ellipse	Data logging
PT100 9	5th ellipse	Data logging
PT100 10	4th ellipse	Data logging
PT100 11	5th ellipse	Data logging
PT100 12	3rd ellipse	Data logging
PT100 13	Baffle bracket plate	Data logging
PT100 14	Frontal ring	Data logging
PT100 15	HT MLI – internal surface	Data logging
Thermocouple 16	IR lamps	Temperature control
PT 100 17	Hot plate	Data logging
PT100 18	Cryostat	Data logging
PT100 19	Nitrogen circuit – IN	Data logging
PT100 20	Nitrogen circuit – OUT	Data logging

Table 4-2 Position of sensors employed during tests on HRIC baffle

The position of the sensors is shown in the following figures: circles have been used to mark sensors which detect and record temperatures, squares indicate sensors which detect and control temperatures (being electrically linked to the PID controllers).

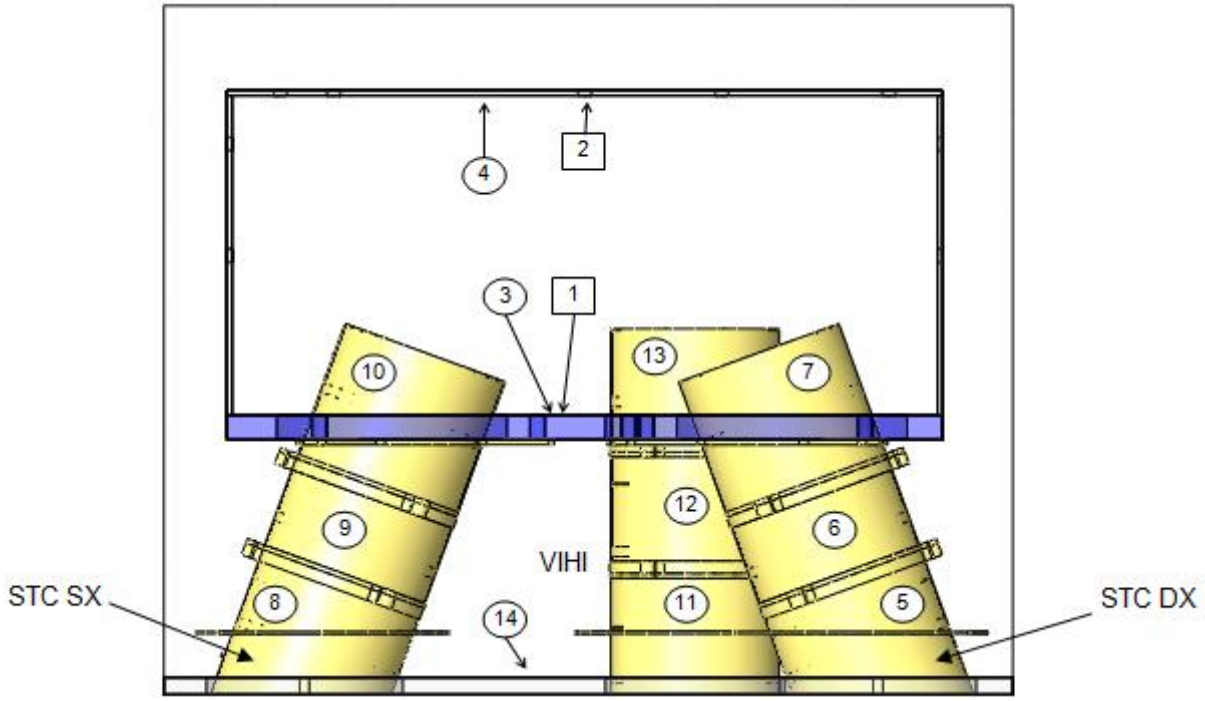

Fig. 4-11 Position of temperature sensors on STC – VIHI baffles unit: sensors from #5 to #13 are applied on baffles, sensor #14 is applied on the internal side of the HT MLI; sensors from #1 to #4 detect and control temperature of baffles I/F and aluminum box

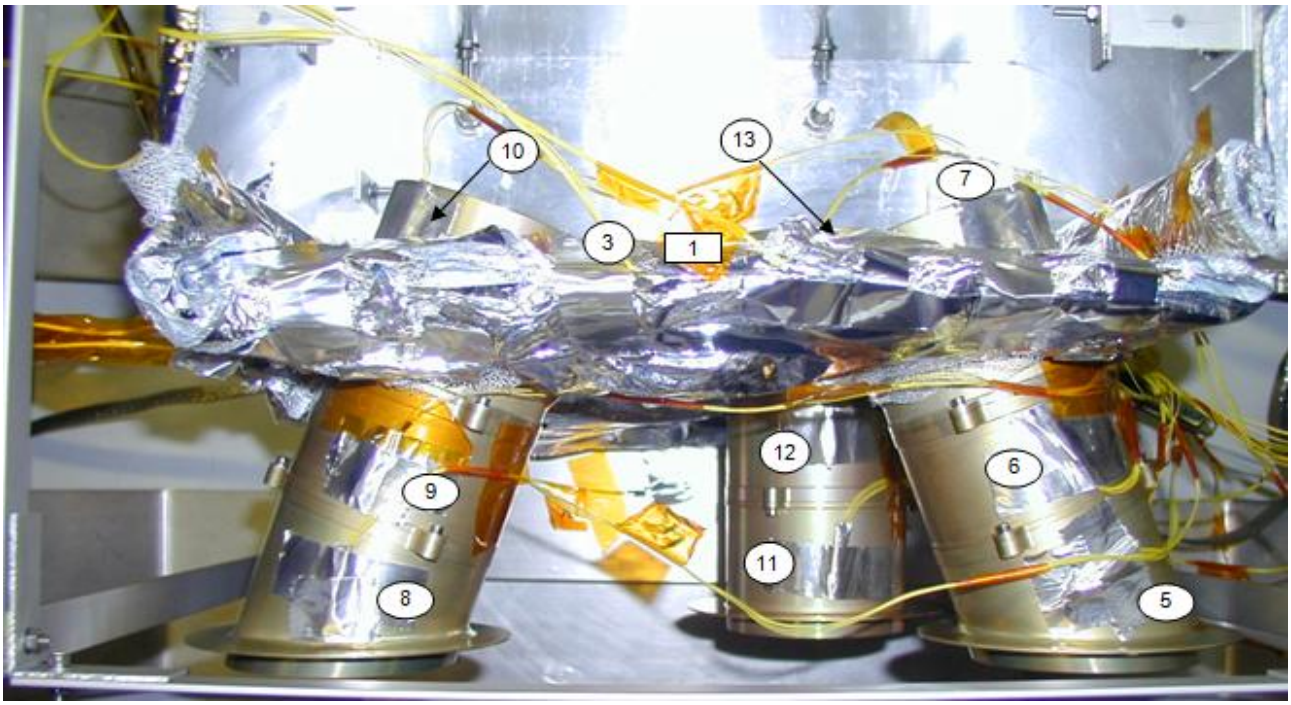

Fig. 4-12 Position of temperature sensors on STC – VIHI unit: PT100 #1 and #3 are not visible since they are applied on the baffle bracket plate, which is covered by standard MLI

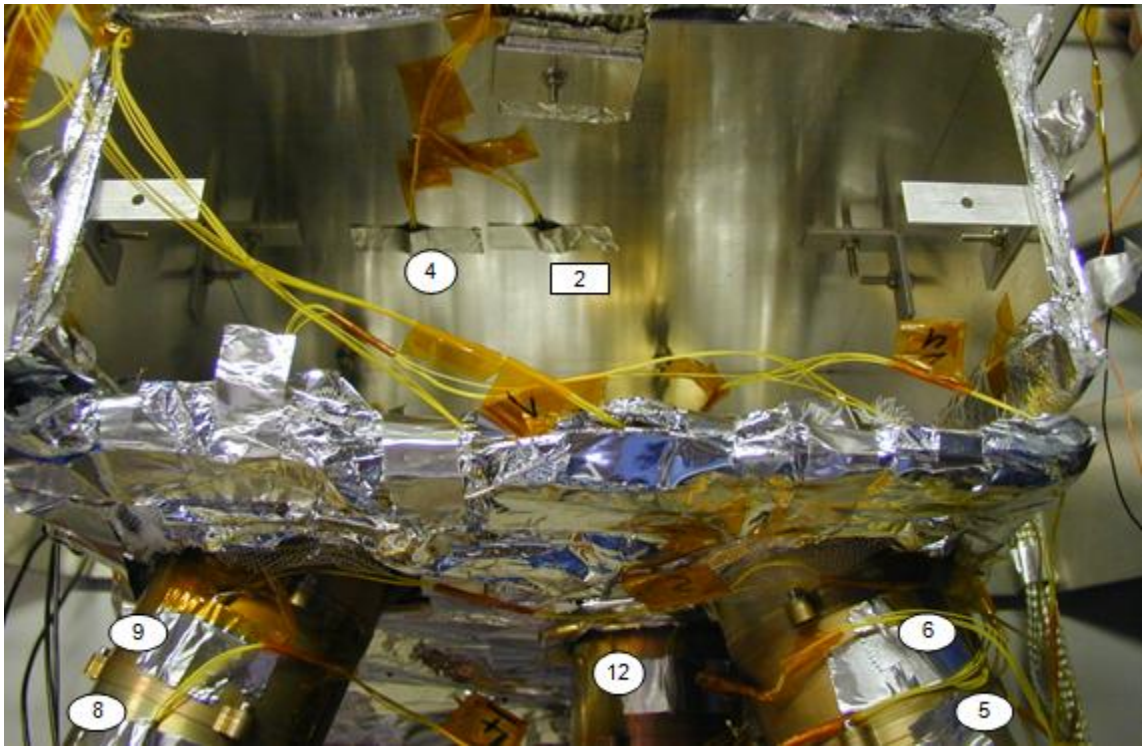

Fig. 4-13 Position of temperature sensors on STC – VIHI unit

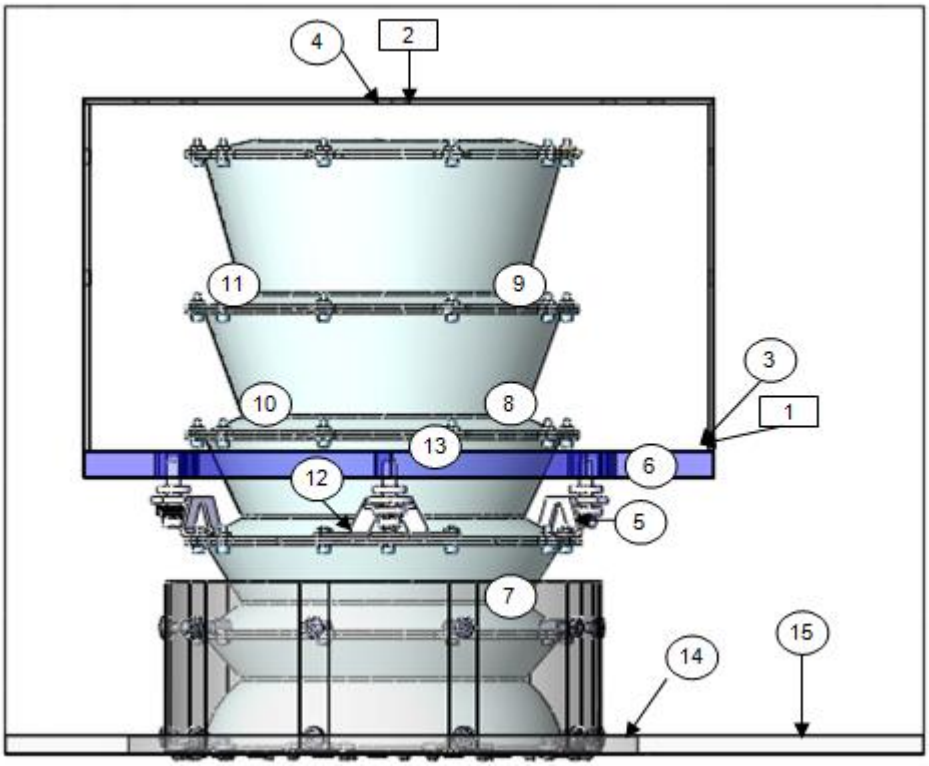

Fig. 4-14 Position of temperature sensors on HRIC baffle unit: sensors from #5 to #14 are applied on baffle, sensor #15 is applied on the internal side of the HT MLI; sensors from #1 to #4 control and detect temperature of baffle I/F and aluminum box

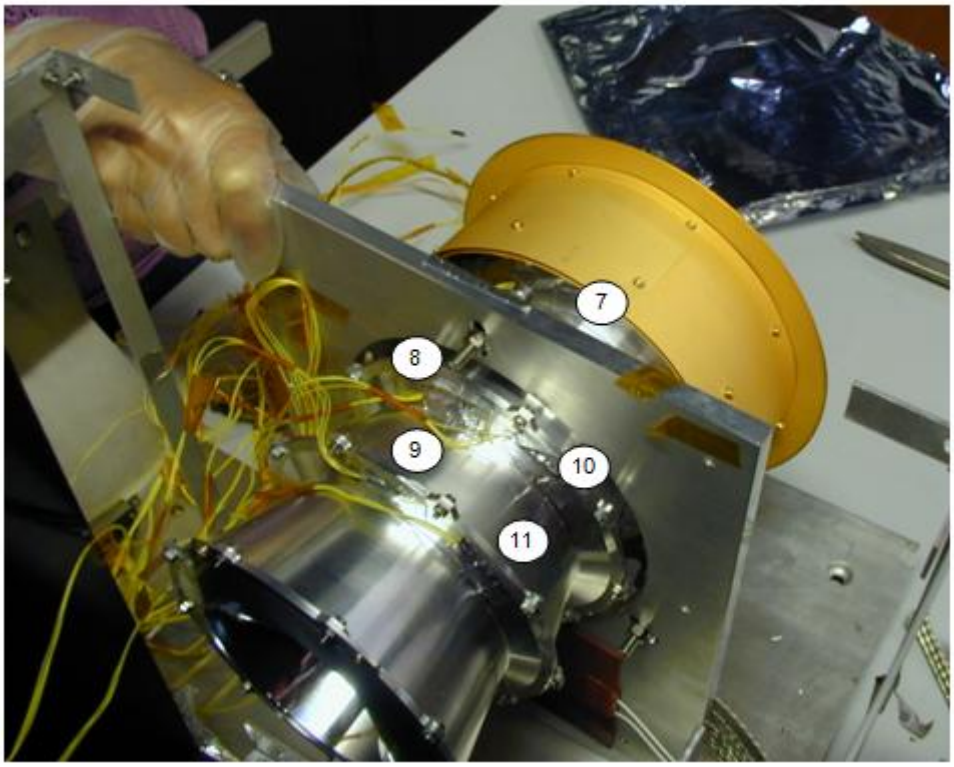

Fig. 4-15 Position of some temperature sensors on HRIC baffle during assembling operations

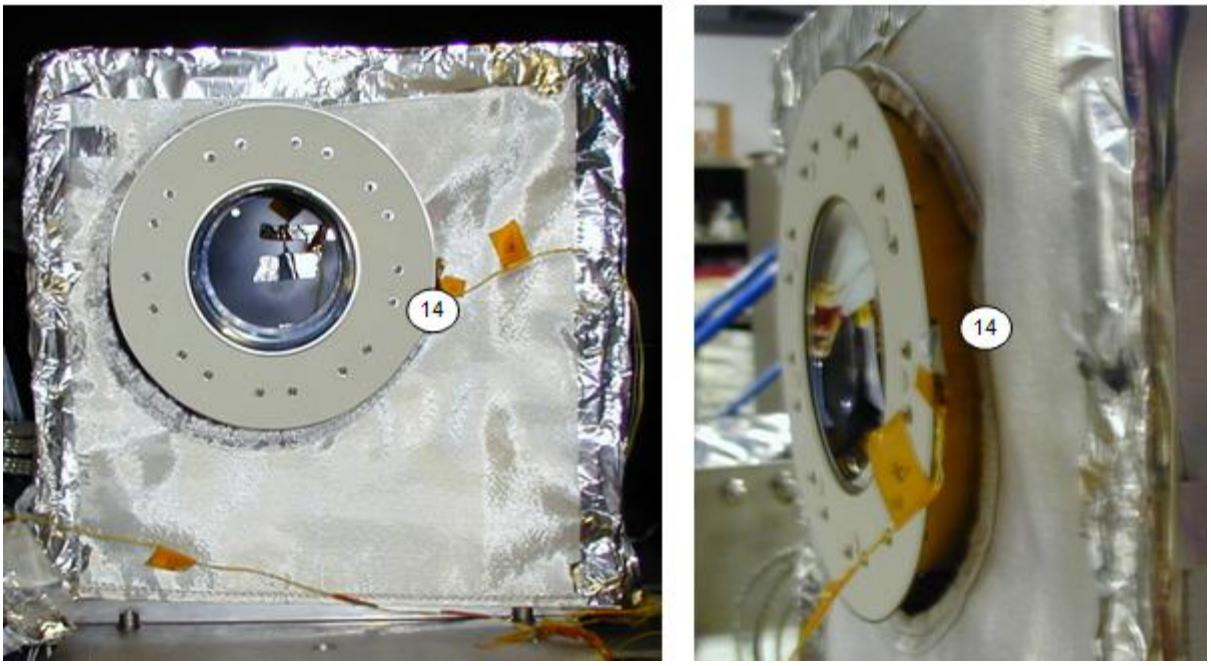

Fig. 4-16 Position of temperature sensor behind the frontal ring of the baffle

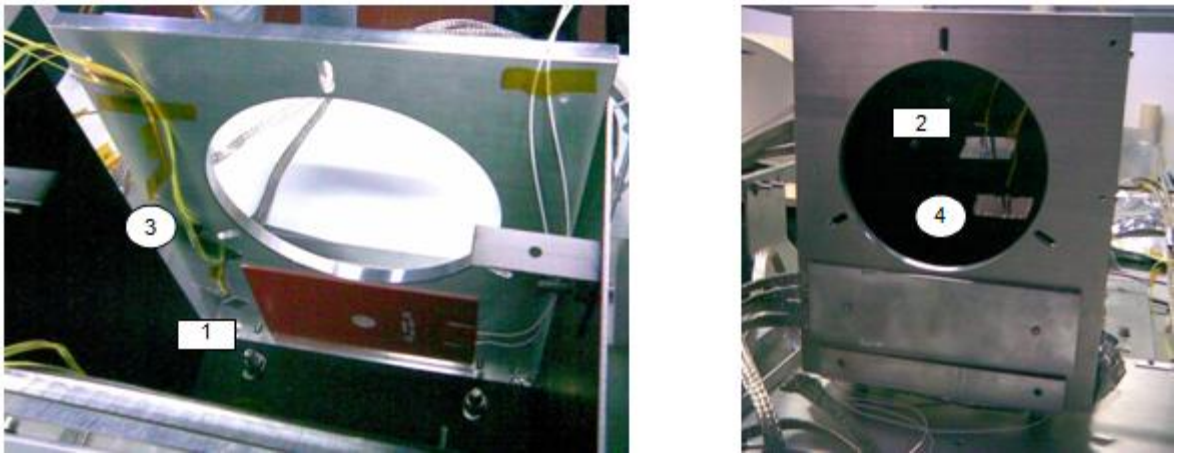

Fig. 4-17 Position of temperature sensors on the baffle bracket plate and on the aluminum box

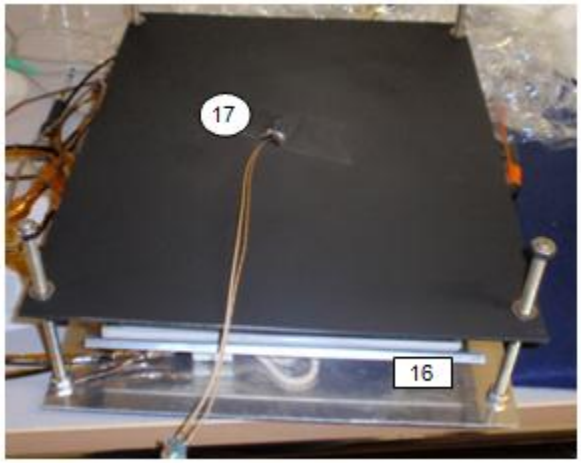

Fig. 4-18 Position of temperature sensors on the hot black plate: sensor #16 is a type K thermocouple, sensor #17 is a 4 wires PT100

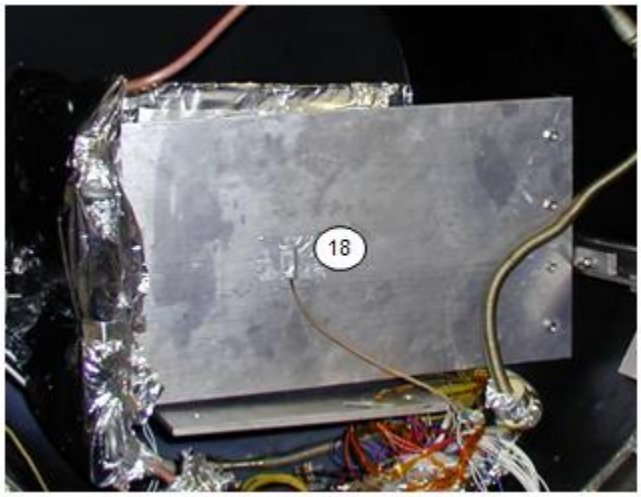

Fig. 4-19 Position of temperature sensor #18 on the cold plate or cryostat

4.3 Test levels

Preliminary analytical calculation and numerical simulations have been performed to evaluate the worst thermal case, depending on the position of the spacecraft above the surface of the planet and the position of Mercury around the Sun. The following tables show the maximum and minimum heat fluxes incident on the nadir surface of MPO with the spacecraft orbiting above the planet's illuminated and shadowed surface respectively. q_{IR}, q_A and q_S are the infrared, albedo and solar fluxes.

Maximum fluxes [W·m^{-2}]			
S/C orbiting above the illuminated surface			
	Perihelion	**Aphelion**	**Autumn/Spring**
q_{IR}	4496.1	4087.4	390.6
q_A	613.2	557.46	56.07
q_S	8509.5	4798.4	0
S/C orbiting above the dark surface			
q_{IR}	4.3	2.4	//
q_A	0	0	//
q_S	8509.5	4798.4	//

Table 4-3 Maximum heat fluxes incident on the nadir surface of MPO spacecraft

Minimum fluxes [W·m^{-2}]			
S/C orbiting above the illuminated surface			
	Perihelion	**Aphelion**	**Autumn/Spring**
q_{IR}	5.7	2.4	320.8
q_A	0.3	0.0	43.5
q_S	0	0	0
S/C orbiting above the dark surface			
q_{IR}	3.7	2.2	//
q_A	0	0	//
q_S	0	0	//

Table 4-4 Minimum heat fluxes incident on the nadir surface of MPO spacecraft

From the previous tables it can be noticed that MPO orbit at Perihelion is characterized by the highest IR thermal input, due to the proximity to the Sun; therefore tests on STM are based on the simulation of the orbital thermal environment at Perihelion.
Two different situations have been simulated separately in TVC for each instrument unit:

a. Hot case: S/C orbiting above Mercury illuminated surface at Perihelion. Three different tests have been performed:
    i. Initially lamps have been switched on in order to obtain an incident heat flux on the instrument box frontal side equivalent to the incident planetary heat flux at Perihelion (4496.1 W/m^2), emitted by Mercury illuminated surface. With this assumption, supposing to employ 4 lamps with a surface mean temperature of 417°C and a heat flux on a reference surface of 17 kW/m^2, a temperature of about 220°C has been imposed on the hot black surface; then the thermal stability has been reached.
    ii. Subsequently the temperature has been increased in order to achieve a value closer to the Planet hot surface temperature; considering that surface mean temperature of IR lamps is 417°C, this value has been imposed to the IR lamps PID controller as maximum set – point temperature.
    iii. An additional hot case test has been foreseen for Stavroudis baffle: active and passive thermal control devices (heaters and copper braids) have been disabled inside the instrumentation box (on the baffle bracket plate and on the aluminum black box) and only IR lamps have been kept switched on, in order to evaluate the free thermal behavior of the system, without heat sinks inside the instrumentation box. Set – point temperature of the hot plate has been imposed equal to 220°C during this simulation.
b. Cold case: S/C orbiting above Mercury cold surface at Perihelion. TVC has been opened, the lamps have been removed, a rectangular aluminum cryostat (simulating the cold planet surface) provided with an internal coil and heaters has been positioned opposite to the instrumentation box, the cryostat has been switched on allowing the liquid nitrogen to flow inside the circuit and the surface temperature decreased, reaching a temperature close to the cold surface of the Planet (minimum 100 K): a temperature of about -130°C has been reached on the cryostat during simulations on STC – VIHI baffles unit, of about -150°C during simulations on Stavroudis baffle unit.

The boundary temperature of the aluminum plate (baffle bracket plate) has been adjusted to different values according to each condition, in order to follow the temperature profile of the correspondent mechanical and thermal I/F during S/C orbit at Perihelion. The temperature profile of the baffle bracket plate, obtained thanks to numerical simulations, is shown in the following figure (and it is evidenced by a black arrow), as a function of MPO orbital position. The minimum temperature occurs when the S/C orbits above the cold surface of the planet, the highest one occurs when the S/C orbits on the illuminated surface of Mercury.

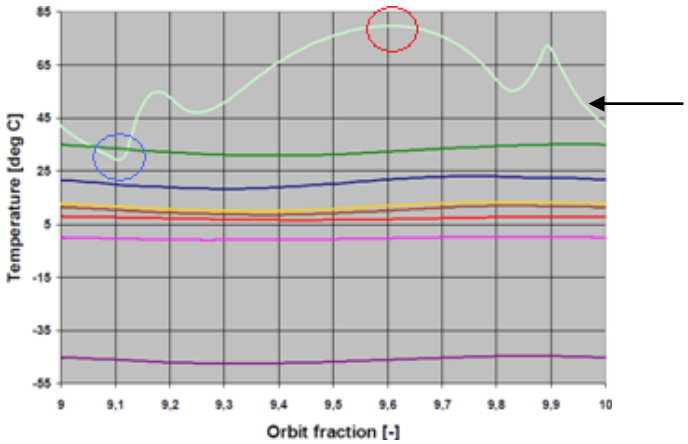

Fig. 4-20 Temperature profile of the baffle bracket plate as a function of MPO orbital position: the blue circle mark the minimum temperature, the red circle the maximum one

Referring to hot case simulation and cold case simulation, the following temperatures have been imposed on the baffle bracket plate, according to the graph above:

a. S/C orbiting above Mercury illuminated surface: taking into account of the ±12°C accuracy for temperature determination in the TMM and considering that the baffle bracket nominal temperature value is equal to 80°C, the temperature to be reached on the I/F is 92°C.
b. S/C orbiting above Mercury cold surface: taking into account of the ±12°C accuracy for temperature determination in the TMM and considering that the baffle bracket nominal temperature value is equal to 30°C, the temperature to be reached on the I/F is 18°C.

The boundary temperature of the aluminum box behind the baffles was different for simulations on STC – VIHI baffles unit and on HRIC baffle unit:

a. For STC – VIHI baffles, the aluminum box represents the thermal environment of the S/C, which is at 50°C at Perihelion.
b. For HRIC baffle, the aluminum box represents the BK7 filter behind HRIC baffle, which is at about 35°C at Perihelion.

Temperature levels imposed to the heat sources and the heat sinks (baffle bracket plate and aluminum box) are listed in the following tables: the first one refers to tests on STC-VIHI baffles, the second one to tests on HRIC baffle.

Case	Description	Temperature [°C]			
		Hot source	Cryostat	Baffle bracket plate	Aluminum box
HOT	S/C orbiting above Mercury hot surface	A) 220[3]	//	92	50
		B) 417[4]			
COLD	S/C orbiting above Mercury cold surface	//	-130	18	50

Table 4-5 Detail of temperature values applicable to heat sources and heat sinks during Thermal Vacuum Tests on STC – VIHI baffles unit

Case	Description	Temperature [°C]			
		Hot source	Cryostat	Baffle bracket Plate	Aluminum box
HOT	S/C orbiting above Mercury hot surface	A) 220[3]	//	92	35
		B) 220[3]		//	//
	Additional case	C) 417[4]		92	35
COLD	S/C orbiting above Mercury cold surface	//	-150	18	35

Table 4-6 Detail of temperature values applicable to heat sources and heat sinks during Thermal Vacuum Tests on HRIC baffle unit

[3] Hot plate temperature set point
[4] IR lamps temperature set point

4.4 Test summary results

In this paragraph test results are summarized, first for STC and VIHI baffles, then for HRIC baffle.

4.4.1 Tests on STC and VIHI baffles

4.4.1.1 Test A – Hot case

During hot case, the following nominal test levels have been assured:

- Baffle bracket plate @ 92°C;
- Hot source @ 220°C.

Stability of 1°C/hr has been verified under these conditions during 2 hours. Subsequently hot source temperature has been increased up to 350°C for a short time, in order to evidence temperature gradients along baffles. The following table summarizes test levels for hot case simulations on STC – VIHI baffles unit:

Boundary surface	Temperature	Description
Baffle bracket plate	92°C	PT100 #3
Hot plate	a) 220°C	PT100 #17
	b) 350°C	

Table 4-7 Test levels for hot case simulations on STC – VIHI baffles unit

The following graph shows the variation of the temperature of baffle bracket plate (BB – T3) and aluminum box (S/C – T4).

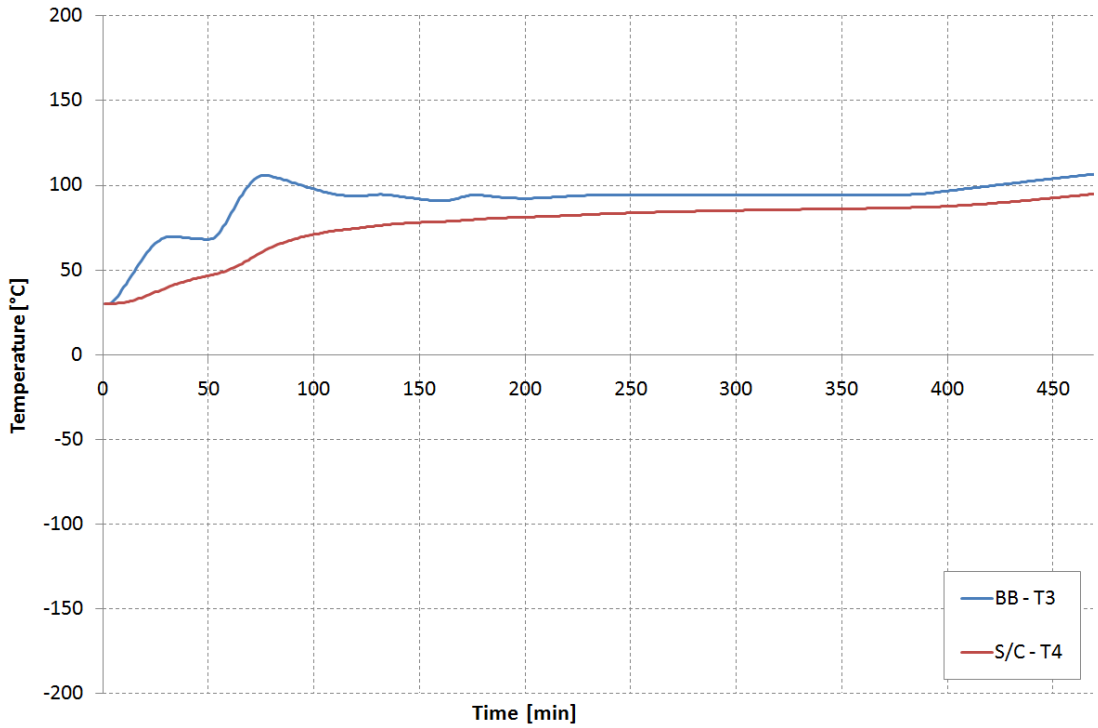

Fig. 4-21 Temperature profile of baffle bracket plate (BB – T3) and aluminum box (S/C – T4) during hot case tests on STC – VIHI baffles unit

The next figure shows the temperature detected by the sensors attached to the baffles vanes (from T5 to T13 in the graph, represented with continuous line) and the internal surface of the HT MLI (HT MLI - T14 in the graph, represented with dotted line).

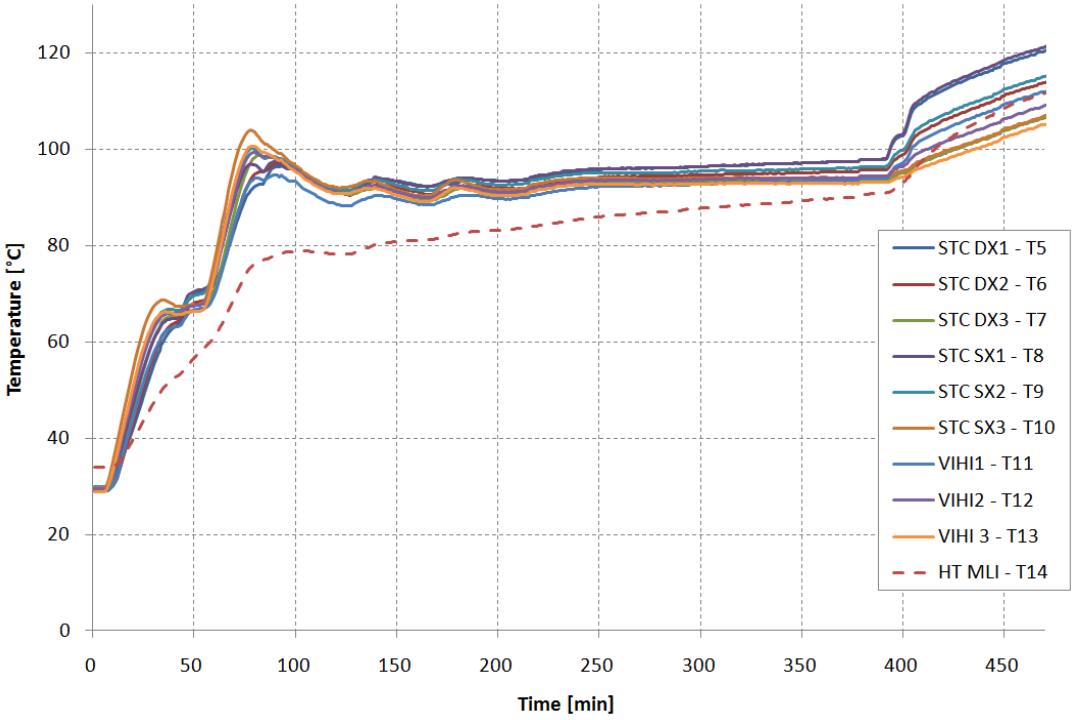

Fig. 4-22 Temperature profile of the baffle vanes (from T5 to T13) and of the internal surface of HT MLI (HT MLI - T14, dotted line) during hot case tests on STC – VIHI baffles unit

Looking at the previous graph, from 400 minute to the end of the test, temperature gradient between different baffle vanes increases, if compared with the gradient from 250 to 400 minute, since, at 375 minute, IR lamp set – point has been increased up to 350°C.

4.4.1.2 Test B – Cold case

During cold case, the following nominal test levels at thermal interfaces have been assured:

- Baffle bracket plate @ 18°C;
- Aluminum box (which represents S/C environment) @ 50°C;
- Cryostat temperature reached a medium value of -130°C during test.

Stability of 1°C/hr has been verified under these conditions during 2 hours.
The following table summarizes test levels for cold case simulations on STC – VIHI baffles unit:

Boundary surface	Temperature	Description
Baffle bracket plate	18°C	PT100 #3
Aluminum box	50°C	PT100 #4
Cryostat	-130°C	PT100 #18

Table 4-8 Test levels for cold case simulations on STC – VIHI baffles unit

The following graphs show the variation of the temperature of baffle bracket plate (BB – T3), aluminum box (S/C – T4), cryostat (CRIO – T18) during cold case simulation and the variation of the temperature detected by the sensors positioned on baffles vanes (from T5 to T13 in the graph,

represented with continuous line) and on HT MLI (HT MLI - T14 in the graph, represented with dotted line) respectively.

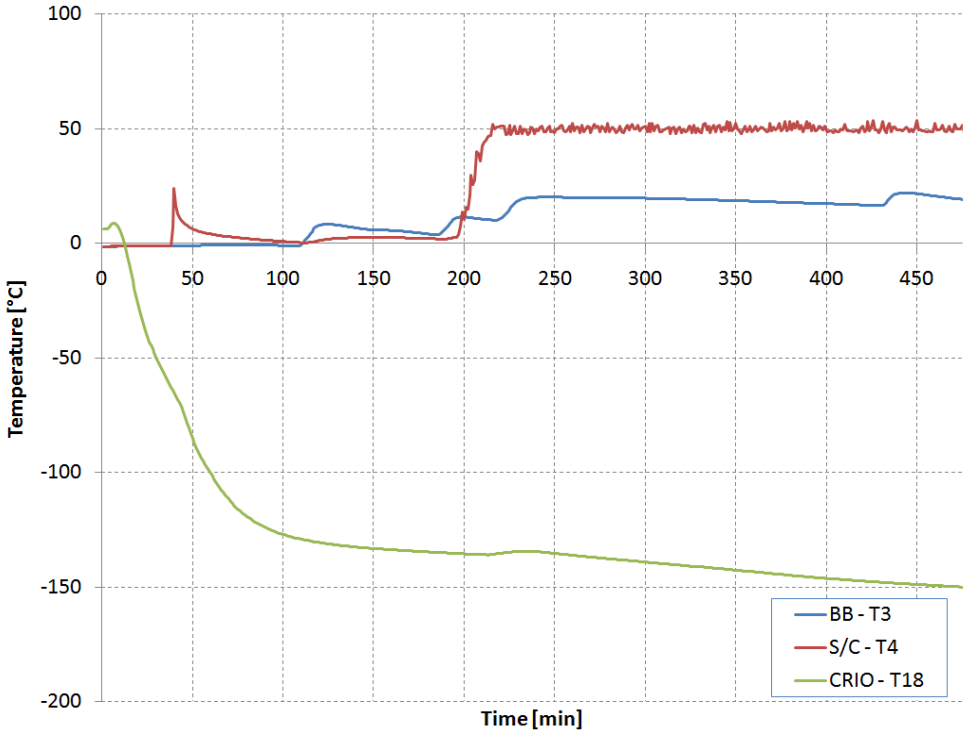

Fig. 4-23 Temperature profile of I/F at controlled temperature during cold case tests on STC – VIHI baffles unit: baffle bracket plate (BB - T3), aluminum box (S/C - T4) and cryostat (CRIO - T18)

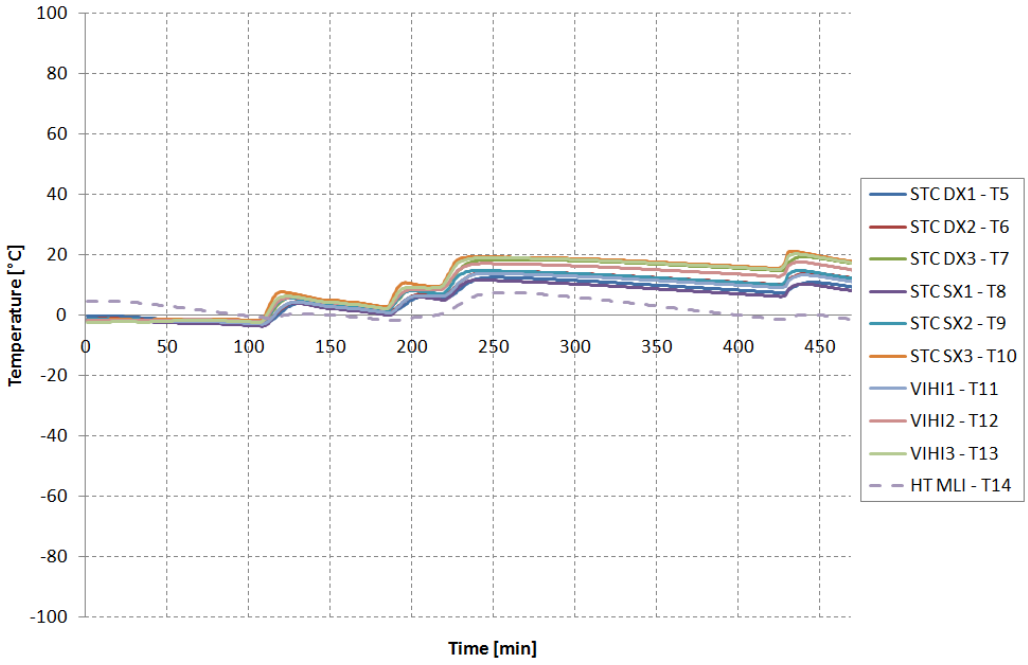

Fig. 4-24 Temperature profile of the baffle vanes (from T5 to T13) and of the internal surface of HT MLI (HT MLI - T14, dotted line) during cold case tests on STC – VIHI baffles unit.

4.4.2 Tests on Stavroudis baffle

Tests on HRIC baffle have been performed in 4 different steps: the first 3 tests refer to orbital hot case at Perihelion, the last one refers on orbital cold case at Perihelion.

Hot cases are different because of the imposed boundary conditions at controlled interfaces, as described below.

4.4.2.1 Test A – Hot case

During test A, the following nominal test levels have been assured:

- Baffle bracket plate @ 92°C;
- Aluminum box (which represents Stavroudis filter) @ 35°C;
- Hot source @ 220°C.

The following table summarizes test levels for test A on HRIC baffle unit:

Boundary surface	Temperature	Description
Baffle bracket plate	92°C	PT100 #3
Aluminum box	35°C	PT100 #4
Hot plate	220°C	PT100 #17

Table 4-9 Test levels for test A on HRIC baffle unit

The following graph shows the variation of the temperature of the hot plate (HOT PLATE – T17), the baffle bracket plate (BB – T3), the aluminum box (FILTER – T4) during simulation.

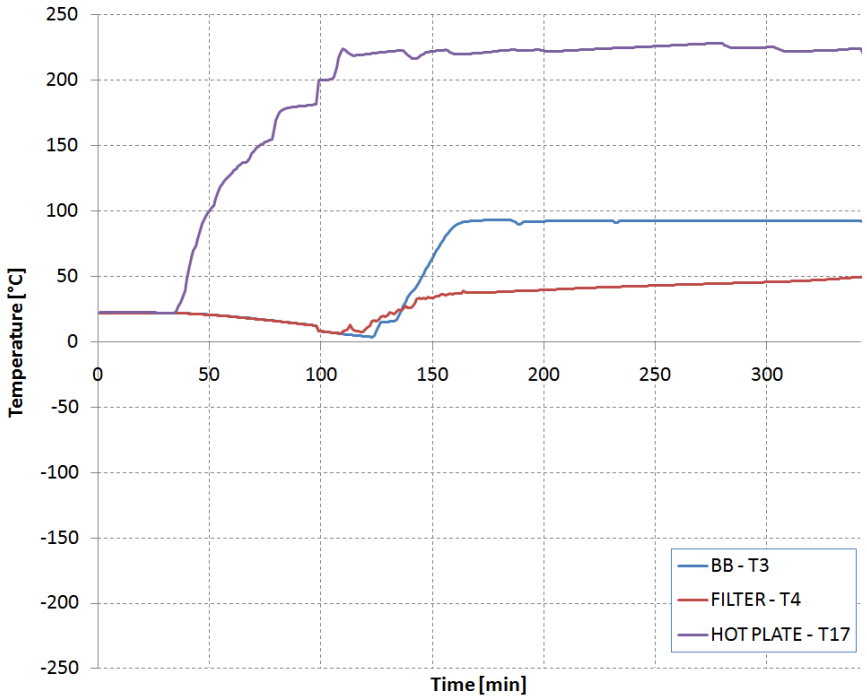

Table 4-10 Temperature profile of I/F at controlled temperature during test A – Hot case on HRIC baffle unit: hot plate (HOT PLATE - T17), baffle bracket plate (BB - T3) and aluminum box (FILTER - T4)

The next figure shows the temperature detected by the sensors positioned on the baffle (T5, T7, T8, T9, T10, T11, T12), on the internal surface of HT MLI (HT MLI - T14, represented with dotted line), on the baffle bracket plate (BB - T6 and BB - T13, represented with continuous green lines).

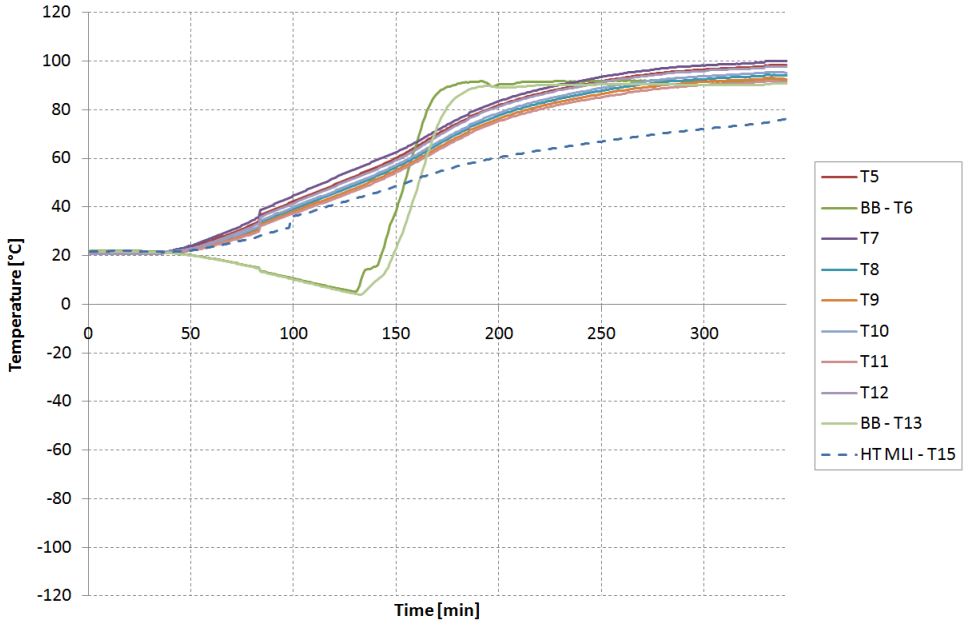

Fig. 4-25 Temperature profile of point of interest on baffle and internal surface of HT MLI (HT MLI - T15 – dotted line) during first hot case simulation on HRIC baffle; continuous green lines represent temperature of baffle bracket plate (BB – T6 and BB – T13)

4.4.2.2 Test B – Hot case

During test B, no boundary conditions inside instrumentation box have been fixed, in order to evaluate the free thermal evolution of Stavroudis baffle subjected to a stable heat source at 220°C. Therefore temperature stability of monitored points of interest along baffle has not been verified.
The following graph shows the variation of the temperature of the hot plate (HOT PLATE – T17), the baffle bracket plate (BB – T3), the aluminum box (FILTER – T4) during test B.

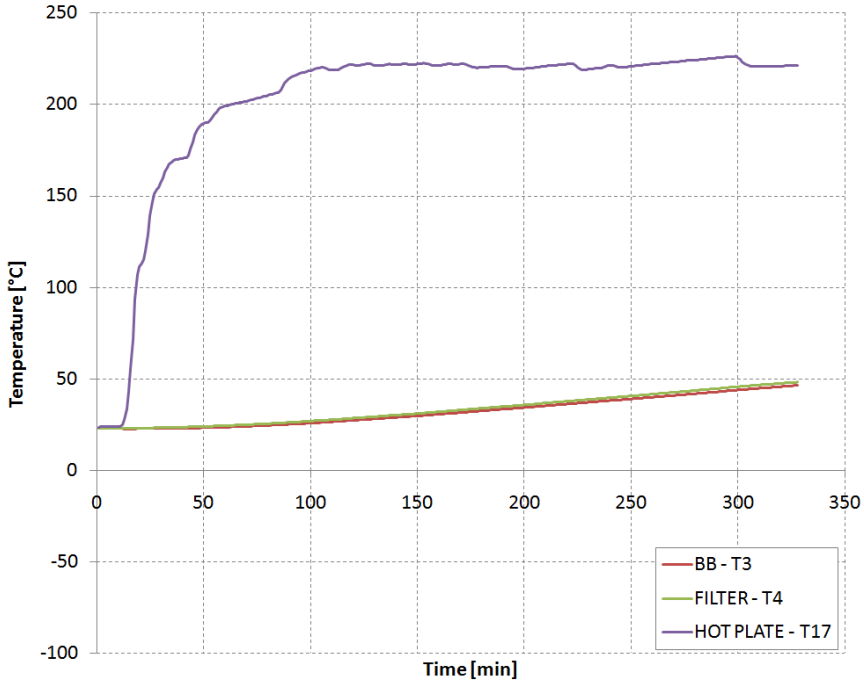

Fig. 4-26 Temperature profile of hot plate (HOT PLATE - T17), baffle bracket plate (BB - T3) and aluminum box (FILTER - T4) during test B – Hot case on HRIC baffle unit

The next figure shows the temperature detected by the sensors positioned on the baffle and other points of interest:

- Green continuous lines represents the temperature of the baffle bracket plate (BB - T6 and BB - T13 in the graph);
- Other continuous lines represent the temperature of points of interest along Stavroudis baffle (T5, T7, T8, T9, T10, T11, T12);
- Black dotted line represents the temperature of the internal surface of the external ring of Stavroudis baffle (EXT.RING - T14);
- Blue dotted line represents the temperature of the internal surface of the HT MLI (HT MLI - T15).

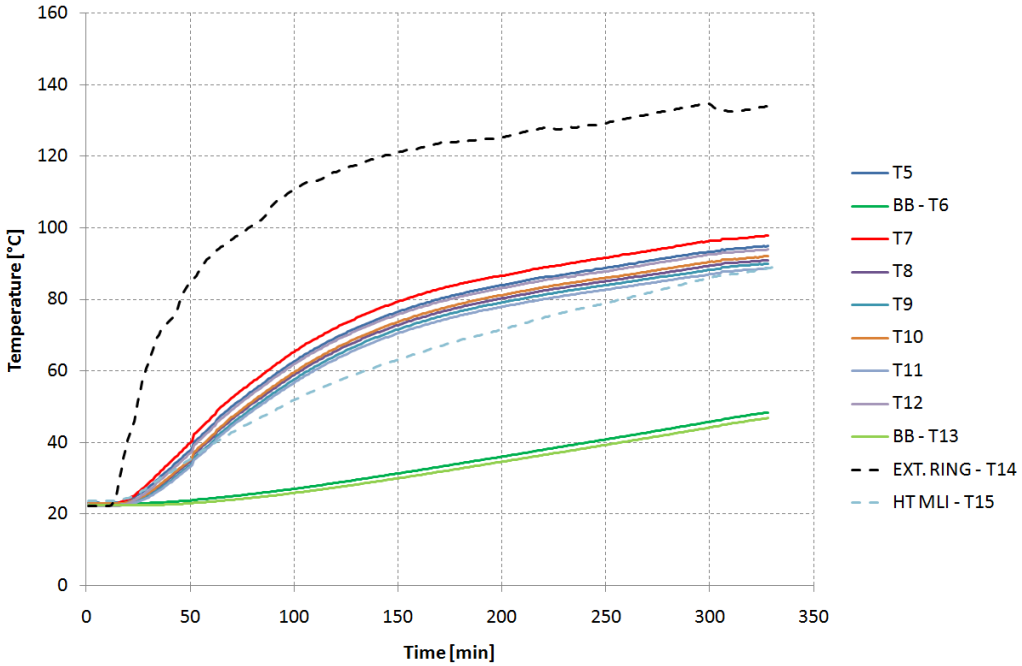

Fig. 4-27 Temperature profile of all point of interest along baffle (from T5 to T13, continuous lines) and internal surface of HT MLI (HT MLI - T15 – dotted line) during second hot case simulation on HRIC baffle; black dotted line (EXT.RING – T14) represents the temperature of the internal side of the external ring of the baffle

4.4.2.3 Test C – Hot case

During test C, the following nominal test levels have been assured:

- Baffle bracket plate @ 92°C;
- Aluminum box (which represents Stavroudis filter) @ 35°C;
- Hot source @ 310°C.

The following table summarizes test levels for test C on HRIC baffle unit:

Boundary surface	Temperature	Description
Baffle bracket plate	92°C	PT100 #3
Aluminum box	35°C	PT100 #4
Hot plate	310°C	PT100 #17

Table 4-11 Test levels for test C on HRIC baffle unit

The following graph shows the variation of the temperature of the hot plate (HOT PLATE – T17), the baffle bracket plate (BB – T3), the aluminum box (FILTER – T4) during the third hot case simulation.

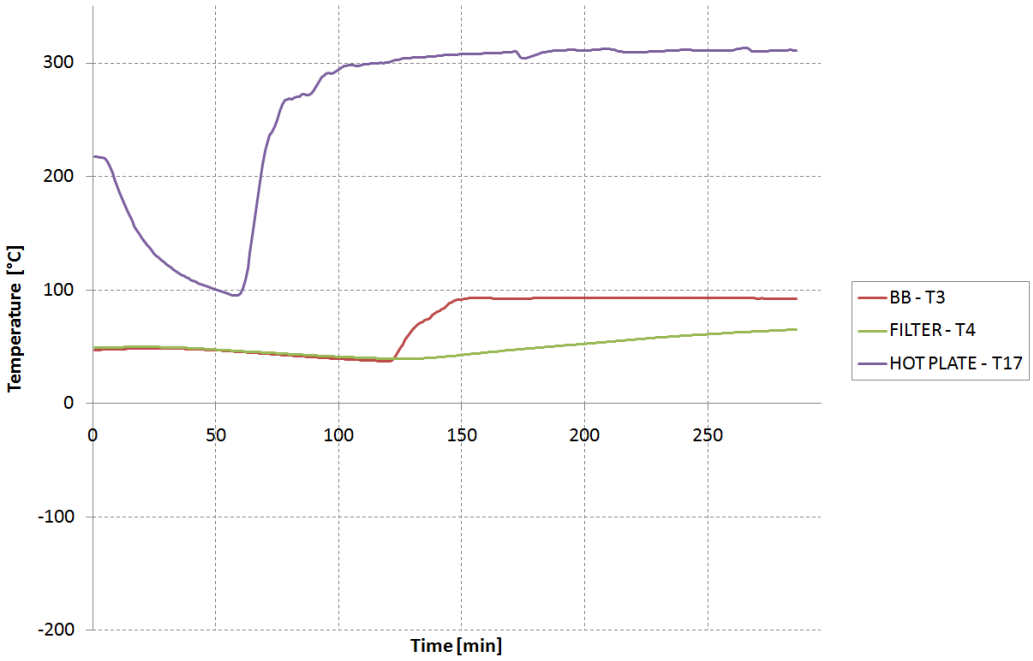

Fig. 4-28 Temperature profile of I/F at controlled temperature during test C – Hot case on HRIC baffle unit: hot plate (HOT PLATE - T17), baffle bracket plate (BB - T3), aluminum box (FILTER - T4)

The next figure shows the temperature detected by the sensors positioned on the baffle and other points of interest:

- Green continuous lines represents the temperature of the baffle bracket plate (BB - T6 and BB - T13 in the graph);
- Other continuous lines represent the temperature of points of interest along Stavroudis baffle (T5, T7, T8, T9, T10, T11, T12);
- Black dotted line represents the temperature of the internal surface of the external ring of Stavroudis baffle (EXT.RING - T14);
- Blue dotted line represents the temperature of the internal surface of the HT MLI (HT MLI - T15).

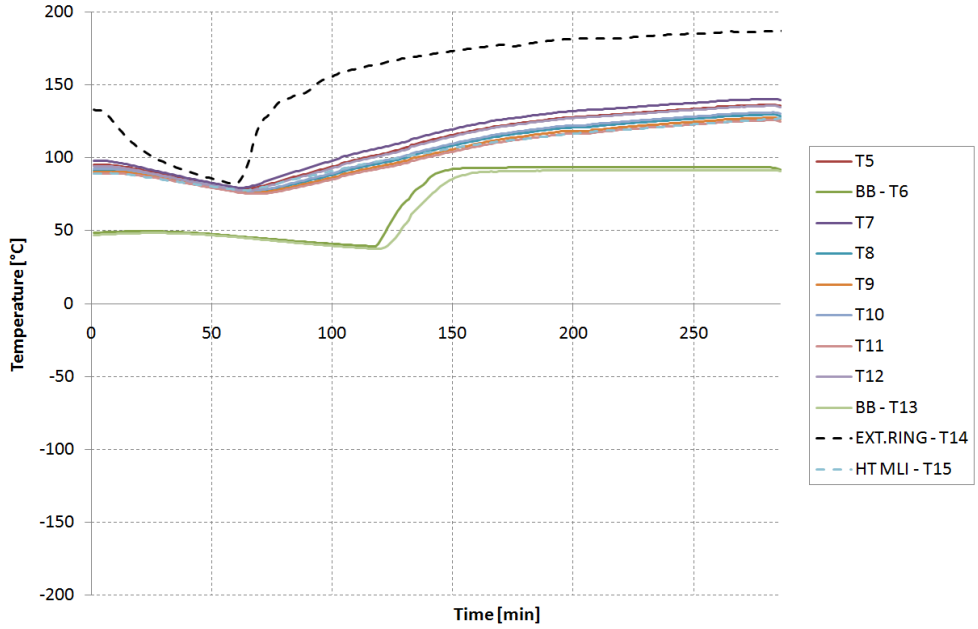

Fig. 4-29 Temperature profile of all point of interest along baffle (from T5 to T13, continuous lines) and internal surface of HT MLI (HT MLI - T15 – dotted line) during third hot case simulation on HRIC baffle; black dotted line (EXT.RING – T14) represents the temperature of the internal side of the external ring of the baffle

4.4.2.4 Test D – Cold case

During cold case, the following nominal test levels at interfaces have been assured:

- Baffle bracket plate @ 18°C;
- Aluminum box (which represents Stavroudis filter) @ 35°C;
- Cryostat temperature reached a stable value of -152°C during test.

Stability of 1°C/hr has been verified under these conditions during 2 hours.
The following table summarizes test levels for cold case simulations on HRIC baffle unit:

Boundary surface	Temperature	Description
Baffle bracket plate	18°C	PT100 #3
Aluminum box	35°C	PT100 #4
Cryostat	-152°C	PT100 #18

Table 4-12 Test levels for cold case simulations on HRIC baffle unit

The following graph shows the variation of the temperature of baffle bracket plate (BB – T3), aluminum box (FILTER – T4), cryostat (CRIO – T18) during simulation.

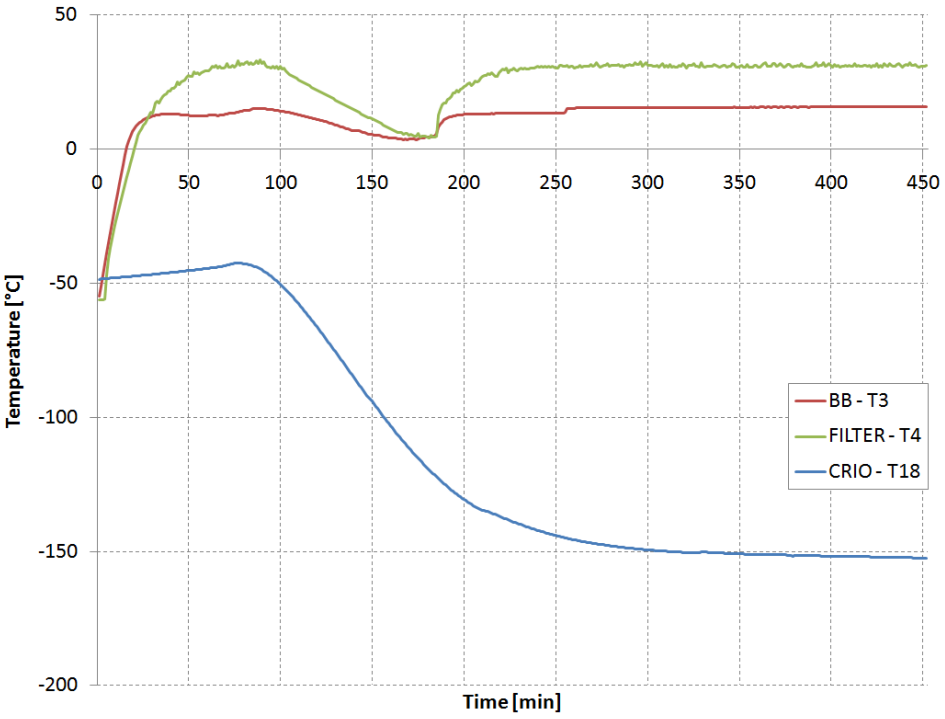

Fig. 4-30 Temperature profile of I/F at controlled temperature during cold case tests on HRIC baffle unit: baffle bracket plate (BB - T3), aluminum box (FILTER - T4) and cryostat (CRIO - T18)

The next figure shows the temperature detected by the sensors positioned on the baffle and other points of interest:

- Green continuous lines represents the temperature of the baffle bracket plate (BB - T6 and BB - T13 in the graph);
- Other continuous lines represent the temperature of points of interest along Stavroudis baffle (T5, T7, T8, T9, T10, T11, T12);
- Black dotted line represents the temperature of the internal side of the external ring of Stavroudis baffle (EXT.RING - T14);

- Blue dotted line represents the temperature of the internal surface of the HT MLI (HT MLI - T15).

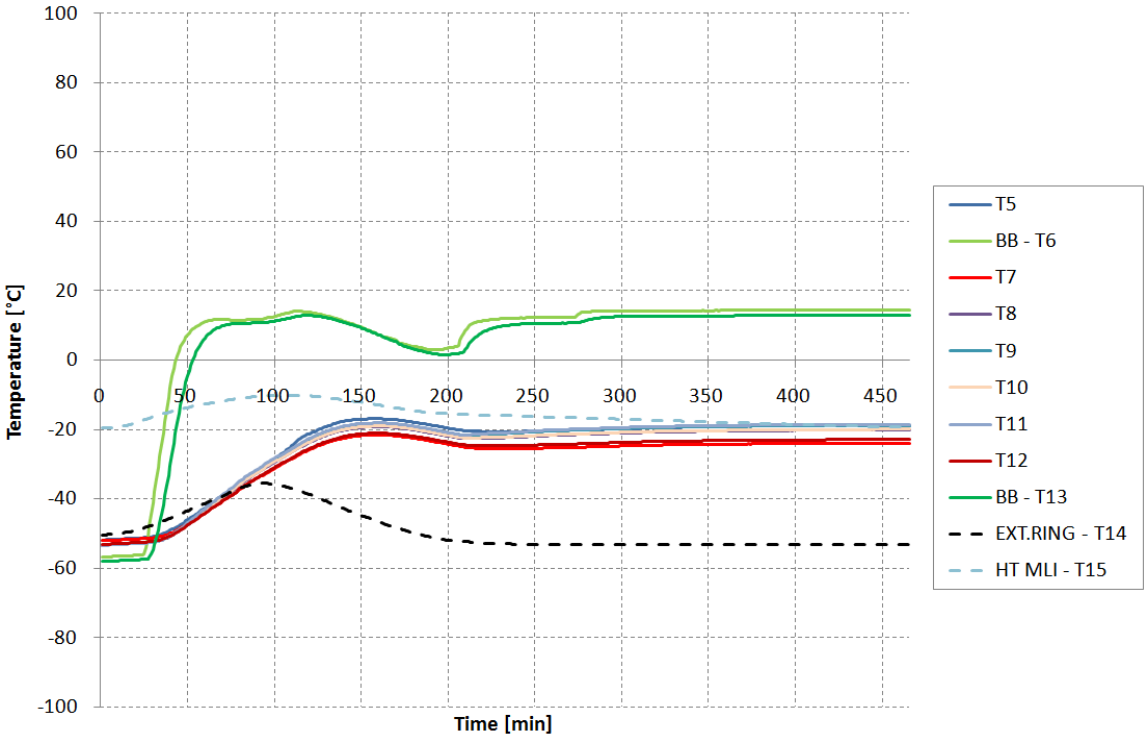

Fig. 4-31 Temperature profile of all point of interest along baffle (from T5 to T13, continuous lines) and internal surface of HT MLI (HT MLI - T15 – dotted line) during cold case simulation on HRIC baffle; black dotted line (EXT.RING – T14) represents the temperature of the internal side of the external ring of the baffle

5. Validation of the TMMs of the baffles STMs

5.1 Introduction

In this chapter the geometrical mathematical models (GMMs) of the test-beds, generated with ESATAN – TMS thermal suite, and the results of the thermal analyses are described; the results obtained numerically have been compared with the experimental results of the test campaign which took place at CISAS premises in September 2010 (and reported in the previous chapter), in order to validate the Thermal Mathematical Models (TMMs) of the STMs of the baffles. The following figure illustrates the correlation procedure: once the TMMs of the baffles have been defined (figure on the left) and test campaign has been performed (on the top), the TMM of the baffle is introduced inside the TMM of the test-bed, representative of the TVC and all thermal I/Fs inside it (figure on the right); the thermal analysis is performed, the numerical results obtained are compared with the experimental ones and modifications can be introduced in the original TMM in order to minimize the difference between the results.

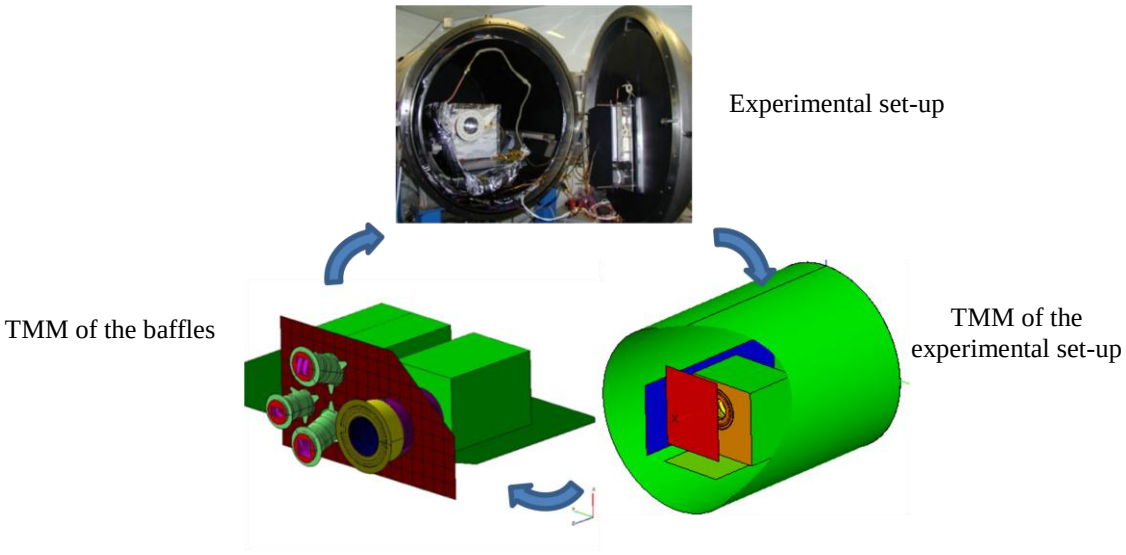

Fig. 5-1 Correlation process

In general, in numerical thermal simulations, the spacecraft and the thermal environment are simulated and approximated by means of a mathematical model, which is a dumped parameters model: the geometry is subdivided into several nodes, in which all the physical properties are suppose to be concentrated. The interconnections between couples of nodes depend on the thermal conductive (GL) and radiative (GR) couplings. The behavior of the network of nodes and the physical properties are described by means of a discrete set of coupled equations, in which the coefficients depend on the following parameters:

- Thermal capacity;
- Heat output;
- Heat input;

- Conductance between adjacent nodes (GL);
- Radiative exchanges between nodes (GR);
- Temperature, when it is a boundary condition.

As for finite difference methods, the system can be easily solved building a matrix which contains these coefficients and solving the associated linear system by means of iterative algorithms.
Once the system of equations is solved, the thermal results are obtained: they can be compared either with the requirements or with the experimental results; the model can be modified and new numerical simulations are performed.
In this section the thermal analysis steps are described in general:

- The thermal analysis starts with the complete description of the spacecraft or the system (e.g. the TVC) configuration, which is simplified and idealized: the geometrical model is composed by primitive shells, simple bi-dimensional or three-dimensional bodies. Shells are combined thanks to logic operations (such as sum or subtraction).
- Then the thermal-optical properties are assigned to each surface and the material properties are assigned to each body.
- The system is meshed into a convenient number of nodes.
- A radiative case is generated: it includes all the information regarding the mission, such as orbital parameters, and, in general, the spacecraft orientation and position respect to the heat sources. In this phase the computational accuracy can be set.
- View factors (VFs) or radiative exchange factors (REFs) computation, by means of Monte Carlo ray-tracing technique.
- Computation of the conductive links (GLs) between adjacent nodes.
- Computation of the heat fluxes (HFs) incoming from the environment and due to the radiation, such as solar, albedo and planetary fluxes, by means of ray-tracing techniques.
- The mathematical model, which includes the information about the view factors, the radiative exchange factors, the thermal conductive and radiative couplings, is solved. The obtained results can then visualized and interpreted (post-processing phase).

The following block diagram summarizes the followed approach in thermal analyses.

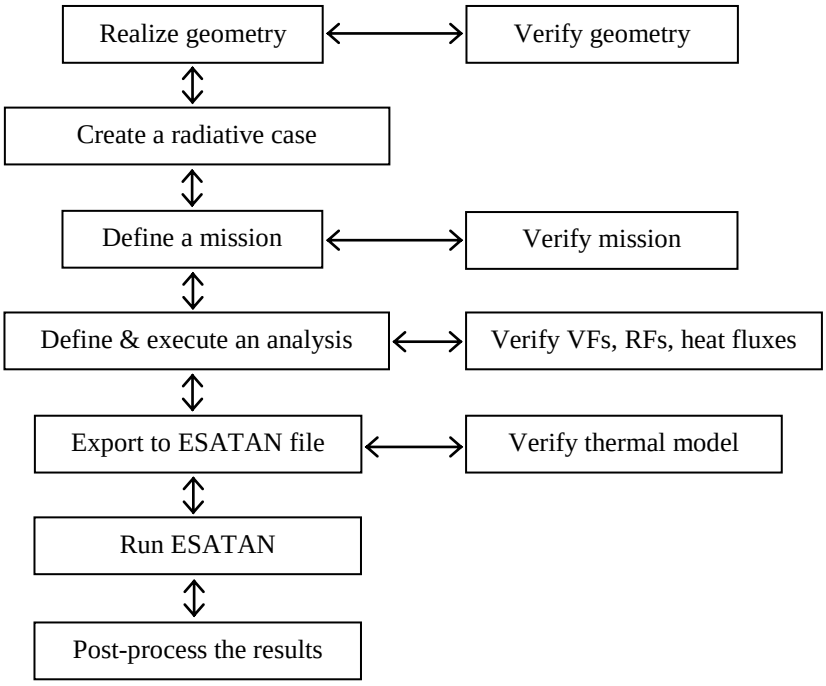

Fig. 5-2 Thermal analysis phases

5.2 Validation of the Thermal Mathematical Models of the STMs of STC – VIHI baffles

5.2.1 Introduction

In this section the correlation between the results of the thermal analysis on STC-VIHI baffles set-up and the experimental results, obtained during the test campaign, is reported.
The following thermal models have been produced:

- Geometrical Mathematical Model (GMM) of the test set-up for the radiative exchange factors (GRs) computation;
- Thermal Mathematical Model (TMM) in ESATAN format, for the thermal analysis execution.

During the test campaign two main steady – state conditions have been simulated inside the TVC: a hot case steady - state condition, by means of IR lamps, and a cold case steady - state condition, by means of a cold plate cooled by liquid Nitrogen. The test object (STC and VIHI baffles) has been placed inside an instrumentation box covered by HT-MLI and fixed on an Aluminum plate (which represents the baffle bracket plate) at controlled temperature, depending on the case which has been simulated. An aluminum box situated behind the aluminum plate represents the thermal environment of the S/C. In the figures below the instrumentation box for STC-VIHI baffles unit with the internal thermal I/Fs is shown.

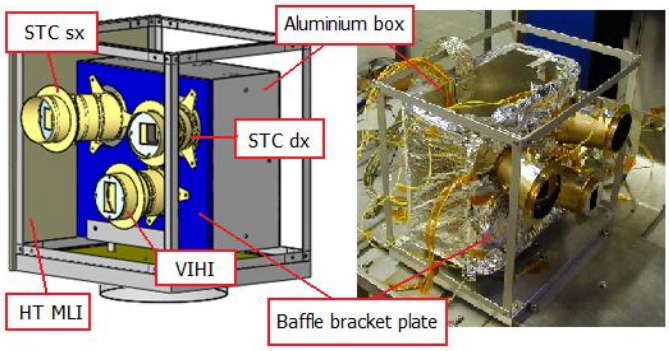

Fig. 5-3 Thermal I/Fs inside the instrumentation box (on the left) and STC - VIHI baffles unit during assembling operations (on the right).

5.2.2 Thermal cases

5.2.2.1 Hot case test levels and experimental results

During hot case simulation the following values have been assured on the thermal I/Fs with a stability of at least 1°C/hr for at least 2 hours:

- IR lamps @ about 220°C: this imposed value allows to obtain an incident flux on the frontal side of the instrumentation box equivalent to the maximum incident planetary heat flux at Perihelion (4496.1 W/m^2), employing a set of 4 IR lamps with a surface mean temperature of 417°C and a heat flux on a reference surface of 17 kW/m^2.
- Baffle bracket plate @ about 92°C, which is the maximum nominal value of the baffle bracket plate temperature (taking into account the ±12°C accuracy in temperature determination with TMM), reached with the S/C orbiting above Mercury illuminated surface at Perihelion.
- A cold plate (cryostat) @ about -6.8°C has been conductively connected to the baffle bracket plate and to the aluminum box by means of copper braids, in order to control the temperature of these I/Fs.

- In these conditions, the aluminum box reached a steady state value of about 85 °C.

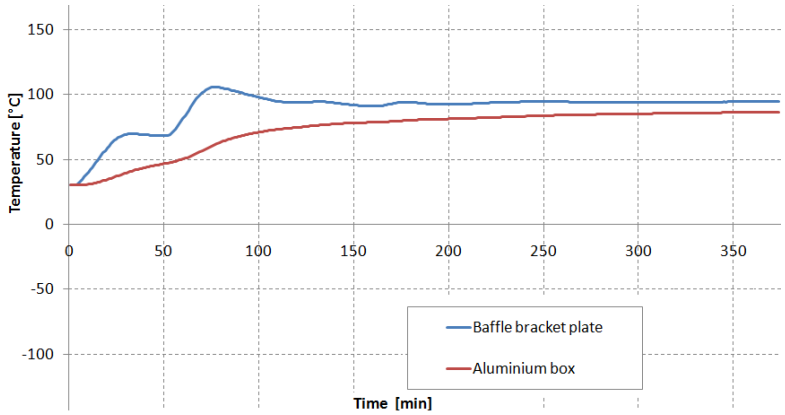

Fig. 5-4 Temperature profile of thermal I/Fs during hot case simulation on STC-VIHI baffles unit (baffle bracket plate and aluminum box)

The following graph shows the temperature of relevant points on the baffles surfaces and on the internal surface of the HT MLI.

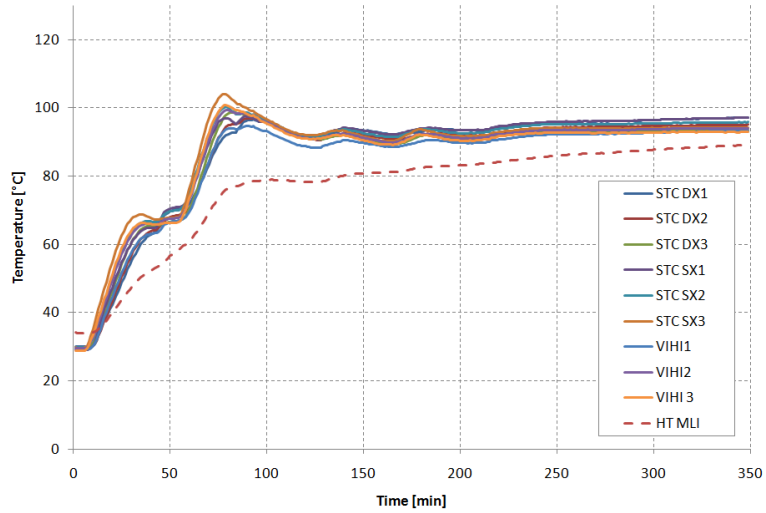

Fig. 5-5 Temperature profile of points of interest on the baffles and on the internal surface of the HT MLI during hot case simulation on STC-VIHI baffles.

5.2.2.2 Cold case test level and experimental results

During cold case simulation the following values have been assured on the thermal I/Fs with a stability of at least 1°C/hr for at least 2 hours:

- Cold plate @ about -140°C, which has been the minimum reachable value during simulations.
- Baffle bracket plate @ about 18°C, which is the minimum nominal value of the baffle bracket plate temperature (taking into account the ±12°C accuracy in temperature determination with TMM), reached with the S/C orbiting above Mercury cold surface at Perihelion.
- Aluminum box @ about 50°C, which is the temperature of the radiative thermal environment of the S/C.

The following graph summarizes the imposed test level.

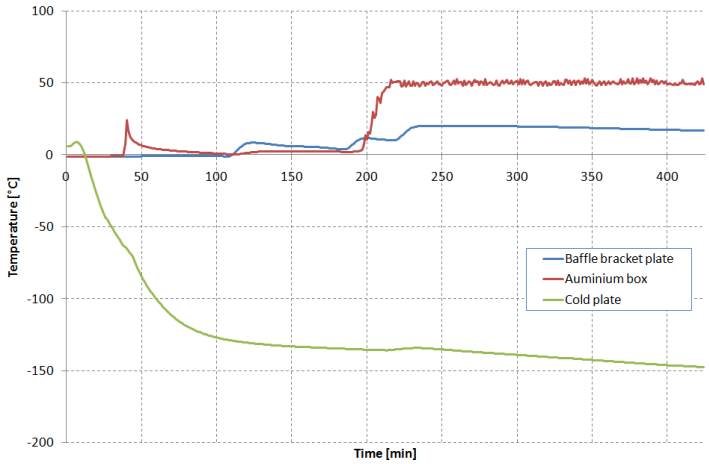

Fig. 5-6 Temperature profile of thermal I/Fs during cold case simulation on STC-VIHI baffles unit (cold plate, baffle bracket plate and aluminum box).

The following graph shows the temperature of relevant points on the baffles surfaces and on the internal surface of the HT MLI.

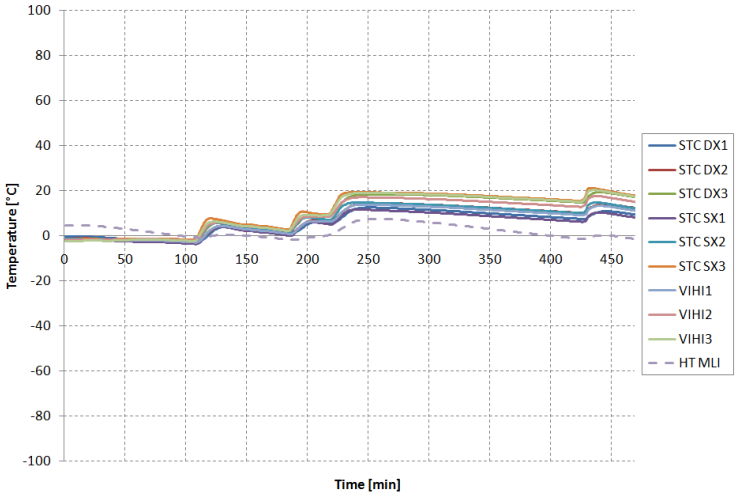

Fig. 5-7 Temperature profile of points of interest on the baffles and on the internal surface of the HT MLI during hot case simulation on STC-VIHI baffles.

5.2.3 Description of the set-upTMMs

Since two different steady – state experimental simulations have been carried on, two different thermal cases have been analyzed. The GMMs are different for each thermal case and are described in the following paragraph.

5.2.3.1 Nodal breakdown thermo-optical properties

The proposed TMM of the experimental set – up has been carried out according to the following approach:

- It is representative of all thermal I/Fs (both radiative and conductive) included inside the TVC used during the test campaign.
- All the structural parts have been simplified as much as possible.
- Once all thermal and mechanical I/Fs inside the TVC have been modeled, the TMM of the baffles has been included inside the model.
- Adjacent nodes presenting low thermal differences have been merged into one single node.

In the following figure the GMM and the node numbering are shown: the GMM represents all thermal and mechanical I/Fs which have been used during hot case and cold case simulations.

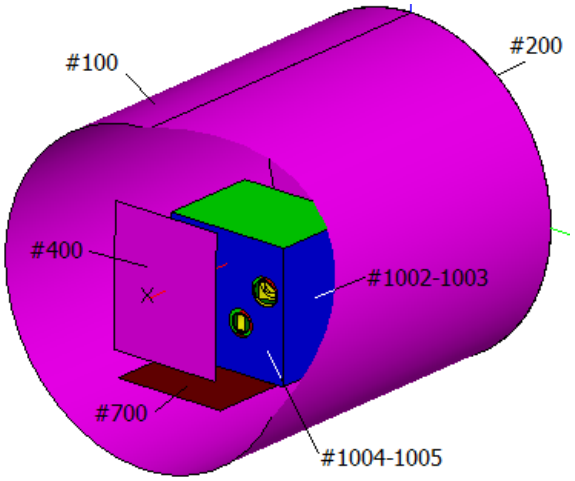

Fig. 5-8 Overall of the GMM for the hot and the cold case simulations

The following figures show the instrumentation box covered by HT MLI and standard MLI with the baffles inside it.
Internally also the baffle bracket plate (node #60800) and the aluminum box (nodes #1100 – 1900) are visible.

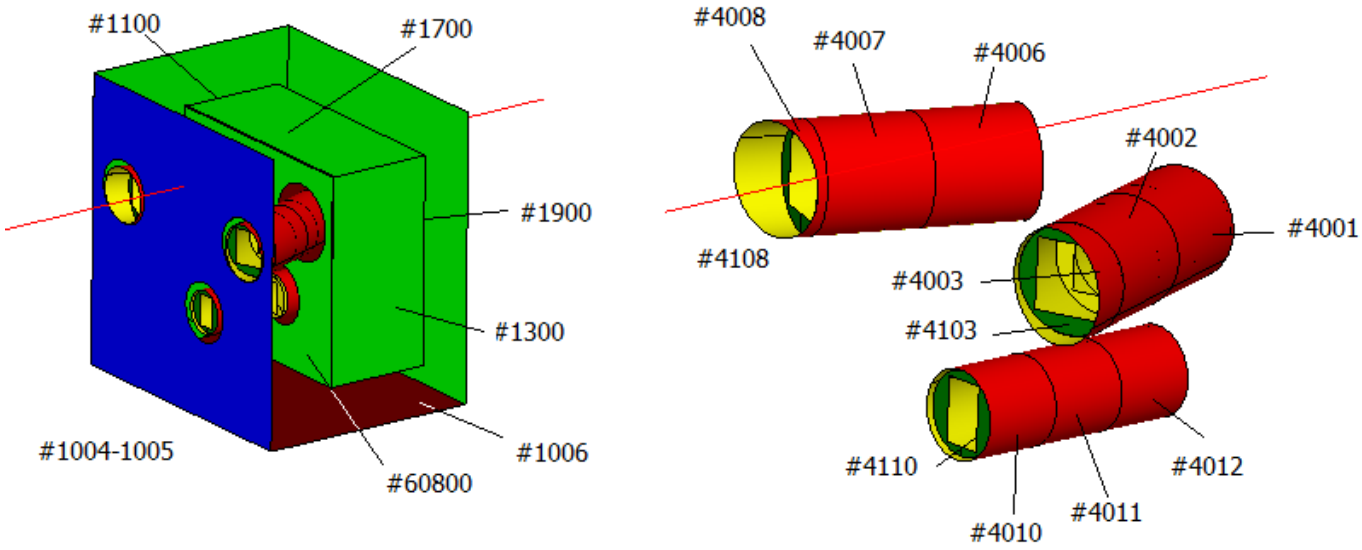

Fig. 5-9 Nodes numbering of the instrumentation box and STC-VIHI baffles

The following table reports a list of the nodes, specifying the material and the optical properties for each node. Node #400 represents the IR lamps in the hot case simulation (*), the cold plate in the cold case simulation (**).

Node	Type	Name	Material	Thermal finish	α_S	ρ_S^D	ρ_S^S	ε_{IR}	ρ_{IR}^D	ρ_{IR}^S
100	D	Cryostat	AISI 316	Black	1.00	0.00	0.00	1.00	0.00	0.00
200	D	Cryostat	AISI 317	Black	1.00	0.00	0.00	1.00	0.00	0.00
300	D*/B**	Cryostat	AISI 318	Black	1.00	0.00	0.00	1.00	0.00	0.00
400	B D	Hot plate* Cold plate**	Aluminum Aluminum	Black Black	1.00	0.00	0.00	1.00	0.00	0.00
700	D	Base plate	Aluminum	Rough Aluminum	0.15	0.85	0.00	0.03	0.97	0.00

1000	D	Lat1 instr. Box ext.	//	HT MLI	0.23	0.39	0.39	0.87	0.07	0.07
1001	D	Lat1 instr. Box int.	//	STD MLI	0.50	0.25	0.25	0.04	0.48	0.48
1002	D	Lat2 instr. Box int.	//	STD MLI	0.50	0.25	0.25	0.04	0.48	0.48
1003	D	Lat2 instr. Box ext.	//	HT MLI	0.23	0.39	0.39	0.87	0.07	0.07
1004	D	Front instr. Box int.	//	STD MLI	0.50	0.25	0.25	0.04	0.48	0.48
1005	D	Front instr. Box ext.	//	HT MLI	0.23	0.39	0.39	0.87	0.07	0.07
1006	D	Bottom instr. Box	Aluminum	Rough Aluminum	0.15	0.85	0.00	0.03	0.97	0.00
1008	D	Top instr. Box ext.	//	STD MLI	0.50	0.25	0.25	0.04	0.48	0.48
1009	D	Top instr. Box int.	//	STD MLI	0.50	0.25	0.25	0.04	0.48	0.48
1010	D	Back instr. Box ext	//	STD MLI	0.50	0.25	0.25	0.04	0.48	0.48
1011	D	Back instr. Box int	//	STD MLI	0.50	0.25	0.25	0.04	0.48	0.48
4001-4003	D	STC baffle DX	Aluminum 7075	Alodine	0.35	0.65	0.00	0.15	0.85	0.00
				Anodized Al	0.90	0.10	0.00	0.80	0.20	0.00
4101-4103	D	STC baffle vanes DX	//	Polished	0.12	0.00	0.88	0.05	0.00	0.95
				Anodized Al	0.90	0.10	0.00	0.80	0.20	0.00
4006-4008	D	STC baffle SX	Aluminum 7075	Alodine	0.35	0.65	0.00	0.15	0.85	0.00
				Anodized Al	0.90	0.10	0.00	0.80	0.20	0.00
4106-4108	D	STC baffle vanes SX	//	Polished	0.12	0.00	0.88	0.05	0.00	0.95
				Anodized Al	0.90	0.10	0.00	0.80	0.20	0.00
4010-4012	D	VIHI baffle	Aluminum 7075	Alodine	0.35	0.65	0.00	0.15	0.85	0.00
				Anodized Al	0.90	0.10	0.00	0.80	0.20	0.00
4110-4112	D	VIHI baffle vanes	//	Polished	0.12	0.00	0.88	0.05	0.00	0.95
				Anodized Al	0.90	0.10	0.00	0.80	0.20	0.00
60800	B	Baffle bracket plate	Aluminum	STD MLI	0.50	0.25	0.25	0.04	0.48	0.48
1100	D	Lat1 Al. Box	Aluminum	STD MLI	0.50	0.25	0.25	0.04	0.48	0.48
				Rough Aluminum	0.15	0.85	0.00	0.03	0.97	0.00
1300	D	Lat1 Al. Box	Aluminum	STD MLI	0.50	0.25	0.25	0.04	0.48	0.48
				Rough Aluminum	0.2	0.9	0	0	0.97	0
1500	D	Bottom Al. Box	Aluminum	STD MLI	0.50	0.25	0.25	0.04	0.48	0.48
				Rough Aluminum	0.15	0.85	0.00	0.03	0.97	0.00
1700	D	Top Al. Box	Aluminum	STD MLI	0.50	0.25	0.25	0.04	0.48	0.48
				Rough Aluminum	0.2	0.9	0	0	0.97	0
1900	B	Back Al. Box	Aluminum	STD MLI	0.50	0.25	0.25	0.04	0.48	0.48
				Rough Aluminum	0.15	0.85	0.00	0.03	0.97	0.00
99998	X	Inactive node	//	//	//	//	//	//	//	//
99999	B	Environment	//	//	//	//	//	//	//	//

Table 5-1 Node list and surface properties.

The following table shows a list of the materials used in the TMM.

Material	ρ [kg/m^3]	c_p [J/kg K]	λ [W/mK]
Rough Al	2800	850	130
Al7075	2801	829.45	170
AISI 316	8030	504	16.3

Table 5-2 materials properties

5.2.3.2 Conductive thermal couplings

In this paragraph two tables describe the conductive thermal couplings between each couple of nodes. The first one refers to the hot case, the second one to the cold case.

Node i	Node j	GL[W/K]	Node i	Node j	GL[W/K]
4110	4111	0.33882	4111	60800	0.5
4111	4112	0.33882	4101	60800	0.5
4106	4107	0.51867	4106	60800	0.5
4107	4108	0.95412	1900	1500	0.3059
4101	4102	0.51867	1900	1300	0.0217
4102	4103	0.95412	1900	1100	0.0217
4001	4101	1000.0	1100	1500	0.0217
4002	4102	1000.0	1300	1500	0.0217
4003	4103	1000.0	60800	1500	0.159
4006	4106	1000.0	1006	700	7.8871
4007	4107	1000.0	1002	1003	0.003569
4008	4108	1000.0	1000	1001	0.003569
4010	4110	1000.0	1008	1009	0.002003
4011	4111	1000.0	1010	1011	0.002595
4012	4112	1000.0	1004	1005	0.004045

Table 5-3 Hot case – internal conductive couplings

Node i	Node j	GL[W/K]	Node i	Node j	GL[W/K]
4110	4111	0.33882	4101	60800	0.5
4111	4112	0.33882	4106	60800	0.5
4106	4107	0.51867	300	400	8.5167
4107	4108	0.95412	1900	1500	0.3059
4101	4102	0.51867	1900	1300	0.0217
4102	4103	0.95412	1900	1100	0.0217
4001	4101	1000.0	1100	1500	0.0217
4002	4102	1000.0	1300	1500	0.0217
4003	4103	1000.0	60800	1500	0.159
4006	4106	1000.0	1006	700	7.8871
4007	4107	1000.0	1002	1003	0.003569
4008	4108	1000.0	1000	1001	0.003569
4010	4110	1000.0	1008	1009	0.002003
4011	4111	1000.0	1010	1011	0.002595
4012	4112	1000.0	1004	1005	0.004045
4111	60800	0.5			

Table 5-4 Cold case – internal conductive couplings

5.2.4 Numerical results

5.2.4.1 Hot case results

In the table below the main results of the thermal analysis are shown and compared with the experimental ones.

Node	Name	Type	Experimental [°C]	Model [°C]	Δ [°C]
4003	STC dx 1	D	97.5	99.2	-1.7
4002	STC dx 2	D	95.3	98.5	-3.2
4001	STC dx 3	D	93.5	96.5	-3.0
4008	STC sx 1	D	97.4	99.4	-2.0
4007	STC sx 2	D	96.0	98.7	-2.7
4006	STC sx 3	D	94.1	96.6	-2.5
4010	VIHI 1	D	93.5	96.2	-2.7
4011	VIHI 2	D	94.1	95.4	-1.3
4012	VIHI 3	D	93.0	95.4	-2.4
1004	HT MLI int.	D	90.0	95.9	-5.9
60800	Baffle bracket plate	B	94.3	94.3	0.0
1900	Al box	B	84.4	84.4	0.0
300	Cryostat	B	-6.8	-6.8	0.0
400	IR lamps	B	220.0	220.0	0.0

Table 5-5 Hot case – Comparison between experimental results and numerical results

From the previous tables it can be noticed that the maximum difference between experimental and numerical results appears on the 2nd vane of STC baffle on the right and is equal to -3.2 °C.
Fig. 5-22 and Fig. 5-23 show the temperature profile for each node of the model of the experimental set – up and the nodal thermal distribution on the STMs of the baffles.

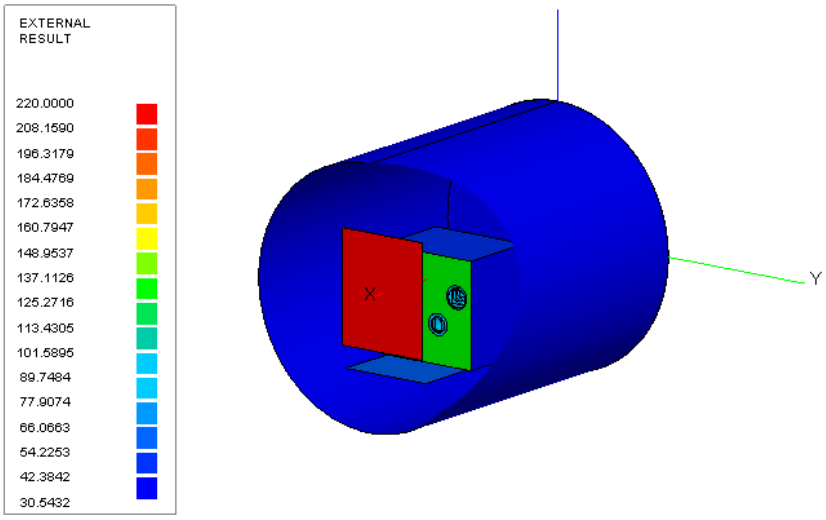

Fig. 5-10 Temperature profile of the mechanical and thermal I/Fs inside the TVC

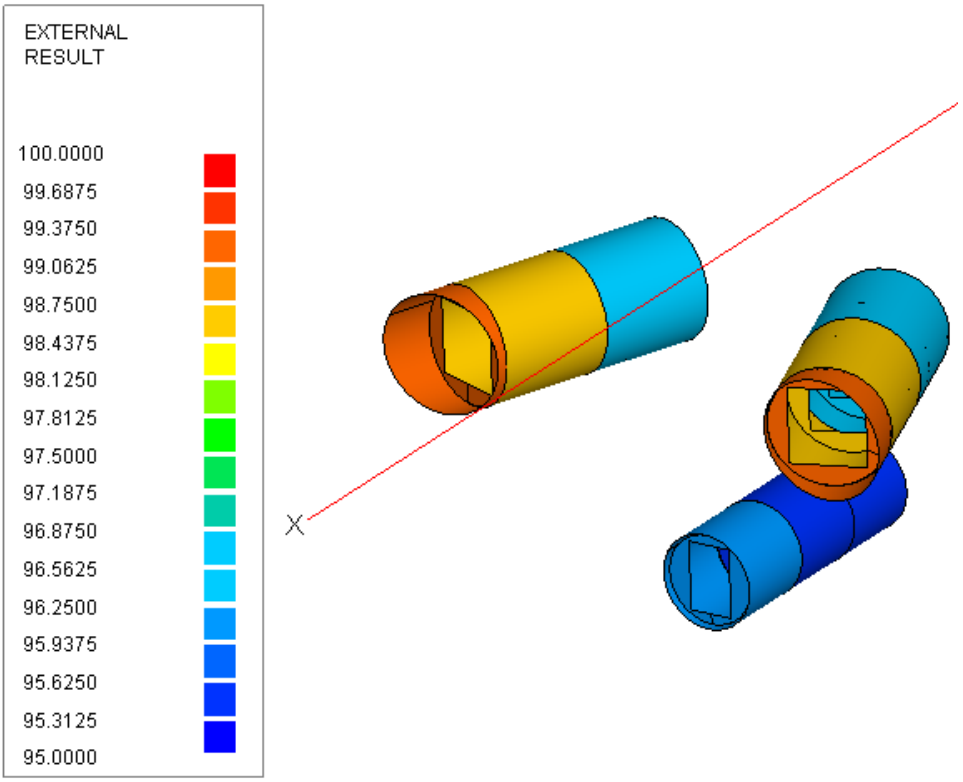

Fig. 5-11 Temperature of STC and VIHI baffles

5.2.4.2 Cold case results

In the following table the main results of the thermal analysis are compared with the experimental ones.

Node	Name	Type	Experimental [°C]	Model [°C]	Δ [°C]
4003	STC dx 1	D	10.4	15.5	-5.1
4002	STC dx 2	D	12.8	16.0	-3.1
4001	STC dx 3	D	17.2	17.4	-0.2
4008	STC sx 1	D	10.3	15.5	-5.2
4007	STC sx 2	D	12.8	16.0	-3.1
4006	STC sx 3	D	17.9	17.4	0.5
4010	VIHI 1	D	11.9	17.1	-5.2
4011	VIHI 2	D	15.4	18.1	-2.7
4012	VIHI 3	D	17.6	18.3	-0.7
60800	Baffle bracket plate	B	18.8	18.8	0.0
1900	Al box	B	50.1	50.1	0.0
300	Cryostat	B	-141.2	-141.2	0.0

Table 5-6: Cold case - Comparison between experimental results and numerical results

From the previous tables it can be noticed that the maximum difference between experimental and numerical results appears on the 1st vane of STC baffle on the left and is equal to -5.2 °C.
The following figures show the temperature profile for each node of the model of the experimental set – up and the nodal thermal distribution on the STMs of the baffles.

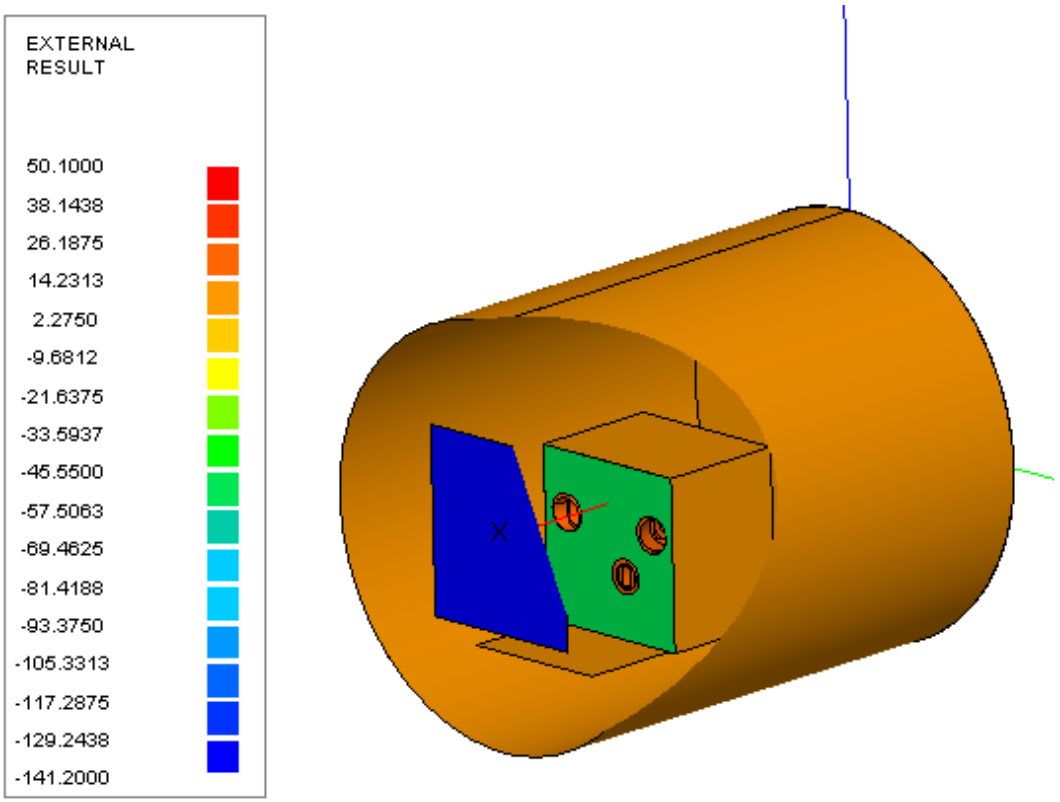

Fig. 5-12: Temperature profile of the mechanical and thermal I/Fs inside the TVC

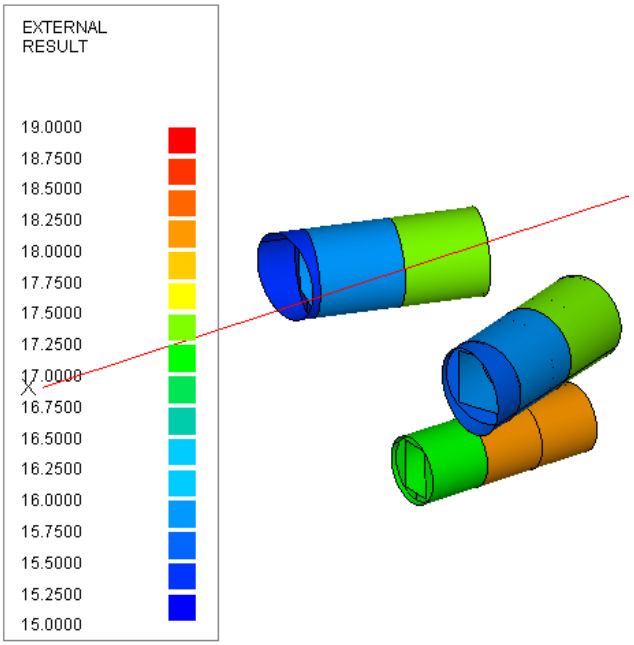

Fig. 5-13: Temperature of STC and VIHI baffles

5.3 Validation of the Thermal Mathematical Models of the STM of Stavroudis baffle

5.3.1 Introduction

In this section the correlation between the results of the thermal analysis on Stavroudis baffle set-up and the experimental results, obtained during the test campaign, is reported.
The following thermal models have been produced:

- Geometrical Mathematical Model (GMM) of the test set-up for the radiative exchange factors (GRs) computation;
- Thermal Mathematical Model (TMM) in ESATAN format, for the thermal analysis execution.

During the test campaign two main steady – state conditions have been simulated inside the TVC: a hot case steady - state condition, by means of a hot plate heated up by IR lamps, and a cold case steady - state condition, by means of a cold plate cooled by liquid Nitrogen. The test object (Stavroudis baffle) has been placed inside an instrumentation box covered by HT-MLI and fixed on an Aluminum plate (which represents the baffle bracket plate) at controlled temperature, depending on the case which has been simulated. An aluminum box situated behind the aluminum plate represents HRIC filter placed behind the Stavroudis baffle.

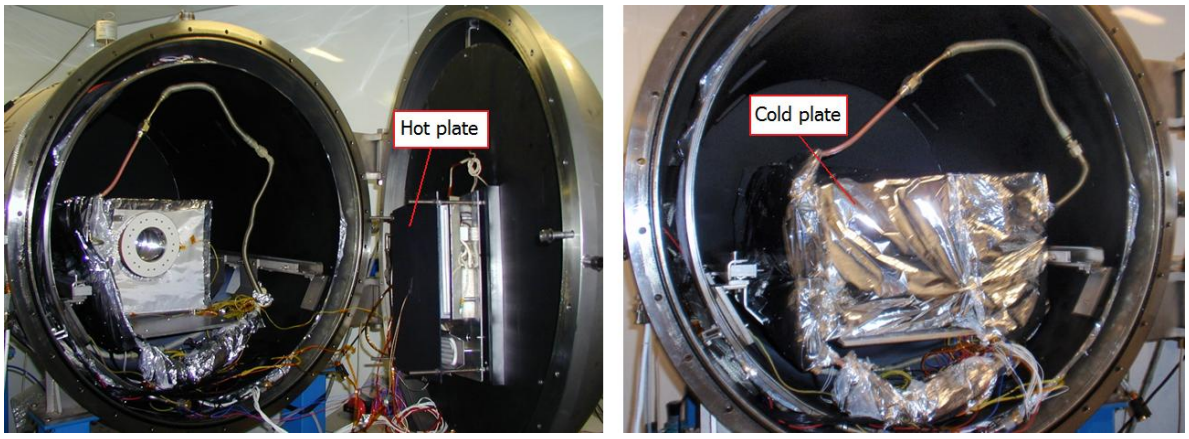

Fig. 5-14: HRIC baffle set – up inside TVC before hot case and cold case simulations

In the figures below the instrumentation box for HRIC baffle unit with the internal thermal I/Fs is shown.

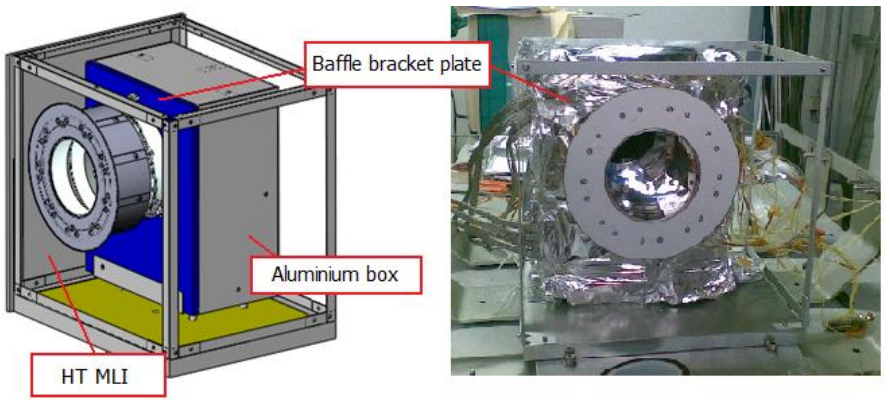

Fig. 5-15: Thermal I/Fs inside the instrumentation box and HRIC baffle unit during assembling operations

5.3.2 Thermal cases

5.3.2.1 Hot case test level and experimental results

During hot case simulation the following values have been assured on the thermal I/Fs with a stability of at least 1°C/hr for at least 2 hours:

- Hot plate @ about 220°C: this imposed value allows to obtain an incident flux on the frontal side of the instrumentation box equivalent to the maximum incident planetary heat flux at Perihelion (4496.1 W/m^2), employing a set of 4 IR lamps with a surface mean temperature of 417°C and a heat flux on a reference surface of 17 kW/m^2.
- Baffle bracket plate @ about 92°C, which is the maximum nominal value of the baffle bracket plate temperature (taking into account the ±12°C accuracy in temperature determination with TMM), reached with the S/C orbiting above Mercury illuminated surface at Perihelion.
- A cold plate @ about -178°C has been conductively connected to the baffle bracket plate and to the aluminum box by means of copper braids, in order to control the temperature of these I/Fs.

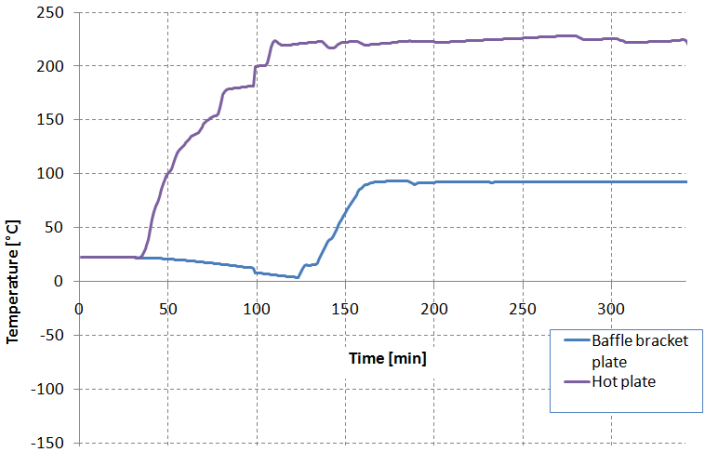

Fig. 5-16: Temperature profile of thermal I/Fs during hot case simulation on HRIC baffle unit (hot plate and baffle bracket plate)

The following graph shows the temperature of relevant points on the baffle surface, on the internal surface of the HT MLI, on the aluminum box.

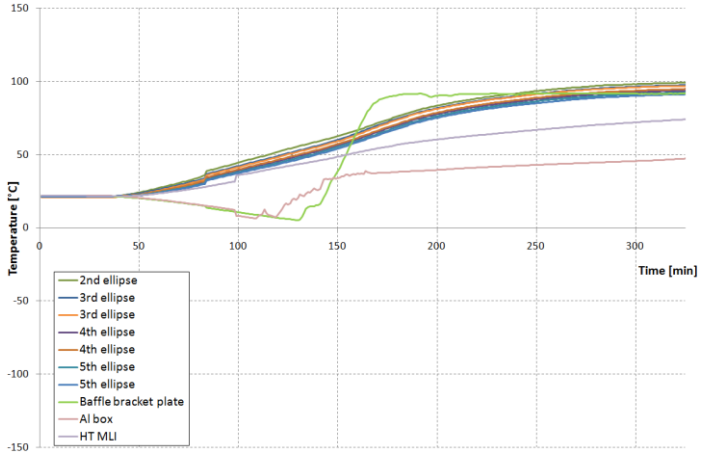

Fig. 5-17: Temperature profile of points of interest on the baffle, on the internal surface of the HT MLI and on the aluminum box during hot case simulation on HRIC baffle

5.3.2.2 Cold case test level and experimental results

During cold case simulation the following values have been assured on the thermal I/Fs with a stability of at least 1°C/hr for at least 2 hours:

- Cold plate @ about -152°C, which has been the minimum reachable value during simulations.
- Baffle bracket plate @ about 18°C, which is the minimum nominal value of the baffle bracket plate temperature (taking into account the ±12°C accuracy in temperature determination with TMM), reached with the S/C orbiting above Mercury cold surface at Perihelion.
- Aluminum box @ about 35°C, which is the temperature of the BK7 filter behind HRIC baffle at Perihelion.

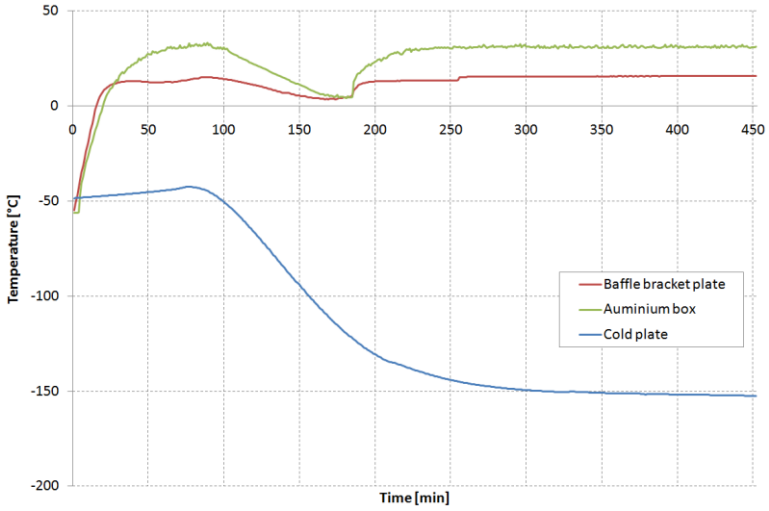

Fig. 5-18: Temperature profile of thermal I/Fs during cold case simulation on HRIC baffle unit (cold plate, baffle bracket plate and aluminum box)

The following graph shows the temperature of relevant points on the baffle surface, on the internal surface of the HT MLI, on the aluminum box.

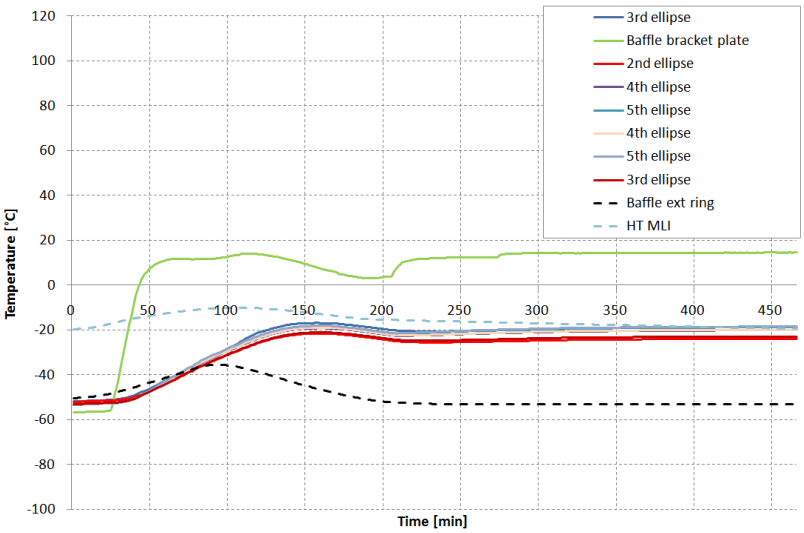

Fig. 5-19: Temperature profile of points of interest on the baffle, on the internal surface of the HT MLI and on the aluminum box during hot case simulation on HRIC baffle

5.3.3 Description of the set-up TMM

Since two different steady – state experimental simulations have been carried on, two different thermal cases have been analyzed. The GMMs are different for each thermal case and are described in the following paragraph.

5.3.3.1 Nodal breakdown thermo-optical properties

The proposed TMM of the experimental set – up has been carried out according to the following approach:

- It is representative of all thermal I/Fs (both radiative and conductive) included inside the TVC used during the test campaign.
- All the structural parts have been simplified as much as possible.
- Once all thermal and mechanical I/Fs inside the TVC have been modeled, the TMM of the Stavroudis baffle has been included inside the model.
- Adjacent nodes presenting low thermal differences have been merged into one single node.

In the following figures the geometric model and the node numbering are shown.
The first figure represents all thermal and mechanical I/Fs which have been used during hot case simulation:

- Node #400 is the hot plate;
- Node #3000 is the cold plate connected to the internal aluminum box by copper braids;
- Node #700 is the plate which supports the instrumentation box.

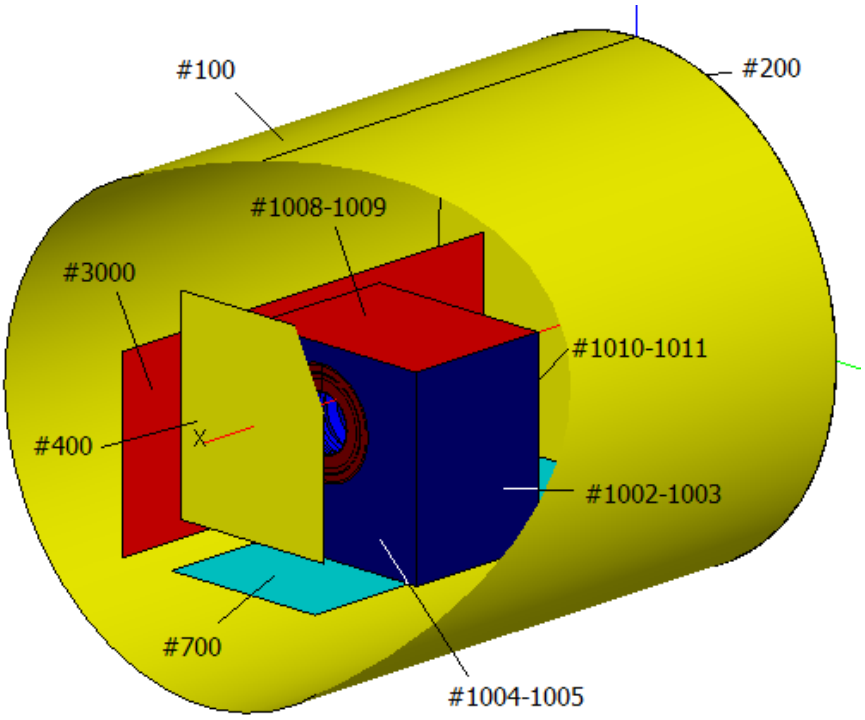

Fig. 5-20: Overall of the GMM for the hot case simulation

The following figures show the instrumentation box covered by HT MLI and standard MLI with the Stavroudis baffle inside it (nodes #58210 – 58234, #96 – 97); internally also the baffle bracket plate (node #99996) and the aluminum box (nodes #1100 – 1900) are visible.

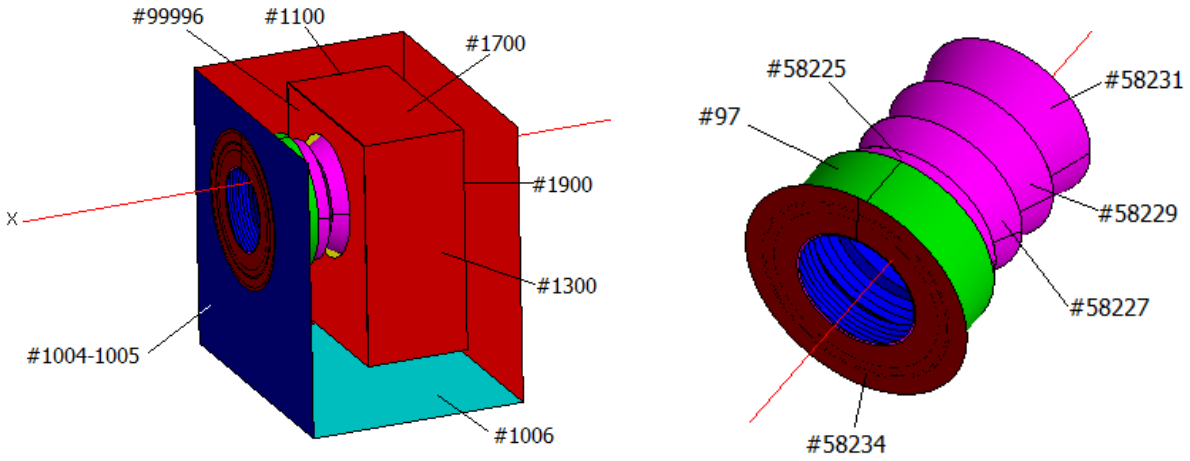

Fig. 5-21: Nodes numbering of the instrumentation box and Stavroudis baffle

The following table reports a list of the nodes, specifying the material and the optical properties for each node. Node #400 represents the hot plate in the hot case simulation (*), the cold plate in the cold case simulation (**); node #3000 represents the cold plate employed during hot case simulation (*) in order to control the temperature of thermal I/Fs.

Node	Type	Name	Material	Thermal finish	α_S	ρ_S^D	ρ_S^S	ε_{IR}	ρ_{IR}^D	ρ_{IR}^S
100	D	Cryostat	AISI 316	Black	1.00	0.00	0.00	1.00	0.00	0.00
200	D	Cryostat	AISI 317	Black	1.00	0.00	0.00	1.00	0.00	0.00
300	D	Cryostat	AISI 318	Black	1.00	0.00	0.00	1.00	0.00	0.00
400	B	Hot plate*	Aluminum	Black	1.00	0.00	0.00	1.00	0.00	0.00
	B	Cold plate**	Aluminum	Black						
500	D	MLI cold plate ext.**	//	STD MLI	0.50	0.25	0.25	0.04	0.48	0.48
501	D	MLI cold plate int.**	//	STD MLI	0.50	0.25	0.25	0.04	0.48	0.48
600	D	MLI cold plate ext.**	//	STD MLI	0.50	0.25	0.25	0.04	0.48	0.48
601	D	MLI cold plate int.**	//	STD MLI	0.50	0.25	0.25	0.04	0.48	0.48
700	D	Base plate	Aluminum	Rough Aluminum	0.15	0.85	0.00	0.03	0.97	0.00
3000	B	Cold plate*	Aluminum	STD MLI	0.50	0.25	0.25	0.04	0.48	0.48
1000	D	Lat1 instr. Box ext.	//	HT MLI	0.23	0.39	0.39	0.87	0.07	0.07
1001	D	Lat1 instr. Box int.	//	STD MLI	0.50	0.25	0.25	0.04	0.48	0.48
1002	D	Lat2 instr. Box int.	//	STD MLI	0.50	0.25	0.25	0.04	0.48	0.48
1003	D	Lat2 instr. Box ext.	//	HT MLI	0.23	0.39	0.39	0.87	0.07	0.07
1004	D*/B**	Front instr. Box int.	//	STD MLI	0.50	0.25	0.25	0.04	0.48	0.48
1005	D	Front instr. Box ext.	//	HT MLI	0.23	0.39	0.39	0.87	0.07	0.07
1006	D	Bottom instr. Box	Aluminum	Rough Aluminum	0.15	0.85	0.00	0.03	0.97	0.00
1008	D	Top instr. Box ext.	//	STD MLI	0.50	0.25	0.25	0.04	0.48	0.48
1009	D	Top instr. Box int.	//	STD MLI	0.50	0.25	0.25	0.04	0.48	0.48
1010	D	Back instr. Box ext	//	STD MLI	0.50	0.25	0.25	0.04	0.48	0.48
1011	D	Back instr. Box int	//	STD MLI	0.50	0.25	0.25	0.04	0.48	0.48
58210-58219	D	Stavroudis - 1st ell.	Aluminum sintered	Polished	0.12	0.03	0.85	0.05	0.05	0.90
				Aluminum	0.15	0.85	0.00	0.05	0.95	0.00
58220-58224	D	Stavroudis - 1st hyp-ell.	Aluminum sintered	Polished	0.12	0.03	0.85	0.05	0.05	0.90
				Aluminum	0.15	0.85	0.00	0.05	0.95	0.00
58225-	D	Stavroudis - 2nd hyp-	Aluminum	Polished	0.12	0.03	0.85	0.05	0.05	0.90

58226		ell.	sintered	Aluminum	0.15	0.85	0.00	0.05	0.95	0.00
58227-58228	D	Stavroudis - 3rd hyp-ell.	Aluminum sintered	Polished	0.12	0.03	0.85	0.05	0.05	0.90
				Aluminum	0.15	0.85	0.00	0.05	0.95	0.00
58229-58230	D	Stavroudis - 4th hyp-ell.	Aluminum sintered	Polished	0.12	0.03	0.85	0.05	0.05	0.90
				Aluminum	0.15	0.85	0.00	0.05	0.95	0.00
58231-58232	D	Stavroudis - 5th hyp-ell.	Aluminum sintered	Polished	0.12	0.03	0.85	0.05	0.05	0.90
				Aluminum	0.15	0.85	0.00	0.05	0.95	0.00
58233	D	Stavroudis Vane Zero	Aluminum sintered	Polished	0.12	0.03	0.85	0.05	0.05	0.90
				Aluminum	0.15	0.85	0.00	0.05	0.95	0.00
58234	D	Stavroudis Front ring	Titanium	Ceramic	0.44	0.56	0.00	0.76	0.24	0.00
				Gold	0.35	0.65	0.00	0.05	0.95	0.00
96	D	Titanium ext. shield	Titanium	Gold	0.35	0.65	0.00	0.05	0.95	0.00
97	D	Titanium int. shield	Titanium	Gold	0.35	0.65	0.00	0.05	0.95	0.00
99996	B	Baffle bracket plate	Aluminum	STD MLI	0.50	0.25	0.25	0.04	0.48	0.48
1100	D	Lat1 Al. Box	Aluminum	STD MLI	0.50	0.25	0.25	0.04	0.48	0.48
				Black	1.00	0.00	0.00	1.00	0.00	0.00
1300	D	Lat1 Al. Box	Aluminum	STD MLI	0.50	0.25	0.25	0.04	0.48	0.48
				Black	1.00	0.00	0.00	1.00	0.00	0.00
1500	D	Bottom Al. Box	Aluminum	STD MLI	0.50	0.25	0.25	0.04	0.48	0.48
				Black	1.00	0.00	0.00	1.00	0.00	0.00
1700	D	Top Al. Box	Aluminum	STD MLI	0.50	0.25	0.25	0.04	0.48	0.48
				Black	1.00	0.00	0.00	1.00	0.00	0.00
1900	D*/B**	Back Al. Box	Aluminum	STD MLI	0.50	0.25	0.25	0.04	0.48	0.48
				Black	1.00	0.00	0.00	1.00	0.00	0.00
99998	X	Inactive node	//	//	//	//	//	//	//	//
99999	B	Environment	//	//	//	//	//	//	//	//

Table 5-7 Node list and surface properties

The following table shows a list of the materials used in the TMM.

Material	ρ [kg/m^3]	c_P [J/kg K]	λ [W/mK]
Aluminum	2800.00	850.00	130.00
Titanium	4420	560	7.3
Aluminum Sintered	2700.00	900.00	170.00
AISI 316	8030	504	16.3

Table 5-8: materials properties

5.3.3.2 Conductive thermal couplings

In this paragraph two tables describe the conductive thermal couplings between each couple of nodes. The first one refers to the hot case, the second one to the cold case.

Node i	Node j	GL [W/K]	Node i	Node j	GL [W/K]
58210	58211	26.0504	58210	58234	0.035
58211	58212	25.6194	58225	99996	0.00723
58212	58213	24.9126	58226	99996	0.00723
58213	58214	23.9462	58225	58226	1.72493
58214	58215	22.7412	96	58210	0.09193

58215	58216	21.322	96	58234	0.01574
58216	58217	19.7146	96	58222	0.09026
58217	58218	17.9454	96	58221	0.09026
58218	58219	16.0398	96	97	0.95528
58219	58220	9.0554	1900	1500	0.3059
58220	58221	6.9764	1900	1300	0.0217
58221	58222	2.4866	1900	1100	0.0217
58222	58223	12.3668	1100	1500	0.0217
58223	58224	10.4482	1300	1500	0.0217
58224	58225	4.13	99996	1500	0.159
58226	58227	2.7894	1006	700	7.8871
58227	58228	1.3989	1900	3000	0.04
58228	58229	1.231	1002	1003	0.00356867
58229	58230	0.98652	1000	1001	0.00356867
58230	58231	1.0587	1008	1009	0.00200278
58231	58232	0.81278	1010	1011	0.00259538
58233	58210	3.3534	1004	1005	0.00350735

Table 5-9: hot case – internal conductive couplings

Node i	Node j	GL [W/K]	Node i	Node j	GL [W/K]
58210	58211	26.0504	58226	99996	0.00723
58211	58212	25.6194	58225	58226	1.72493
58212	58213	24.9126	96	58210	0.09193
58213	58214	23.9462	96	58234	0.01574
58214	58215	22.7412	96	58222	0.09026
58215	58216	21.322	96	58221	0.09026
58216	58217	19.7146	96	97	0.95528
58217	58218	17.9454	1900	1500	0.3059
58218	58219	16.0398	1900	1300	0.0217
58219	58220	9.0554	1900	1100	0.0217
58220	58221	6.9764	1100	1500	0.0217
58221	58222	2.4866	1300	1500	0.0217
58222	58223	12.3668	99996	1500	0.159
58223	58224	10.4482	1006	700	7.8871
58224	58225	4.13	1002	1003	0.00356867
58226	58227	2.7894	1000	1001	0.00356867
58227	58228	1.3989	1008	1009	0.00200278
58228	58229	1.231	1010	1011	0.00259538
58229	58230	0.98652	1004	1005	0.00350735
58230	58231	1.0587	400	501	1000
58231	58232	0.81278	500	600	1000
58233	58210	3.3534	501	601	1000
58210	58234	0.035	500	501	0.0005336
58225	99996	0.00723	600	601	0.006322

Table 5-10 – Cold case: internal conductive couplings

5.3.4 Numerical results

5.3.4.1 Hot case results

In the table below the main results of the thermal analysis are shown and compared with the experimental ones.

Node	Name	Type	Experimental [°C]	Model [°C]	Δ [°C]
58222-58224	2nd ell.	D	100.2	97.6	2.7
58226	3rd ell.	D	98.0	96.1	1.9
58228	4th ell.	D	94.9	94.7	0.2
58230	5th ell.	D	92.5	93.0	-0.5
1900	Al box	D	50.8	55.8	-5.1
1004	HT MLI int.	D	77.0	80.1	-3.1
99996	Baffle bracket plate	B	92.1	92.1	0.0
3000	Cold plate	B	-177.7	-177.7	0.0
400	Hot plate	B	220.2	220.1	0.1

Table 5-11: Hot case– Comparison between experimental results and numerical results

From the previous tables it can be noticed that the maximum difference between experimental and numerical results appears on the 2nd ellipsoid and is equal to 2.7 °C. The difference decreases as the measurement is performed moving towards the inner conic surfaces of the baffle.
Fig. 5-22 and Fig. 5-23 show the temperature profile for each node of the model of the experimental set – up and the nodal thermal distribution on the STM of the baffle.

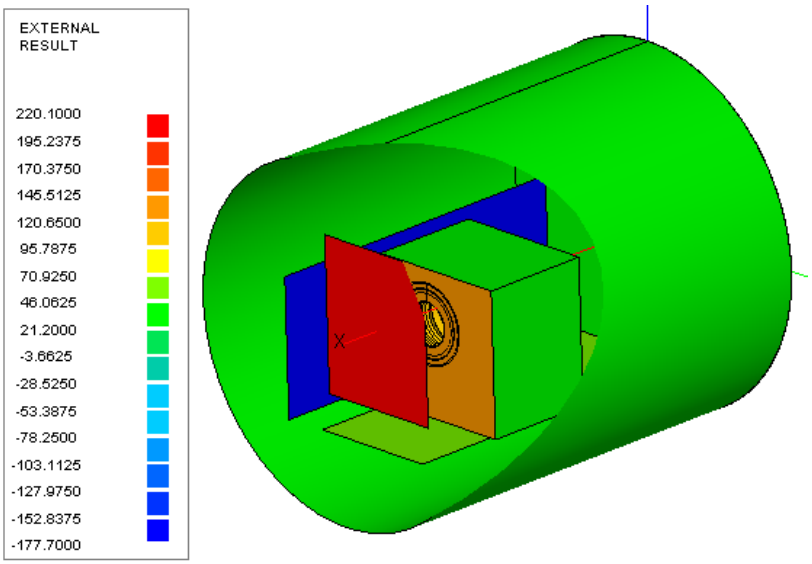

Fig. 5-22 : Temperature profile of the mechanical and thermal I/Fs inside the TVC

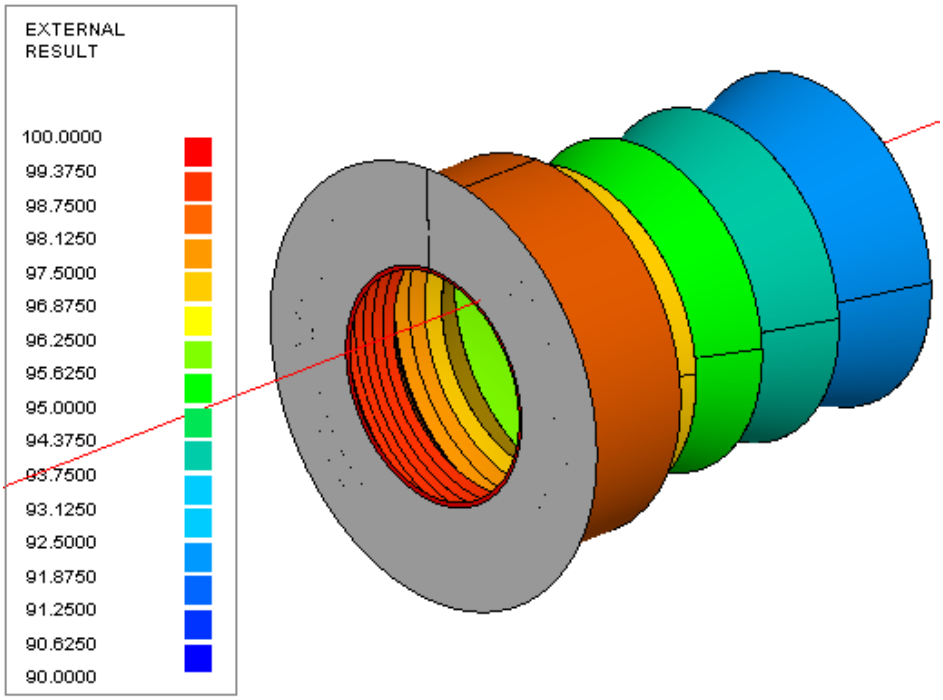

Fig. 5-23: Temperature of the Stavroudis baffle

5.3.4.2 Cold case results

In the following table the main results of the thermal analysis are compared with the experimental ones.

Node	Name	Type	Experimental [°C]	Model [°C]	Δ [°C]
58222-58224	2nd ell.	D	-24.0	-22.1	-1.9
58226	3rd ell.	D	-20.9	-20.8	-0.1
58228	4th ell.	D	-20.1	-19.7	-0.4
58230	5th ell.	D	-18.8	-18.4	-0.4
58234	Front ring	D	-53.3	-56.2	2.9
1900	Al box	B	31.1	31.1	0.0
1004	HT MLI int.	B	-19.6	-19.6	0.0
99996	Baffle bracket plate	B	14.0	14.0	0.0
400	Cold plate	B	-152.4	-152.4	0.0

Table 5-12: Cold case - Comparison between experimental results and numerical results

From the previous tables it can be noticed that the maximum difference between experimental and numerical results appears on the front ring and is equal to 2.9 °C. The following figures show the temperature profile for each node of the model of the experimental set – up and the nodal thermal distribution on the STM of the baffle.

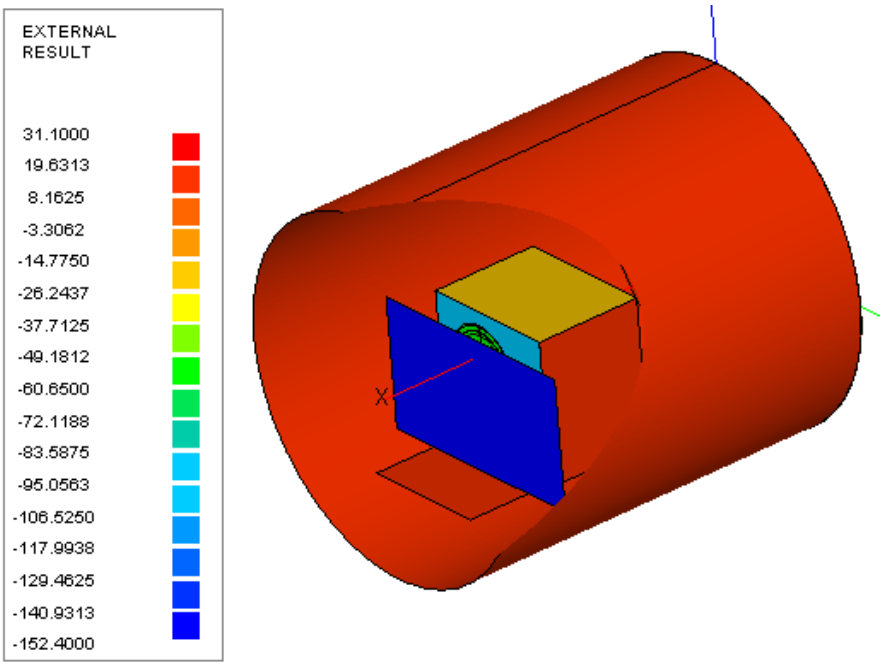

Fig. 5-24: Temperature profile of the mechanical and thermal I/Fs inside the TVC

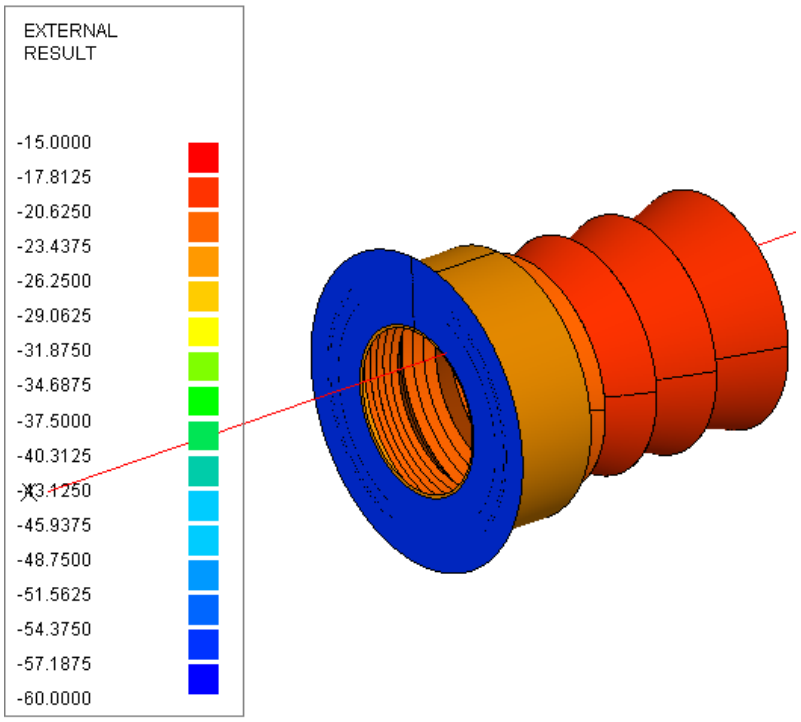

Fig. 5-25: Temperature of the Stavroudis baffle

5.4 **Conclusions**

Thanks to the correlation and the comparison between the numerical and experimental results, the TMMs of the STMs of the baffles have been validated and some useful and original modifications have been implemented into the TMM of the Flight Model of the baffles (as an example, the conductance between the frontal ring of the Stavroudis baffle and the first vane has been changed).

6. Thermal test activity on the QM of HRIC baffle

6.1 Introduction

This section reports the design phases of the test-bed for the test campaign on the Qualification Model of Stavroudis baffle and the test procedure.
The Thermal Vacuum Tests described are aimed to:

1. Verify the thermal behaviour of the QM of the baffle up to the temperature range limits (operative and non-operative).
2. Verify the thermal behaviour of the QM of the baffle in the most critical orbital conditions, basing on the temperature measured on the TIRD (Thermal Infrared Rejection Device) simulator placed behind the baffle.

6.2 Test object

Test object is the QM of HRIC baffle, which is represented in the following figure.

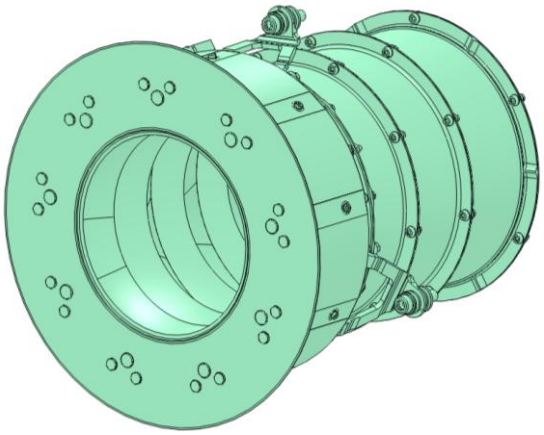

Fig. 6-1 Stavroudis baffle QM

6.3 Test equipment

The test facility used for the TVTs is composed of 2 main parts: an innovative Solar Simulator, designed, developed and characterized at CISAS "G.Colombo" of University of Padova, and a custom TVC, which hosts equipment to be tested and thermally controlled I/Fs.
Three different types of test are foreseen for HRIC baffle test campaign:

1. Test A: performance measurements;
2. Test B: qualification test;
3. Test C: test in space-like environment.

A brief description of different types of test with related equipment to be used is reported below:

1. Test A: performance measurements.

Performance measurements will be made in order to evaluate possible effects of thermal loads and critical boundary conditions on the baffle performance. The performance will be estimated subjecting the baffle to the solar simulator flux and measuring the temperature of a black surface placed behind the baffle (here named TIRD simulator), in steady state conditions, since the temperature of the TIRD simulator can give an estimation of incident heat on the TIRD filter. In order to evaluate the effect of the thermal loads, the performance measurements will take place:

- Before qualification tests, at the beginning of the test campaign (see the following figure);
- After qualification tests (see the following figure);
- At the end of the test campaign, after tests in space-like environment (see the following figure).

2. Test B: qualification test on the baffle.
   During this phase, minimum and maximum qualification temperature will be imposed on the conductive and radiative interfaces, taking into account the ±10°C qualification margin. Thermally controlled surfaces inside the TVC (shrouds and plates with PID controlled heaters and liquid Nitrogen circuits) will provide interfaces to be used for qualification test.
3. Test C: the baffle will be subjected to the most critical orbital conditions.
   During orbits around Mercury, SIMBIO-SYS baffles are exposed to direct solar illumination, albedo and infrared radiation from Mercury, and are subjected to heat exchange with the sky background.
   To reproduce the thermal environment the baffle will face in orbit, the test object will be subjected to:
   - Solar flux, incoming from a beam generated by a Solar Simulator outside the TVC.
   - Infrared flux, incoming from:
     - A black plate illuminated by IR lamps (hot plate), which will simulate radiation generated by the day-side surface of Mercury planet and will be placed inside the TVC, facing the external ring of the baffle.
     - A black shroud cooled by liquid Nitrogen, which will simulate radiation generated by the shaded surface of Mercury planet and by the sky-background.

The following scheme summarizes the flow tests (on the left) and equipment to be used for each phase (on the right).

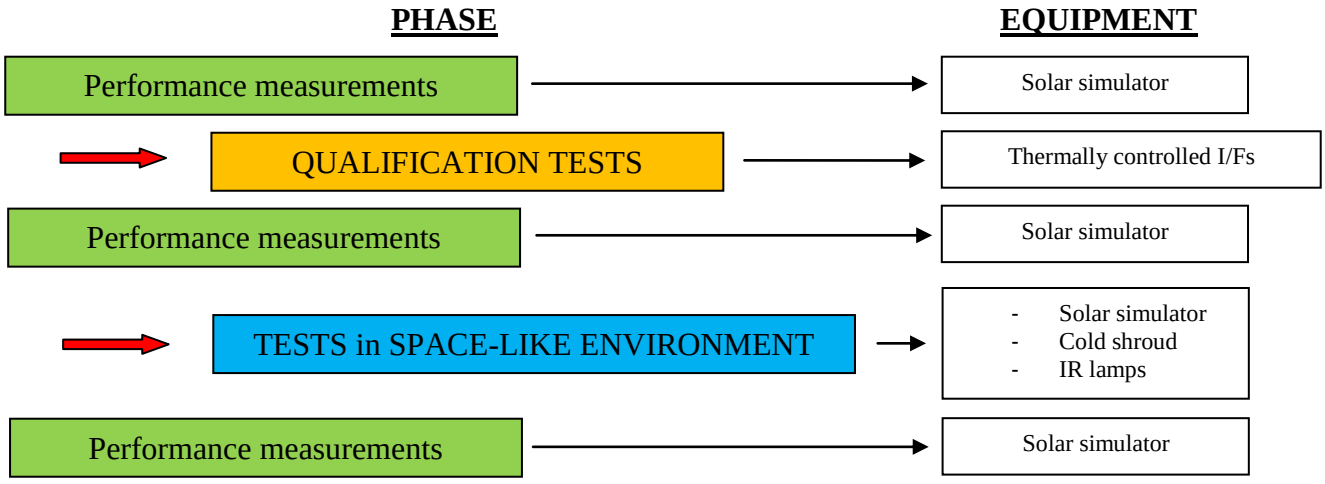

Fig. 6-2 Operations sequence during TVTs

6.3.1 CISAS Thermal Vacuum Chamber

The test facility available is suitable for flight units and is installed inside a ISO 8 (100000 Federal Standard) class clean-room.
A stainless steel vessel AISI 304 with a volume of about 1.2 m^3 (available room inside cryostat 0.8 m^3) mainly composes the TVC. All flanges are CF type with metal gaskets (copper material) except for the main opening (front door) in which a Viton O-ring is present. The thermal vacuum facility is equipped with several electrical feed-through. A HP 34970A data-logger for temperature measurements is able to manage up to 30 RTD PT100 (class A), four wires measurements.
Three main sub-systems are available:

1. Vacuum sub-system, controlled via a dedicated PLC able to reduce the internal pressure up to 10^{-3} Pa. The pump group is constituted of one rotating pump, for the pre-vacuum, and one turbo-molecular pump. Vacuum gauges which are used are: a Pirani vacuometer, for the pressure range of 100 ÷10^{-3} mbar, a capacitive vacuum sensor (pressure range 10 to 10^{-3} mbar) and a ionizing sensor (hot cathode), for the pressure range of $6{\cdot}10^{-3}$ to $2{\cdot}10^{-11}$ mbar. The system, managed from a controller, gives the possibility to fill with gaseous nitrogen the climatic chamber, before opening it to the atmosphere.
2. The shroud is mainly composed by an aluminum cylinder with a dedicated pipe in which a Joule-Thompson expansion of liquid allows to achieve a temperature value of about 90K. To improve the reproducibility of radiative flux exchanged between shroud and equipment to be tested, a high and constant emissivity painting (Aeroglaze) covers the inner surface of the shroud, while a customized thermal blanket covers the external surface of the shroud itself.
3. Suprasil viewport window (diameter 270 mm) to allow the Solar Simulator light beam to enter the chamber. An external shutter is available to blind the solar simulator light source (see the figure below).

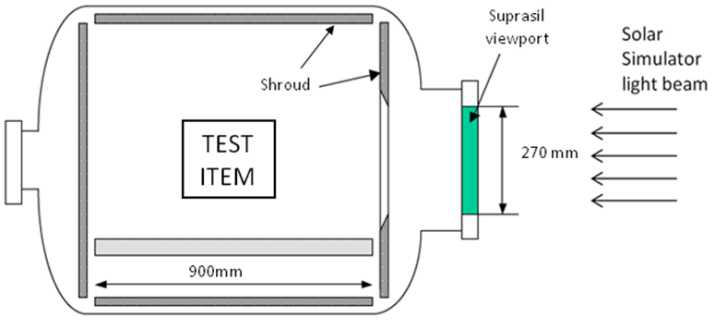

Fig. 6-3 Solar simulator facility and TVC layout

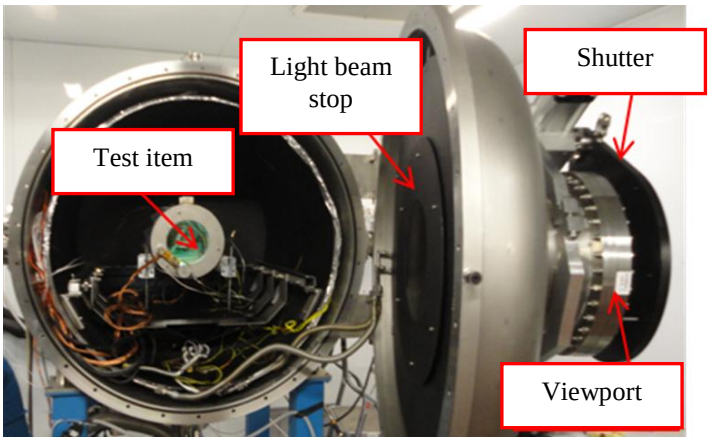

Fig. 6-4 TVC with test item inside it

6.3.2 Solar Simulator

CISAS Solar Simulator, placed externally to the TVC, produces a nearly – collimated (divergence < 30') steady beam with a homogeneous flux distribution (uniformity better than 5%) across an aperture of 270 mm diameter and allows to reach up to 6-7 Solar Constant flux intensity.
The optical design of the solar simulator is based on a series of multiple different reflecting surfaces mounted on a common thermally - controlled optical bench. The light is generated by a Xenon arc lamp placed in the focus of an ellipsoid mirror and able to produce a flux with a spectral distribution similar to that of the Sun (spectrum extents from the visible range up to the ultraviolet), a small concentrated arc and a high irradiance value. The beam oriented by the reflecting ellipsoid is then deviated by a folding mirror towards a primary spherical mirror, a fly – eye integrator (which uniforms the flux) and a secondary spherical 500 mm-diameter mirror. After multiple reflections, the beam is directed towards the thermal vacuum chamber, whose entrance window is provided with a dedicated cooled shutter in order to shield instrumentation under test without switching off the light source, preserving therefore the life cycle of the lamp.
Once aligned and correctly positioned with respect to the thermal vacuum chamber, the solar simulator has been characterized by means of a spectrometer, both outside and inside the thermal vacuum chamber.
The following figures show the optical bench of the Solar Simulator with main optical reflective components mounted on it and the TVC with its dedicated shutter.

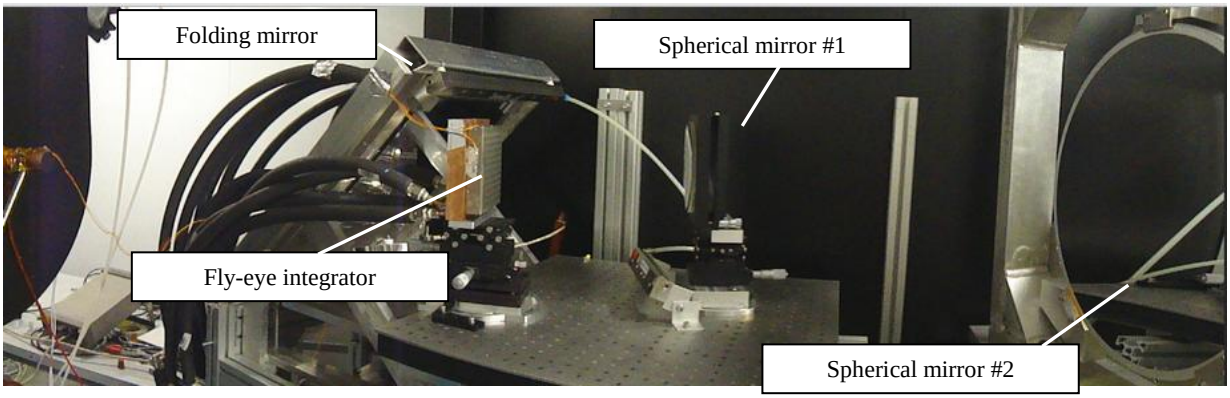

Fig. 6-5 Detail of the Solar Simulator optical bench

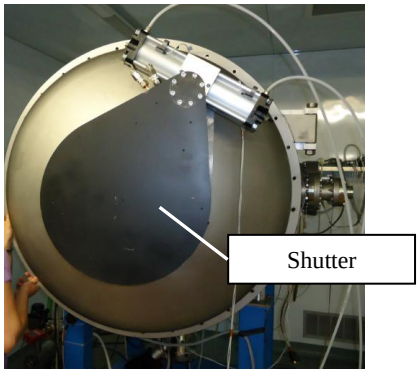

Fig. 6-6 TVC with the shutter on the viewport

The following figures show the solar spectra obtained outside and inside the TVC: blue curve refers to full power supplied to the light source, red curve to the minimum power supplied.

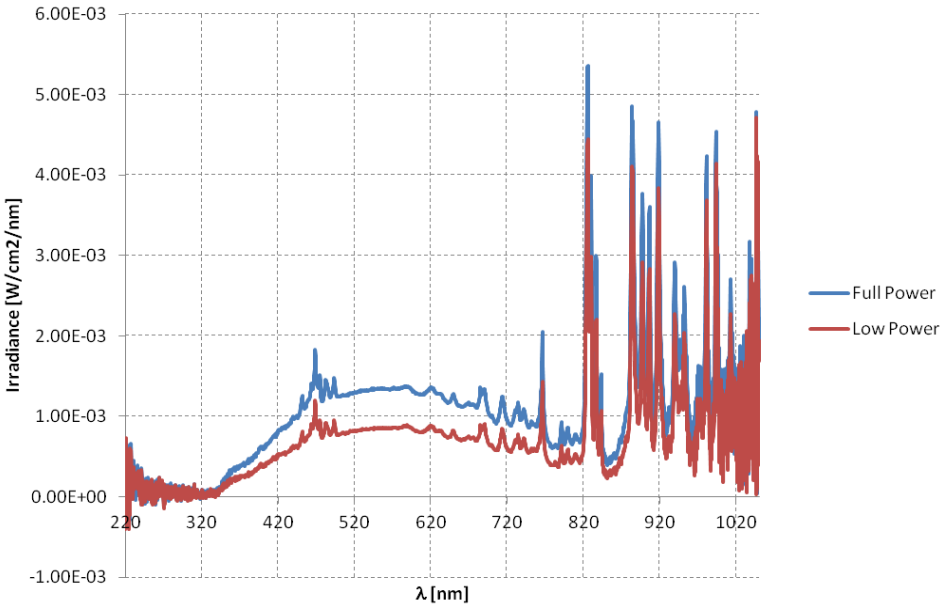

Fig. 6-7 Solar spectra outside the TVC

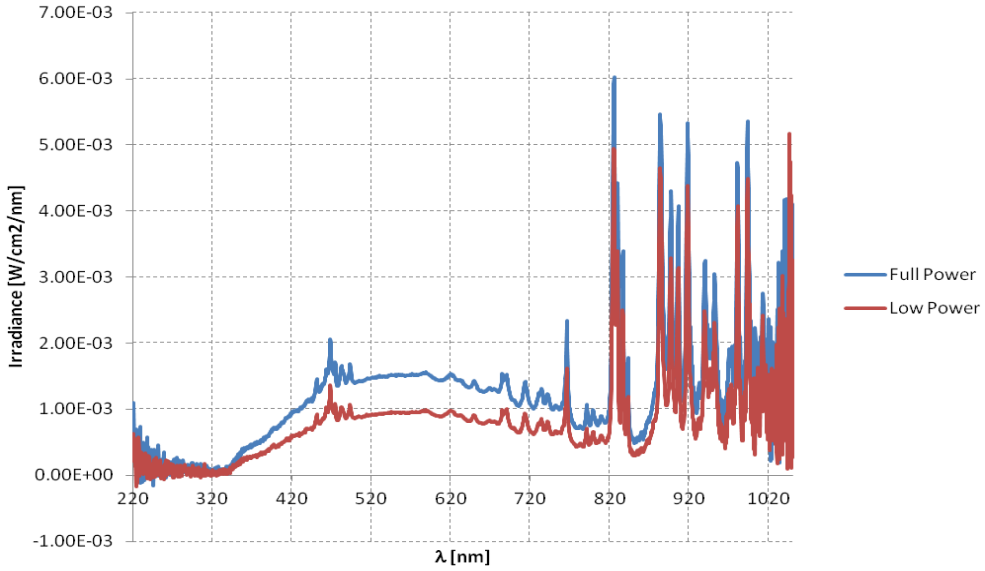

Fig. 6-8 Solar spectra inside the TVC

6.3.3 Thermal Vacuum Chamber test set-up

6.3.3.1 Performance measurements

Performance measurements will be performed three times during the test campaign (see Fig. 6-2):

- At the beginning of the test campaign, before qualification tests.
- In the middle of the test campaign, after qualification tests.
- At the end of the test campaign, after tests in space-like environment.

For this reason, in order to minimize operations during TVTs:

- The test-bed used for the first performance measurements will be similar to the test-bed used during qualification test;

- The test-bed used for the second and third measurement will be similar to the test-bed used during tests in space-like environment.

In both cases the same instrumental set-up will be used.
Performance measurements will be made in thermal vacuum chamber at environment temperature, subjecting the baffle to the solar simulator flux and measuring the temperature detected at the TIRD simulator placed behind the baffle in steady state condition.
In this paragraph, only the test-bed used for the first performance measurement is described in detail; second and third measurement test-bed is the same described in paragraph 6.3.3.3.
During first performance measurement, the baffle will be supported by a (240×293×10) mm^3 Aluminum plate thanks to three M6 screws; this aluminum plate will be attached to a horizontal aluminum plate, removable from the TVC (and provided with PID controlled heaters and a liquid Nitrogen circuit).
Behind the baffle a black-painted plate, thermally insulated respect to the horizontal plate thanks to threaded bars, will simulate the TIRD and will host temperature sensors in order to provide an estimation of the baffle performance. The backwards surface of the TIRD plate will be covered with standard MLI in order to reduce radiative exchange with the surrounding environment.
High Temperature MLI will be placed behind the frontal ring of the baffle and will be supported by an aluminum frame in order to shield the baffle body with respect to the solar beam.
During performance measurements, the angle between the normal to the plate which supports baffle and the solar vector is 38° (see paragraph 6.4.3 for further details). The following figure shows a sketch of the test-bed during the first performance measurement.

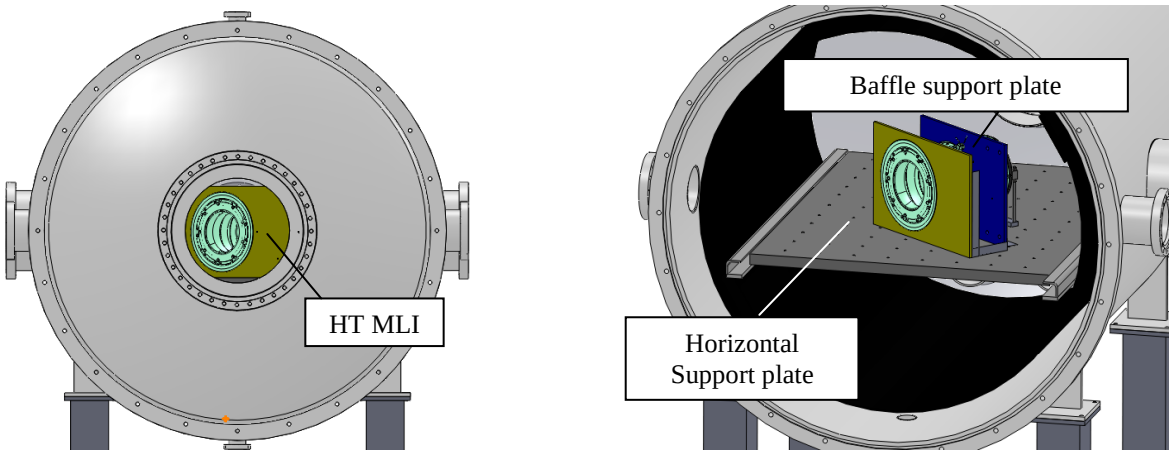

Fig. 6-9 Sketch of the test bed inside the TVC

The following figure is a detailed view of the test bed inside the TVC.

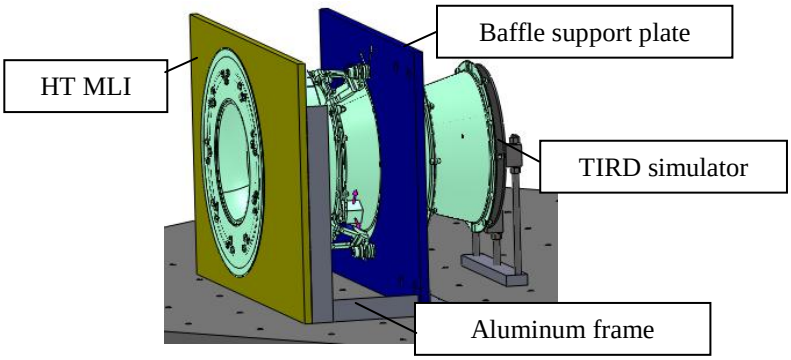

Fig. 6-10 Detailed view of the test bed

The chamber (internal diameter equal to 1100 mm, length equal to 1130 mm) can reach a vacuum of 10^{-6} mbar. During the performance measurements, the following parameters will be monitored, thanks

to electrical interconnections between sensors and the acquisition system, which will be performed through a service flange:

- Internal chamber pressure;
- Progressive time of cycle;
- Temperature of the components reported in the table below:

Temperature sensor location	**Quantity**	**Label**	**Responsible for the positioning**	**Notes**
Cylindrical shroud	3	#1,2,3	CISAS	
Aluminum plate supporting baffle	3	#4,5,6	CISAS	Near baffle attachment points
Horizontal plate	2	#7,8	CISAS	
HT MLI – frontal surface	1	#9	CISAS	
Black disc behind the baffle (TIRD)	5	#10-14	CISAS	
Baffle	10	#15-24	CISAS	1 sensor/couple of vanes (ellips.& hyp.), the first couple excluded

Table 6-1 Number and location of temperature sensors

The following figures show the position of the sensors.

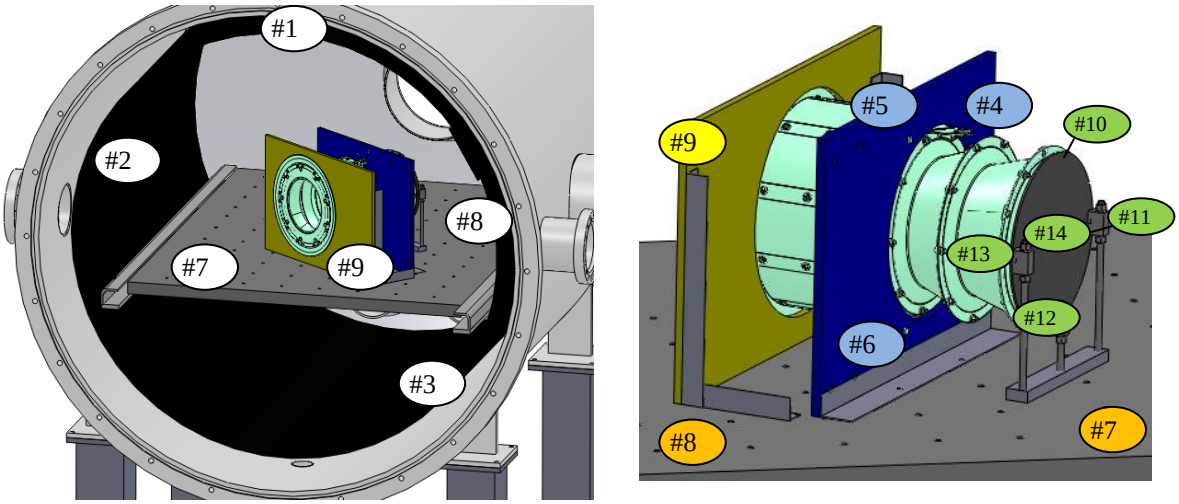

Fig. 6-11 Position of the temperature sensors during the first performance measurement

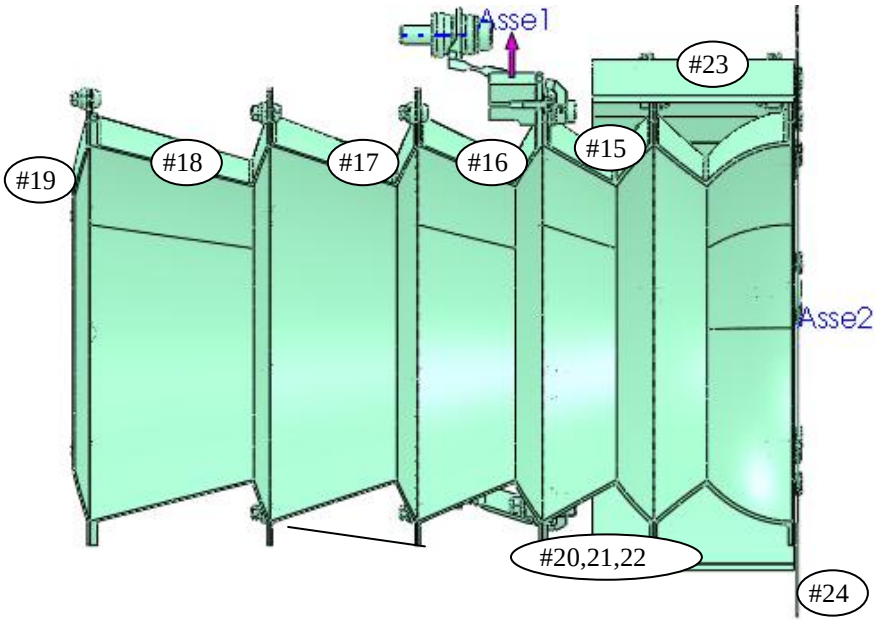

Fig. 6-12 Position of the temperature sensors on the Stavroudis baffle

6.3.3.2 Qualification test

Qualification test on the test object will be performed in the TVC reproducing minimum and maximum qualification temperature on the conductive and radiative interfaces.
The test bed is very similar to that described in the previous paragraph (mechanical interfaces are unchanged).
During qualification tests solar simulator will not be activated, whereas the horizontal supporting plate temperature will be driven to the lowest and highest qualification temperature levels, by means of its internal liquid Nitrogen circuit and PID controlled heaters. Since temperature of the aluminum plate supporting baffle has to be controlled (it represents the baffle conductive interface), this plate will be thermally coupled with respect to the active-controlled horizontal plate, by means of copper braids. Temperature will be stabilized thanks to heaters placed on the aluminum plate.
In addition radiative interfaces will be reproduced thanks to a cryostat (a copper shell) which will be attached to the horizontal plate and will define the limited control volume around the baffle.
In order to thermally insulate the cryostat from the remaining volume of the TVC, MLI will be used around it.
The following figure shows a sketch of the test-bed (external MLI is not shown).

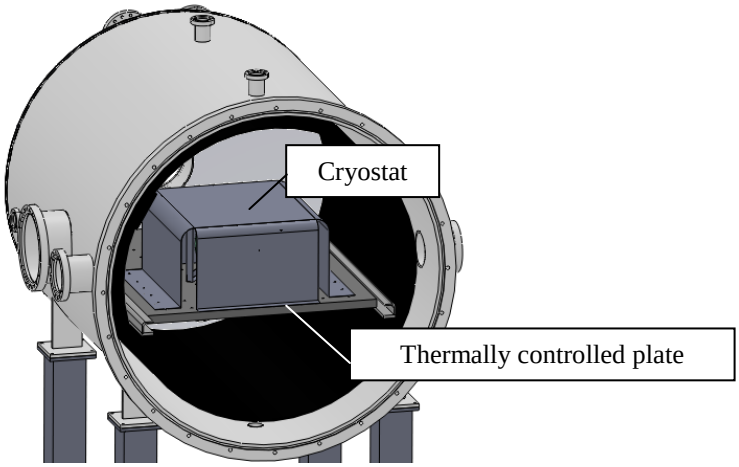

Fig. 6-13 Sketch of the test bed inside the TVC

During qualification test, the following parameters will be monitored, thanks to electrical interconnections between sensors and the acquisition system, which will be performed through a service flange:

- Internal chamber pressure;
- Progressive time of cycle;
- Temperature of the components reported in the table below:

Temperature sensor location	Quantity	Label	Responsible for the positioning	Notes
Cylindrical Shroud	3	#1,2,3	CISAS	
Aluminum plate supporting baffle	3	#4,5,6	CISAS	Near baffle attachment points
Horizontal plate	2	#7,8	CISAS	
HT MLI – frontal surface	1	#9	CISAS	
Black disc behind the baffle (TIRD)	5	#10- 14	CISAS	
Baffle	10	#15-24	CISAS	1 sensor/couple of vanes (ellips.& hyp.), the first couple excluded
Cryostat	4	#25,26,27,28		

Table 6-2 Number and location of temperature sensors

The following figure shows the position of the sensors (for sensors from #1 to #24 see Fig. 6-11 and Fig. 6-12).

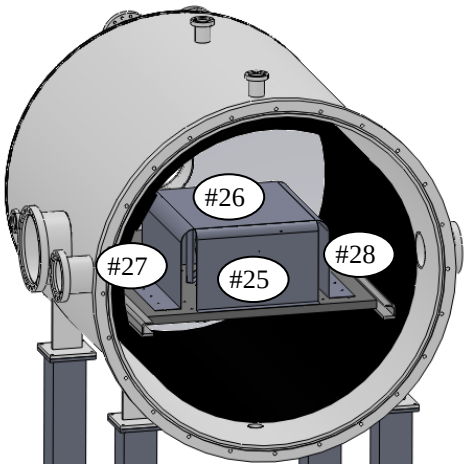

Fig. 6-14 Position of the temperature sensors during qualification tests

6.3.3.3 Tests in space-like environment

During tests in space-like environment, Thermal Vacuum Chamber will host the test object and the thermally controlled heat sources , used to simulate the IR fluxes (cold case and hot case).
The baffle will be supported by a (240×293×10) mm^3 Aluminum plate and the baffle-plate system will be placed inside a (250×288×360) mm^3 box thermally insulated with respect to the heat sources by means of HT and standard MLI (frontal and lateral surfaces of the box, directly exposed to the solar simulator beam, will be covered by HT MLI, whereas standard MLI will covered the upper surface).

Thanks to a rotation stage supporting the box, the baffle will be oriented alternatively towards the solar simulator beam and the thermally controlled heat sources, which will simulate hot (690 K) and cold (100 K) Mercury surfaces. Hot surface of the planet will be simulated thanks to a black plate heated up by IR lamps; cold surface of the planet and the sky-background will be simulated by a cylindrical shroud and a disc surface placed on the rear side of the TVC front door, both connected to the liquid Nitrogen circuit. The following figure shows a sketch of the test-bed.

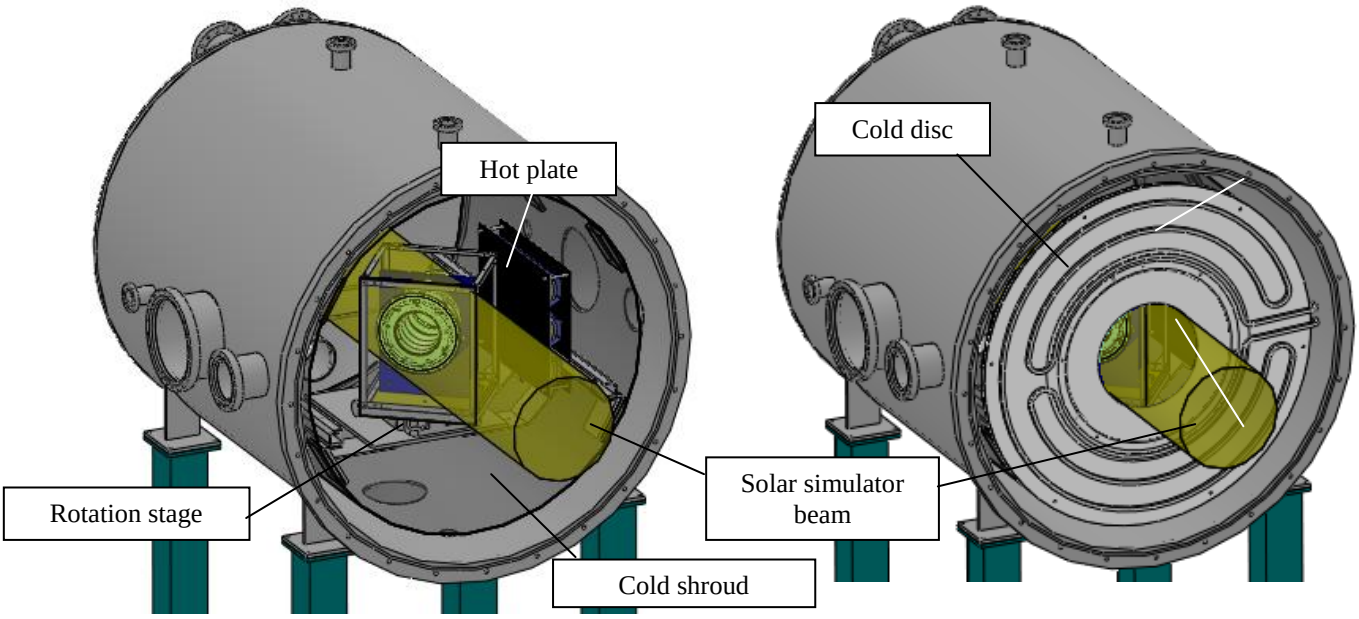

Fig. 6-15 Sketch of the test bed inside the TVC

Stavroudis baffle will be fixed to the supporting plate thanks to three M6 screws; the supporting plate will be radiatively insulated with respect to the surrounding environment thanks to MLI and conductively insulated with respect to the horizontal plate of the box thanks to PEEK washers interposed between the plate itself and the supporting clamps. Plate supporting baffle will not be thermally controlled, since, during the operative phase, such interface follows baffle behavior from a thermal point of view. Behind the baffle, a black disc (simulating the TIRD) will be supported by three M5 threaded bars in order to reduce thermal exchange due to conduction: it will host temperature sensors in order to provide an estimation of the baffle performance. The backwards surface of the disc will be covered with standard MLI in order to reduce radiative exchange with the surrounding environment. In addition a MLI ring will join the black disc to the baffle. The following figure shows the instrument box (MLI is not shown).

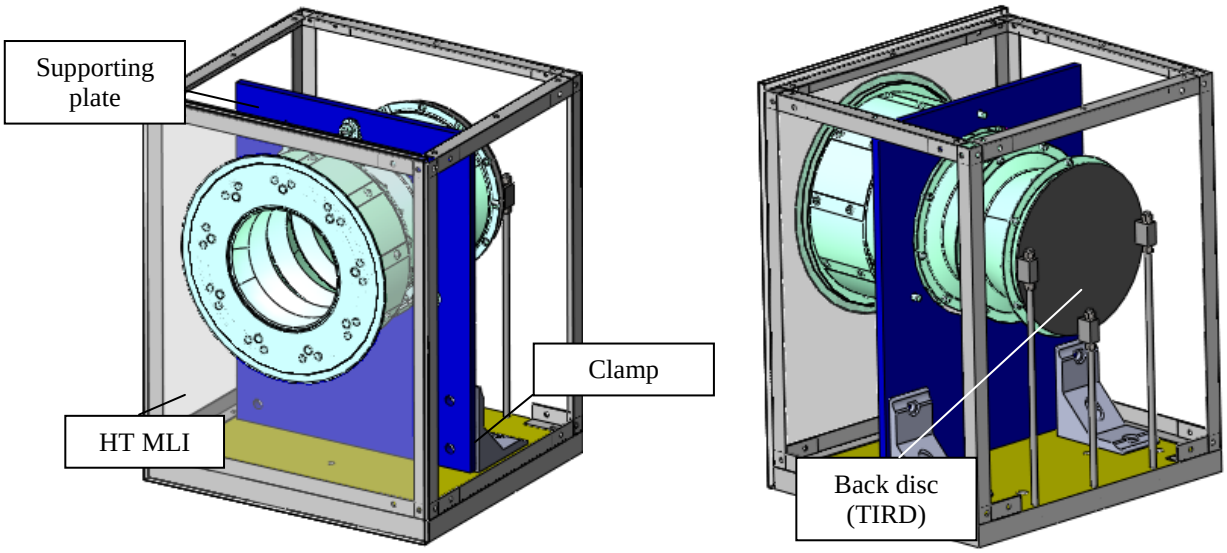

Fig. 6-16 Instrument box with test object in it

The test-bed previously described will be used both for tests in space-like environment and for second and third performance measurements:

1. During tests in space-like environment, all thermal I/Fs inside the TVC and solar simulator will be activated in sequence (as described in paragraph 6.4.3), in order to simulate orbital IR and solar heat fluxes.
2. During second and third performance measurements, only solar simulator will be activated and TIRD simulator temperature will be monitored to provide an estimation of baffle rejection performance (as described in paragraph 6.4.1).

During TVTs in space-like environment, second and third performance measurements, the following parameters will be monitored, thanks to electrical interconnections between sensors and the acquisition system, which will be performed through a service flange:

- Internal chamber pressure;
- Progressive time of cycle;
- Rotation angle profile;
- Temperature of the components reported in the table below:

Temperature sensor location	**Quantity**	**Label**	**Responsible for the positioning**	**Notes**
Cylindrical shroud	3	#1,2,3	CISAS	#2,3 on the cyl. shroud, #1 on the frontal disc
Hot plate	2	#4, 5	CISAS	#4 for monitoring, #5 for controlling, only during tests in space-like environment
Aluminum plate supporting baffle	3	#6, 7, 8	CISAS	Near baffle attachment points
Horizontal plate of the instrument box	1	#9	CISAS	
Horizontal plate of the supporting structure	1	#10	CISAS	
HT MLI – frontal surface	1	#11	CISAS	

Black disc behind the baffle (TIRD)	5	#12 - 16	CISAS	
Baffle	10	#17-26	CISAS	1 sensor/couple of vanes (ellips.& hyp.), the first couple excluded

Table 6-3 Number and location of temperature sensors

The following figures show the position of the sensors.

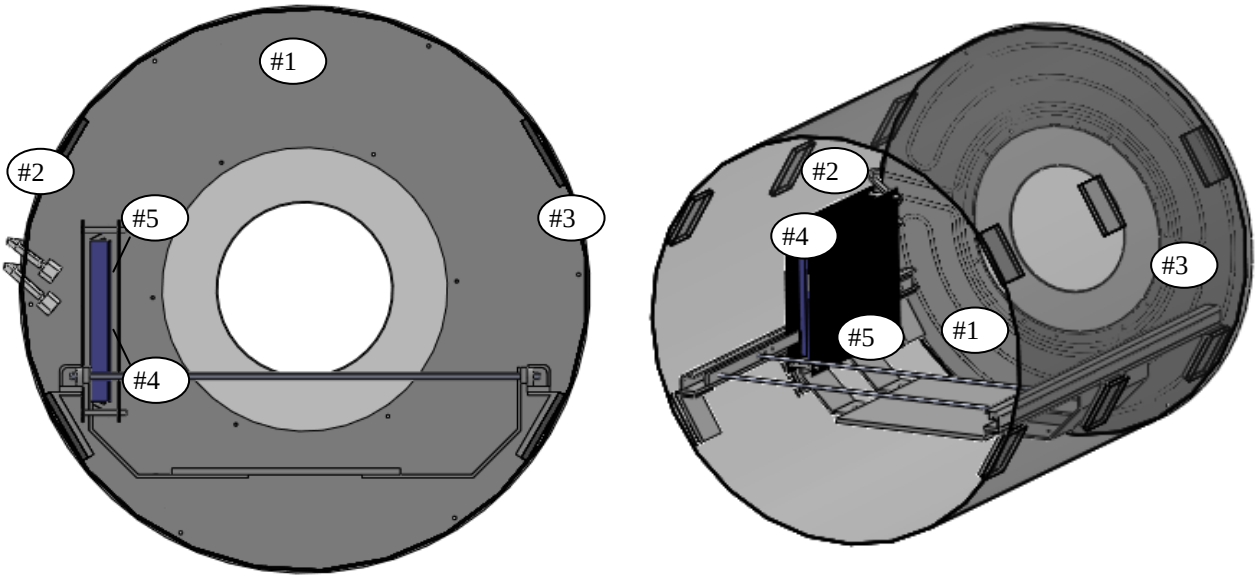

Fig. 6-17 Position of the temperature sensors on the cylindrical shroud, on the frontal plate and on the hot plate

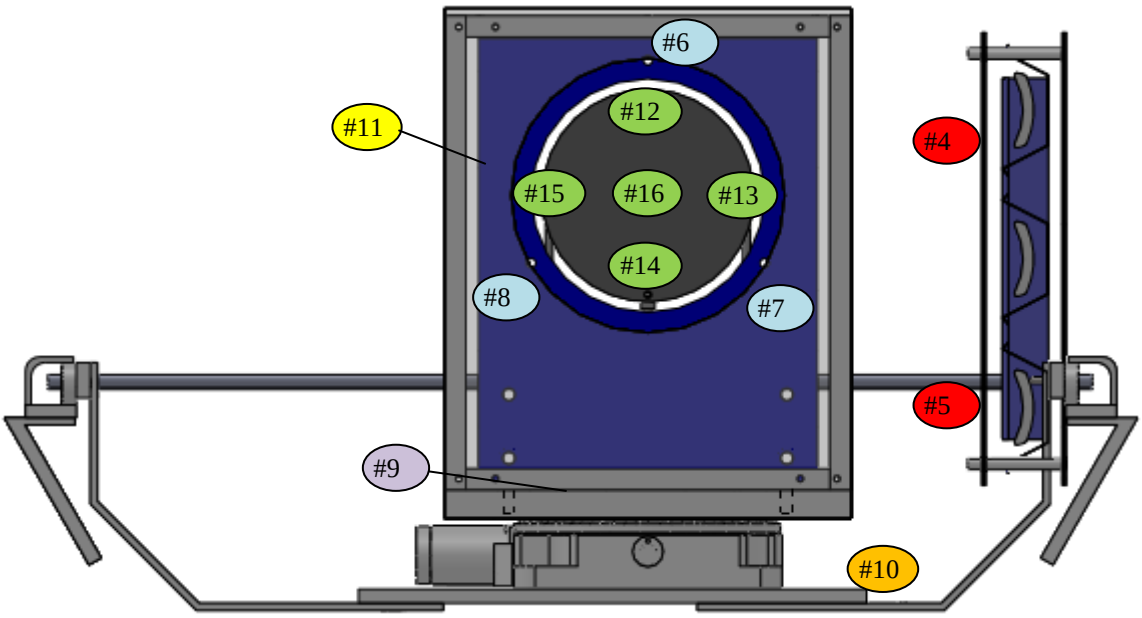

Fig. 6-18 Position of the temperature sensors on baffle bracket plate (light blue dots), TIRD simulator (green dots), hot plate (red dots), support plates (violet and orange dots), HT MLI (yellow dot)

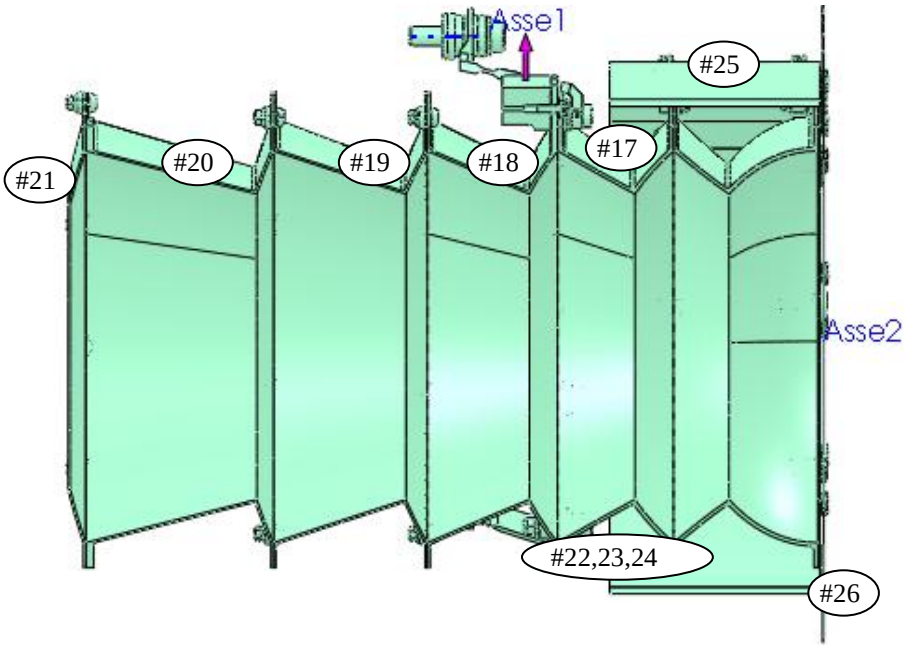

Fig. 6-19 Position of the temperature sensors on the Stavroudis baffle

6.4 General procedure

6.4.1 Performance measurements

6.4.1.1 Objectives

The objective of the performance measurements is to verify that baffle performance, measured before and after TVTs, are unchanged despite the severe thermal loads imposed to the unit during qualification test and tests in space-like environment.

6.4.1.2 Test conditions and test levels

During this test:

1. The unit will be mounted inside the TVC with and angle of 38.3° between the baffle axis and the solar beam direction.
2. The solar simulator will be switched on and the TVC shutter will be opened in order to make the solar simulator flux gets into the TVC through the viewport.
3. All mechanical interfaces inside the TVC will not be thermally controlled.
4. Initial temperature inside the TVC will be about 20°C (clean room temperature).

Performance will be estimated basing on the temperature of the TIRD simulator after thermal stability will be reached (within 1°C/hr).

6.4.2 Qualification tests

6.4.2.1 Objectives

The objective of the qualification tests is to reproduce the qualification minimum and maximum temperature (taking into account the ±10°C margin) at the conductive and radiative interfaces of the baffle, the aluminum plate supporting baffle and the cryostat (copper shell) respectively.

6.4.2.2 Test conditions and test levels

Qualification test will be performed controlling the temperature of the horizontal plate supporting equipment inside the TVC and the temperature of the plate supporting baffle, by means of 2 dedicated PID controllers.
A margin of ± 10°C shall be applied to minimum and maximum temperature levels, which are reported in the following table:

QUALIFICATION QM		
	T_{MIN} [°C]	T_{MAX} [°C]
Operating	-50 (-40-10)	+75(+65+10)
Non-operating	-50 (-40-10)	+85(*)

(*) a margin of 20°C has been assumed taking in to account the thermal analysis result at S/C level (based on BC-EST-TN-04748 is 03 rev 4)

Table 6-4 Qualification temperature levels

The temperatures are referred to the three temperature sensors placed on the aluminum plate supporting baffle, which simulates baffle bracket plate, and the temperature sensors placed on the cryostat, which represents the radiative boundary.
The QM shall be subjected to the TVT temperature profiles as specified in figure and table below: since operating and non – operating temperature levels are equal, standard non-operative sequence, which usually takes place at the beginning of the complete qualification thermal vacuum cycle, is skipped. Only one cycle will be performed during qualification test.

Step	T start [°C]	T end [°C]	Slope [°C/min]
AB	20	20	-
BC	20	85	2
CD	85	85	-
DE	85	-50	2
EF	-50	-50	-
FG	-50	20	2
GH	20	20	-

Table 6-5 Detail of temperature profiles applicable to baffle bracket plate and the cryostat

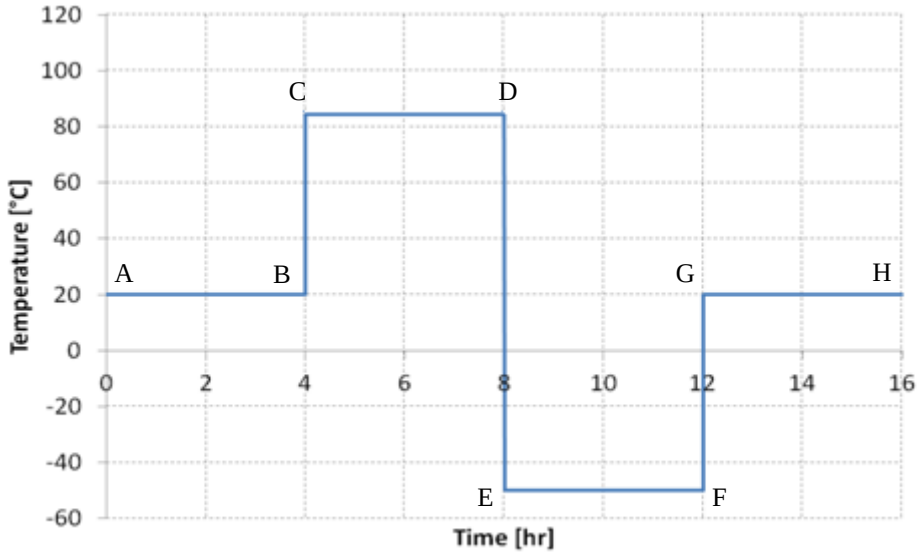

Fig. 6-20 Temperature profiles applicable to baffle bracket plate and the cryostat

The increasing/decreasing of the temperature shall be performed with a rate comprised between [2-10]°C/min and the requested stability is within 1°C/hr. During the cycle the temperature sensors will be continuously recorded by a dedicated PC.

6.4.3 Tests in space-like environment

6.4.3.1 Objectives

The main test objectives of the TVTs in space-like environment are to:

- Simulate the most critical orbital conditions indoor;
- Verify baffle behavior against most critical simulated conditions.

6.4.3.2 Test conditions

From a thermal point of view, at Perihelion, the S/C operates in 3 different conditions:

1) The S/C passes above the dark side of the planet.
2) The S/C exits from the eclipse: in this condition, S/C nadir pointing surfaces are subjected both to the IR flux coming from the shadowed surface of the planet and to the solar flux at the same time.
3) The S/C passes above the illuminated side of the planet.
4) The S/C entries into the eclipse (this point is similar to point 2).

The following figure illustrates this sequence.

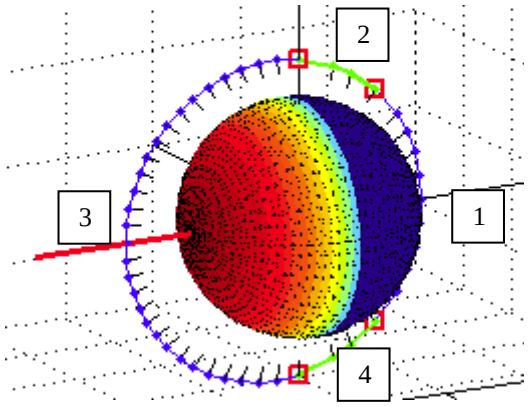

Fig. 6-21 Orbital conditions at Perihelion

Along one orbit around Mercury, the solar flux incident to the S/C surfaces is maximum (most critical condition) when the sun angle (angle between the normal to the S/C illuminated surface and the solar vector) is minimum. The following figure is a representation of the sun angle.

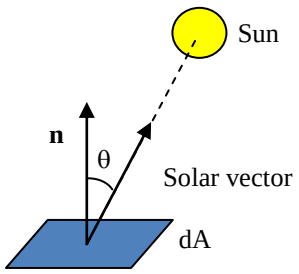

Fig. 6-22 Sun angle (θ)

The minimum sun angle which occurs along each orbit of the S/C around Mercury varies as a function of the position of Mercury along its orbit around the Sun (true anomaly), as represented in the graph below.

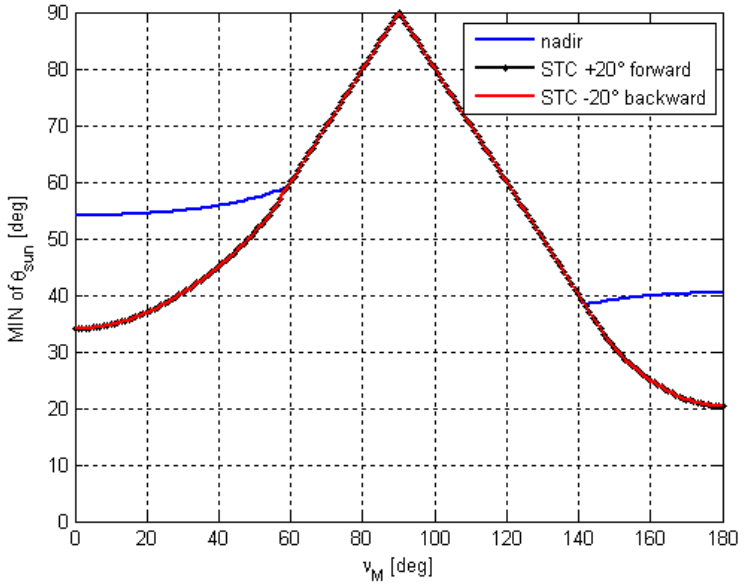

Fig. 6-23 Minimum sun angle variation as a function of Mercury true anomaly

Most critical condition from a thermal point of view in terms of incident fluxes occurs at Perihelion, where:

- Temperature of Mercury illuminated surface is 689 K and IR flux is 4496 W/m^2.
- Solar flux is 8510 W/m^2.
- The minimum sun angle is about 54° ($\nu_M = 0$).

The TVC test-bed has been designed in order to simulate the operational sequence described above at Perihelion. The following table and the following figure describe the general procedure for one test cycle: each operational phase is associated to a precise configuration in the set-up.
Eight thermal cycles will be performed during test campaign.

#	Condition on orbit	Fluxes to be simulated	Operation/configuration
1	The S/C passes above the dark side of the planet	Cold IR	A. Cold shroud is activated B. Baffle is rotated until the angle between the instrument nadir direction and the solar beam direction is equal to θ_{MIN} C. Shutter is closed
2	The S/C exits from the eclipse	• Cold IR • Solar	Shutter is opened and solar simulator is switched on in order to make the solar simulator flux gets into the TVC though the viewport ($\theta_{MIN} = 54°$)
3	The S/C passes above the illuminated side of the planet	Hot IR	A. Shutter is closed B. Baffle is rotated in order to bring the frontal surface of the baffle // to the hot plate surface C. Hot plate is switched on
4	The S/C entries into the eclipse	• Cold IR	A. Hot plate is switched off B. Baffle is rotated until the angle

		• Solar	between the instrument nadir direction and the solar beam direction is equal to θ_{MIN} C. Shutter is opened in order to make the solar simulator flux gets into the TVC though the viewport (θ_{MIN} = 54°)

Table 6-6 Sequence of operations for one thermal cycle

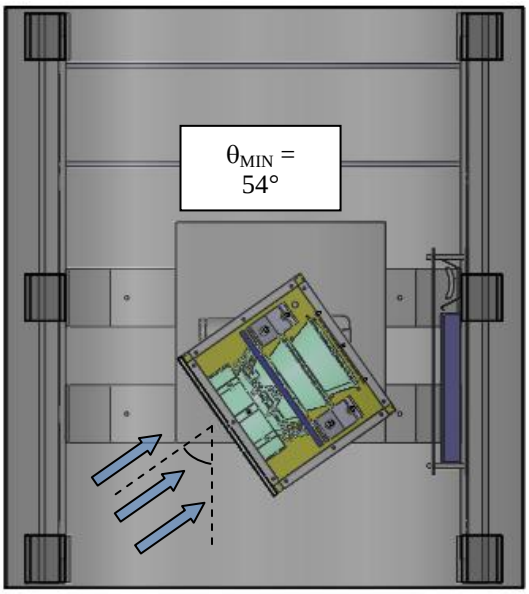

Fig. 6-24 Baffle subjected to the cold IR flux (S/C above Mercury cold surface)

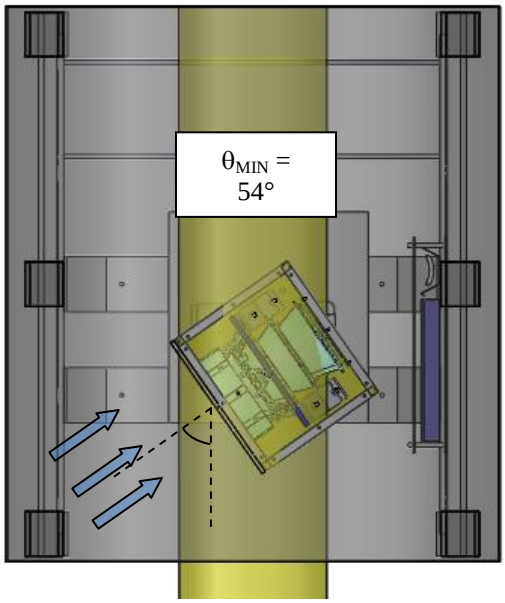

Fig. 6-25 Baffle subjected to the cold IR flux and to the solar flux (S/C exiting from the eclipse)

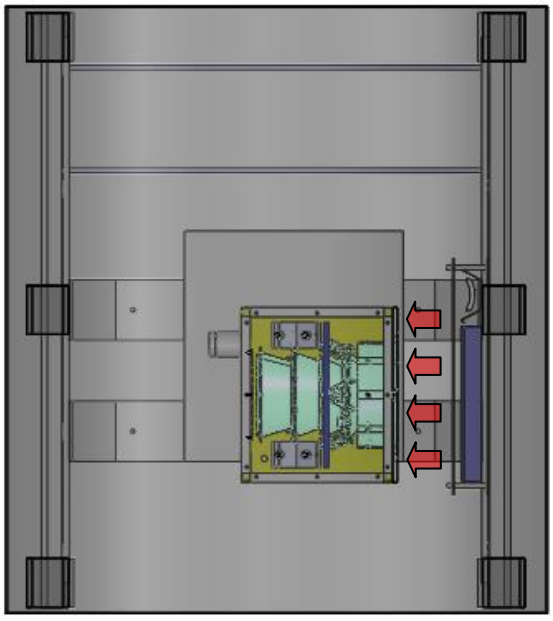

Fig. 6-26 Baffle subjected to the hot IR flux (S/C above Mercury illuminated surface)

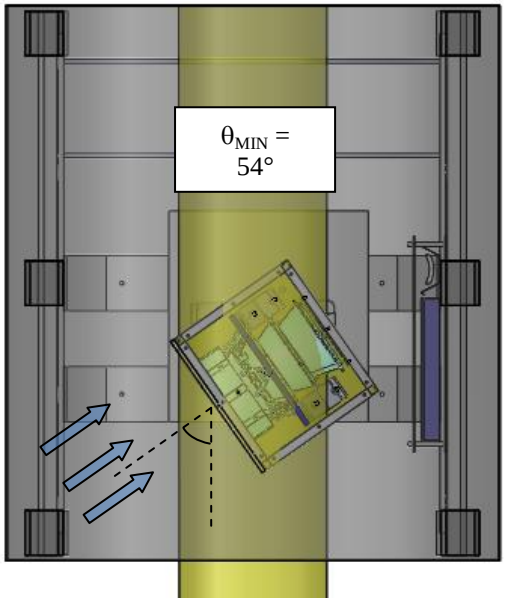

Fig. 6-27 Baffle subjected to the cold IR flux and to the solar flux (S/C entering into the eclipse)

The following figures show a frontal view of the TVC during test conditions #1, 2, 4: it can be noticed that the solar simulator beam entirely hits the Stavroudis baffle frontal section (HT MLI on the lateral surfaces of the instrument box is not shown).

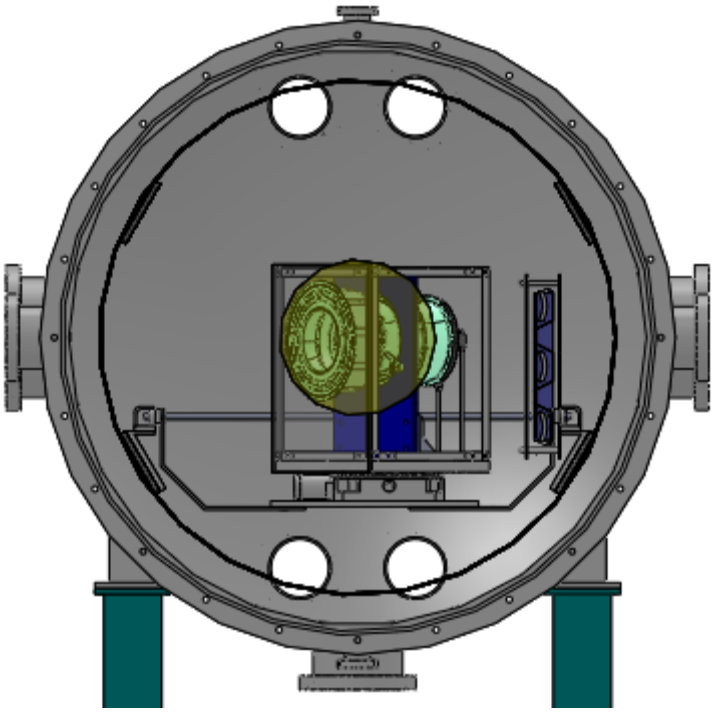

Fig. 6-28 Frontal view of the TVC during simulation of cases #1, 2, 4

In addition to Perihelion case simulation, this set-up allows to simulate the minimum sun angle condition (θ_{MIN} = 38°), which occurs when ν_M is 141.8°.
The following figure illustrates the minimum solar angle condition: baffle is subjected to IR cold flux and solar flux at the same time.
Operations sequence reported in Table 6-6 will be repeated to simulate this condition; 8 test cycles will be performed.

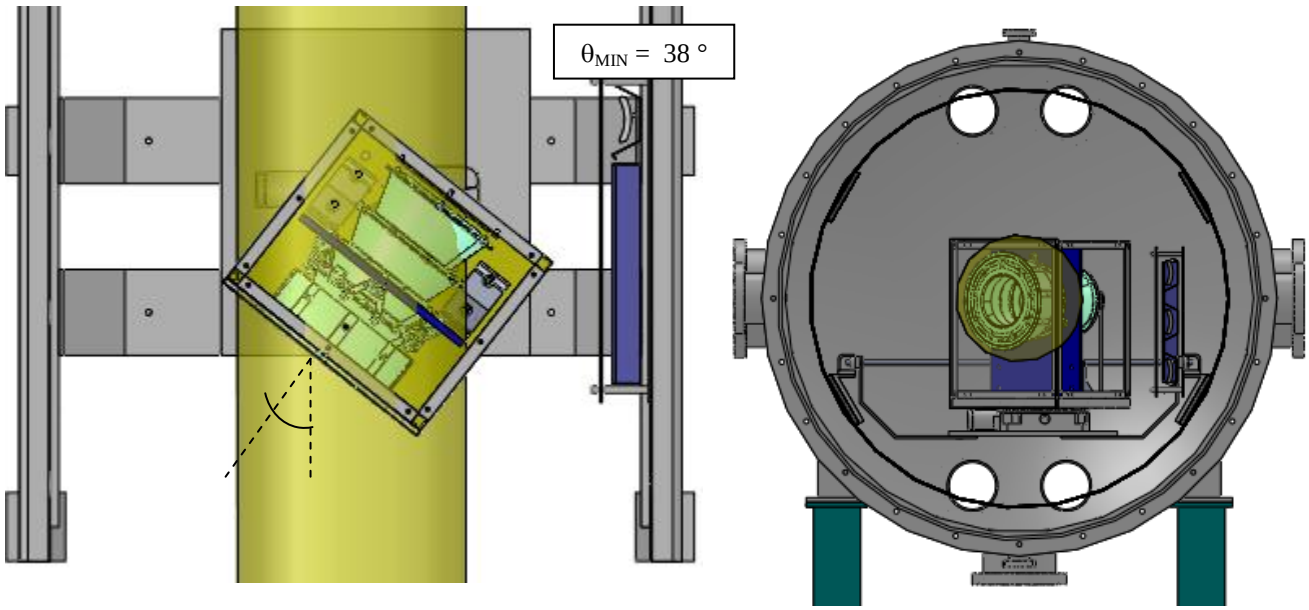

Fig. 6-29 Simulation of minimum solar angle condition

6.4.3.3 Test levels

In order to reproduce test conditions described in the previous paragraph, the following test levels will be assured:

1. Cold IR case (S/C orbiting above Mercury cold surface): the shroud will be cooled in order to reach a temperature close to 100 K, which is minimum temperature of Mercury surface. In particular a temperature of -150°C ($T_{IR\ COLD}$) will be assured. Then thermal stability on the controlled surface will be reached.
2. S/C exiting from the eclipse – case: temperature of the cryostat (shroud and frontal disc) will be maintained @-150°C and the solar simulator will be activated.
3. Hot IR case (S/C orbiting above Mercury hot surface): IR lamps will be switched on in order to obtain an incident heat flux on the instrument box frontal side equivalent to the incident planetary heat flux at Perihelion (4496.1 W/m^2), emitted by Mercury illuminated surface. With this assumption, supposing to employ 4 lamps with a surface mean temperature of 417°C and a heat flux on a reference surface of 17 kW/m^2, a temperature of about 220°C ($T_{IR\ HOT}$) will be imposed on the hot black surface; then the thermal stability on the hot plate will be reached.
4. S/C entering into the eclipse – case: shroud will be cooled in order to reach a temperature of -150°C and the solar simulator will be activated.

The following table summarizes test levels.

Case	Description	Hot plate		Shroud		Solar simulator	θ [°]
		Status	Temperature [°C]	Status	Temperature [°C]	Status	
1	S/C orbiting above Mercury cold surface	OFF		ON	-150	OFF	54
							38
2	S/C exiting from the eclipse	OFF		ON	-150	ON	54
							38
3	S/C orbiting above Mercury hot surface	ON	220	ON	-150	OFF	-90
4	S/C entering into the eclipse	OFF		ON	-150	ON	54
							38

Table 6-7 Detail of temperature values imposed at thermally controlled I/Fs during TVT

The following figure is a representation of one TVT cycle.

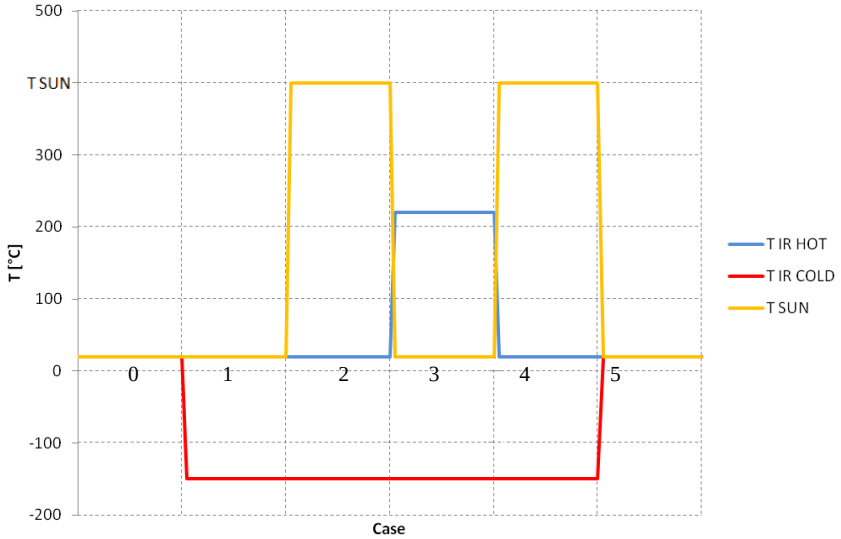

Fig. 6-30 Thermal cycle

The increasing/decreasing of the temperature shall be performed with a rate comprised between [2-10]°C/min and the requested stability is within 1°C/hr. During the cycle the temperature sensors will be continuously recorded by a dedicated PC.

6.5 Step-by-step procedure

Before the test, a baking of the test-bed inside the TVC will be performed.
The following test sequence will be applied during the thermal vacuum tests on baffle QM. During the whole test, item will be mounted inside the thermal vacuum chamber.

1. Perform TVT001 preliminary operation procedure: the unit and all mechanical interfaces are assembled and mounted inside the TVC on the horizontal aluminum plate. All auxiliary sensors are placed on the proper location. Thermal and electrical connections are provided.
2. Perform TVT002: first performance measurement with the solar simulator.
3. Perform TVT003: TVC is opened and qualification test-bed is prepared. All auxiliary sensors are placed on the proper location. Thermal and electrical connections are provided.
4. Perform TVT004: qualification TVTs.
5. Perform TVT005: TVC is opened and test-bed for the second performance measurement is set up. Also hot plate with IR lamps is placed inside the TVC; all auxiliary sensors are placed on the proper location. Thermal and electrical connections are provided.
6. Perform TVT006: second performance measurement with the solar simulator.
7. Perform TVT007: TVTs in space-like environment.
8. Perform TVT008: third performance measurement with the solar simulator.
9. Perform TVT009: all final operations are performed.

6.5.1 QM test sequence

6.5.1.1 Performance measurements

As described before, this sequence will be repeated 3 times during test campaign (see Fig. 6-2).

- Temperature sensors acquisition system switched on;
- Start with operation sequence described in paragraph 6.4.1.2:
    - Check orientation of the baffle: this operation is trivial for the first performance measurement, necessary for the second and third performance measurements, when instrumentation box is placed on the rotary stage (angle between the baffle axis and the solar direction has to be equal to 38°);
    - Check temperature sensors on the baffle bracket plate (which has to be equal to the environment temperature);
    - Switch on the solar simulator;
    - Open TVC shutter;
    - Wait for the stabilization of temperature until the variation is under 1°C/hr;
- Switch off the solar simulator and close the shutter;
- Switch off the temperature sensors acquisition system.

6.5.1.2 Qualification tests

- Temperature sensors acquisition system switched on;
- Start with the TVC cycle described in Table 6-4 and Fig. 6-20:
    - Open the liquid Nitrogen circuit and switch on the heaters;
    - Check the baffle bracket plate and cryostat temperature reaches the value of +85°C±1°C in the expected time;
    - Wait the stabilization until the variation is under 1°C/hr;

  - Check the baffle bracket plate and cryostat temperature reaches the value of -50°C±1°C in the expected time;
  - Wait the stabilization until the variation is under 1°C/hr;
  - Check the baffle bracket plate and cryostat temperature reaches the value of +20°C±1°C in the expected time,
  - Wait the stabilization until the variation is under 1°C/hr;
- Close the liquid Nitrogen circuit & switch off the heaters;
- Switch off the temperature sensors acquisition system.

6.5.1.3 Tests in space-like environment

- Temperature sensors acquisition system switched on;
- Start with the TVC cycle described in Table 6-7 and Fig. 6-30:
  - Rotate the instrumentation box until the angle between the baffle axis and the solar beam direction is equal to θ_{MIN} (minimum solar angle at Perihelion);
  - Cool the shroud by means of liquid Nitrogen and check the temperature sensors (PT100) on the cryostat until temperature reaches $T_{IR\ COLD}$ (±1°C) in the expected time;
  - Wait for the stabilization until the variation of flux source temperature is under 1°C/hr;
  - Switch on solar simulator and open TVC shutter;
  - Check cryostat temperature and TIRD simulator temperature and wait for steady state condition;
  - Close the shutter;
  - Switch on IR lamps;
  - Rotate the instrumentation box until the frontal face of the instrumentation box is parallel to the hot plate.
  - Check hot plate temperature until its temperature reaches $T_{IR\ HOT}$ (±1°C) in the expected time;
  - Wait for the stabilization until the variation of flux source temperature is under 1°C/hr;
  - Switch off IR lamps;
  - Rotate the instrumentation box until the nadir direction is tilted of an angle equal to 54° with respect to the direction of solar flux coming from solar simulator;
  - Open the TVC shutter;
  - Check cryostat temperature and TIRD simulator temperature and wait for steady state condition;
- Repeat this sequence 8 times;
- Switch off the temperature sensors acquisition system.

The previous test sequence can be repeated one time to simulate the condition of minimum sun angle of 38°.

6.5.2 Test procedure

6.5.2.1 QM preliminary operations

Name of test: TVT001 QM preliminary operations			
Description of step	**Reference value**	**Measurement**	**Remarks**
TVT001.1 Place HT MLI on the baffle			

TVT001.2 Fix the baffle on its proper aluminum supporting plate			
TVT001.3 Fix the supporting plate with the baffle on the horizontal aluminum plate			
TVT001.4 Fix the frame supporting HT MLI on the horizontal aluminum plate and the dummy TIRD on the instrument plate			
TVT001.5 Place sensors on the points of interest			
TVT001.6 Cover the dummy TIRD and the baffle support plate with standard MLI			
TVT001.7 Check sensors on the baffle and on other points of interest			
TVT001.8 Place sensors on the shroud and on the horizontal plate and fix them by means of aluminum tape (in order to reduce radiative exchange)			
TVT001.9 Put the baseplate inside the TVC			
TVT001.10 Perform all electrical and thermal interconnections inside and outside the TVC			
TVT001.11 Close the TVC			
TVT001.12 Start temperature recording			

6.5.2.2 First performance measurement

Name of test: TVT002 First performance measurement			
Description of step	**Reference value**	**Measurement**	**Remarks**
TVT002.1 Reduce TVC internal pressure to 1×10^{-6} bar (TBC)			
TVT002.2 Wait for stabilization of the pressure (TBC)			
TVT002.3 Switch on solar simulator and open the shutter			
TVT002.4 Read the temperature of the TIRD simulator (TRP). Wait for stabilization (1°C/hr).	TRP = T_{TIRD}		
TVT002.5 Close the TVC shutter			
TVT002.6 Switch off the solar simulator			
TVT002.7 Temperature sensors acquisition data switched off			

6.5.2.3 Qualification test-bed preparation

Name of test: TVT003 Qualification test-bed preparation			
Description of step	**Reference value**	**Measurement**	**Remarks**
TVT003.1 Switch off TVC			
TVT003.2 Open the TVC			

TVT003.3 Disconnect all electrical interconnections			
TVT003.4 Remove the base-plate from the TVC			
TVT003.5 Place temperature sensors on the shroud			
TVT003.6 Place the shroud on the base-plate			
TVT003.7 Cover the shroud with standard MLI			
TVT003.8 Put the baseplate with its supporting structure and all I/Fs inside the TVC			
TVT003.9 Perform all electrical and thermal interconnections inside and outside the TVC			
TVT003.10 Close the TVC			
TVT003.11 Start temperature recording			

6.5.2.4 QM Qualification TVT

Name of test: TVT004 QM Qualification TVT			
Description of step	**Reference value**	**Measurement**	**Remarks**
TVT004.1 Reduce TVC internal pressure to 1×10^{-6} bar			
TVT004.2 Wait for stabilization of the pressure			
TVT004.3 Verify the synchronization between external PC and controllers			
TVT004.4 Initialize the temperature profile of heat sources to PC and controllers			
TVT004.5 Open the liquid Nitrogen circuit			
TVT004.6 Read the temperature of the baffle bracket plate (TRP1) and the shroud (TRP2) until value is equal to +85 °C, and wait for stabilization (1°C/hr).	TRP1 = 85 °C TRP2 = 85 °C		
TVT004.7 Wait 2 hours at the stabilized temperature			
TVT004.8 Read the temperature of the baffle bracket plate (TRP1) and the shroud (TRP2) until value is equal to -50 °C, and wait for stabilization (1°C/hr).	TRP1 = -50°C TRP2 = -50°C		
TVT004.9 Wait 2 hours at the stabilized temperature			
TVT004.10 Read the temperature of the baffle bracket plate (TRP1) and the shroud (TRP2) until value is equal to environment temperature	TRP1 ~ 20°C TRP2 ~ 20°C		
TVT004.11 Temperature sensors acquisition data switched off			

TVT004.12 Close the liquid Nitrogen circuit			
TVT004.13 Controllers and heaters switched off			

6.5.2.5 Test-bed for the second performance measurement preparation

Name of test: TVT005 Test-bed for the second performance measurement preparation			
Description of step	**Reference value**	**Measurement**	**Remarks**
TVT005.1 Switch off TVC			
TVT005.2 Open the TVC			
TVT005.3 Disconnect all electrical interconnections			
TVT005.4 Dismount QM and all I/Fs and components from TVC			
TVT005.5 Mount rotation stage on the aluminum baseplate externally to the TVC			
TVT005.6 Fix the aluminum plate which supports instrumentation box on the rotation stage			
TVT005.7 Fix clamps which support the baffle bracket plate on the aluminum plate of the instrumentation box			
TVT005.8 Fix aluminum plate supports baffle on the aluminum plate which supports instrument box, thanks to the devoted clamps			
TVT005.9 Fix the frame on the aluminum plate, the baffle on its supporting plate and the dummy TIRD on the instrument plate			
TVT005.10 Place sensors on the points of interest			
TVT005.11 Cover the dummy TIRD and the baffle support plate with standard MLI			
TVT005.12 Check sensors on the baffle and on other points of interest			
TVT005.13 Cover the instrument box with HT and standard MLI			
TVT005.14 Fix the hot plate with the IR lamps on the supporting structure of the base plate			
TVT005.15 Place sensors on the shroud and on the hot plate and fix them by means of aluminum tape (in order to reduce radiative exchange)			
TVT005.16 Put the baseplate with its supporting structure and all I/Fs inside the TVC			
TVT005.17 Perform all electrical and thermal interconnections inside and outside the TVC			

TVT005.18 Close the TVC			
TVT005.19 Start temperature recording			

6.5.2.6 Second performance measurement

Name of test: TVT006 Second performance measurement			
Description of step	**Reference value**	**Measurement**	**Remarks**
TVT006.1 Reduce TVC internal pressure to 1×10^{-6} bar (TBC)			
TVT006.2 Wait for stabilization of the pressure (TBC)			
TVT006.3 Check baffle orientation (angle between baffle axis and solar direction shall be 38°)			
TVT006.4 Switch on solar simulator and open the shutter, wait for stabilization			
TVT006.5 Read the temperature of the TIRD simulator (TRP1) and wait for stabilization (1°C/hr).	TRP = T_{TIRD}		
TVT006.1 Close the TVC shutter			
TVT006.2 Switch off the solar simulator			
TVT006.3 Temperature sensors acquisition data switched off			

6.5.2.7 Tests in space-like environment

Name of test: TVT007 Tests in space-like environment			
Description of step	**Reference value**	**Measurement**	**Remarks**
TVT007.1 Verify the synchronization between the rotation stage and external PC			
TVT007.2 Verify the synchronization between external PC and controllers			
TVT007.3 Initialize the temperature profile of heat sources to PC and controllers			
TVT007.4 Initialize the rotation angle profile to rotation stage controller			
TVT007.5 Open the liquid Nitrogen circuit			
TVT007.6 Read the temperature of the cryostat (TRP1) until value is equal to $T_{IR\ COLD}$ and of the hot plate (TRP2), wait for stabilization (1°C/hr).	TRP1 = $T_{IR\ COLD}$ TRP2 = 20°C		
TVT007.7 Wait 2 hours at the stabilized temperature			
TVT007.8 Switch on solar simulator and open the shutter			
TVT007.9 Read the temperature of the cold plate (TRP1) and check that its value is equal to $T_{IR\ COLD}$. Read the temperature of	TRP1 = $T_{IR\ COLD}$ TRP2 = T_{TIRD}		

the TIRD simulator (TRP2). Wait for stabilization (1°C/hr).			
TVT007.10 Close the TVC shutter			
TVT007.11 Switch on IR lamps			
TVT007.12 Read the temperature of the hot plate (TRP1) until value is equal to $T_{IR\ HOT}$, wait for stabilization (1°C/hr).	TRP1 = $T_{IR\ HOT}$		
TVT007.13 Wait 2 hours at the stabilized temperature			
TVT007.14 Switch off IR lamps			
TVT007.15 Open TVC shutter			
TVT007.16 Read the temperature of the cold plate (TRP1) and check that its value is equal to $T_{IR\ COLD}$. Read the temperature of the TIRD simulator (TRP2) and wait for stabilization (1°C/hr).	TRP1 = $T_{IR\ COLD}$ TRP2 = T_{TIRD}		
TVT007.17 Temperature sensors acquisition data switched off			
TVT007.18 Close the liquid Nitrogen circuit			
TVT007.19 Controllers switched off			

6.5.2.8 Third performance measurement

Name of test: TVT008 Third performance measurement			
Description of step	**Reference value**	**Measurement**	**Remarks**
TVT008.1 Check baffle orientation (angle between baffle axis and solar direction shall be 38°)			
TVT008.2 Read the temperature of the TIRD simulator (TRP) and check that its value is at environment temperature	TRP ~ 20°C		
TVT008.3 Switch on solar simulator and open the shutter, wait for stabilization			
TVT008.4 Read the temperature of the TIRD simulator (TRP1) and wait for stabilization (1°C/hr).	TRP = T_{TIRD}		
TVT008.5 Close the TVC shutter			
TVT008.6 Switch off the solar simulator			
TVT008.7 Temperature sensors acquisition data switched off			

6.5.2.9 TV Final operations

Name of test: TVT009 TV Final operations			
Description of step	**Reference value**	**Measurement**	**Remarks**
TVT009.1 Switch off TVC			
TVT009.2 Open the TVC			
TVT009.3 Disconnect electrical cables			
TVT009.4 Disconnect thermal			

interconnections			
TVT009.5 Dismount QM and all I/Fs from TVC			

7. Design of two thermal vacuum chambers for the calibration activity on SIMBIO-SYS instruments

7.1 Introduction

This chapter describes the design process which has been followed to realize two thermal vacuum chambers for the calibration and the qualification of STC-VIHI and HRIC units. The TVCs will be delivered in 2013 to Selex ES S.p.A., which is responsible for the manufacturing and the delivery to the Italian Space Agency (ASI) of the SIMBIO-SYS units. The calibration represents a fundamental step of a space instrument life cycle, since it allows to obtain the Key Data Parameters which are used in a following phase by specific algorithms to obtain the Mercury topographical data, mineralogy composition and basic information necessary for stereo 3D reconstruction of the planet surface (Digital Terrain Model).
Both TVCs for STC-VIHI and HRIC support compatibility with a double operating mode, realizable with a single interchangeable mechanical flange:

- Without baffles: this operating mode is dedicated to test units performance in vacuum conditions;
- With baffles: for stray-light measurements and on-ground validation.

The activity started with the conceptual design, followed by the detailed design, the procurement of the components, the realization and the test of the TVCs. The last paragraph describes thermal tests performed on the thermal vacuum chamber of HRIC.

7.2 TVC for STC and VIHI

7.2.1 Introduction

This paragraph describes the mechanical, thermal and electrical interfaces of the TVC for the calibration of STC.VIHI units and the overall configuration, which has been defined in order to fulfill some specific technical requirements, which are hereafter listed. Several structural and thermal analyses have been performed in order to size the components and all mechanical and thermal interfaces.

7.2.2 General requirements

Requirements which have been defined by Selex ES are hereafter summarized. The following scheme sketches the list and the types of requirements:

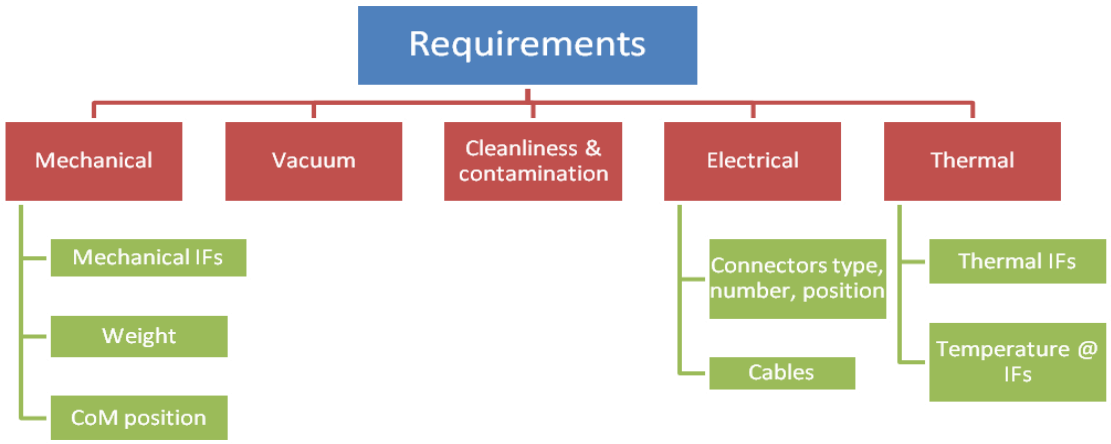

Fig. 7-1 Type of requirements to be fulfilled in the TVC design

7.2.2.1 Mechanical requirements

M1. The unit (STC-VIHI) under test has to be ideally included inside an envelope with the following dimensions: 300 mm in *x* direction, 320 mm in *y* direction and 250 mm in *z* direction. The reference system is represented in the following figure.

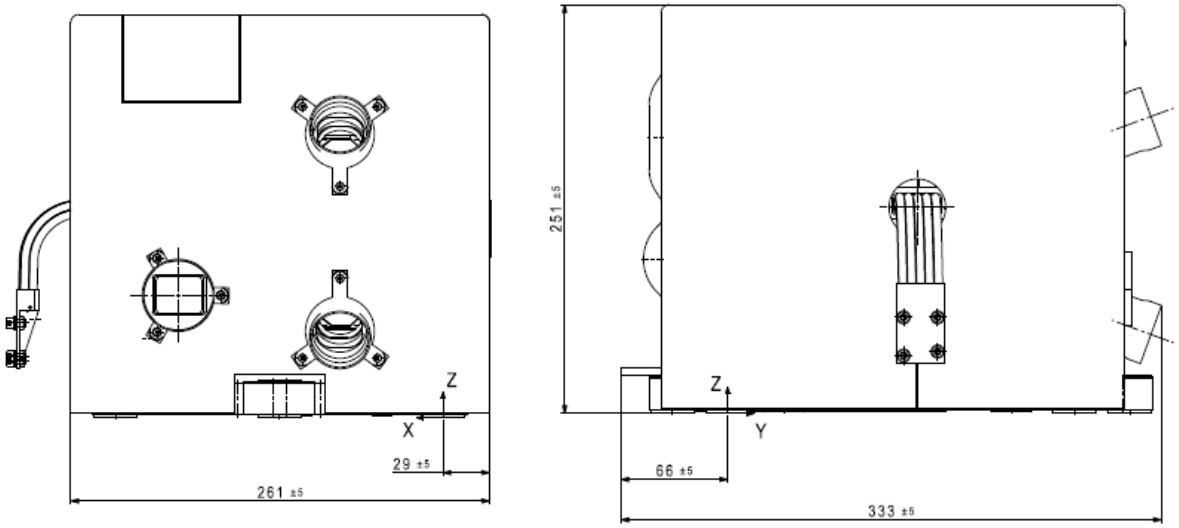

Fig. 7-2 Reference frame of STC-VIHI unit

M2. STC-VIHI channels have to be rotated of 90° w.r.t. the flight configuration in order to have the 2 sub-channels apertures horizontal. The TVC has to be fixed thanks to a dedicated mechanical I/F on a rotary stage, in order to minimize the number of rotations actuators to explore both STC sub-channels and simplify the operations (azimuthal rotation instead of zenithal one).

M3. The TVC has to be provided with 2 mechanical parts: a bottom part has to be fixed to the rotary stage and to the optical bench, the top part has to be removable and provided with mounting columns in order to guarantee the repeatability of operations and avoid any damages to the instruments during mounting operations.

M4. Thermal flanges (dedicated to thermal connections), electrical flanges (dedicated to the electrical connections), vacuum flange (dedicated to the vacuum pump group) have to be placed on the fixed bottom part of the TVC, in order to easily remove the upper part without interfere with the performed connections and minimize the weight of the upper part (which has to be lifted during mounting operations).

M5. The TVC has to be provided with a stainless steel "L-shape" I/F: on this I/F other plates have to be mounted, according to the following scheme.

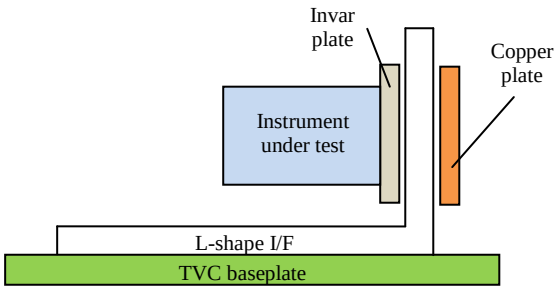

Fig. 7-3 Main mechanical I/Fs inside the TVC

M6. According to the previous figure, a copper plate, thermally actively controlled, has to be fixed to the stainless steel "L-shape" structure and thermally decoupled with respect to the support structure itself, in order to guarantee the thermal control of the instrument plane (invar plate).

M7. According to the previous figure, the instrument support plate is an invar plate, which has to be fixed on the stainless steel I/F and thermally decoupled with respect to the I/F itself.

M8. A 3 points regulation system has to be foreseen on the instrument plane, in order to guarantee the pitch/roll regulation (yaw regulation is performed thanks to the rotation stage) with a resolution of 20 arcsec (100 μrad).

M9. The maximum distance between the STC structure and the external surface of the optical window is 175 mm, measured in the direction normal to the STC-VIHI structure wall (in order to avoid vignetting with OGSE).

M10. Residual vibrations incoming from the external environment have to be minimized. Therefore the vacuum pump has to be switched off during some measurements and vacuum inside the TVC should be maintained (maximum value of 10^{-5} mbar for at least 30 minutes).

M11. TVC weight in its operative configuration with all parts mounted on it (e.g. pumps) has to be lower than 250 kg. This value is given by the maximum load which the rotation stage is able to outstand (the rotation stage is a Newport RV 350 HAHLT-F).

M12. The CoG of the TVC in its operative configuration has to be contained in the mechanical I/Fs perimeter shown in the following figure and very close to the centre of the circle, which passes though the rotation stage axis. Service-weights can be used in order to fulfill this requirement.

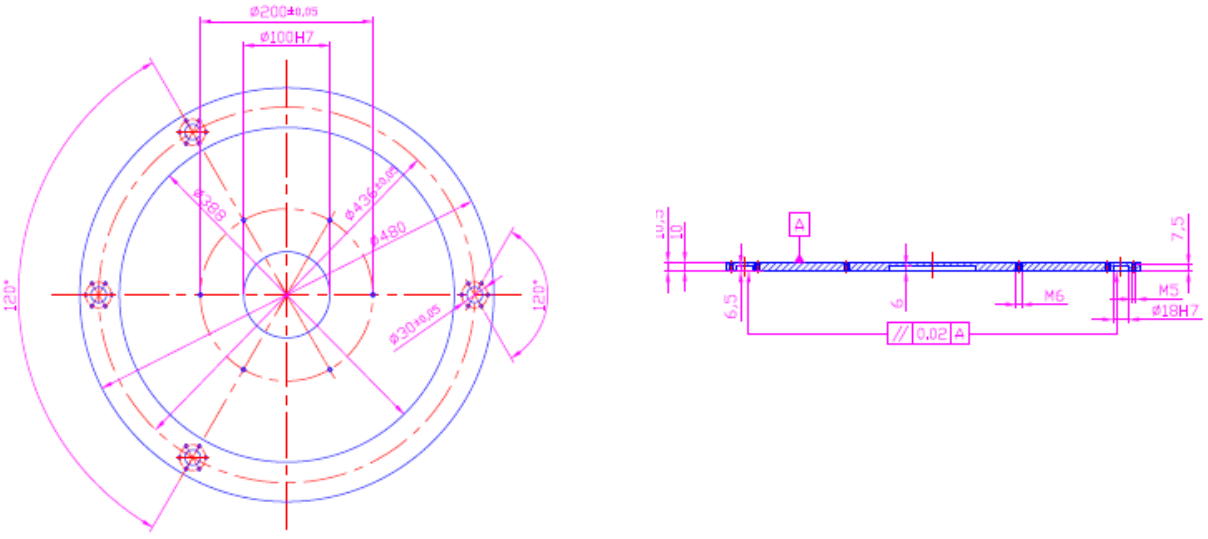

Fig. 7-4 Mechanical I/F of the STC-VIHI TVC: the pattern allows coupling with the rotation stage

M13. TVC has to be provided with external hooks which allow to lift and move it.

M14. The I/F with the rotary stage (see previous figure) has to be directly soldered form exterior to the bottom part of the TVC.

M15. According to the previous figure, the TVC interfaces with the rotation stage with its rotation axis along the local vertical and passing through STC pivot point (within 5 mm tolerance), which is the intersection between the 2 STC channels optical axes. Required details can be realized if the TVC bottom support plate thickness is at least 10.5 mm. Given the properties of the Newport rotation stage, the relation between the vertical load and the misalignment between the rotation stage axis and the axis passing through the load CoG is:

$$W \leq \frac{W_{\max}}{1 + \frac{d}{A}}$$

where W[N] is the vertical load, $W_{\max}$ [N] is the maximum admissible load for the rotation stage, d [mm] is the misalignment between the rotation stage axis and the axis passing through the load CoG, A [mm] is an intrinsic rotation stage parameters equal to 100 mm. For our purposes, the maximum admissible misalignment ($d_{\max}$) is equal to 5 cm.

M16. The TVC has to be transportable with the instrument mounted and fixed inside it. Therefore all I/Fs will be separated from the TVC surface and cleanliness requirements will be guaranteed by pumping dry Nitrogen through the TVC valves. This requirement derives from the need to perform the straylight measurements outside the cleanroom, with only electrical interfaces mounted on the TVC.

M17. The TVC material has to be selected in order to minimize its weight and guarantee the vacuum requirements.

M18. A remotely driven shutter has to be placed inside the TVC, in front of the VIHI entrance port. Its sizes and distance from the aperture has to be sufficient to completely cover the VIHI entrance port when it is closed and without causing any vignetting when it is commanded open. In order to reduce the shutter emissivity, the internal surface, facing to the VIHI channel, has to be manufactured in reflecting material. This tool allows to perform a dark current measurement of the VIHI instrument.

M19. The TVC has to be provided with an external optical reference cube, located on the same flange hosting the optical windows. The optical quality requirements has to be guaranteed on at least two faces (front and lateral ones) and the cube side has to be at least 25 mm long. Perpendicularity between the reflecting faces and the face fixed on the TVC external surface has to be within 5arcmin. By this cube, which defines the TVC reference frame, the direction of the TVC (and hence STC-VIHI) rotating axis with respect to the OGSE reference frame can be measured. This measurement together with the angles between STC-VIHI optical reference frame and the TVC reference frames, allows to figure out the STC-VIHI reference frame with respect to the OGSE one.

M20. The TVC has to be provided with three BK7 windows, provided by Selex ES: two windows are dedicated to the two STC sub-channels and have to be large enough to guarantee the simultaneous view of the STC entrance ports and relevant lateral face of the STC reference mirror along the direction normal to the faces. Each window has to be located in front of the STC entrance port perpendicularly, within ±1° accuracy, to the relevant optical axis .The third one is dedicated to the total view of the STC reference mirror front face (along its normal direction).

M21. The TVC has to be provided with a quartz window, large enough to view the VIHI entrance port without obscuring the VIHI entrance beam in whole Field Of View. It has to be located in front of the VIHI entrance port perpendicularly, within ±1° accuracy, to the optical axis. The material has been chosen considering its transparency in the Near IR wavelength spectrum.

M22. The TVC has to be provided with a BK7 window, placed in front of the STC/VIHI reference mirror perpendicularly, within ±1° accuracy, to the optical axis.

M23. Optical windows have to be accommodated on a dedicated flange easily removable from the TVC vessel. The mechanical I/Fs of the optical windows have to be perpendicular to each optical axis. In this way the internal of the TVC in easily accessible, by using a quick-lock system to fix the windows mechanical I/Fs to the TVC.

M24. Measurements with baffles, performed at 1 bar pressure, foreseen that baffles can be accommodate in their final flight configuration inside the TVC by means of a devoted mechanical I/F. The maximum distance between the STC-VIHI structure and the baffle flange is 65 mm in the *y* direction. Also the TVC flange hosting the baffles has to be easily removable. During measurements with baffles the internal volume has to be filled with dry Nitrogen in order to have a minimum over-pressure with respect to the ambient one avoiding contamination. The following figure shows the unit with baffles in its flight configuration. Holes have to be practiced on the mechanical flange, in order to accommodate the baffles.

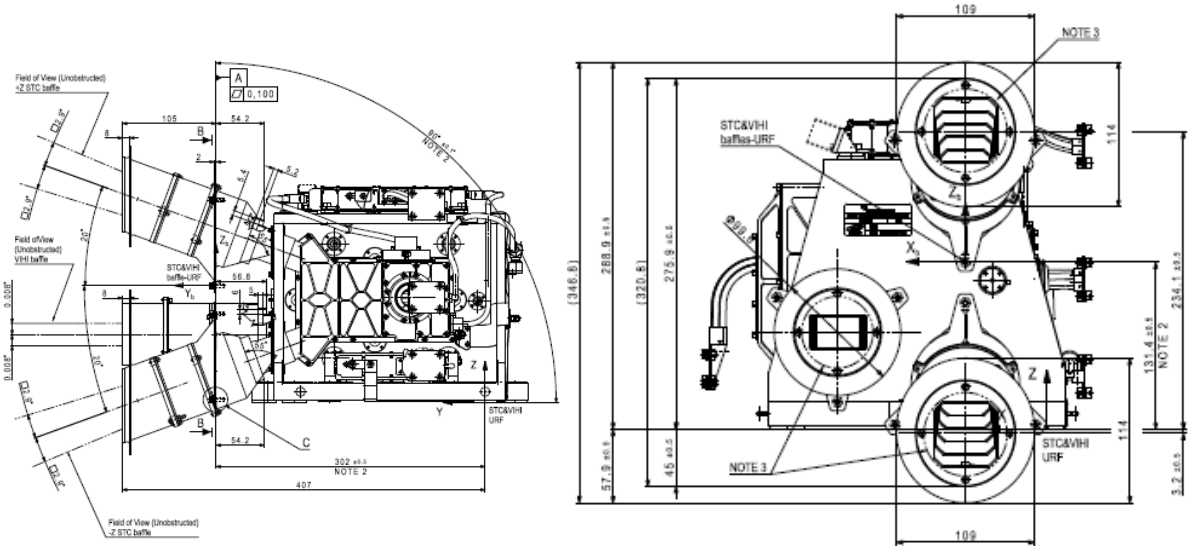

Fig. 7-5 STC-VIHI unit with baffles

M25. Gaskets which will not frequently removed during test campaign have to be realized in Copper, gasket of removable flanges in rubber.

M26. All electrical and thermal I/Fs have to be placed on the fixed bottom part of the TVC, in order to simplify mounting operations. Harness length have to be minimized and thermal flange has to be placed as closest as possible to the thermal I/Fs.

M27. The alignment between the upper and bottom part of the TVC has to be guaranteed thanks to 3 auto-centre columns (tolerance on the columns diameter of 0.1 mm).

7.2.2.2 Vacuum requirements

V1. Pressure inside the TVC has to be equal to 10^{-6} mbar with rotary and turbo-molecular pumps activated.

V2. The vacuum level has to be guaranteed with the pumping system switched off for at least 30 minutes. Maximum allowed pressure after 30 minutes is 10^{-5} mbar. In this way some critical measurements can be performed (e.g. PSF measurements) in vacuum without the vibrations inducted by the pumping system.

7.2.2.3 Cleanliness and contamination requirements

C1. Since tests will be performed on Flight Models of the units, materials compliant with contaminations requirements have to be used. Non-metallic materials can be used

taking into account their out-gassing rate, their amount and location and their configuration. The following table is considered as guideline:

Applied Material Mass Range	Outgassing Parameters (%)		
	Total Mass Loss	Collected Volatile Condensed Material	Recovered Mass Loss
> 100 gr		≤ 0.01	≤ 0.1
10 ÷ 100 gr		≤ 0.05	≤ 0.5
< 10 gr	≤ 1.0	≤ 0.1	

Table 7-1 Outgassing parameters

All components inside the TVC (cables, sensors, mechanical parts) have to be submitted to dedicated clean and outgassing processes.

C2. An easily accessible cold trap has to be included inside the TVC: this cold trap, maintained at temperature lower than the lowest environmental one, is realized by means of an external dewar and an internal dedicated removable cold plate able to catalyze eventual volatile particles inside the TVC. The optimal position of the cold trap is on the upper part of the chamber, with the dewar placed in vertical position (in order to maximize its efficiency).

C3. The external dewar should have an autonomy of at least 24 hours, thanks to a dedicated internal Nitrogen reservoir or by an external liquid Nitrogen line.

C4. A DN_2 valve has to be foreseen since dry Nitrogen is needed to avoid contamination during tests at ambient pressure. During tests with baffles, the holes of the baffles act as outlet valves; purging connectors of the instrument can be used as inlet valves.

7.2.2.4 Electrical requirements

TVC has to be provided with the following connectors, which should be placed on the same flange in order to minimize cables length, on the bottom fixed part of the TVC:

- Two 15 pins MDM (SRIMD2006-15) connectors for STC-VIHI spacewire data.
- Two 37 pins Dsub connectors, for power supply and service purposes.
- One 50 pins Dsub connector, for service purposes.

7.2.2.5 Thermal requirements

T1. Three thermal I/Fs have to be designed inside the TVC:

a. The Cold Heat Pipe Simulator, connected to the thermal strap dedicated to VIHI detector;
b. The Hot Heat Pipe Simulator, connected to the thermal straps dedicated to STC-VIHI Proximity Electronics (PEs) and STC detector;
c. The invar plate which supports the unit.

The following table summarizes the thermal levels and the dissipation values which have to be guaranteed at the different I/Fs (values are obtained taking into account the ±10°C qualification margin):

Thermal I/Fs	Cold case		Hot case	
	T_{min} [°C]	Minimum internal power to be subtracted [W]	T_{max} [°C]	Minimum internal power to be subtracted [W]
Hot Heat Pipe	-20	4.71	24	8.46
Cold Heat Pipe	-70	0.06	-6.5	2.46
Mounting feet	-50	This power derives directly from the thermal	+50	This power derives directly from the

		analysis results [referred to reduced model provided to the supplier] combined with the TVC thermal model		thermal analysis results [referred to reduced model provided to the supplier] combined with the TVC thermal model

Table 7-2 Temperature and dissipation levels at the different thermal I/Fs for STC-VIHI TVC

The thermal cycle to be reproduced is reported in the following figure:

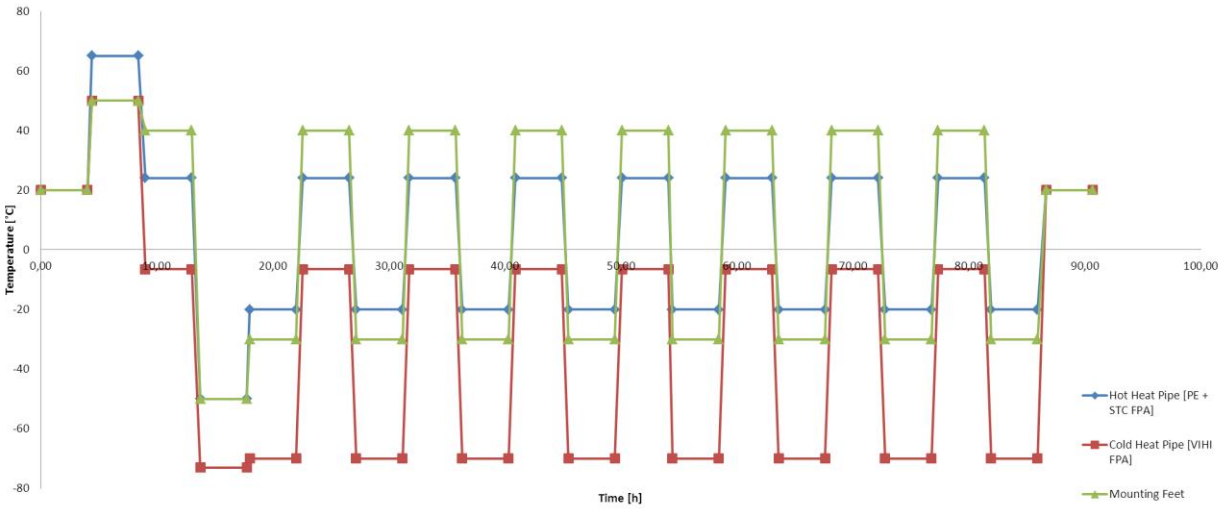

Fig. 7-6 Thermal cycle to be assured on the thermal I/Fs of STC-VIHI TVC

The number of cycles has been deduced accordingly to EID-A requirements for thermal tests; dwell time duration is 4 hours and change temperature rate is 2°C/minute; in fact the real temperature rate can be different for different heat pipes. The required stability is 1°C/hour. The previous thermal cycle is imposed taking into account that TVC will be used for alignment, performance, qualification and calibration test activities.

T2. The TVC has to be provided with an external thermal conditioning system able to achieve the temperature values defined before, separately for each heat pipe simulator.

T3. The length of the external pipes connecting the cryostat to the TVC thermal flange has to be minimized, in order to minimize heat losses along the connections.

T4. The heat pipes and all thermal I/Fs (excluding the invar support plate) have to be produced in copper.

T5. Ten temperature sensors have to be supplied, for monitoring purposes. The request accuracy is 0.1°C. The temperature of the following critical points will be monitored:

- 4 positions close to the 4 instrument thermal straps extremities (STC and VIHI detectors, STC and VIHI PEs)
- 2 points on the baseplate
- Other points still TBC.

Also controllers have to be supplied.

7.2.3 Conceptual design

Taking into account the requirements summarized in the previous paragraph, the conceptual design of the TVC has been performed. The system can be conceived as composed of the following parts:

1. Thermal vacuum chamber, realized in stainless steel (AISI 316) and characterized by a cylindrical shape. The chamber is composed of two different parts:
   - a bottom part, which is fixed, interfaces with the rotation stage (by means of the pattern represented in Fig. 7-4) and hosts flanges for electrical, thermal and vacuum interconnections.
   - An upper removable part, which hosts the flanges for the viewports and the cold trap.

   Inside the TVC the mechanical I/Fs for supporting units and thermal I/Fs are present, together with the cold plate of the cold trap, heaters and temperature sensors for the thermal control.
2. Pumping system, composed of a turbo-molecular pump and a rotary pump, with their devoted vacuum (pressure) sensors (Pirani and Penning sensors) and controllers.
3. An ultra cryostat for the thermal control of the internal thermal I/Fs.
4. An external dewar containing liquid Nitrogen for the supply of the cold trap.
5. Cabling and connectors, together with the controllers for the thermal control.

The following figure sketches the system briefly described before:

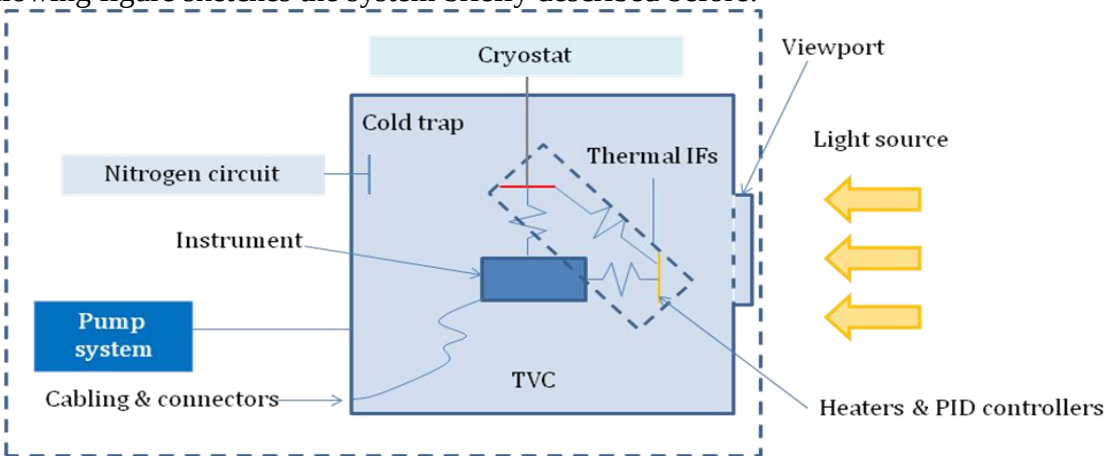

Fig. 7-7 Conceptual scheme of the system

The thermal control of the 3 different thermal I/Fs to be controlled (Hot Heat Pipe Simulator, Cold Heat Pipe Simulator and invar plate supporting the unit) is based on the following principle: the copper plate attached on the "L-shape" stainless steel represented in Fig. 7-3 is provided with an internal coil and can be actively controlled by means of a liquid circulating along the coil; the fluid is a Thermal HY-Baysilone-Oel M3 liquid operating in the range -80°C up to +55°C and it can be heated and cooled thanks to a FP89-ME Julabo Ultra Cryostat, operating in the range -90°C up to 100°C and provided with its proper temperature controller. The copper plate is connected to the invar plate and to the heat pipe simulators (hot and cold) by means of copper thermal straps and, thanks to this conductive link, acts as a heat sinks with respect to the other I/Fs. All the copper plates are covered with MLI in order to reduce the thermal exchange through radiation with the internal parts of the TVC. In addiction the thermal I/Fs (cold and hot heat pipe simulators and invar plate) are provided with a dedicated heater and a PT100 (one for each thermal I/F), connected to 3 CAL9900 controllers, which allow the fine regulation of the temperature on the different I/Fs. In the previous figure, the red segment sketches the copper plate provided with coil and connected to the external ultra-cryostat, the yellow segment represents the thermal I/Fs, thermally connected by conduction to the actively controlled copper plate.
The following figures show the final drawings of the Thermal Vacuum Chamber: in the first 2 figures the main components of the top part are evidenced (external view), in the 3rd and 4th figures the main components of the bottom part are evidenced (both internal and external view). Numbers identify the different vacuum flanges, which are described in the following table.

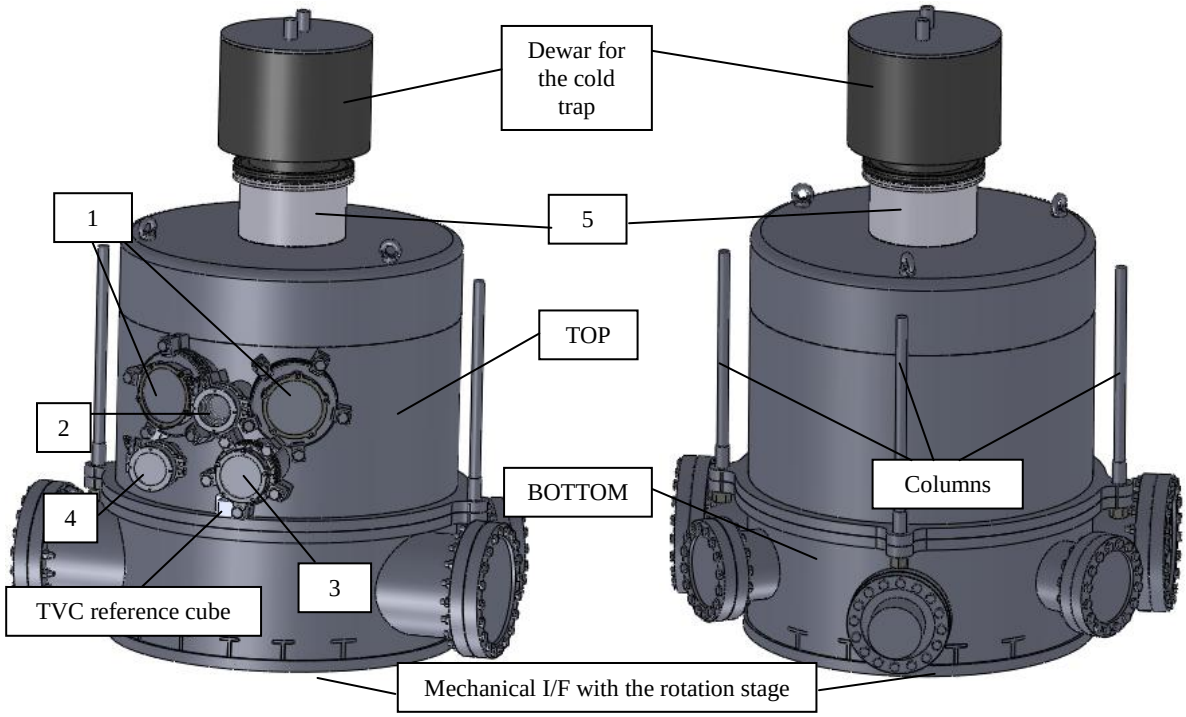

Fig. 7-8 Main components of the TVC (external view)

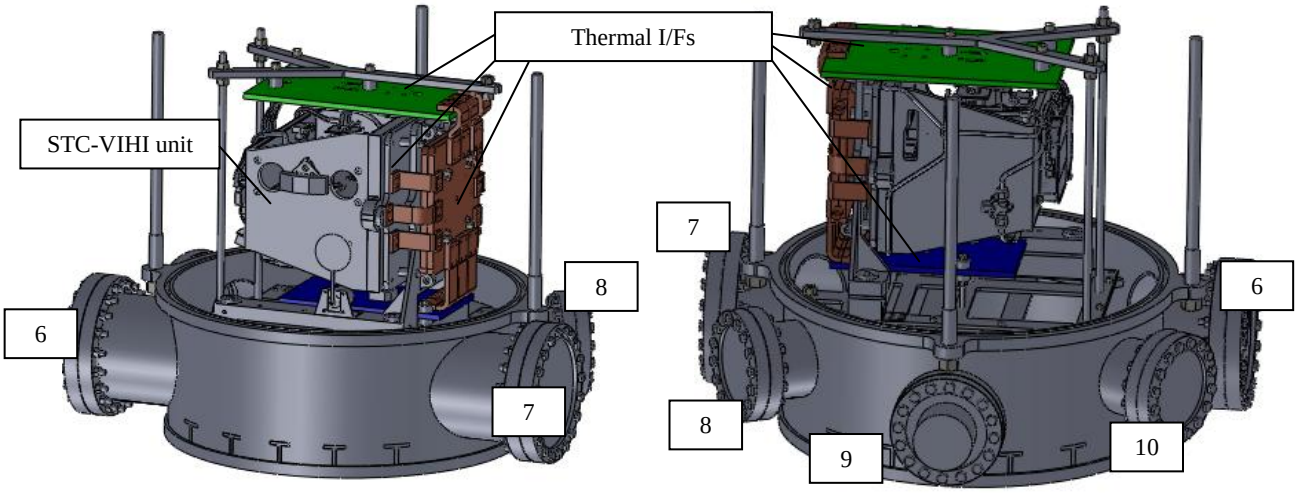

Fig. 7-9 Main components of the TVC (external and internal view)

Number	Type of flange	Description	Position
1	ISO100	STC channels viewports	Top part
2	NW40	STC reference cube viewport	
3	ISO63	VIHI channel viewport	
4	NW40	Unit reference cube viewport	
5	ISO 160	Dewar	
6	CF150	Flange for the electrical interconnections (2×15 pins MDM connectors, 2×37 pins Dsub connectors, 1×50 pins Dsub connector)	Bottom part
7	CF150	Flange for the thermal interconnections (1×CF40 for PT100, 1×CF40 for fluid feedthrough)	
8	CF100	Flange for the dry Nitrogen valve (1×CF16), the Pirani (1×NW16) and Penning (1×CF40) gauges	
9	CF100	Gate for the turbo-molecular pump	
10	CF100	Service flange for 2 additional Dsub 37 pins connectors	

Table 7-3 Position and description of the vacuum flanges present on the TVC

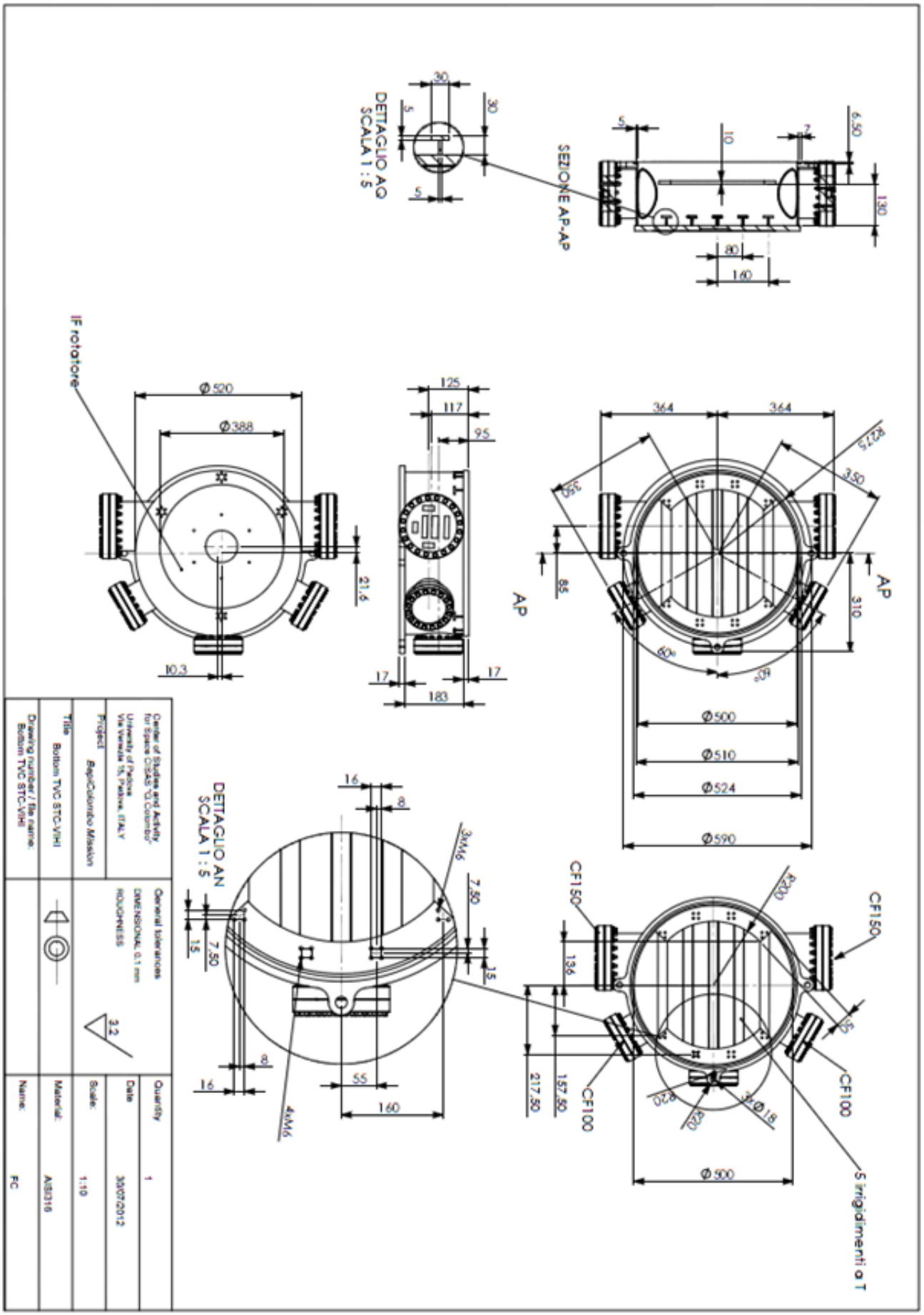

Fig. 7-10 Final drawing of the bottom part of the TVC

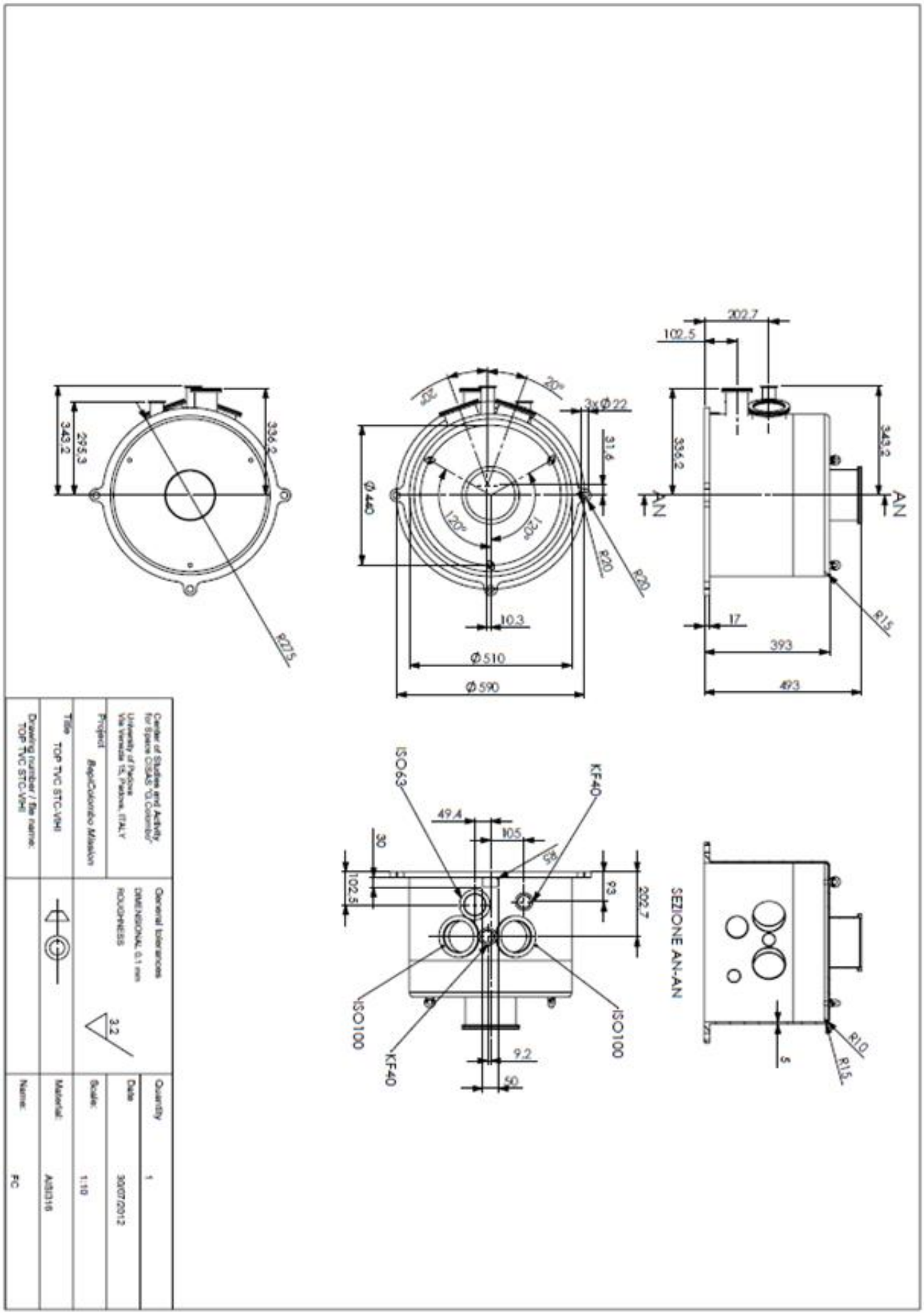

Fig. 7-11 Final drawing of the top part of the TVC

7.2.4 Mechanical interfaces

In this paragraph mechanical I/Fs of the TVC are listed and described, both for the vacuum configuration and for the configuration at ambient pressure devoted to the measurements with baffles.
The second operating mode (at ambient pressure) is derived from the first operating mode (in vacuum) simply lifting the top part of the TVC and replacing it with an aluminum flange for supporting the baffles. Therefore the bottom part remains unchanged and fixed to the rotation stage passing from the first to the second configuration, simplifying the test procedures and the operations.

7.2.4.1 Configuration in vacuum

As described before, the TVC is a cylindrical body in AISI316 characterized by the following main properties:

Property	Value
Total weight	235 kg
Internal Diameter	500 mm
External diameter	510 mm
Cylindrical body height	610 mm
Dewar protrusion	307 mm
Total height	917 mm

Table 7-4 Main mechanical properties of the TVC

From the previous table, it can be seen that the requirement on the maximum weight of 250 kg (M11) is fulfilled.
According to M12 and M15, the CoM of the TVC has been kept as closest as possible to the rotation axis of the rotary stage, which passes through the Pivot axis. As shown in the following figure, the pattern on the mechanical I/F between the TVC and the rotation stage has been de-centered with respect to the cylindrical body in order to fit with M15 requirement: in particular the axis of rotation is about 10.3 mm far in z direction (in the TVC reference frame, represented in the figure below) and 21.6 mm far in x direction from the TVC cylindrical axis.

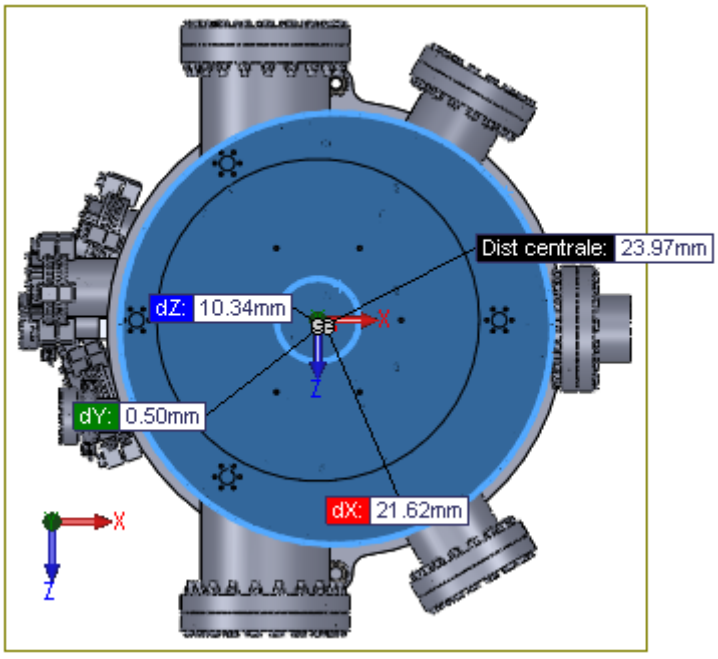

Fig. 7-12 Position of the rotation axis with respect to the cylindrical axis

The CoM is about 32.3 mm far from the rotation axis, which is lower than the 50 mm of the requirement (M15 requirement is fulfilled).
The top part (393 mm high) interfaces with the bottom part (217 mm high) thanks to a custom flange (having an external diameter of 550 mm) which hosts a rubber seal and three 18 mm-diameter holes for the columns which allow to align the top part with the bottom part. The following figure shows the alignment procedure between the top and bottom parts.

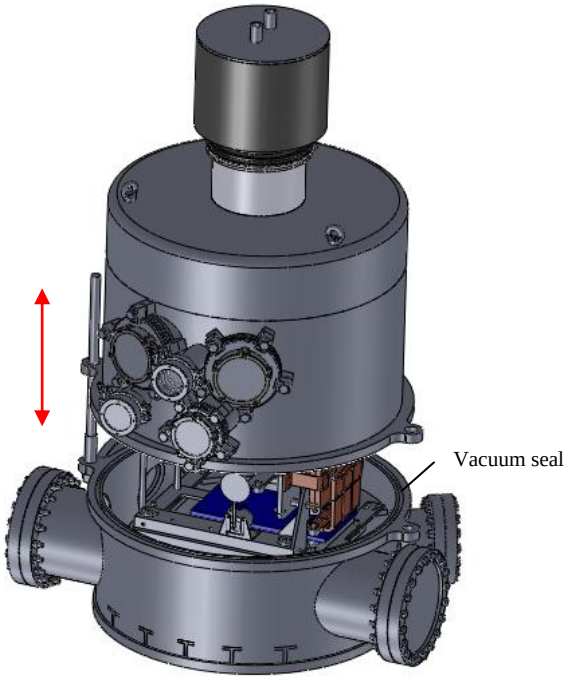

Fig. 7-13 Alignment procedure between the top and bottom part of the TVC

Internally the bottom part is provided with four T-section beams which support an AISI316 frame on which the "L-shape" structure described in M5 and 6 threaded bars are fixed: three longer M10 threaded bars support the hot heat pipe simulator, 3 shorter M6 threaded bars support the cold heat pipe simulator ("L-shape" structure and the heat pipe simulator plates are not shown in the figure).

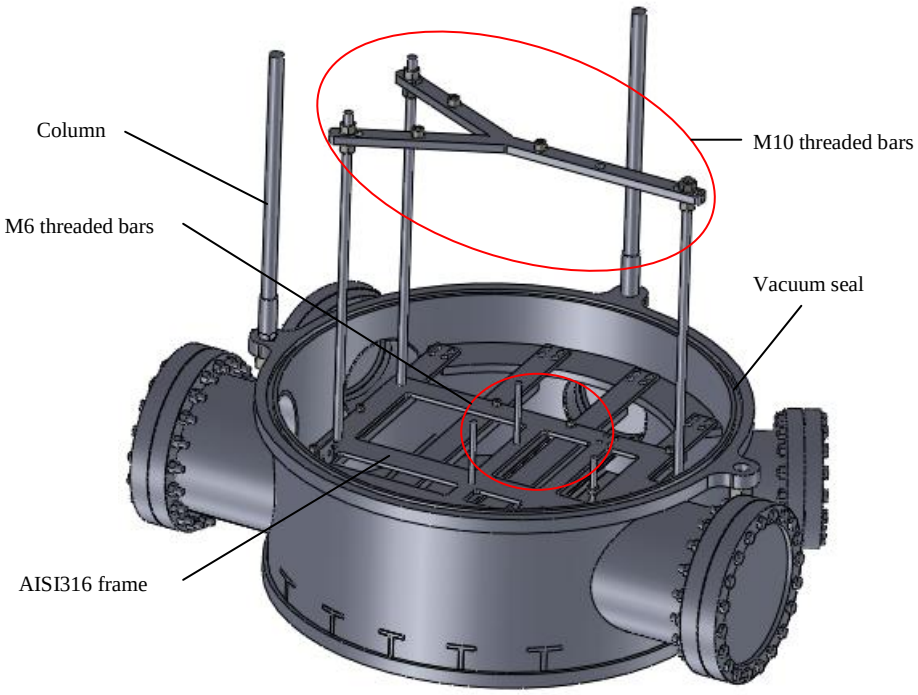

Fig. 7-14 Internal structural components of the TVC (1)

The following figure shows the components which are fixed to the AISI316 frame: the “L-shape” stainless steel structure, which supports the copper plate (on the right) by means of four M6 screws and the invar plate (on the left) by means of eight M5 screws, and the heat pipe simulators (green and blue plate), which are fixed to the threaded bars.

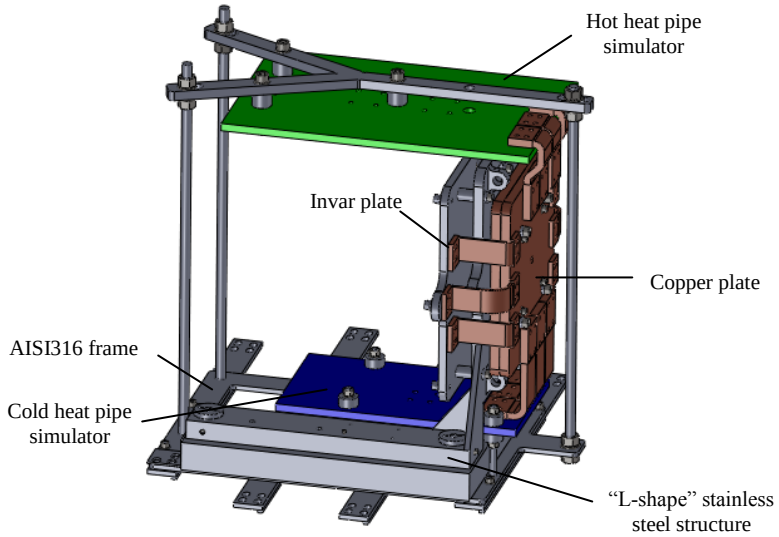

Fig. 7-15 Internal structural components of the TVC (2)

The copper plate and the invar plate are not directly attached to the “L-shape” structure, in order to guarantee different thermal levels to the plate themselves: therefore several PEEK washers have been foreseen around the screws, minimizing the thermal exchange for conduction between different I/Fs.

Finally the unit is directly attached to the invar plate by means of six M5 screws, as in flight configuration, evidenced with circles in the following figure. Squares evidence the M4 holes for the fixation of the thermal straps.

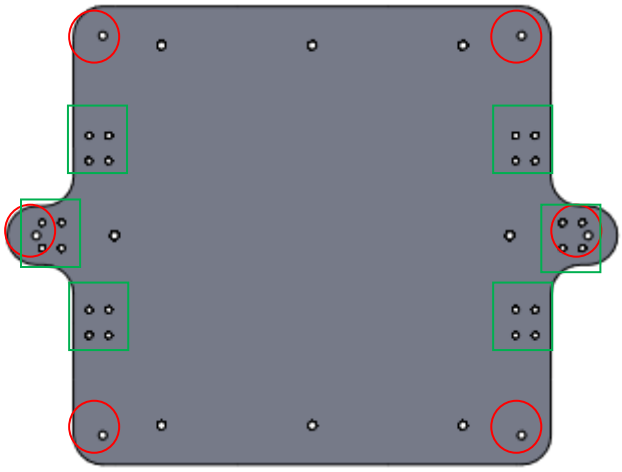

Fig. 7-16 Mechanical I/F of the instrument

The pitch – roll regulation (foreseen by M8 requirement) and regulation of the vertical distance of the instrument with respect to the TVC body is provided thanks to three M30 screws and three spherical joints, which are represented in the following figure. The spherical joints can rotate inside a hollow practiced inside a fixed part of the “L-shape” structure, whereas the M30 screws, stiffly connected to the spherical joints, can rotate inside three threaded holes practiced in a movable part of the “L-shape” structure. Once the final position is reached, the M30 screws can be easily blocked.

Considering the distance between the centre of the screws and the pitch of the screw (2 mm), it can be simply verified that the required accuracy on the position can be reached.

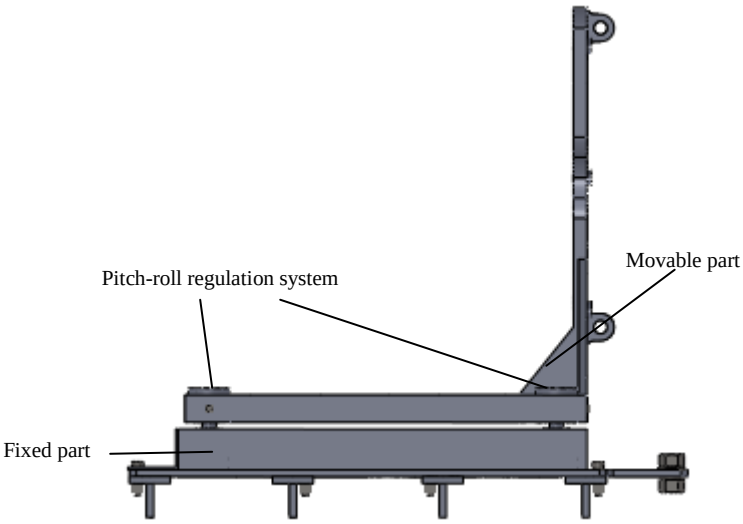

Fig. 7-17 Fixed and movable part of the "L-shape" structure

The following figure shows in detail the pitch-roll regulation system: only the regulation and the fixed part of the "L-shape" structure are visible.

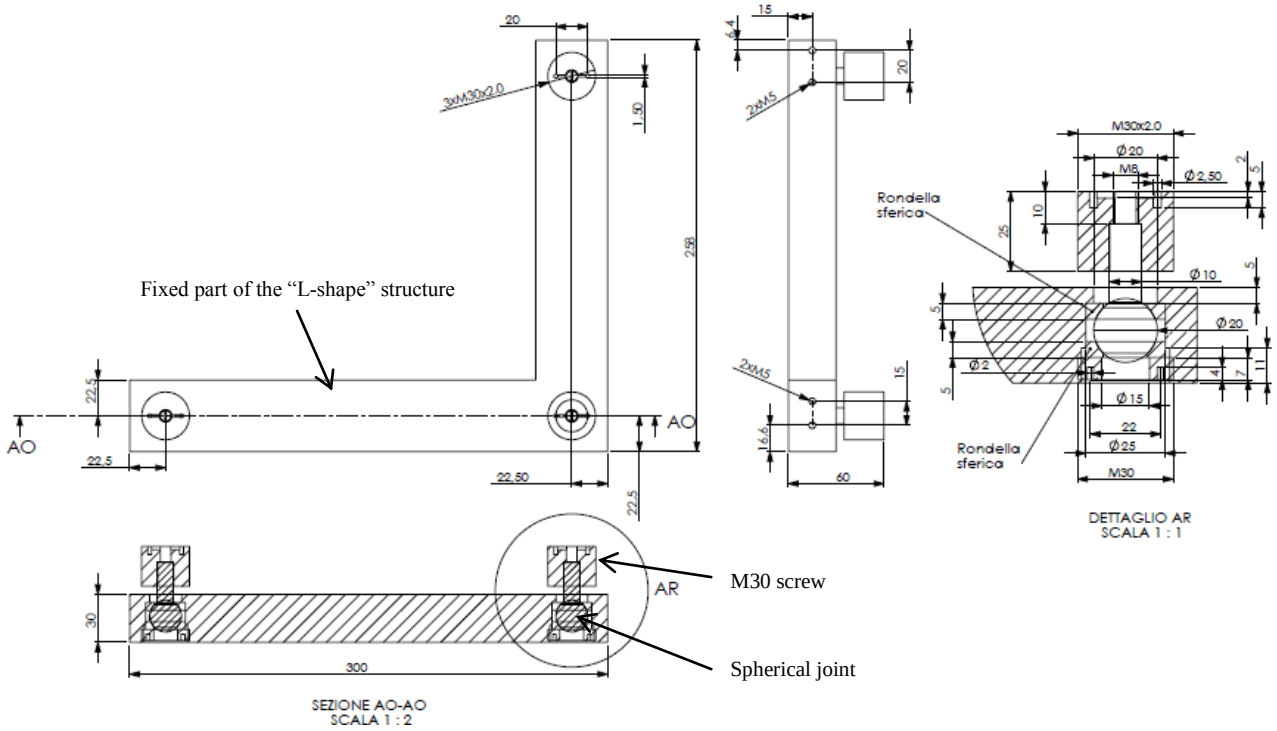

Fig. 7-18 Pitch-roll regulation system

Once all internal parts are mounted inside the bottom part, the top part can be fixed to the bottom part in order to perform tests in vacuum.

At last, the cold trap is a system is composed of two components:

- A cylindrical tank which is filled up by means of and external portable dewar with liquid Nitrogen; the tank is provided with a double wall so that the cavity between the internal and external walls can be evacuated, avoiding thermal exchange by convection within the cavity and providing a thermal insulation for the internal liquid Nitrogen.
- A circular plate which is in contact with the liquid Nitrogen on the upper surface and faces with the internal TVC environment on the other side, acting as a cold trap which catalyze the volatile particles inside the TVC. This circular plate is directly soldered to the tank.

These two components are fixed on the vacuum ISO 160 flange placed on the top of the TVC cap, as shown in Fig. 7-8.
The following figures show the dewar: the holes which allow to perform vacuum inside the cavity, without the necessity to introduce an additional pump (once vacuum is performed inside the TVC, it is also performed inside the gap of the dewar) are indicated; the plane which delimits the internal volume for the internal volume of the TVC is represented with dotted lines.

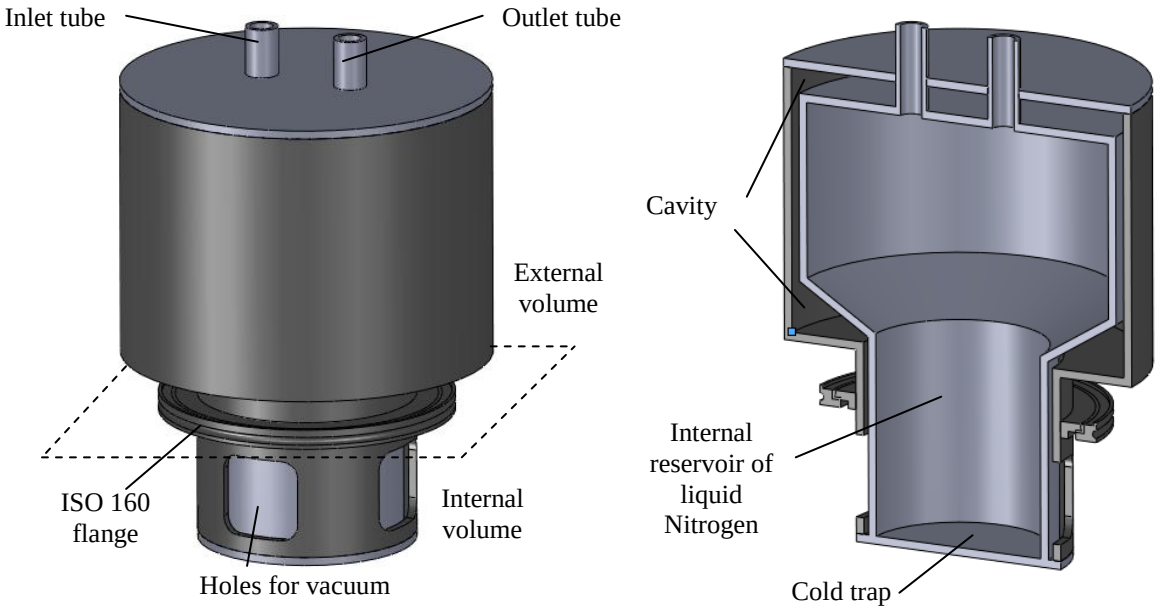

Fig. 7-19 Dewar and cold trap

The following figures show the thermal vacuum chamber assembled: the first figure shows the bottom part with all thermal I/Fs inside it, the second one the top cap with the viewports and the dewar.

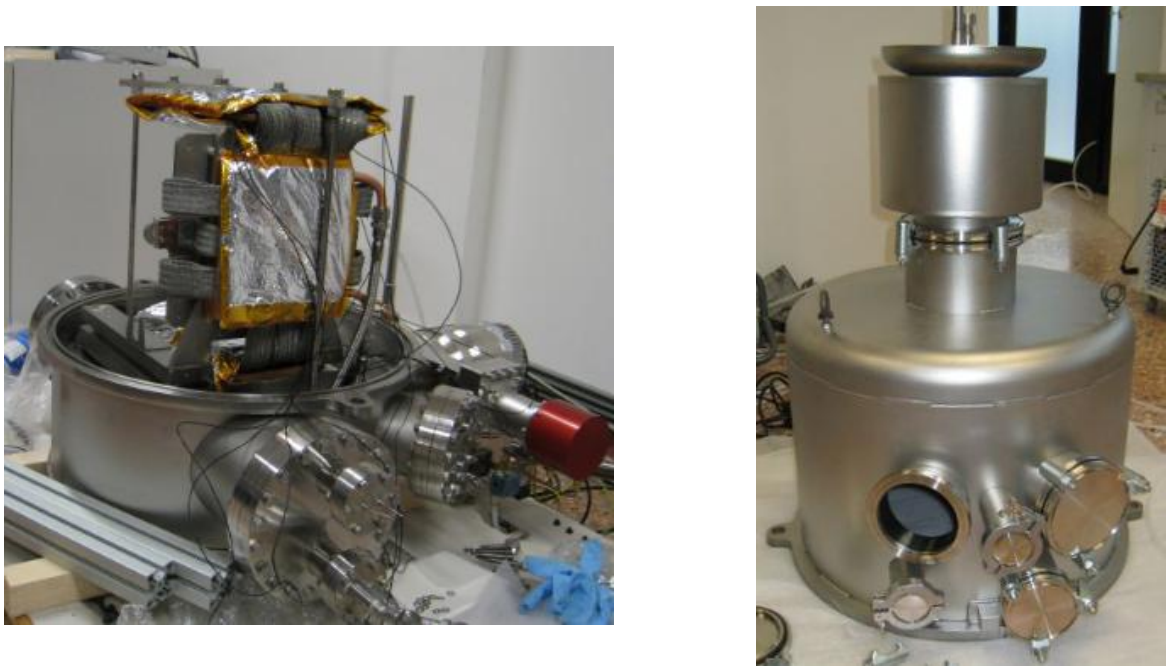

Fig. 7-20 Bottom part and top cap of the TVC for STC-VIHI

7.2.4.2 Configuration with baffles

Operations at ambient pressure with baffles are performed removing the cap and fixing an aluminum plate to the "L-shape" structure by means of 2 threaded bars: baffles are attached to the 5-thickness aluminum plate in the flight position; finally a black box is fixed to the plate in order to reduce the control volume around the instrument, which is filled with dry Nitrogen for cleanliness and contamination purposes.
During operations with baffles the thermal I/Fs (copper plate and heat pipe simulators) are removed from the structure and the total weight is reduced to about 176 kg.
The following figure shows the configuration with baffles: it can be seen the upper cap and thermal I/Fs have been removed since they are not used.

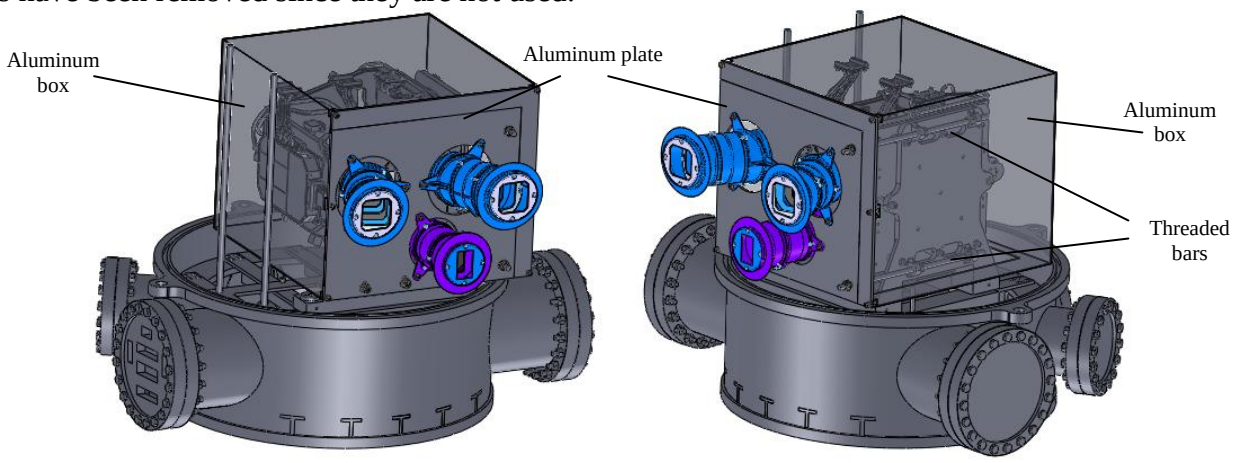

Fig. 7-21 Configuration with baffles

7.2.5 Thermal interfaces

7.2.5.1 Components

As written before, the thermal I/Fs to be controlled are:

- The cold heat pipe simulator (8 mm thickness copper plate), attached to the thermal strap of the VIHI detector;
- The hot heat pipe simulator (8 mm thickness copper plate), attached to the thermal straps of STC-VIHI PEs and STC detector;
- The invar plate, on which the unit is attached.

These I/Fs are linked by means of 12 copper thermal straps to the copper plate connected to the external cryostat, which drives the temperature of the whole system. In order to maximize the thermal contact between the straps and the I/Fs, indium foils, characterized by an high conductivity, have been interposed.
The fine regulation of the temperature on the different I/Fs is obtained thanks to different heaters realized with a resistor covered by adhesive Kapton, operating in the whole requested operative range. The thermal I/Fs are covered with MLI in order to minimize the thermal exchange by radiation with the internal components of the TVC.
The sizing of thermal straps and heaters derives by a detailed thermal analysis which is described in the following paragraph.
The thermal control system, in addition to the plates, the thermal straps and the heaters, is composed of 3 PT100 devoted to monitor the temperature of the I/Fs and 3 CAL9900 controllers, which have been chosen once the total current absorbed by the heaters has been calculated.

7.2.5.2 Thermal analysis and results

7.2.5.2.1 Introduction

The scopes of the thermal analysis described in this paragraph are:

1. Verify if a single commercial ultra-cryostat, able to remove up to 200 W heat flux at a temperature of -80°C, is suitable to reach the thermal levels (specified in Fig. 7-6) at the different I/Fs;
2. Design the thermal control system, in other words design the thermal strap, determine the power of the heaters before the procurement, choose the controllers, taking into account the maximum amount of current of the heaters.

The following figure represents the components reproduced in the thermal model; the top cap is not represented in the figure, but it has been simulated in the model as a boundary node:

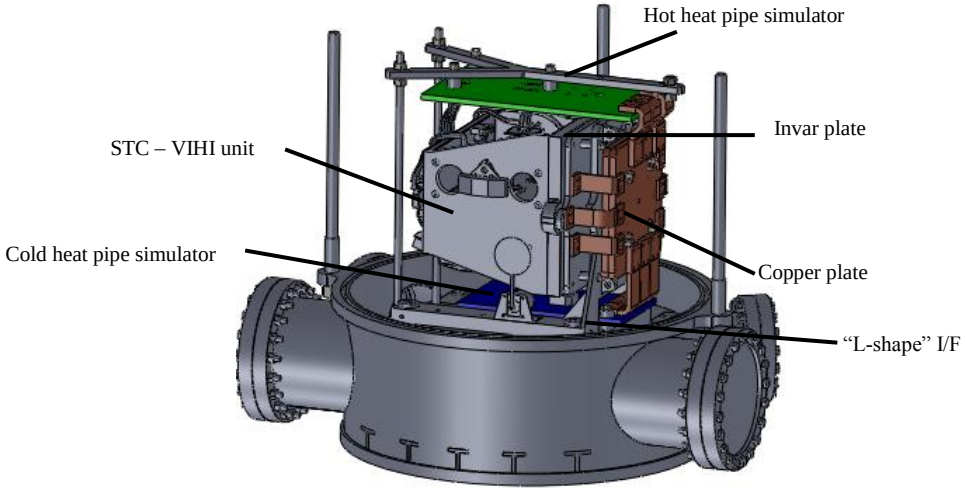

Fig. 7-22 Components simulated in the thermal model of STC-VIHI TVC

7.2.5.2.2 Thermal model architecture

The thermal model of the whole system has been obtained including the reduced thermal model of the unit provided by Selex ES into the thermal model of the TVC will all thermal I/Fs inside it.

The TVC has been simulated as a raw stainless steel cylinder with $\varepsilon = 0.14$. All the I/Fs inside the TVC and STC-VIHI unit are covered with MLI ($\alpha = 0.5$, $\varepsilon = 0.03$ for critical I/Fs, $\alpha = 0.5$, $\varepsilon = 0.1$ for STC-VIHI unit).

The copper plate, which drives the temperature of the whole system thanks to the link to the external cryostat, is thermally connected to the following components:

1. The invar plate, by means of 6 copper thermal straps (1.05 W/K total conductance);
2. Cold heat pipe simulator, by means of 3 copper thermal straps (0.92 W/K total conductance): CHPS is then connected to VIHI detector by means of its dedicated thermal strap (2 W/K contact conductance, according to the instrument reduced thermal model).
3. Hot heat pipe simulator, by means of 3 copper thermal straps (1.05 W/K total conductance): HHPS is then connected to STC-VIHI PEs and STC detector by means of dedicated thermal straps (2 W/K contact conductance for each strap, according to the instrument reduced thermal model).
4. "L-shape" support, by means of PEEK washers (0.03 W/K total conductance).

The invar plate which supports the instrument is conductively decoupled with respect to the "L-shape" support structure by means of PEEK washers (0.03 W/K total conductance); according to the instrument reduced thermal model, the conductance between the instrument and the invar plate is 0.046 W/K.

In general, the conductance of the thermal straps has been calculated considering a full copper strap characterized by the same volume of the copper braid and multiplying the obtained value by an empirical reduction factor (0.7), which provides and estimation of the lower amount of material of the braid with respect to the full copper strap. The conductance of the strap (GL_{strap}) has been calculated by means of the following relation:

$$GL_{strap} = \left(k \cdot \frac{A}{d}\right) 0.7 \tag{7.1}$$

where *k* is the conductivity of the copper, *A* is the transversal section of the strap, *d* is the length of the strap, 0.7 is the empirical reduction factor.
In order to increase the conductance of a single strap, several braids have been overlapped and brazed: in this case the total conductance of the strap (GL_{strap}^{tot}) is estimated considering several straps in parallel and becomes:

$$GL_{strap}^{tot} = N \cdot GL_{strap} \tag{7.2}$$

where *N* is the total number of braids which constitute the thermal strap.
The total conductance GL_{ij} from the node *i* (e.g. the copper plate) and the node *j* (e.g. the invar plate) has been then estimated considering also the series with the contact conductance ($GL_{contact}$) and the conductance of the indium layers (GL_{indium}) interposed between the strap and the thermal I/Fs. As an example:

$$GL_{ij} = \left(\frac{n}{GL_{contact}} + \frac{m}{GL_{indium}} + \frac{1}{GL_{strap}^{tot}}\right)^{-1} \tag{7.1}$$

where *n* and *m* are the number of contacts between the different I/Fs and the number of indium layers respectively.

The following picture shows some thermal straps and the indium foils: it can be seen that braids are brazed with two copper flanges at the extremities and fixation with the thermal I/Fs is provided thanks to 4 holes for each flange.

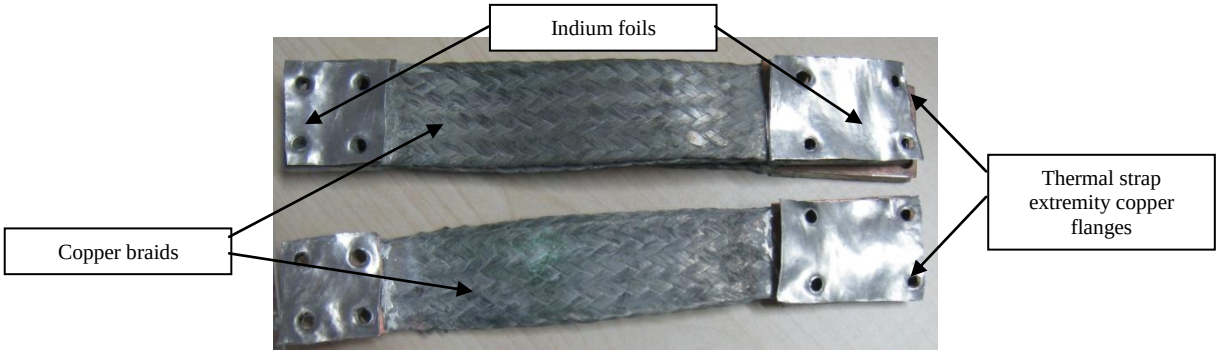

Fig. 7-23 Thermal straps and indium foils

The following figure shows the geometrical mathematical model of the TVC with all I/Fs inside it and the geometrical mathematical model of STC-VIHI unit. Node numbering and the reference frame are shown.
External sides of TVC cylinder are simulated as boundary nodes at 20°C.

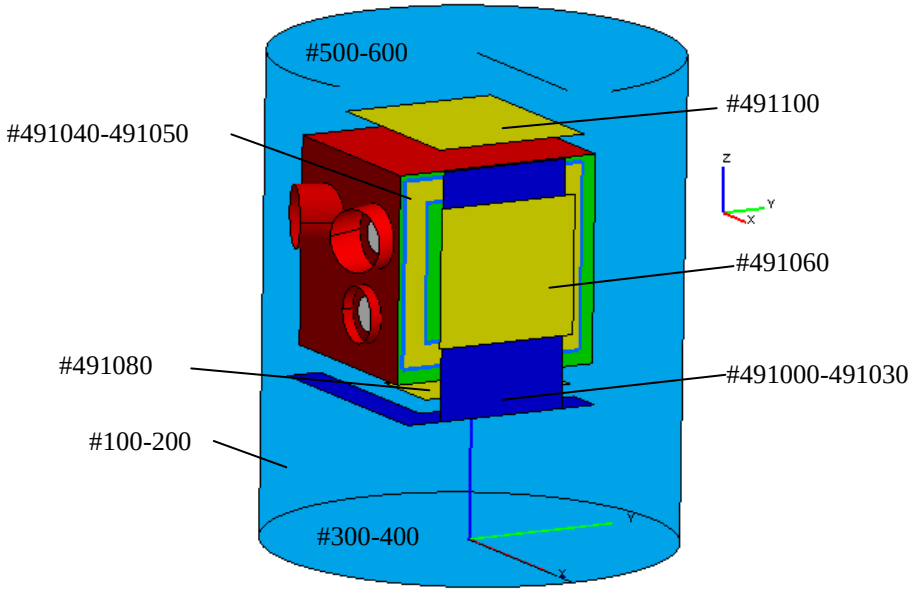

Fig. 7-24 Geometrical mathematical model of STC-VIHI TVC

7.2.5.2.3 Nodal breakdown, bulk and thermo-optical properties

A brief description of node numbering is given in the following table:

Node number	Description	Notes
BOUNDARY NODES		
B100	TVC cylinder	External wall
B400	TVC bottom plate	External wall
B500	TVC top plate	External wall
B99999	External environment	
DIFFUSIVE NODES		
D200	TVC cylinder	Internal side
D300	TVC bottom plate	Internal side
D600	TVC top plate	Internal side
D491000-491030	“L-shape” I/F	
D491040	Invar plate	-X side
D491050	Invar plate	+X side
D491060	Copper plate	
D491080	CHPS	
D491100	HHPS	
D68401-68405	STC-VIHI MLI	
D68406	STC-VIHI honeycomb	
D68407	STC OB, items & cover	
D68408	STC detector cage	
D68428	STC detector strap end	
D68416	VIHI OB, items & cover	
D68417	VIHI detector cage	
D68429	VIHI detector strap end	
D68420	STC PE	
D68422	STC PE strap end	
D68425	VIHI PE	
D68427	VIHI PE strap end	

Table 7-5 Thermal model node numbering

The following table summarizes the nodal breakdown and the thermal-optical properties.

Node	Name	Material	Thermal finish	α_S	ρ_S^D	ρ_S^S	ε_{IR}	ρ_{IR}^D	ρ_{IR}^S
100	TVC cylinder	AISI316	Raw SS	0.47	0.53	0.0	0.14	0.86	0.0
200	TVC cylinder	AISI316	Raw SS	0.47	0.53	0.0	0.14	0.86	0.0
300	TVC bottom plate	AISI316	Raw SS	0.47	0.53	0.0	0.14	0.86	0.0
400	TVC bottom plate	AISI316	Raw SS	0.47	0.53	0.0	0.14	0.86	0.0
500	TVC top plate	AISI316	Raw SS	0.47	0.53	0.0	0.14	0.86	0.0
600	TVC top plate	AISI316	Raw SS	0.47	0.53	0.0	0.14	0.86	0.0
491000-491030	“L-shape” I/F	AISI316	Raw SS	0.47	0.53	0.0	0.14	0.86	0.0
491040	Invar plate	Invar	MLI_CISAS	0.5	0.25	0.25	0.03	0.97	0.0
491050	Invar plate	Invar	MLI_CISAS	0.5	0.25	0.25	0.03	0.97	0.0
491060	Copper plate	Copper	MLI_CISAS	0.5	0.25	0.25	0.03	0.97	0.0
491080	CHPS	Copper	MLI_CISAS	0.5	0.25	0.25	0.03	0.97	0.0
491100	HHPS	Copper	MLI_CISAS	0.5	0.25	0.25	0.03	0.97	0.0
68401-68405	STC-VIHI MLI	MLI	MLI	0.5	0.25	0.25	0.1	0.45	0.45
68406	STC-VIHI honeycomb	Honeycomb	CFRP	/	/	/	0.85	0.15	0.0
68407	STC OB, items & cover	Aluminum	internal	/	/	/	/	/	/
68408	STC detector cage	Aluminum	internal	/	/	/	/	/	/
68428	STC detector strap end	Copper	internal	/	/	/	/	/	/
68416	VIHI OB, items & cover	Titanium	internal	/	/	/	/	/	/
68417	VIHI detector cage	Titanium	internal	/	/	/	/	/	/
68429	VIHI detector strap end	Copper	internal	/	/	/	/	/	/
68420	STC PE	Aluminum	internal	/	/	/	/	/	/
68422	STC PE strap end	Copper	internal	/	/	/	/	/	/
68425	VIHI PE	Aluminum	internal	/	/	/	/	/	/
68427	VIHI PE strap end	Copper	internal	/	/	/	/	/	/

Table 7-6 Node list and surface properties

The following table shows a list of the materials used in the thermal mathematical model.

Material	ρ[kg/m^3]	c_P [J/kg K]	λ [W/mK]
AISI316	8000.0	500.0	16.3
Copper	8930.0	385.0	398.0
Invar	8050.0	515.0	10.15

Table 7-7 Material properties

7.2.5.2.4 Conductive thermal couplings

The linear conductor chain is listed in the table below.

Node i	Node j	GL [W/K]	Description
100	200	0.963941 / ((0.00250000 / k_aisi316) + (0.00250000 / k_aisi316))	TVC body
300	400	0.202683 / ((0.00250000 / k_aisi316) + (0.00250000 / k_aisi316))	
500	600	0.202683 / ((0.00250000 / k_aisi316) + (0.00250000 / k_aisi316))	
491000	491010	0.0239144 / ((0.00500000 / k_aisi316) + (0.00500000 / k_aisi316))	“L-shape” supporting structure
491020	491030	0.0421066 / ((0.00500000 / k_aisi316) + (0.00500000 / k_aisi316))	

491000	491030	0.19	
491010	491020	0.19	
491010	200	0.01	
491040	491050	0.0570960 / ((0.00400000 / k_invar) + (0.00400000 / k_invar))	Invar plate
491020	491060	0.03	PEEK contact
491030	491050	0.03	
491050	491060	1.05	Invar plate th.straps
491060	491100	1.05	HHPS th. straps
491060	491080	0.92	CHPS th. Straps
68428	491100	2.0	STC Detector Strap Contact
68422	491100	2.0	STC PE Strap Contact
68427	491100	2.0	VIHI PE Strep Contact
68429	491080	2.0	VIHI Detector Strap Contact
68406	491040	0.046	STC&VIHI Structure in Contact with OB Bench
68407	68406	0.097389	STC OB to HoneyComb Structure
68416	68406	0.024347	VIHI OB to HoneyComb Structure
68408	68407	0.247374	STC Detector to OB
68417	68416	0.023157	VIHI Detector to OB
68420	68406	0.065904	STC PE to HoneyComb
68425	68406	0.147316	VIHI PE to HoneyComb
68428	68408	0.49	VIHI PE Th. Strap
68429	68417	0.38	STC PE Th. Strap
68422	68420	0.46	STC Detector Th. Strap
68427	68425	0.35	VIHI Detector Th. Strap

Table 7-8 Internal conductive thermal couplings

7.2.5.2.5 Thermal cases and boundary conditions

As written before, only external sides of the TVC and the external environment are simulated as boundary nodes at 20°C constant temperature.
Different kinds of heat fluxes are simulated:

- Dissipation incoming from the PEs and the FPAs of the unit: these heat fluxes have been defined in the reduced thermal model as a function of the temperature of the nodes themselves. They are null in the non – operative case, whereas, in the operative case, they assume the values derived by the following relations:

Node	Operative dissipation
68408	STC Detector cage: STC Detector dissipation (0.2 W) + STC TEC power consumption
68417	VIHI Detector cage: VIHI Detector dissipation (0.13 W) + VIHI TEC power consumption
68420	STC PE dissipation: 3.01 + (1/0.8-1) · STC TEC power consumption
68425	VIHI PE dissipation: 1.529 + 0.36 · VIHI TEC power consumption

Table 7-9 Operative dissipation of STC-VIHI detectors and PEs

ΔT=f(T68408)	0	5	10	15	20	25	30	35	40	45	50
STC TEC power consumption	0.02	0.052	0.092	0.196	0.324	0.52	0.764	1.198	1.548	2.226	3.262

Table 7-10 STC TEC power consumption

ΔT=f(T68417)	0	5	10	15	20	25	30	35	40	45
VIHI TEC power consumption	0.01	0.038	0.055	0.117	0.17	0.274	0.429	0.642	0.903	1.55

Table 7-11 VIHI TEC power consumption

Within the code of the thermal model, 2 control variables (SIMB3_iSTC & SIMB3_iVIHI) allow the switch on or the switch off of the units (operative and non-operative cases respectively), which corresponds to the activation or to the de-activation of detectors and PEs dissipations:

SIMB3_iSTC	**SIMB3_iVIHI**	**Case**
1	1	Operative
0	0	Non-operative

Table 7-12 Activation and de-activation of the unit (detectors and PEs)

- The thermal cycle which has to be reproduced at the thermal I/Fs is obtained by the following sequence:
    1. Hot non-operative case;
    2. Hot operative case;
    3. Cold non-operative case;
    4. Cold operative case;
    5. Hot operative case;

  Then stages 4 and 5 (hot operative and cold operative cases) are repeated 8 times, according to EID-A.

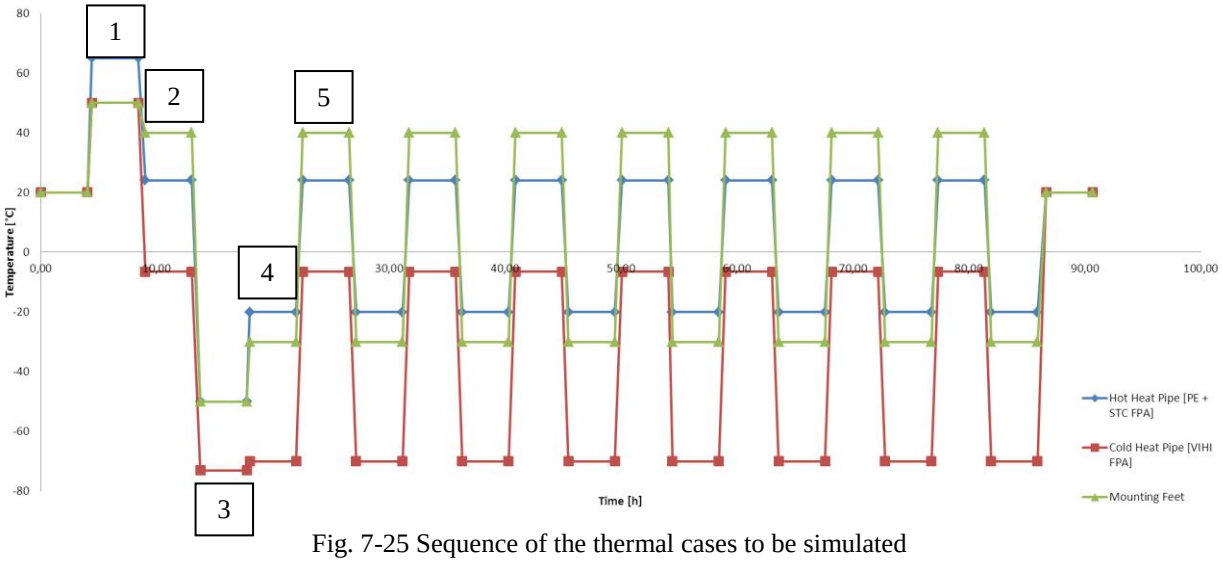

Fig. 7-25 Sequence of the thermal cases to be simulated

Each thermal level specified in the previous graph and corresponding to a different thermal case has been reached in the thermal model implementing a PID control on the thermal I/Fs. In particular Hot Heat Pipe Simulator (HHPS), Cold Heat Pipe Simulator (CHPS) and invar plate (feet HPS) are characterized by a positive internal heat generation, which simulates the presence of the heaters, whereas the copper plate, connected to the cryostat, is characterized by a negative and positive internal heat generation, which simulates the action of the cryostat, able to remove up to 200 W at -80°C and to provide up to 2000 W.
The internal heat generations are provided in the thermal model for at least 4 hours for each phase.

7.2.5.2.6 Results

The following figure shows the temperature reached at the relevant nodes of the thermal model:

- The Hot Heat Pipe Simulator (HHPS, node 491100), represented with the red line;
- The Cold Heat Pipe Simulator (CHPS, node 491080), represented with the yellow line;
- Feet support plate, represented with the blue line (node 491050).
- Copper plate (node 491060), represented with the green line.

It can be seen that the temperatures reached coincides with thermal levels specified in the graph above.

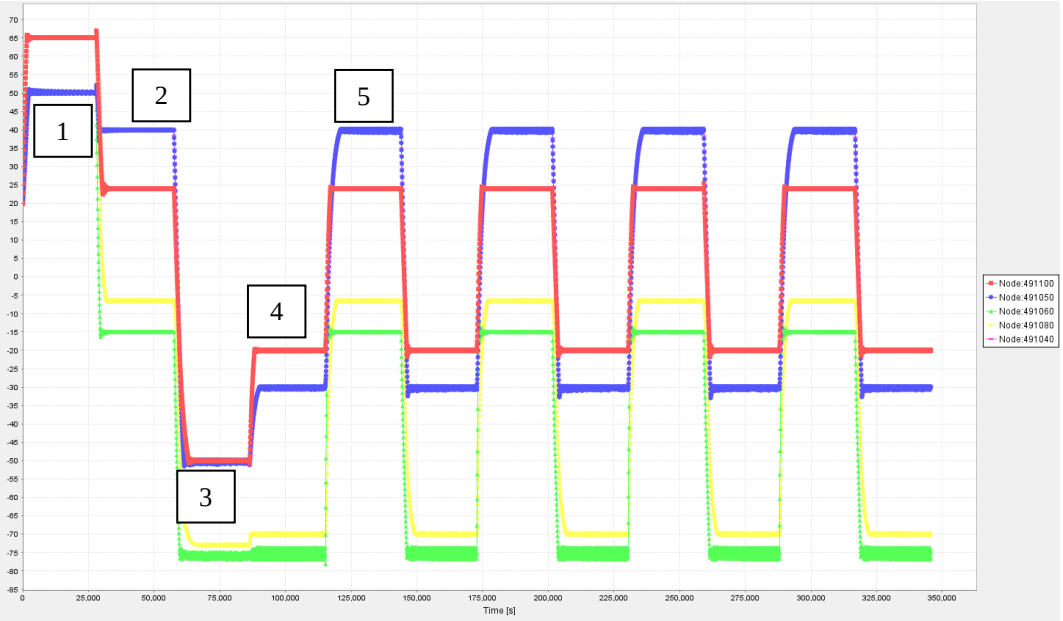

Fig. 7-26 Thermal levels obtained as a result of the thermal analysis

The following graph represents incoming conductor heat flow (red line), the internal heat generation (blue line) and the temperature (green line) of the copper plate (node 491060). It can be seen that, thanks to a maximum dissipation of 200 W at -75°C, the required thermal levels are reached. Therefore a solution based on a single ultra-cryostat for the cooling of the copper plate is feasible.

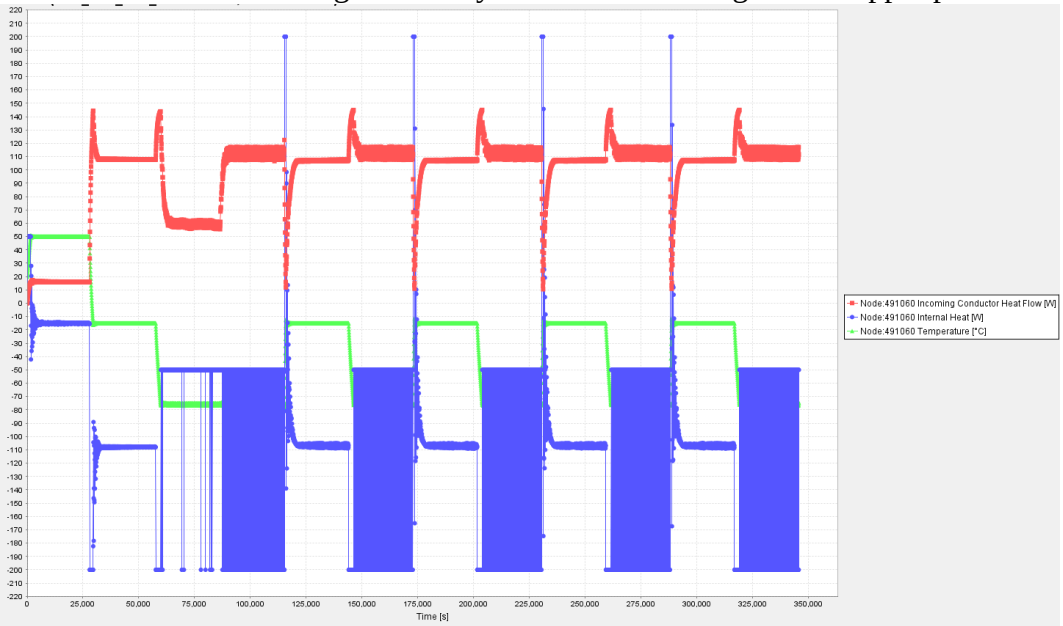

Fig. 7-27 Incoming conductor heat flow, internal heat generation and temperature of node 491060 (copper plate, connected to the cryostat)

The chosen ultra-cryostat is a FP89-ME Julabo Ultra Cryostat, operating in the range -90°C up to 100°C and provided with its proper temperature controller; the fluid is a Thermal HY-Baysilone-Oel M3 liquid operating in the range -80°C up to +55°C. The following table summarizes the main properties of the cryostat:

Parameter	Unit	Value
Operating temperature	°C	-90/+100
Temperature stability	°C	0.02
Refrigerating capacity	°C	+20 0 -20 -40 -60 -80
	kW	1.0 0.92 0.88 0.75 0.58 0.2
Heating capacity	kW	2.0
Dimensions	Cm	56×61×90
Capacity (volume)	L	5.5/8
Weight	Kg	133
Power supply	V/Hz	207-253/50
Absorbed current @ 230 V	A	16
Resolution	°C	0.1
Flux	l/min	11/16
Maximum pressure	Bar	0.22/0.45

Table 7-13 Main properties of the Julabo Ultra-cryostat

In order to reproduce the thermal cycles above, basing on thermal analysis, the following power levels have to be guaranteed at I/Fs for each thermal case.

Case number	Thermal case	Power [W]		
		Hot Heat Pipe Simulator	Cold Heat Pipe Simulator	Feet HPS
1	Hot case – non operative	80	10	23
2	Hot case – operative A	80	10	60
3	Cold case – non operative	40	10	30
4	Cold case – operative A	80	10	50
5	Hot case – operative B	80	10	65
6	Cold case – operative B	80	10	50
	MAX	**80**	**10**	**65**

Table 7-14 Internal heat generation of the thermal I/Fs

The following figure shows the positioning of the heaters on the thermal I/Fs: different heaters have been placed on the plates if necessary in order to guarantee an uniform heat generation.

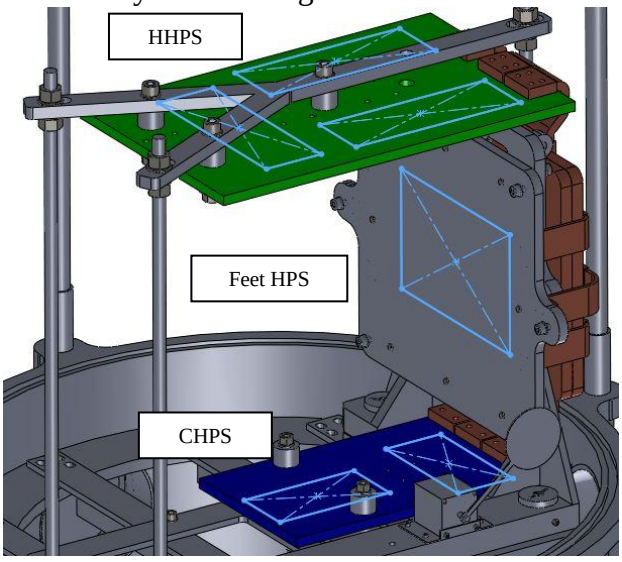

Fig. 7-28 Positioning of the heaters on the thermal I/Fs

Heaters have been chosen considering:

- Maximum power to be supplied at the different thermal I/Fs, whose values are reported in the last rows of Table 7-14;
- Dimension of the heaters, basing on the free area on the thermal I/Fs.

Some margins have been considered in the choice of the heaters, taking into account uncertainty in the estimation of conductance of thermal straps which thermally connect I/Fs with the copper plate controlled by the cryostat.
MINCO Kapton heaters have been chosen: these heaters operating temperature can vary in the range -73°C up to about 200°C.
The following table shows the chosen models for each I/F. For each heater the following properties are reported:

- Dimension (mm^2);
- Number of heaters;
- Resistance and total resistance (when different heaters are connected in series)(Ω);
- Supply voltage (V);
- Current (A);
- Max allowable current (A);
- Maximum nominal power (W), compared with power resulting from thermal model;
- Lead gauge.

Parameter	HHPS	CHPS	Feet HPS
Model	HK5172	HK5422	HK5491
Dimension (mm^2)	50 × 150	50 × 100	100 × 150
Number	3	2	1
Resistance (Ω)	110	10.9	6.4
Total resistance (Ω)	330	21.8	6.4
Supply voltage (V)	220	24	24
Current (A)	0.7	1.1	3.8
Max allowable current (A)	3.0	7.5	7.5
Maximum nominal power	146.7 > 80.0	26.4 > 10.0	90.0 > 65.0
Lead gauge	AWG 30	AWG 24	AWG 24

Table 7-15 Properties of heaters used for STC-VIHI TVC

Since 2 heaters are supplied at 24 V, an additional 24 V power pack has been foreseen in order to supply the loads; the resistor supplied at 220 V a.c. is directly connected to electrical line.
AWG 24 and AWG 30 leads, with a diameter of 0.51 mm and 0.26 mm respectively, are compatible with D-sub connector chosen for the TVC electrical feed-through: these connectors can host wires with a diameter up to 0.6 mm and withstand a working current up to 6.5 A, which is higher than heaters working current (see table above). As an example, the following figure shows the heaters attached to the HHPS (series of 3 heaters).

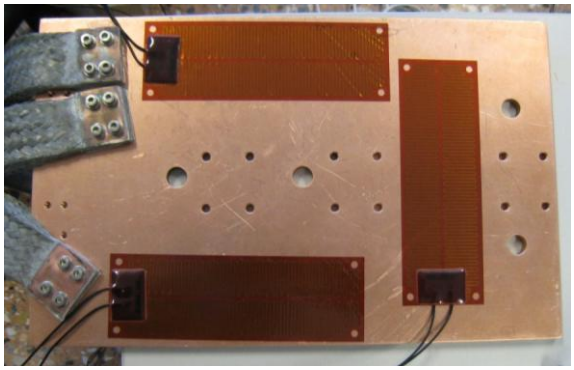

Fig. 7-29 Heaters placed on the HHPS

PID controllers with relays able to withstand 3.75 A have been chosen, considering the maximum working current for heaters (see table above), such as the CAL9900 controllers series, which are characterized by the following features:

- Supply: 220 V a.c.
- Inputs: Thermocouples or PT100.
- Output ratings (2 outputs):
  - Relay (SP1): 5A/250V~
  - Relay (SP2): 3A/250V~

Since these controllers outstand current up to 5A (>3.75A), they can be used to regulate current to the heaters.
In order to increase the safety margins on the current, additional industrial relays, able to outstand current values up to 20A, have been connected to the controllers, acting as amplifier of the control.

7.2.6 Electrical interfaces

As written in paragraph 7.2.3, the electrical connectors have been placed on the bottom part of the TVC, on a CF150 flange and on a CF100 flange. In particular, CF150 flange is provided with:

- 2×15 pins MDM connectors for STC-VIHI spacewire data;
- 2×37 pins Dsub connectors for power supply and service purposes;
- 1×50 pins Dsub connector for service purposes, in other words it hosts the connections for the ten PT100 devoted to the monitoring of the points of interest temperature.

The CF100 flange is provided with 2 additional 37 pins Dsub connector: the first one is used for the power supply of the heaters and the connection of the PT100 devoted to thermal control of the thermal I/Fs; the second one is a spare connector.
The following figure is a scheme of the electrical connections:

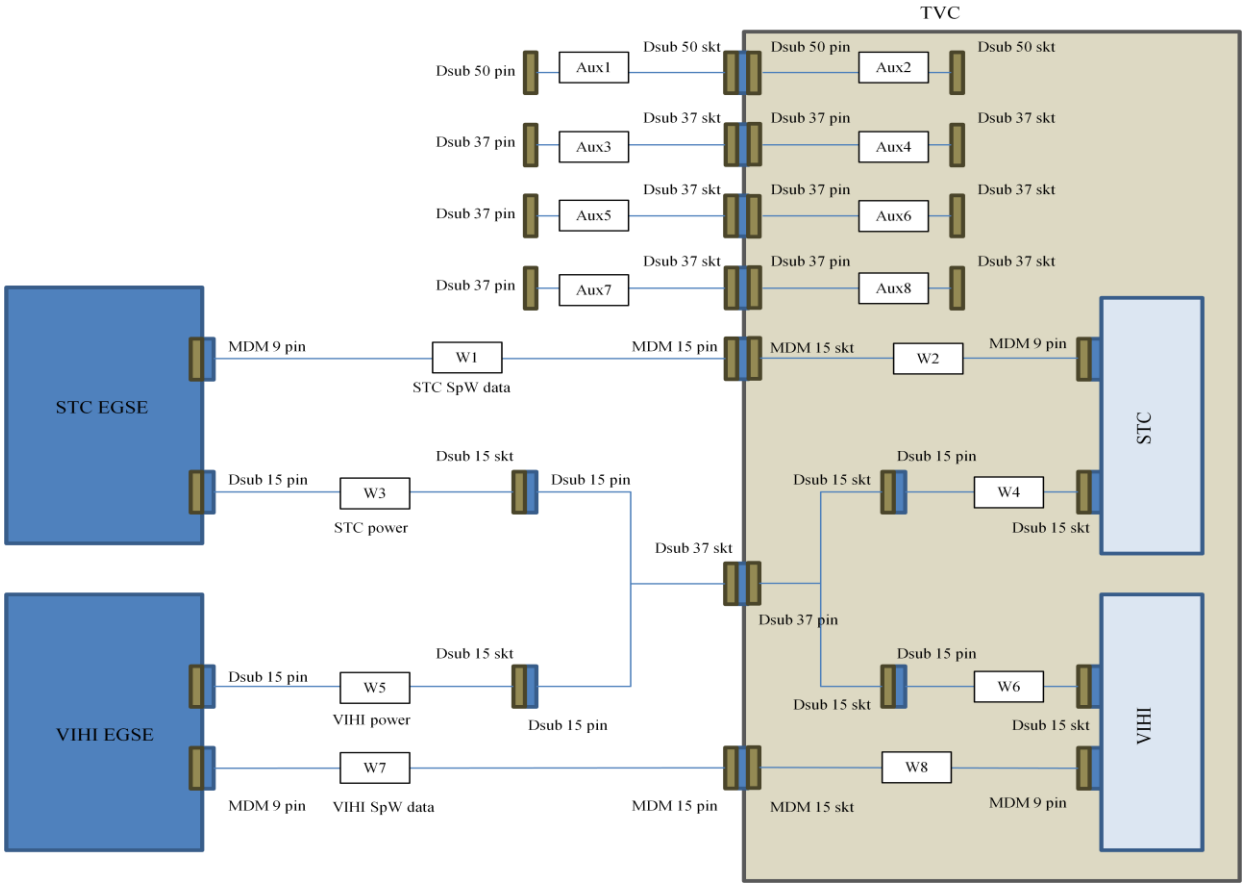

Fig. 7-30 Electrical connection of the STC-VIHI TVC

The following table shows the pin scheme of the 37 pins D-sub connector devoted to the power supply of the heaters and the 3 PT100 for the thermal control. PT100 have been connected with the standard 3-wires scheme (3-wires connection is compliant with controllers properties), while, for heaters, 4 wires have been used for de-rating purposes.

Pin	Component
1, 2, 3	PT100 #1
4, 5, 6	PT100 #2
7, 8, 9	PT100 #3
26, 27, 28, 29	Heater #1
30, 31, 32, 33	Heater #2

Table 7-16 37 pins D-sub connector scheme

The third heater, which is operates at 220 V a.c., is supplied by means of a custom feed-through for safety reasons.
The following table shows the pin scheme of the 50 pins D-sub connector devoted to the PT100 used for monitoring the temperature of the 10 points of interest.

Pin	PT100 cabling	PT100 number	Pin	PT100 cabling	PT100 number
1	PT100_1_V+	PT100_1	20	PT100_6_V+	PT100_6
3	PT100_1_I+		36	PT100_6_I+	
2	PT100_1_V-		21	PT100_6_V-	
4	PT100_1_I-		37	PT100_6_I-	
5	PT100_2_V+	PT100_2	22	PT100_7_V+	PT100_7
7	PT100_2_I+		38	PT100_7_I+	
6	PT100_2_V-		23	PT100_7_V-	
8	PT100_1_I-		39	PT100_7_I-	
9	PT100_3_V+	PT100_3	24	PT100_8_V+	PT100_8
11	PT100_3_I+		40	PT100_8_I+	
10	PT100_3_V-		25	PT100_8_V-	
12	PT100_3_I-		41	PT100_8_I-	
13	PT100_4_V+	PT100_4	26	PT100_9_V+	PT100_9
15	PT100_4_I+		42	PT100_9_I+	
14	PT100_4_V-		27	PT100_9_V-	
16	PT100_4_I-		43	PT100_9_I-	
18	PT100_5_V+	PT100_5	28	PT100_10_V+	PT100_10
34	PT100_5_I+		44	PT100_10_I+	
19	PT100_5_V-		29	PT100_10_V-	
35	PT100_5_I-		45	PT100_10_I-	

Table 7-17 50 pins D-sub connector scheme

Remaining 37 pins Dsub connectors are spare connectors.

Concerning the external cabling of the controllers, the following figures show a possible connection of the controller to the power supply line (220V~) and to the load (heaters), considering that one heater is supplied @220V a.c., the others @24V c.c.

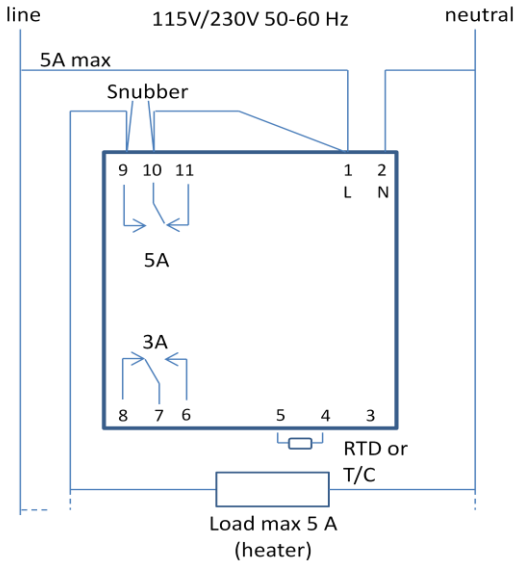

Fig. 7-31 Heater supplied @220V a.c. connected to the controller (supplied @220V a.c.)

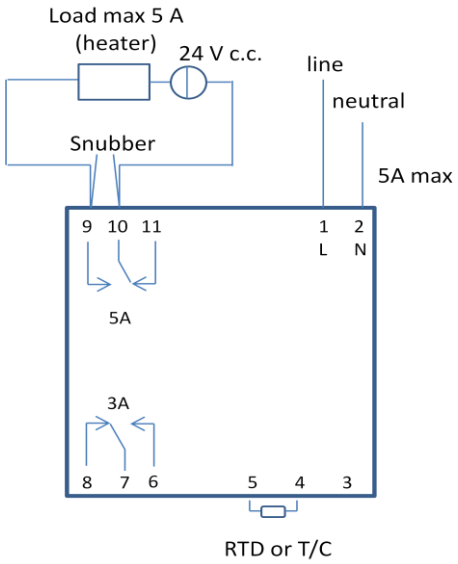

Fig. 7-32 Heater supplied @24V c.c. connected to the controller (supplied @220V a.c.)

The following figure shows a possible connection between different controllers (C_i) and heaters (H_i), supposing that all controllers are supplied @220 a.c., all heaters are supplied @24V c.c.

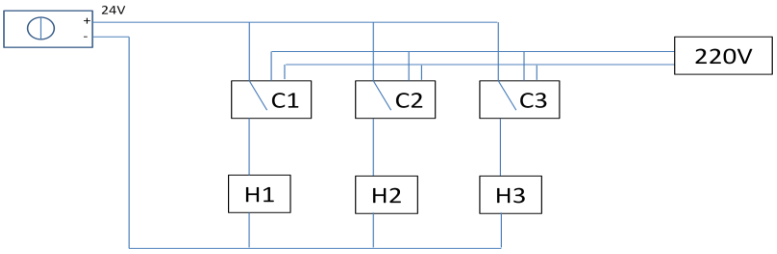

Fig. 7-33 Connections between controllers and heaters

7.3 TVC for HRIC

7.3.1 Introduction

This paragraph describes the mechanical, thermal and electrical interfaces of the TVC for the calibration of HRIC unit and the overall configuration, which has been defined in order to fulfill some specific technical requirements, which are hereafter listed.

7.3.2 General requirements

Requirements which have been defined by Selex ES are hereafter summarized. The types of requirements are the same reported in Fig. 7-1.

7.3.2.1 Mechanical requirements

M1. The unit (HRIC) under test has to be ideally included inside an envelope with the following dimensions: 230 mm in *x* direction, 300 mm in *y* direction and 230 mm in *z* direction. The reference system is represented in the following figure.

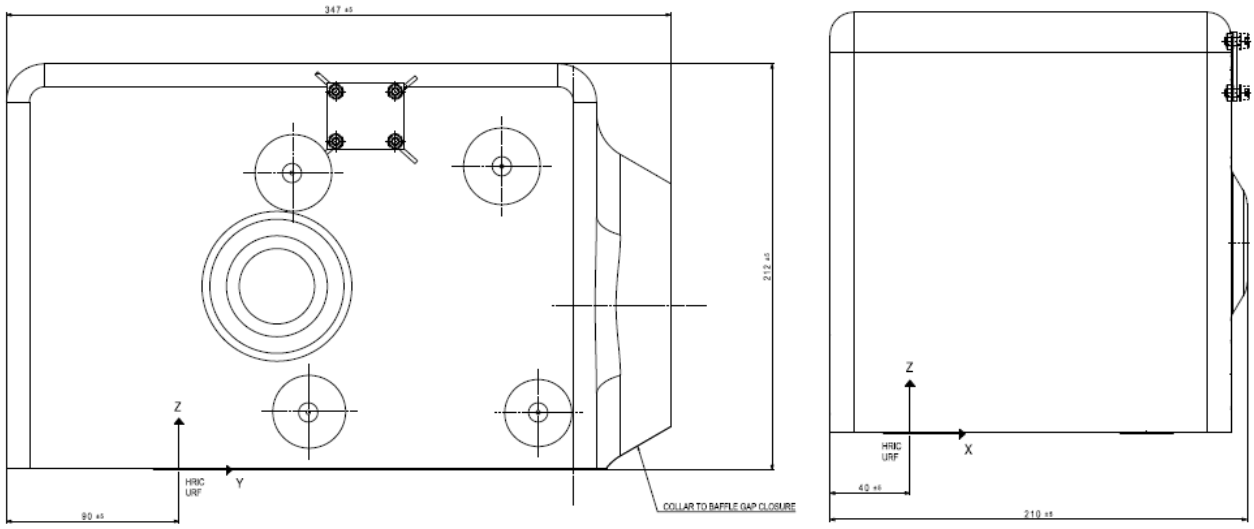

Fig. 7-34 Reference frame of HRIC unit

M2. The HRIC TVC has to be fixed directly on the active isolation optical bench by means of a dedicated mechanical I/F (in this case the rotation stage in not foreseen), in order to minimize the environment vibration effects. A collimator placed on the same optical bench allows to direct the OGSE optical beam thought the HRIC entrance aperture. The support allows to adapt the HRIC optical axis with the collimator optical axis.

M3. As for STC-VIHI TVC, the HRIC TVC has to be provided with 2 mechanical parts: a bottom part has to be fixed to the optical bench, the top part has to be removable and provided with mounting columns in order to guarantee the repeatability of operations and avoid any damages to the instruments during mounting operations.

M4. Thermal flanges, electrical flanges and vacuum flanges have to be placed on the fixed bottom part of the TVC, in order to easily remove the upper part without interfere with the performed connections and minimize the weight of the upper part (which has to be lifted during mounting operations).

M5. The TVC has to be provided with 3 different plates, as shown in the following figure: a stainless steel plate, a copper plate and an invar plate.

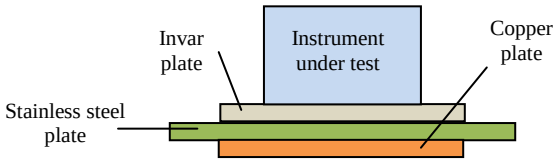

Fig. 7-35 Main mechanical I/Fs inside the TVC

M6. According to the previous figure, a copper plate, thermally actively controlled, has to be fixed to the stainless steel plate and thermally decoupled with respect to the support plate itself, in order to guarantee the thermal control of the instrument plane (invar plate).

M7. According to the previous figure, the instrument support plate is an invar plate, which has to be fixed on the stainless steel I/F and thermally decoupled with respect to the plate itself.

M8. A 3 points regulation system has to be foreseen on the instrument plane, in order to guarantee the pitch/roll regulation (yaw regulation is not requested) with a resolution of 20 arcsec (100 μrad).

M9. The invar plate has to be connected to the copper thermal plate by means of a series of thermal straps.

M10. The maximum distance between the HRIC structure and the external surface of the optical window is 80mm±5mm, measured in the direction normal to the HRIC structure wall

(in order to avoid vignetting with OGSE). If the distance is higher, a preliminary verification within CAD drawings including the ray tracing of the collimator beam can be performed in order check if vignetting occurs.

M11. Residual vibrations incoming form the external environment have to be minimized. Therefore the vacuum pump has to be switched off during some measurements and vacuum inside the TVC should be maintained (maximum value of 10^{-5} mbar for at least 30 minutes).

M12. TVC weight in its operative configuration with all parts mounted on it (e.g. pumps) has to be lower than 250 kg, which is the maximum load acceptable form the optical bench.

M13. TVC has to be provided with external hooks which allow to lift and move it.

M14. The I/F of the bottom part of the TVC with the optical bench has to be directly soldered form exterior to the bottom part of the TVC.

M15. The pattern shown in the following figure has to be realized on the mechanical I/F of the TVC with the optical bench.

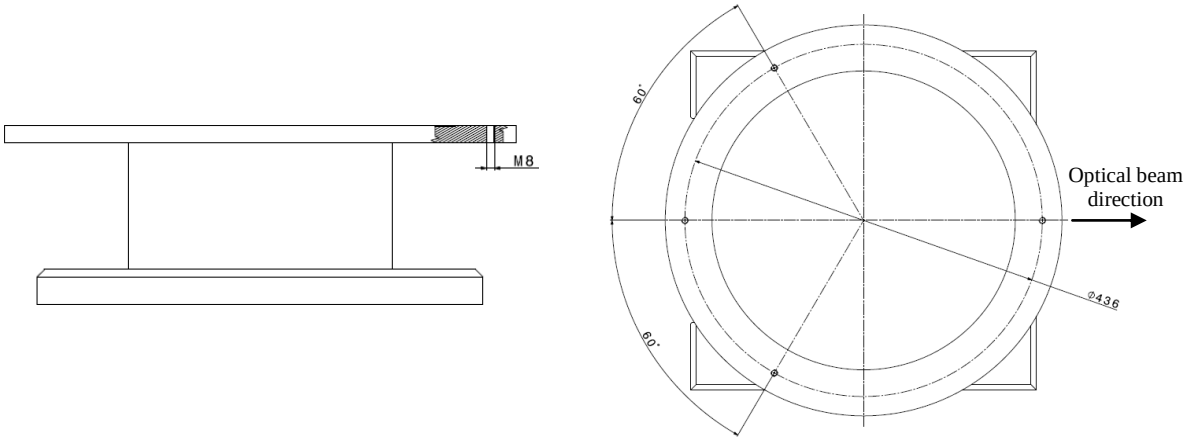

Fig. 7-36 Mechanical I/F of the HRIC TVC: the pattern allows coupling with OGSE

M16. The TVC has to be transportable with the instrument mounted and fixed inside it. Therefore all I/Fs will be separated from the TVC surface and cleanliness requirements will be guaranteed by pumping dry Nitrogen through the TVC valves. This requirement derives from the need to perform the straylight measurements outside the cleanroom, with only electrical interfaces mounted on the TVC.

M17. The TVC material has to be selected in order to minimize its weight and guarantee the vacuum requirements.

M18. The TVC has to be provided with an external optical reference cube, located on the same flange hosting the optical windows. The optical quality requirements has to be guaranteed on at least two faces (front and lateral ones) and the cube side has to be at least 25 mm long. Perpendicularity between the reflecting faces and the face fixed on the TVC external surface has to be within 5arcmin. By this cube, which defines the TVC reference frame, the direction of the TVC rotating axis with respect to the OGSE reference frame can be measured. This measurement together with the angles between HRIC optical reference frame and the TVC reference frames, allows to figure out the HRIC reference frame with respect to the OGSE one.

M19. The TVC has to be provided with two BK7 windows, provided by Selex ES: the first one is dedicated to the frontal face of the HRIC reference mirror along the direction normal to the face, the second one is devoted to HRIC entrance port. The deviation between the windows axes and the relevant optical axes has to be lower than ±1°.

M20. Optical windows have to be accommodated on a dedicated flange easily removable from the TVC vessel. The mechanical I/Fs of the optical windows have to be perpendicular to each optical axis. In this way the internal of the TVC in easily accessible, by using a quick-lock system to fix the windows mechanical I/Fs to the TVC.

M21. Measurements with Stavroudis baffle, performed at 1 bar pressure, foreseen that baffle can be accommodate in its final flight configuration inside the TVC by means of a devoted mechanical I/F. The maximum distance between the HRIC structure and the baffle flange is that specified in the MICDs. Also the TVC flange hosting the baffle has to be easily removable. During measurements with baffle the internal volume has to be filled with dry Nitrogen in order to have a minimum over-pressure with respect to the ambient one avoiding contamination. The following figure shows the unit with Stavroudis baffle in its flight configuration. A hole has to be practiced on the mechanical flange, in order to accommodate the baffle.

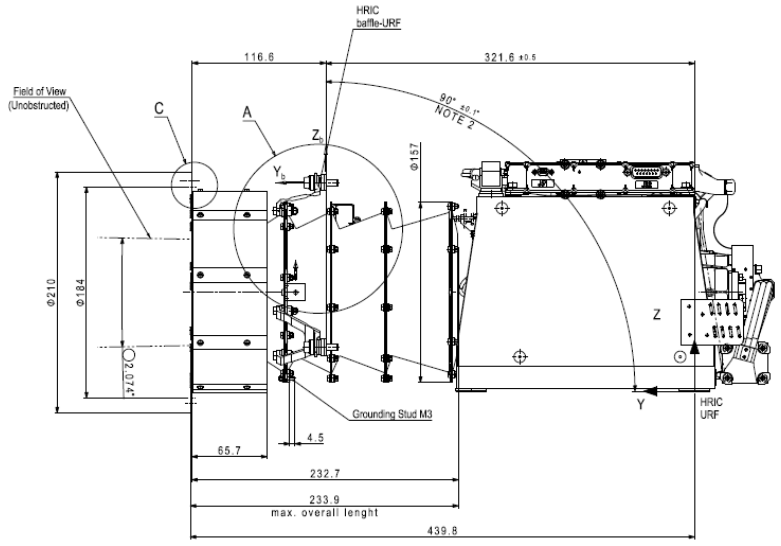

Fig. 7-37 HRIC unit with Stavroudis baffle

M22. Gaskets which will not frequently removed during test campaign have to be realized in copper, gaskets of removable flanges in rubber.

M23. All electrical and thermal I/Fs have to be placed on the fixed bottom part of the TVC, in order to simplify mounting operations. Harness length have to be minimized and thermal flange has to be placed as closest as possible to the thermal I/Fs.

M24. The alignment between the upper and bottom part of the TVC has to be guaranteed thanks to 3 auto-centre columns (tolerance on the columns diameter of 0.1 mm).

7.3.2.2 Vacuum requirements

V1. Pressure inside the TVC has to be equal to 10^{-6} mbar with rotary and turbo-molecular pumps activated.

V2. The vacuum level has to be guaranteed with the pumping system switched off for at least 30 minutes. Maximum allowed pressure after 30 minutes is 10^{-5} mbar. In this way some critical measurements can be performed (e.g. PSF measurements) in vacuum without the vibrations inducted by the pumping system.

7.3.2.3 Cleanliness and contamination requirements

C1. As for STC-VIHI TVC, since tests will be performed on Flight Models of the units, materials compliant with contaminations requirements have to be used. Non-metallic materials can be used taking into account their out-gassing rate, their amount and location and their configuration. Table 7-1 is considered as guideline.

All components inside the TVC (cables, sensors, mechanical parts) have to be submitted to dedicated clean and outgassing processes.

C2. An easily accessible cold trap has to be included inside the TVC: this cold trap, maintained at temperature lower than the lowest environmental one, is realized by means of an external dewar and an internal dedicated removable cold plate able to catalyze eventual volatile particles inside the TVC. The optimal position of the cold trap is on the upper part of the chamber, with the dewar placed in vertical position (in order to maximize its efficiency).

C3. The external dewar should have an autonomy of at least 24 hours, thanks to a dedicated internal Nitrogen reservoir or by an external liquid Nitrogen line.

C4. A DN_2 valve has to be foreseen since dry Nitrogen is needed to avoid contamination during tests at ambient pressure. During tests with baffles, the hole of the baffle acts as an outlet valve; the purging connector of HRIC can be used as inlet valve.

7.3.2.4 Electrical requirements

TVC has to be provided with the following connectors, which should be placed on the same flange in order to minimize cables length, on the bottom fixed part of the TVC:

- One 15 pins MDM (SRIMD2006-15) connector for HRIC spacewire data.
- One 15 pins Dsub connector for HRIC power supply.
- One 37 pins Dsub connector for service purposes.
- One 50 pins Dsub connector, for service purposes.

7.3.2.5 Thermal requirements

T1. Two thermal I/Fs have to be designed inside the TVC:

a. The HRIC Heat Pipe Simulator, connected to the thermal straps dedicated to HRIC PE and HRIC detector;

b. The invar plate which supports the unit.

The following table summarizes the thermal levels and the dissipation values which have to be guaranteed at the different I/Fs (values are obtained taking into account the ±10°C qualification margin):

Thermal I/Fs	Cold case		Hot case	
	T_{min} [°C]	Minimum internal power to be subtracted [W]	T_{max} [°C]	Minimum internal power to be subtracted [W]
HRIC Heat Pipe	-20	3.18	24	6.07
Mounting feet	-50	This power derives directly from the thermal analysis results [referred to reduced model provided to the supplier] combined with the TVC thermal model	+50	This power derives directly from the thermal analysis results [referred to reduced model provided to the supplier] combined with the TVC thermal model

Table 7-18 Temperature and dissipation levels at the different thermal I/Fs for HRIC TVC

The thermal cycle to be reproduced is reported in the following figure:

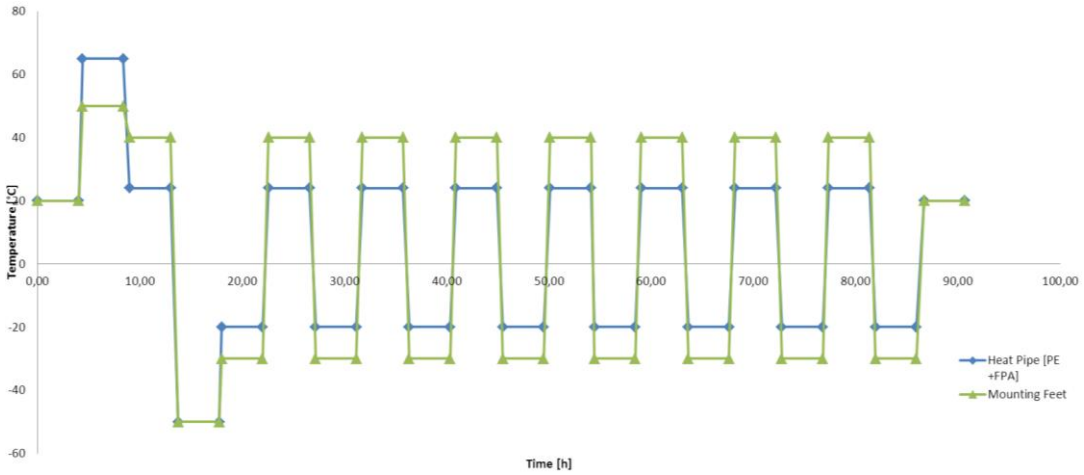

Fig. 7-38 Thermal cycle to be assured on the thermal I/Fs of HRIC TVC

The number of cycles has been deduced accordingly to EID-A requirements for thermal tests; dwell time duration is 4 hours and change temperature rate is 2°C/minute; in fact the real temperature rate can be different for different heat pipes. The required stability is 1°C/hour. The previous thermal cycle is imposed taking into account that TVC will be used for alignment, performance, qualification and calibration test activities.

T2. The TVC has to be provided with an external thermal conditioning system able to achieve the temperature values defined before.

T3. The length of the external pipes connecting the cryostat to the TVC thermal flange has to be minimized, in order to minimize heat losses along the connections.

T4. The heat pipes and all thermal I/Fs (excluding the invar support plate) have to be produced in copper.

T5. Eight temperature sensors have to be supplied, for monitoring purposes. The request accuracy is 0.1°C. The temperature of the following critical points will be monitored:

- 2 positions close to the two instrument thermal straps extremities (HRIC detector and HRIC PE)
- 2 points on the baseplate
- Other points still TBC.

7.3.3 Conceptual design

The conceptual design of the HRIC TVC is the same described in paragraph 7.2.3 The whole system is composed by the following main parts:

1. Thermal vacuum chamber, realized in stainless steel (AISI 316) and characterized by a cylindrical shape. The chamber is composed of two different parts:
   - a bottom part, which is fixed, interfaces with the optical bench (by means of the pattern represented in Fig. 7-36) and hosts flanges for electrical, thermal and vacuum interconnections.
   - An upper removable part, which hosts the flanges for the viewports and the cold trap.

   Inside the TVC the mechanical I/Fs for supporting units and thermal I/Fs are present, together with the cold plate of the cold trap, heaters and temperature sensors.
2. Pumping system, composed of a turbo-molecular pump and a rotary pump, with their devoted vacuum (pressure) sensors (Pirani and Penning sensors) and controllers.
3. An ultra cryostat for the thermal control of the internal thermal I/Fs.
4. An external dewar containing liquid Nitrogen for the supply of the cold trap.
5. Cabling and connectors, together with the controllers for the thermal control.

As written before, the thermal control of the different thermal I/Fs to be controlled (HRIC Heat Pipe Simulator and invar plate supporting the unit) is based on the following principle: the copper plate attached on the stainless steel plate represented in Fig. 7-35 is provided with an internal coil and can be actively controlled by means of a liquid circulating along the coil; the fluid and the ultra-cryostat are the same used for STC-VIHI TVC. The copper plate is connected to the invar plate and to the heat pipe simulator by means of copper thermal straps and acts as a heat sinks with respect to the other I/Fs. All the copper plates are covered with MLI in order to reduce the thermal exchange through radiation with the internal parts of the TVC. In addiction the thermal I/Fs (HRIC heat pipe simulator and invar plate) are provided with a dedicated heater and a PT100 (one for each thermal I/F), connected to CAL9900 controllers, which allow the fine regulation of the temperature on the different I/Fs. Since detector and PE thermal straps extremities are too far to be attached to the same thermal I/F, two separated plates are used as heat pipe simulators: thermal levels and thermal control strategies are the same for these two plates. The following figures show the final drawings of the Thermal Vacuum Chamber: in the first 2 figures the main components of the top part are evidenced (external view), in the 3rd and 4th figures the main components of the bottom part are evidenced (both internal and external view). Numbers identify the different vacuum flanges, which are described in the following table.

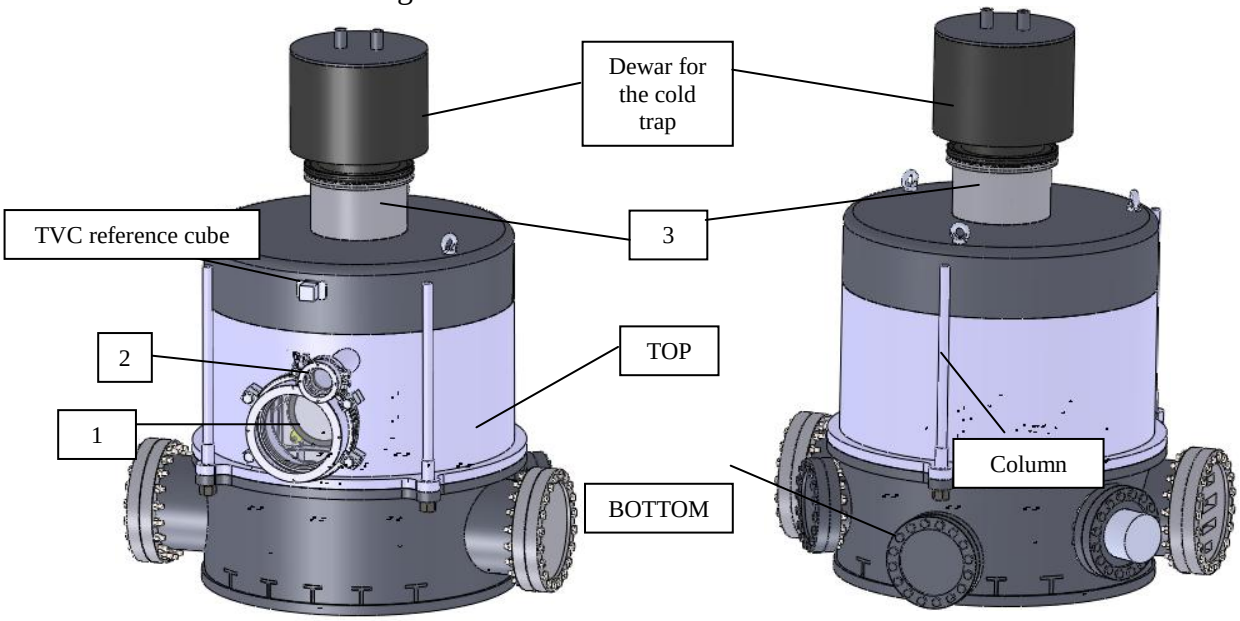

Fig. 7-39 Main components of the TVC (external view)

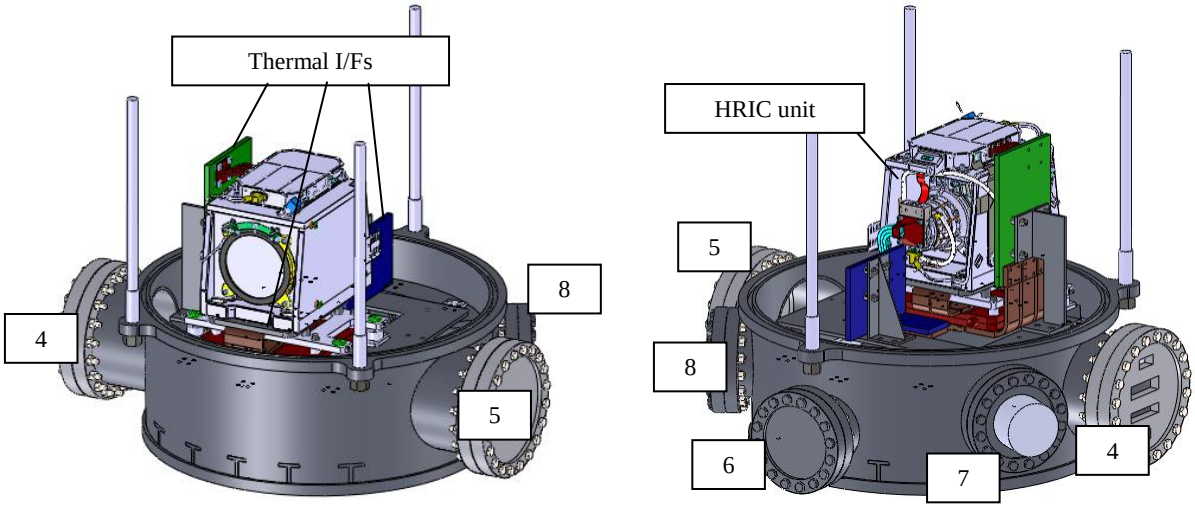

Fig. 7-40 Main components of the TVC (external and internal view)

Number	Type of flange	Description	Position
1	ISO160	HRIC channel viewport	Top part
2	NW40	HRIC reference cube viewport	
3	ISO 160	Dewar	
4	CF150	Flange for the electrical interconnections (1×15 pins MDM connector, 1×15 pins Dsub connector, 1×37 pins Dsub connector, 1×50 pins Dsub connector)	Bottom part
5	CF150	Flange for the thermal interconnections (1×CF40 for PT100, 1×CF40 for fluid feedthrough)	
6	CF100	Service flange for 2 additional Dsub 37 pins connectors	
7	CF100	Gate for the turbo-molecular pump	
8	CF100	Flange for the dry Nitrogen valve (1×CF16), the Pirani (1×NW16) and Penning (1×CF40) gauges	

Table 7-19 Position and description of the vacuum flanges present on the TVC

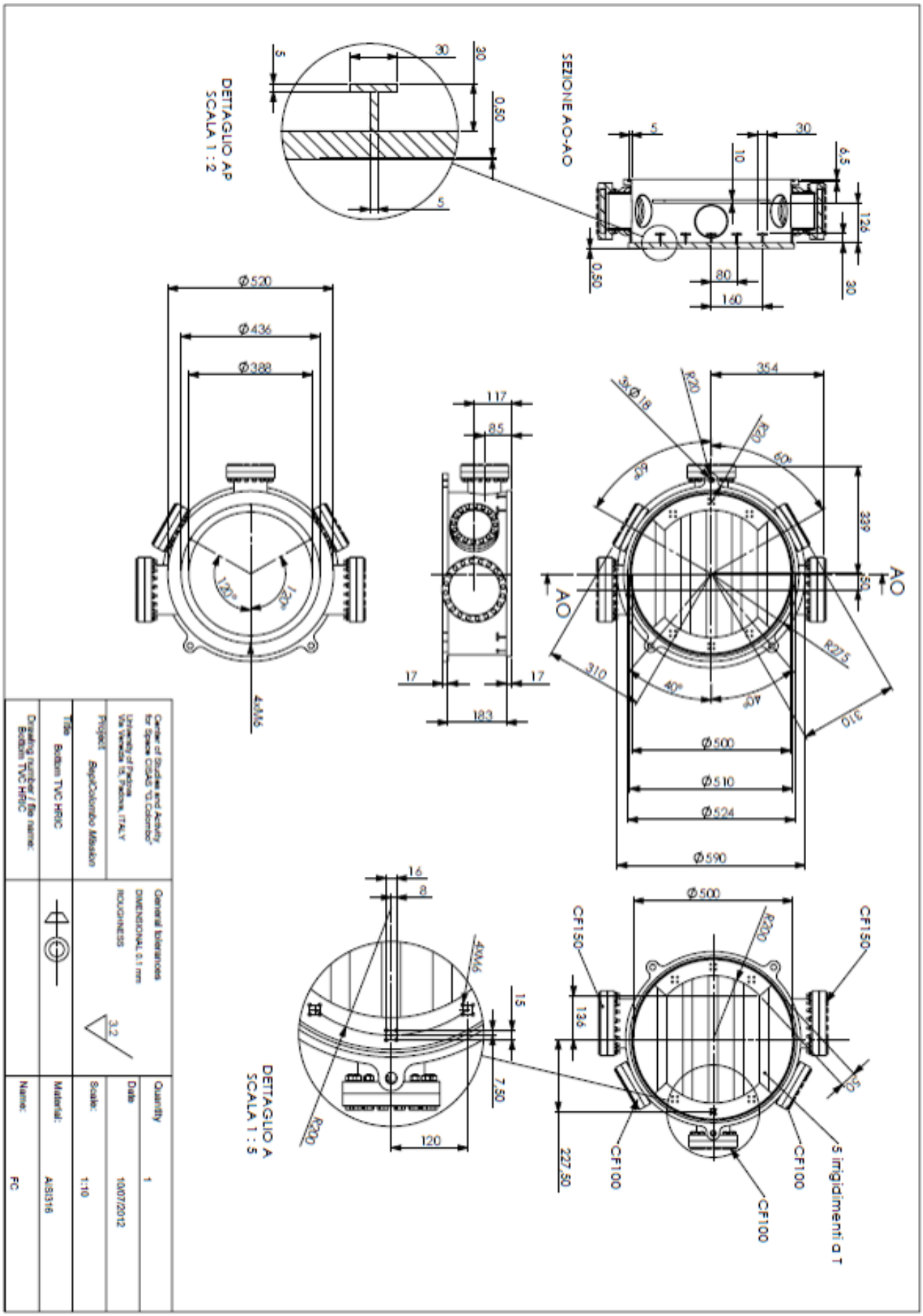

Fig. 7-41 Final drawing of the bottom part of the TVC

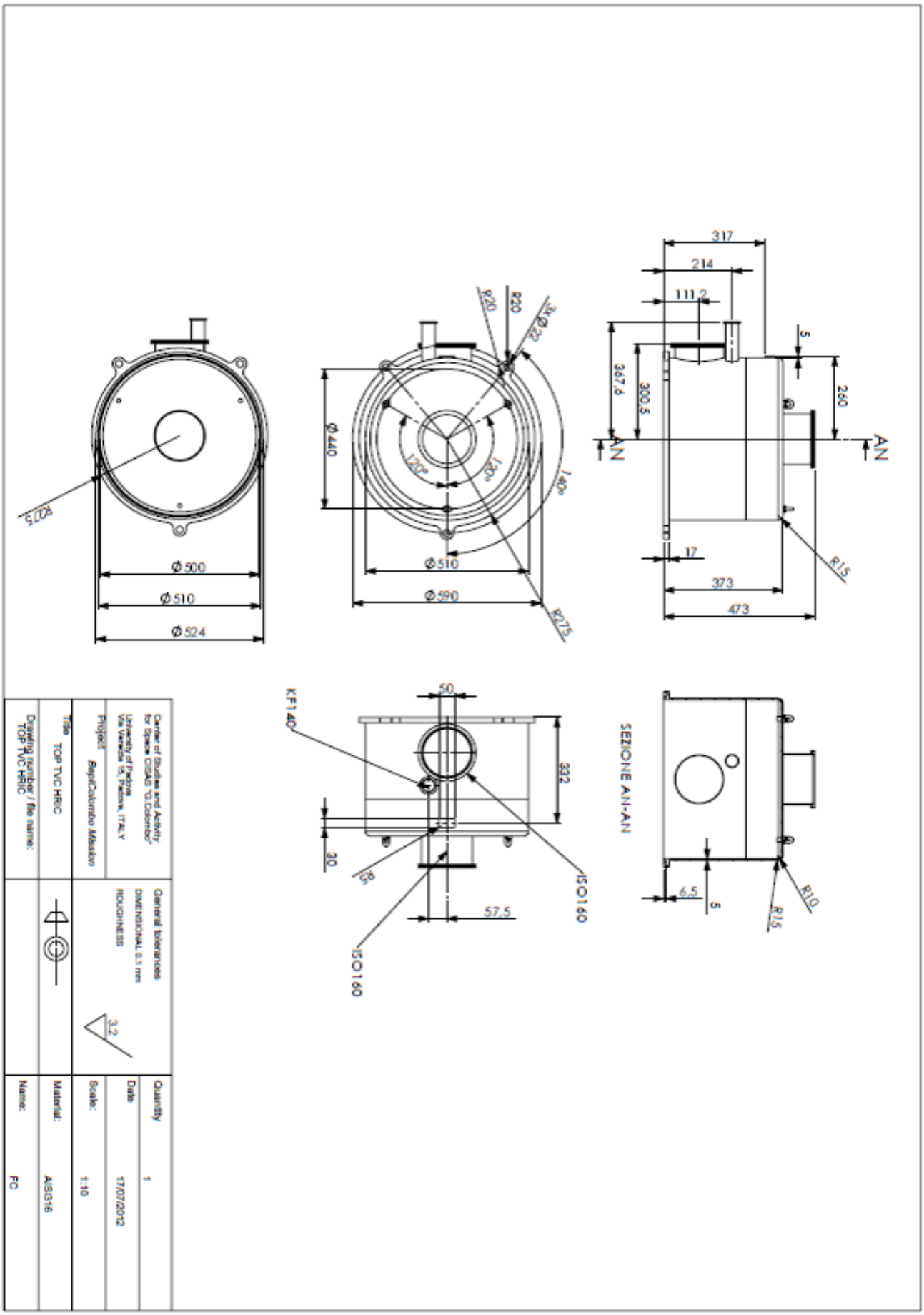

Fig. 7-42 Final drawing of the top part of the TVC

7.3.4 Mechanical interfaces

In this paragraph mechanical I/Fs of the TVC are listed and described, both for the vacuum configuration and for the configuration at ambient pressure. The second operating mode (at ambient pressure) is derived from the first operating mode (in vacuum) simply lifting the top part of the TVC and replacing it with an aluminum flange for supporting the baffle. As for STC-VIHI TVC, the bottom part remains unchanged, simplifying the test procedures and the operations.

7.3.4.1 Configuration in vacuum

As described before, the TVC is a cylindrical body in AISI316 characterized by the following main properties:

Property	Value
Total weight	188 kg
Internal Diameter	500 mm
External diameter	510 mm
Cylindrical body height	590 mm
Dewar protrusion	307 mm
Total height	897 mm

Table 7-20 Main mechanical properties of the TVC

From the previous table, it can be seen that the requirement on the maximum weight of 250 kg is fulfilled.
The top part (373 mm high) interfaces with the bottom part (217 mm high) thanks to a custom flange (having an external diameter of 550 mm) which hosts a rubber seal and three 18 mm-diameter holes for the columns which allow to align the top part with the bottom part. The alignment and mounting procedure is the same shows in Fig. 7-13.
Internally the bottom part is provided with two T-section beams which support an AISI316 frame on which the stainless steel plate described in M5 is fixed

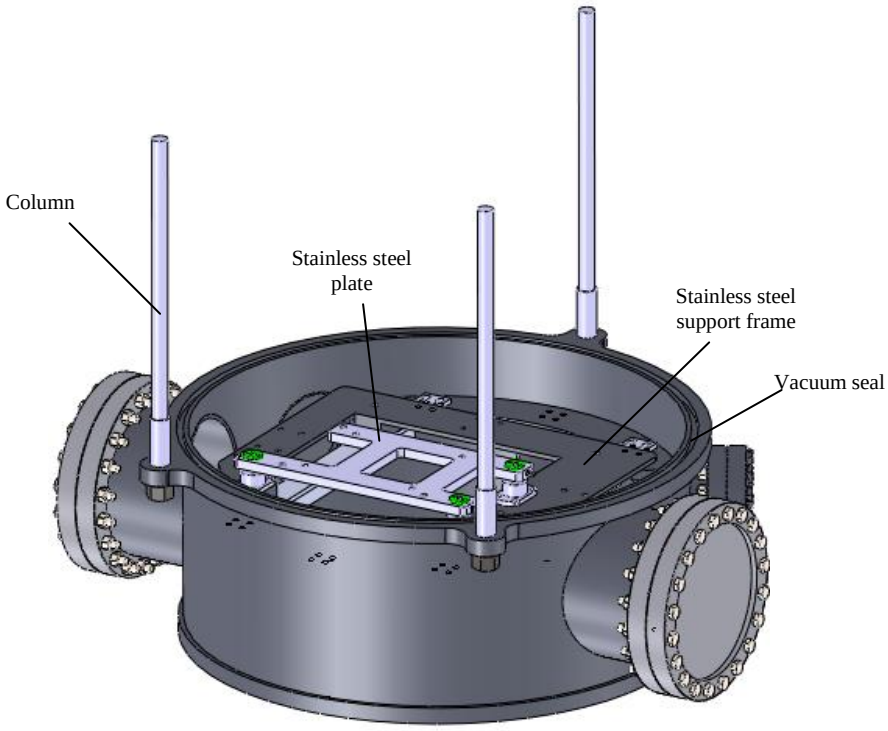

Fig. 7-43 Internal structural components of the TVC (1)

The following figure shows the components which are fixed to the AISI316 frame thanks to their devoted clamps: the stainless steel plate, which supports the copper plate (red plate, under the stainless steel plate) by means of four M5 screws and the invar plate (above the stainless steel plate) by means of four M5 screws, and the heat pipe simulators for the detector and the PE (blue and green plate respectively).

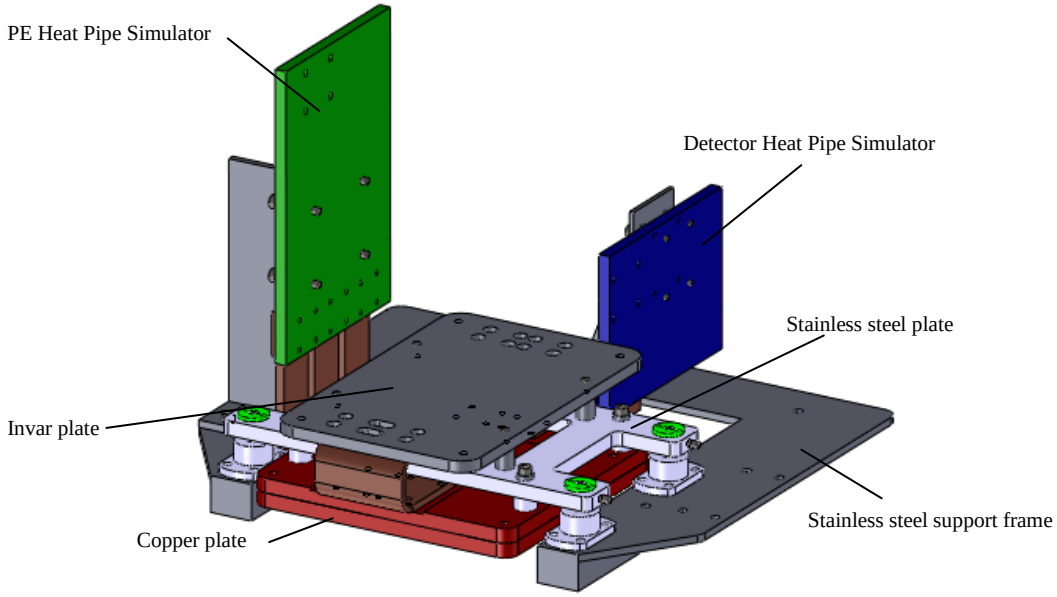

Fig. 7-44 Internal structural components of the TVC (2)

The copper plate and the invar plate are not directly attached to the stainless steel plate, in order to guarantee different thermal levels to the plate themselves: to assure the thermal decoupling, several PEEK washers have been foreseen around the screws, minimizing the thermal exchange for conduction between different I/Fs.
The following figure shows the mechanical I/F with the unit (the invar plate), which is fixed by means of four M5 holes, evidenced below with circles. Squares evidence the M4 holes for the fixation of the thermal straps.

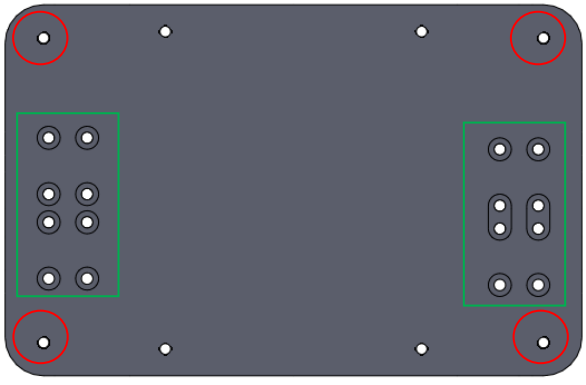

Fig. 7-45 Mechanical I/F of the instrument

The pitch – roll regulation (foreseen by M8 requirement) and regulation of the vertical distance of the instrument with respect to the TVC body is provided thanks to three M20 screws and three spherical joints, which are represented in the following figure. The functioning mechanism is the same described in 7.2.4.1.
Considering the distance between the centre of the screws and the pitch of the screw (1.5 mm), the requirement about the regulation accuracy is fulfilled.

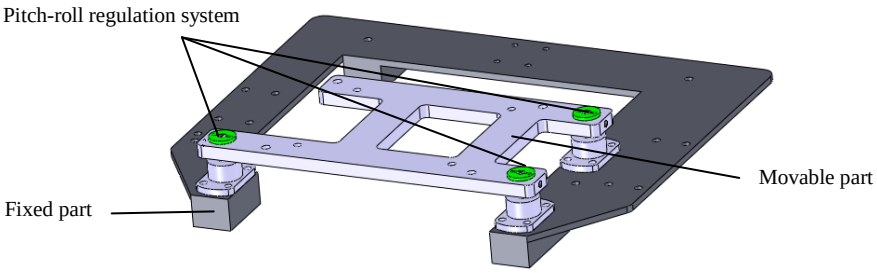

Fig. 7-46 Fixed and movable part inside HRIC TVC

The following figure shows a section view of the pitch-roll regulation system.

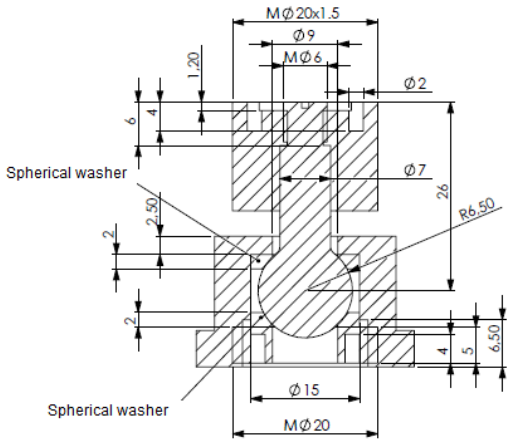

Fig. 7-47 Pitch-roll regulation system

Once all internal parts are mounted inside the bottom part, the top part can be fixed to the bottom part in order to perform tests in vacuum.
The dewar of HRIC TVC is the same described in paragraph 7.2.4.
The following figures show the thermal vacuum chamber assembled: the first figure shows the bottom part with all thermal I/Fs inside it, the second one the top cap with the viewports and the dewar.

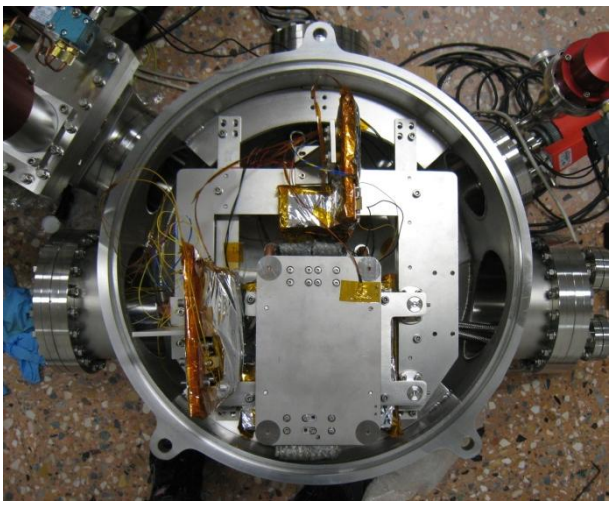

Fig. 7-48 Bottom part and top cap of the TVC for HRIC

7.3.4.2 Configuration with baffles

Operations at ambient pressure with baffles are performed removing the cap and fixing an aluminum plate to the stainless steel support frame by means of clamps and 2 couples of threaded bars: the Stavroudis baffle is attached to the 5-thickness aluminum plate in the flight position; finally a black-painted aluminum box is fixed to the plate in order to reduce the control volume around the instrument, which is filled with dry Nitrogen for cleanliness and contamination purposes.
As for STC-VIHI TVC, all thermal I/Fs can be removed during operation in air, with a consequent reduction of the weight to 116 kg. The following figure shows the configuration with the baffle.

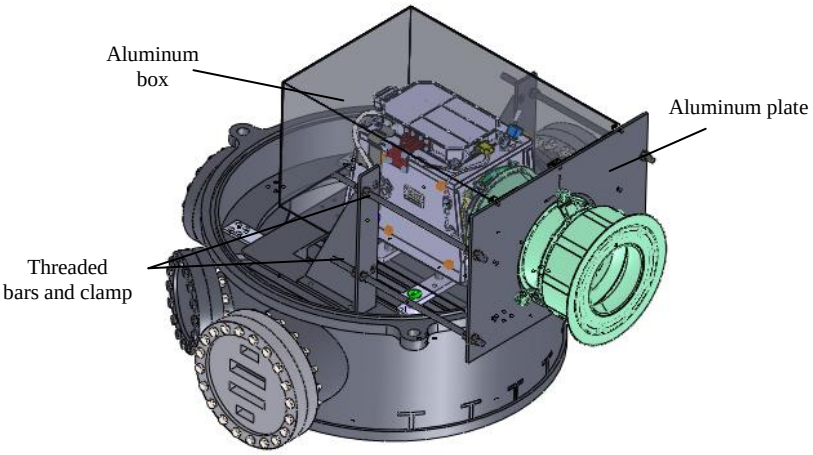

Fig. 7-49 Configuration with Stavroudis baffle

7.3.5 Thermal interfaces

7.3.5.1 Components

As written before, the thermal I/Fs to be controlled are:

- The detector heat pipe simulator (8 mm thickness copper plate), attached to the thermal strap of HRIC detector;
- The PE heat pipe simulator (8 mm thickness copper plate), attached to the thermal straps of HRIC PE;
- The invar plate, on which the unit is attached.

I/Fs are linked by means of 8 copper thermal straps to the copper plate connected to the external cryostat, which drives the temperature of the whole system. Indium foils are interposed between the extremity flanges of the thermal straps and the thermal I/Fs in order to maximize the conductance. As written before, the fine regulation of the temperature on the different I/Fs is obtained thanks to different heaters realized with a resistor covered by adhesive Kapton, operating in the whole requested operative range. MLI is used to thermally insulate the thermal I/Fs with respect to the TVC internal environment.
The thermal control system is then composed of three PT100 (devoted to monitor the temperature of the I/Fs), electrically connected to three CAL9900 controllers.

7.3.5.2 Thermal analysis and results

7.3.5.2.1 Introduction

As for STC-VIHI TVC, the scopes of the thermal analysis described in this paragraph are:

1. Verify if a single commercial ultra-cryostat, able to remove up to 200 W heat flux at a temperature of -80°C, is suitable to reach the thermal levels (specified in Fig. 7-38) at the different I/Fs;
2. Design the thermal control system.

The following figure represents the components reproduced in the thermal model; the top cap is not represented in the figure, but it has been simulated in the model as a boundary node:

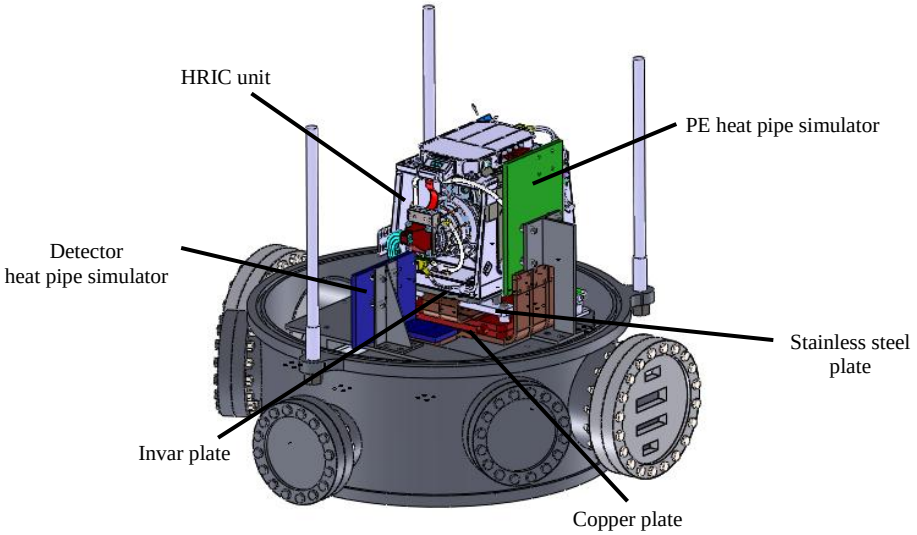

Fig. 7-50 Components simulated in the thermal model of HRIC TVC

7.3.5.2.2 Thermal model architecture

The thermal model of the whole system has been obtained including the reduced thermal model of the unit provided by Selex ES into the thermal model of the TVC will all thermal I/Fs inside it.
The TVC has been simulated as a raw stainless steel cylinder with $\varepsilon = 0.14$. All the I/Fs inside the TVC and STC-VIHI unit are covered with MLI ($\alpha = 0.5$, $\varepsilon = 0.03$ for critical I/Fs, $\alpha = 0.5$, $\varepsilon = 0.1$ for HRIC unit).
The copper plate is thermally connected to the following components:

1. The invar plate, by means of 3 copper thermal straps (0.92 W/K total conductance);
2. PE heat pipe simulator, by means of three copper thermal straps (0.73 W/K total conductance): The PE HPS is then connected to HRIC PE by means of its dedicated thermal strap (2 W/K contact conductance, according to the instrument reduced thermal model).
3. Detector heat pipe simulator, by means of two copper thermal straps (0.75 W/K total conductance): the detector HPS is then connected to HRIC detector by means of dedicated thermal straps (2 W/K contact conductance for each strap, according to the instrument reduced thermal model).
4. Stainless steel support plate, by means of PEEK washers (0.03 W/K total conductance).

The invar plate which supports the instrument is conductively decoupled with respect to AISI 316 support plate by means of PEEK washers (0.03 W/K total conductance); according to the instrument reduced thermal model, the conductance between the instrument and the invar plate is 0.03 W/K.
The method for the estimation of the thermal conductance of the thermal straps is the same described in paragraph 7.2.5.2.2.
The following figure shows the geometrical mathematical model of the TVC with all I/Fs inside it and the geometrical mathematical model of HRIC unit. Node numbering and the reference frame are shown.
External sides of TVC cylinder are simulated as boundary nodes @20°C.

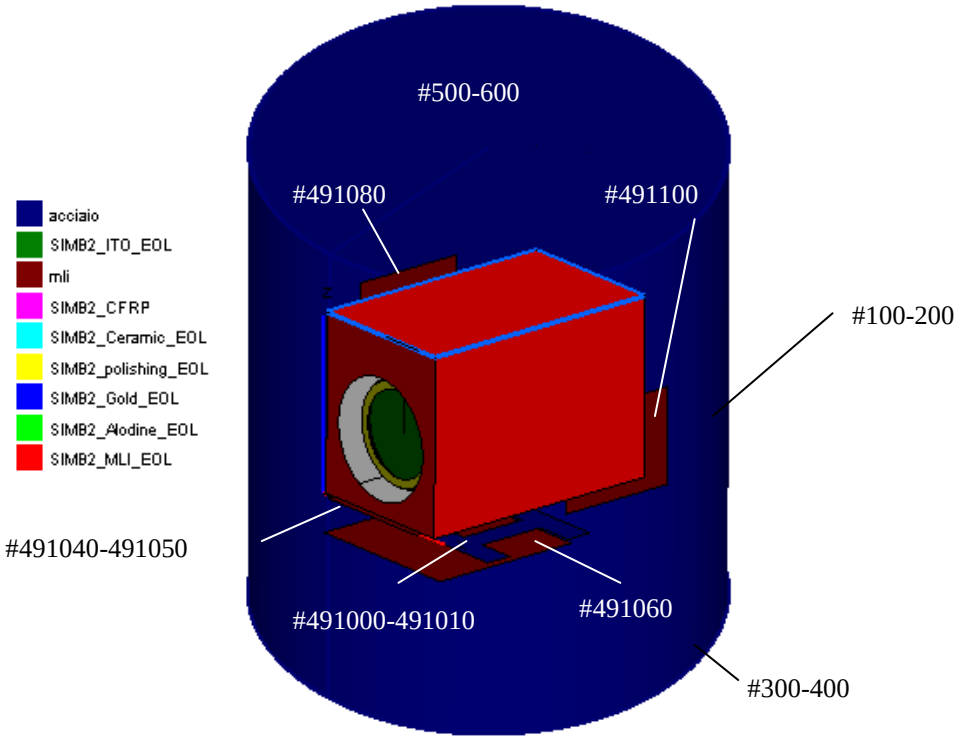

Fig. 7-51 Geometrical mathematical model of HRIC TVC

7.3.5.2.3 Nodal breakdown, bulk and thermo-optical properties

A brief description of node numbering is given in the following table:

Node number	Description	Notes
BOUNDARY NODES		
B100	TVC cylinder	External wall
B400	TVC bottom plate	External wall
B500	TVC top plate	External wall
B99999	External environment	
DIFFUSIVE NODES		
D200	TVC cylinder	Internal side
D300	TVC bottom plate	Internal side
D600	TVC top plate	Internal side
D491000-491010	AISI 316 support plate	
D491040	Invar plate	-X side
D491050	Invar plate	+X side
D491060	Copper plate	
D491080	PE HPS	
D491100	Detector HPS	
D68101	HRIC HC structure	
D68103	HRIC TIRD	
D68111	HRIC sec. mirror group	
D68112	HRIC cyl. Trusses	
D68113	HRIC primary mirror group	
D68114	HRIC Detector Support	
D68115	HRIC Detector Cage	
D68117	HRIC Detector Strap End	
D68116	HRIC PE	
D68118	HRIC PE Strap End	
D68105-68110	HRIC MLI	

Table 7-21 Thermal model node numbering

The following table summarizes the nodal breakdown and the thermal-optical properties.

Node	Name	Material	Thermal finish	α_S	ρ_S^D	ρ_S^S	ε_{IR}	ρ_{IR}^D	ρ_{IR}^S
100	TVC cylinder	AISI316	Raw SS	0.47	0.53	0.0	0.14	0.86	0.0
200	TVC cylinder	AISI316	Raw SS	0.47	0.53	0.0	0.14	0.86	0.0
300	TVC bottom plate	AISI316	Raw SS	0.47	0.53	0.0	0.14	0.86	0.0
400	TVC bottom plate	AISI316	Raw SS	0.47	0.53	0.0	0.14	0.86	0.0
500	TVC top plate	AISI316	Raw SS	0.47	0.53	0.0	0.14	0.86	0.0
600	TVC top plate	AISI316	Raw SS	0.47	0.53	0.0	0.14	0.86	0.0
491000-491010	AISI316 support plate	AISI316	Raw SS	0.47	0.53	0.0	0.14	0.86	0.0
491040	Invar plate	Invar	MLI_CISAS	0.5	0.25	0.25	0.03	0.97	0.0
491050	Invar plate	Invar	MLI_CISAS	0.5	0.25	0.25	0.03	0.97	0.0
491060	Copper plate	Copper	MLI_CISAS	0.5	0.25	0.25	0.03	0.97	0.0
491080	PE HPS	Copper	MLI_CISAS	0.5	0.25	0.25	0.03	0.97	0.0
491100	Detector HPS	Copper	MLI_CISAS	0.5	0.25	0.25	0.03	0.97	0.0
68101	HRIC HC structure	Honeycomb	CFRP	/	/	/	0.85	0.15	0.0
68103	HRIC TIRD	Al + BK7	ITO	0.2	0.03	0.03	0.13	0.42	0.42
68111	HRIC sec. mirror group	Invar + BK7	Internal	/	/	/	/	/	/
68112	HRIC cyl. Trusses	Invar	Internal	/	/	/	/	/	/
68113	HRIC primary mirror group	Invar + BK7	Internal	/	/	/	/	/	/
68114	HRIC Detector Support	Titanium	Internal	/	/	/	/	/	/
68115	HRIC Detector Cage	Aluminum	Internal	/	/	/	/	/	/
68117	HRIC Detector Strap End	Copper	Internal	/	/	/	/	/	/
68116	HRIC PE	Aluminum	Internal	/	/	/	/	/	/
68118	HRIC PE Strap End	Copper	Internal	/	/	/	/	/	/
68105-68110	MLI	MLI	MLI	/	/	/	/	/	/

Table 7-22 Node list and surface properties

The following table shows a list of the materials used in the thermal mathematical model.

Material	ρ[kg/m^3]	c_P [J/kg K]	λ [W/mK]
AISI316	8000.0	500.0	16.3
Copper	8930.0	385.0	398.0
Invar	8050.0	515.0	10.15

Table 7-23 Material properties

7.3.5.2.4 Conductive thermal couplings

The linear conductor chain is listed in the table below.

Node i	Node j	GL [W/K]	Description
100	200	0.916999 / ((0.00250000 / k_aisi316) + (0.00250000 / k_aisi316))	TVC body
300	400	0.200296 / ((0.00250000 / k_aisi316) + (0.00250000 / k_aisi316))	
500	600	0.200296 / ((0.00250000 / k_aisi316) + (0.00250000 / k_aisi316))	
491000	491010	0.0197606 / ((0.00500000 / k_aisi316) + (0.00500000 / k_aisi316))	AISI316 support plate
491010	200	0.01	
491040	491050	0.0326250 / ((0.00400000 / k_invar) + (0.00400000 / k_invar))	Invar plate
491010	491060	0.03	PEEK contact
491000	491050	0.03	
491050	491060	0.92	Invar plate th.straps
491060	491100	0.75	Detector HPS th. Strap
491060	491080	0.73	PE HPS th. Straps
68117	491100	2.0	HRIC Detector Strap Contact
68118	4911080	2.0	HRIC PE Strap Contact
68101	491040	0.003	HRIC Structure in Contact with OB Bench
68101	68103	0.145012	TIRD to HoneyComb Structure
68112	68103	0.000022	Sec. Mirror Group to Cyl. Trusses
68113	68112	0.006249	Cyl. Trusses to Prim. Mirror Group
68113	68101	0.045293	Prim. Mirror Group to HoneyComb
68114	68113	0.036820	Det Sup to Prim Mirr.
68115	68114	0.084112	Detector Cage to Detector Support
68116	68101	0.110861	PE to HoneyComb
68115	68117	0.41	Detecor to Th. Strap ending flange
68116	68118	0.44	PE to Th Strap ending flange

Table 7-24 Internal conductive thermal couplings

7.3.5.2.5 Thermal cases and boundary conditions

As written before, only external sides of the TVC and the external environment are simulated as boundary nodes at 20°C constant temperature.

Different kinds of heat fluxes are simulated:

- Dissipation incoming from the PE and the FPA of the unit, defined in the reduced thermal model as a function of the temperature of the nodes themselves. They are null in the non operative case, they assume the values derived by the following relations in the operative case:

Node	Operative dissipation
68115	HRIC Detector Cage: HRIC Detector dissipation (0.2W) + HRIC TEC power consumption
68116	HRIC PE dissipation: 3.05 + (1/0.8-1) ·HRIC TEC power consumption

Table 7-25 Operative dissipation of HRIC detector and PE

ΔT=f(T68115)	0	5	10	15	20	25	30	35	40	45	50
HRIC TEC power consumption	0.02	0.052	0.092	0.196	0.324	0.52	0.764	1.198	1.548	2.226	3.262

Table 7-26 HRIC TEC power consumption

Within the code of the thermal model, the control variables SIMB2_iHRIC allow the switch on or the switch off of the unit (operative and non-operative cases respectively), which corresponds to the activation or to the de-activation of detector and PE dissipations:

SIMB2_iHRIC	Case
1	Operative
0	Non-operative

Table 7-27 Activation and de-activation of the unit (detector and PE)

- The thermal cycle which has to be reproduced at the thermal I/Fs is obtained by the following sequence:
    1. Hot non-operative case;
    2. Hot operative case;
    3. Cold non-operative case;
    4. Cold operative case;
    5. Hot operative case;

  Then stages 4 and 5 (hot operative and cold operative cases) are repeated 8 times, according to EID-A.

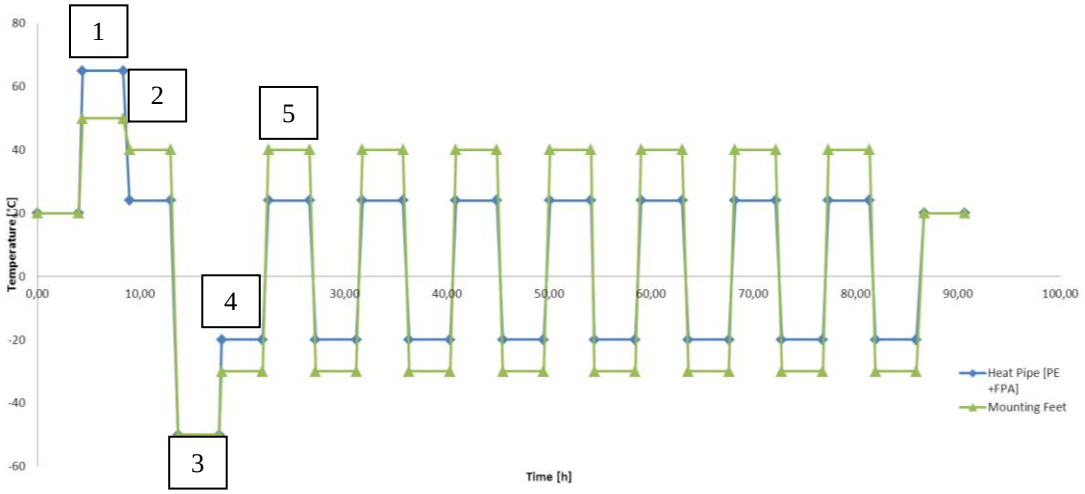

Fig. 7-52 Sequence of the thermal cases to be simulated

Each thermal level specified in the previous graph and corresponding to a different thermal case has been reached in the thermal model implementing a PID control on the thermal I/Fs. In particular PE Heat Pipe Simulator, detector Heat Pipe Simulator and invar plate are characterized by a positive internal heat generation, which simulates the presence of the heaters, whereas the copper plate, connected to the cryostat, is characterized by a negative and positive internal heat generation, which simulates the action of the cryostat, able to remove up to 200 W at -80°C and to provide up to 2000 W.

The internal heat generations are provided in the thermal model for at least 4 hours for each phase.

7.3.5.2.6 Results

The following figure shows the temperature reached at the relevant nodes of the thermal model:

- The detector Heat Pipe Simulator (node 491100), represented with the green line;
- The PE Heat Pipe Simulator (node 491080), represented with the pink line;
- Feet support plate, represented with the red line (node 491040).
- Copper plate (node 491060), represented with the blue line.

It can be seen that the temperatures reached coincides with thermal levels specified in the graph above.

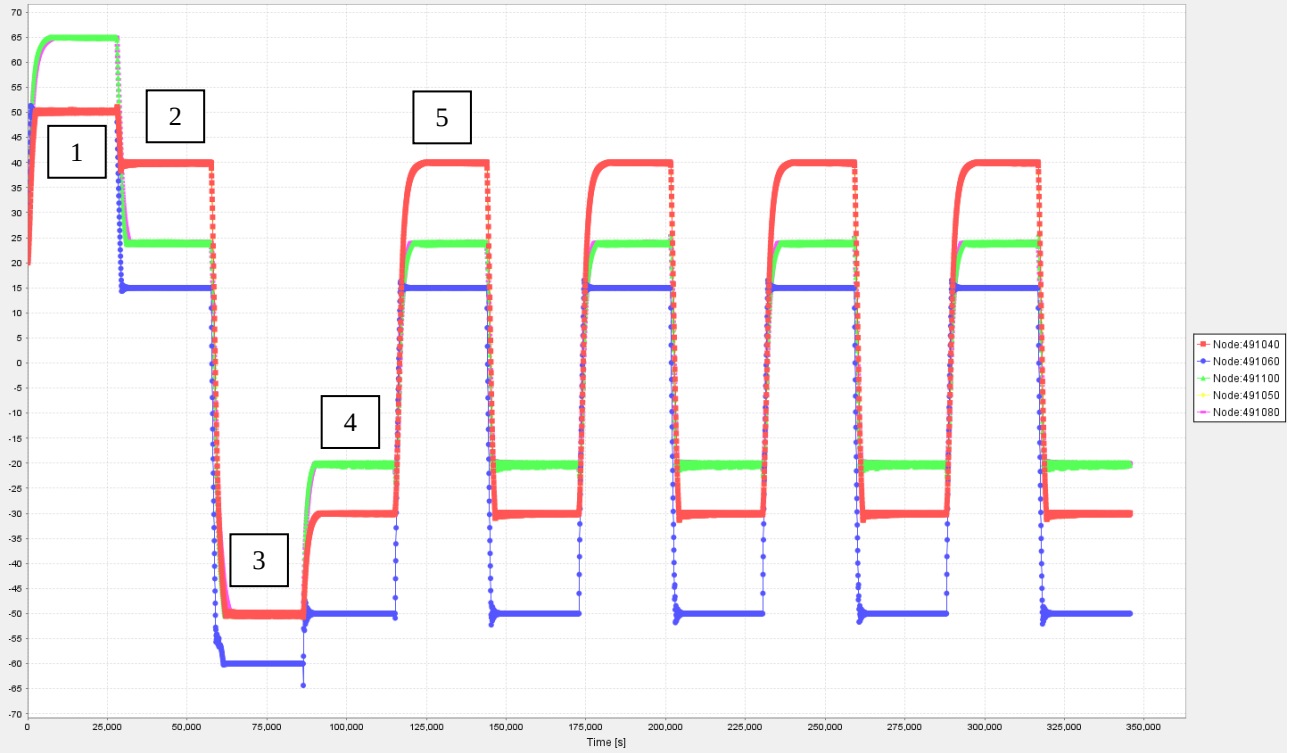

Fig. 7-53 Thermal levels obtained as a result of the thermal analysis

The following graph represents incoming conductor heat flow (blue line), the internal heat generation (green line) and the temperature (red line) of the copper plate (node 491060). Thanks to a maximum dissipation of 200 W at -75°C, the required thermal levels are reached. Therefore a solution based on a single ultra-cryostat for the cooling of the copper plate is feasible and the cryostat used is the same, as for STC-VIHI TVC.

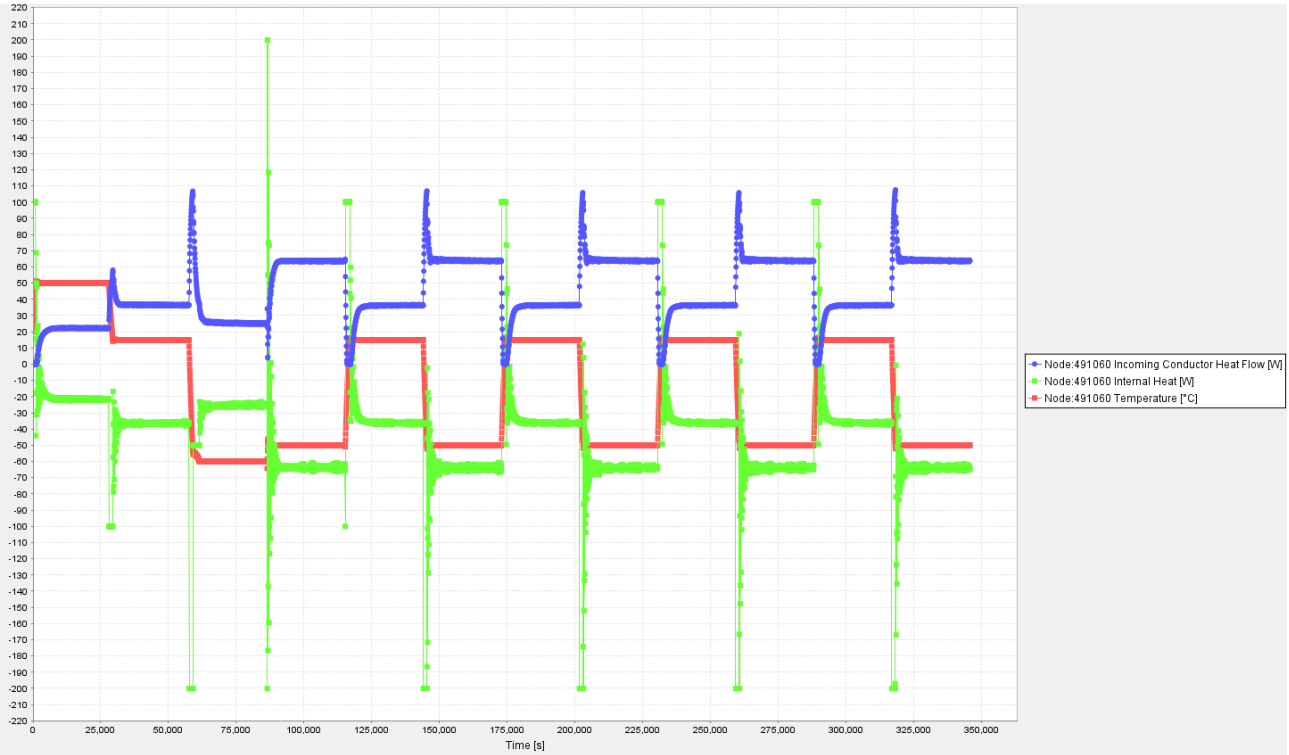

Fig. 7-54 Incoming conductor heat flow, internal heat generation and temperature of node 491060 (copper plate, connected to the cryostat)

The following table summarizes the power levels which have to be guaranteed at the different I/Fs for each thermal case.

Case number	Thermal case	Power [W]		
		Detector HPS	PE HPS	Feet HPS
1	Hot case – non operative	13	14	8
2	Hot case – operative A	8	8	25
3	Cold case – non operative	8	8	10
4	Cold case – operative A	24	21	18
5	Hot case – operative B	8	8	25
6	Cold case – operative B	24	21	18
	MAX	**24**	**21**	**25**

Table 7-28 Internal heat generation of the thermal I/Fs

The following figure shows the positioning of the heaters on the thermal I/Fs.

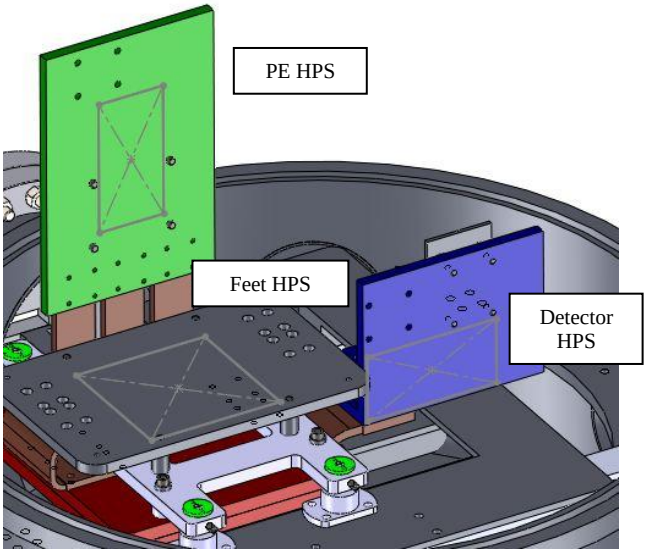

Fig. 7-55 Positioning of the heaters on the thermal I/Fs

Heaters, PID controllers and relays have been chosen with the same strategy described in 7.2.5.2.6. The following table shows the chosen models for each I/F. Since all heaters are supplied at 24 V, an additional 24 V power pack has been foreseen in order to supply the loads.

Parameter	Detector HPS	PE HPS	Feet HPS
Model	HK5422	HK5422	HK5178
Dimension (mm^2)	50 × 100	50 × 100	100 × 100
Number	1	1	1
Resistance (Ohm)	10.4	10.4	11.5
Total resistance (Ohm)	10.4	10.4	11.5
Supply voltage (V)	24	24	24
Current (A)	2.3	2.3	2.1
Max allowable current (A)	7.5	7.5	3.0
Maximum nominal power	55.4 > 24	55.4 > 21	50.1 > 25
Lead gauge	AWG 24	AWG 24	AWG 30

Table 7-29 Properties of heaters used for HRIC TVC

7.3.6 Electrical interfaces

As written in paragraph 7.3.3, the electrical connectors have been placed on the bottom part of the TVC, on a CF150 flange and on a CF100 flange. In particular, CF150 flange is provided with:

- 1×15 pins MDM connector for HRIC spacewire data;
- 1×15 pins Dsub connector for HRIC power supply;
- 1×37 pins Dsub connectors for service purposes;
- 1×50 pins Dsub connector for service purposes, in other words it hosts the connections for the eight PT100 devoted to the monitoring of the points of interest temperature.

The CF100 flange is provided with 2 additional 37 pins Dsub connector: the first one is used for the power supply of the heaters and the connection of the PT100 devoted to thermal control of the thermal I/Fs; the second one is a spare connector.
The following figure is a scheme of the electrical connections:

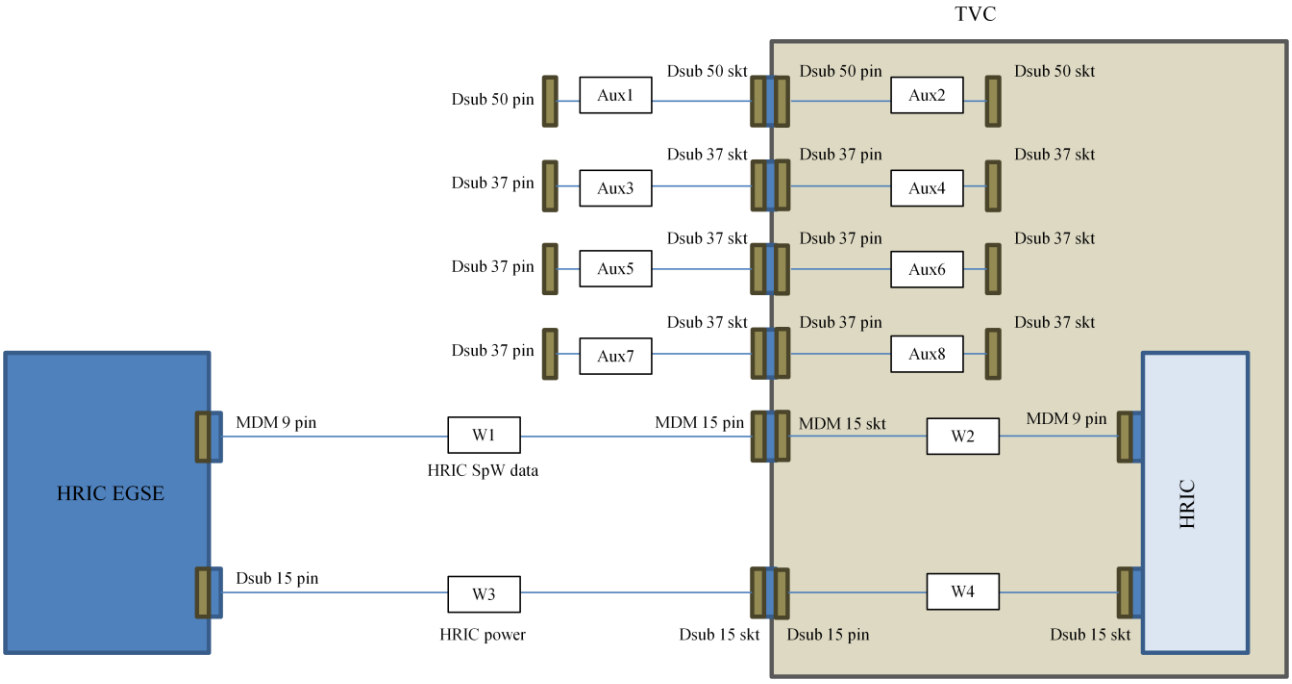

Fig. 7-56 Electrical connection of the HRIC TVC

The following table shows the pin scheme of the 37 pins D-sub connector devoted to the power supply of the heaters and the 3 PT100 for the thermal control. The wiring philosophy is the same described for STC-VIHI TVC.

Pin	Component
1, 2, 3	PT100 #1
4, 5, 6	PT100 #2
7, 8, 9	PT100 #3
26, 27, 28, 29	Heater #1
30, 31, 32, 33	Heater #2
34, 35, 36, 37	Heater #3

Table 7-30 37 pins D-sub connector scheme

The following table shows the pin scheme of the 50 pins D-sub connector devoted to the PT100 used for monitoring the temperature of the 8 points of interest.

Pin	PT100 cabling	PT100 number
1	PT100_1_V+	PT100_1
3	PT100_1_I+	
2	PT100_1_V-	
4	PT100_1_I-	
5	PT100_2_V+	PT100_2

7	PT100_2_I+	
6	PT100_2_V-	
8	PT100_1_I-	
9	PT100_3_V+	PT100_3
11	PT100_3_I+	
10	PT100_3_V-	
12	PT100_3_I-	
13	PT100_4_V+	PT100_4
15	PT100_4_I+	
14	PT100_4_V-	
16	PT100_4_I-	
18	PT100_5_V+	PT100_5
34	PT100_5_I+	
19	PT100_5_V-	
35	PT100_5_I-	
20	PT100_6_V+	PT100_6
36	PT100_6_I+	
21	PT100_6_V-	
37	PT100_6_I-	
22	PT100_7_V+	PT100_7
38	PT100_7_I+	
23	PT100_7_V-	
39	PT100_7_I-	
24	PT100_8_V+	PT100_8
40	PT100_8_I+	
25	PT100_8_V-	
41	PT100_8_I-	
26	PT100_9_V+	PT100_9
42	PT100_9_I+	
27	PT100_9_V-	
43	PT100_9_I-	

Table 7-31 50 pins D-sub connector scheme

Remaining 37 pins Dsub connectors are spare connectors.

7.4 Thermal tests on HRIC TVC

7.4.1 Introduction

This paragraph described thermal tests which have been performed on HRIC thermal vacuum chamber in order to verify the thermal requirements.

7.4.2 Preparation of the test

7.4.2.1 Assembling operations

The following pictures show the thermal interfaces during assembling operations.

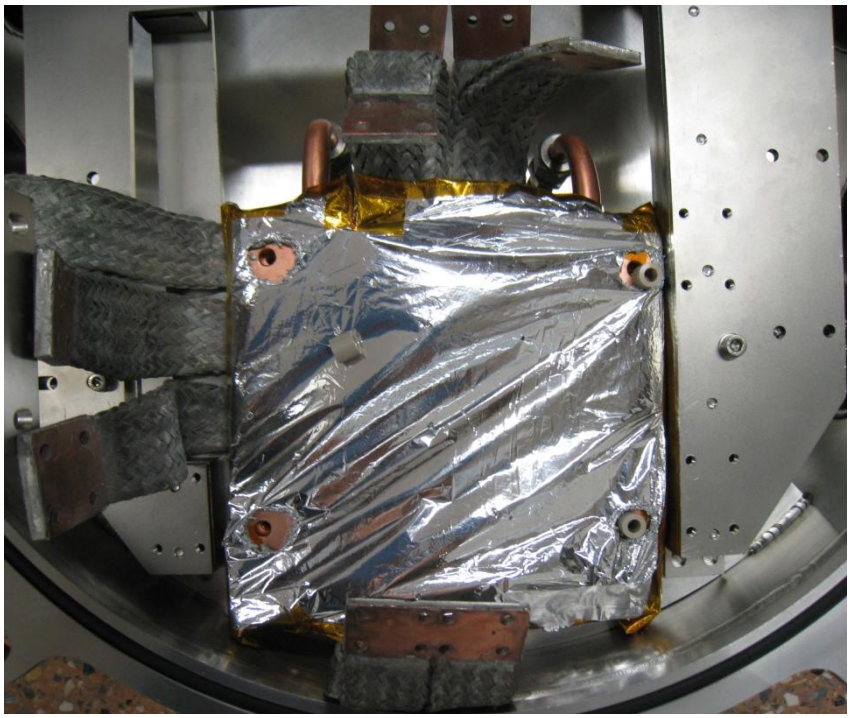

Fig. 7-57 Copper plate with thermal straps and MLI

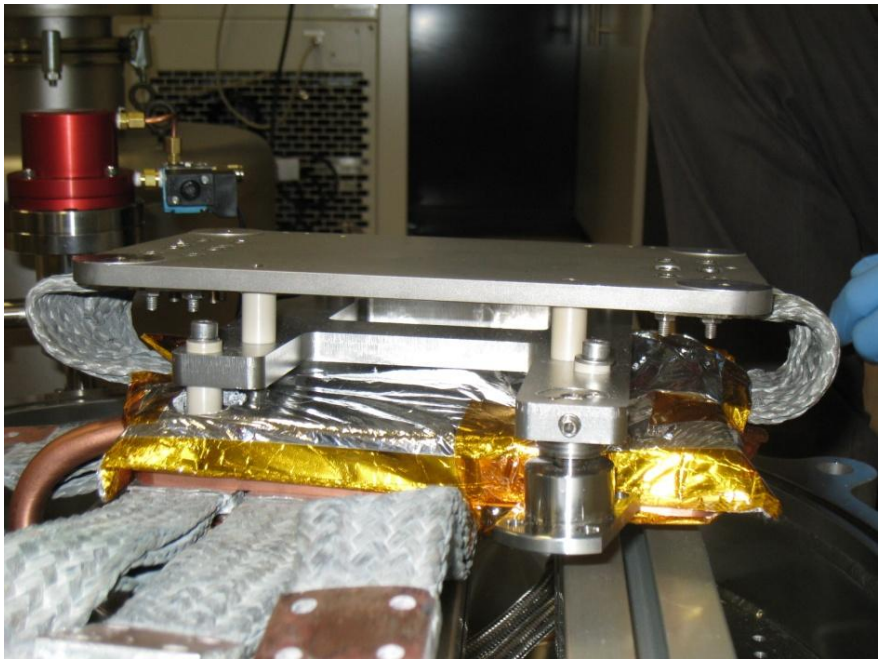

Fig. 7-58 Invar plate connected to the copper plate

Fig. 7-59 PE HPS connected to the copper plate

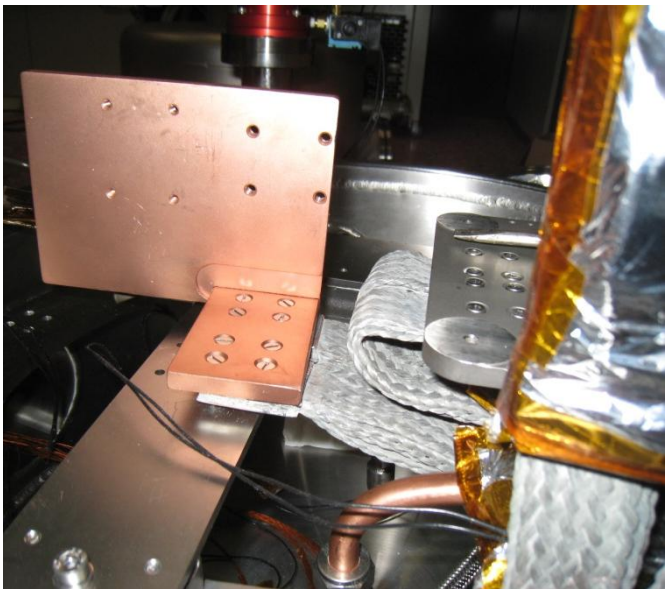

Fig. 7-60 Detector HPS connected to the copper plate

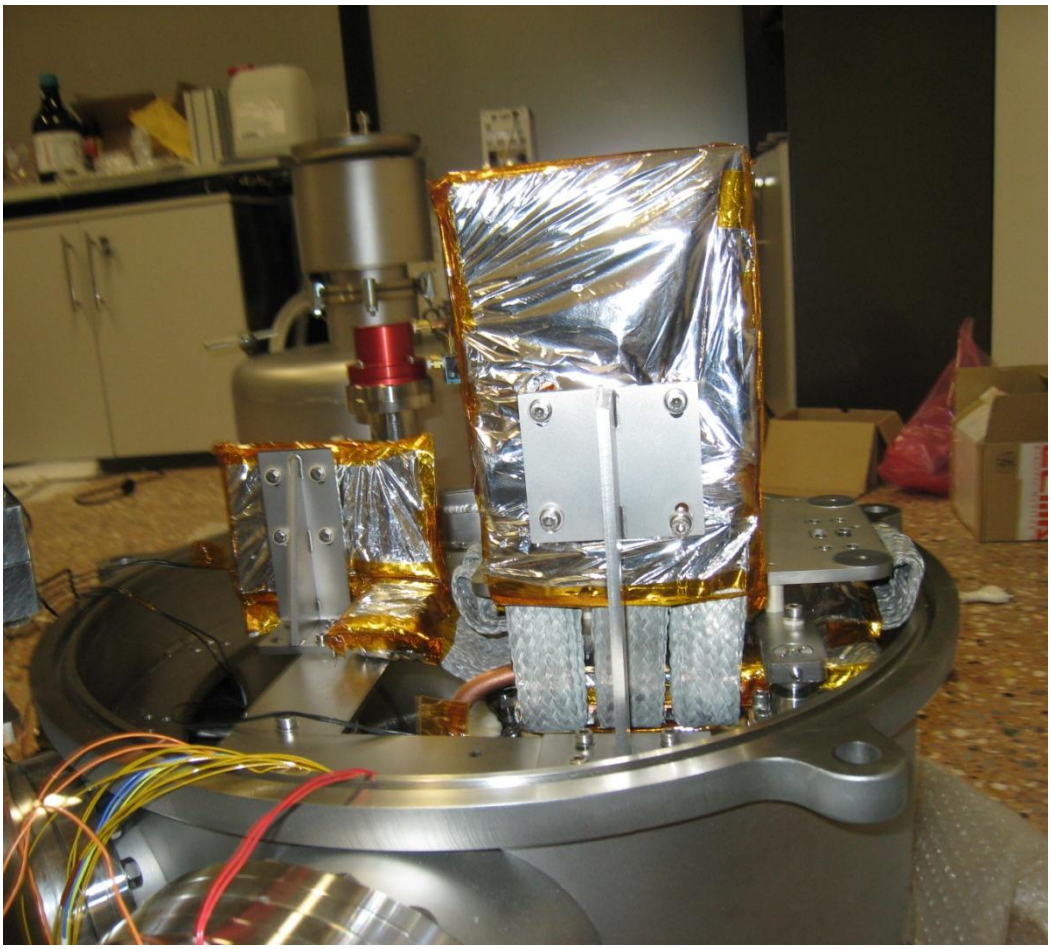

Fig. 7-61 Overall view of the thermal IFs inside the TVC

The following figure shows, from the right, the heaters switch, three CAL9900 controllers (one for each thermal I/F), the 24 V power supply (common for all the heaters), the 20A-220V relays connected to the controllers, the controllers switch.

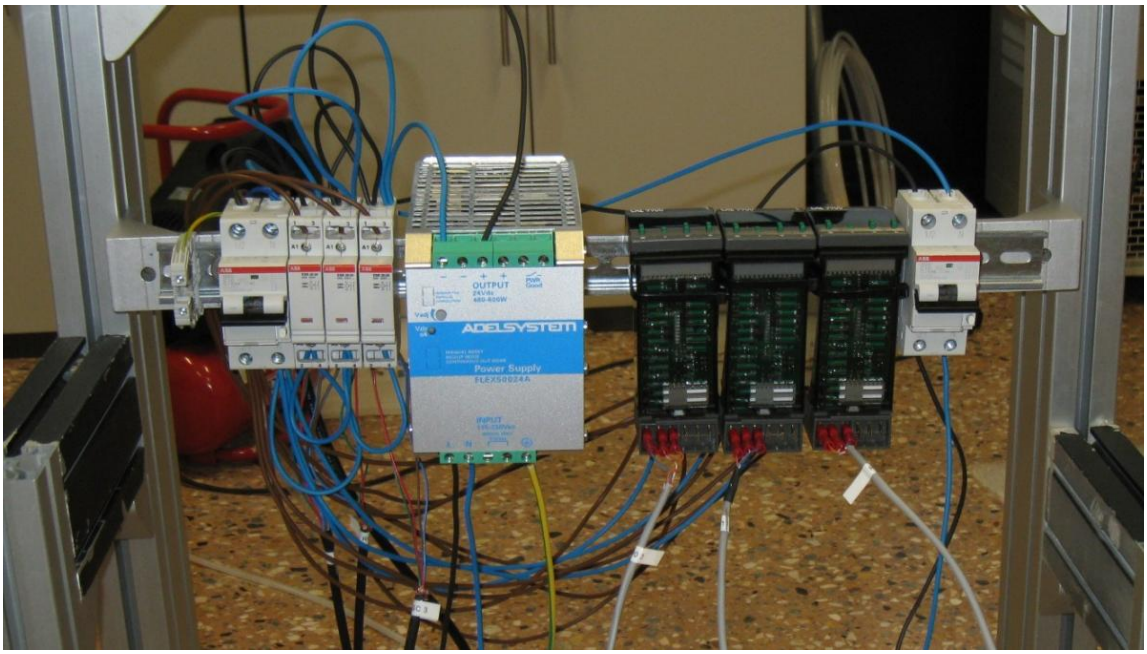

Fig. 7-62 Heaters power supply, relays and controllers

Two additional heaters, provided by Selex ES, have been used to simulate the heat dissipation of the FPA and the PE on the respective Heat Pipe Simulators during the hot and cold operative cases. Such heaters have been supplied by a separated power pack. The following figure shows the power pack used during thermal tests (operative cases only).

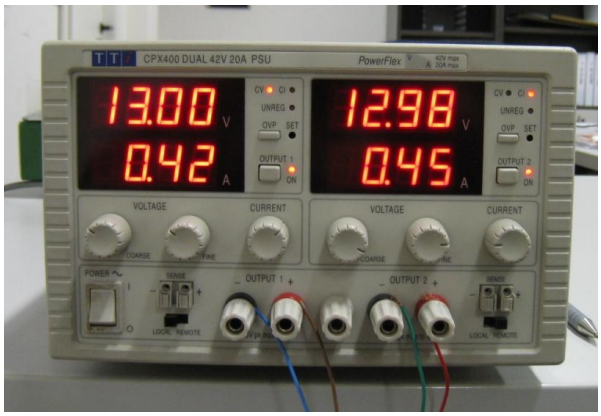

Fig. 7-63 Power pack used to supply the heaters which simulate the heat dissipations of the FPA and the PE in the operative cold and hot cases

7.4.2.2 Sensors position

For these preliminary thermal tests the measurements provided by the 3 PT100 connected to the controllers have been considered as reference. These sensors have been placed near to the heaters of the HPSs.

Temperature sensor number	Position
PT100 #1	Invar plate heater
PT100 #2	PE HPS heater
PT100 #3	Detector HPS heater

Table 7-32 Position of temperature sensors

The following figures evidences the position of the reference sensors during the tests (red circles). Also the heaters which simulates units heat loads (provided by the PE and the FPA) during the operative cases are underlined (with blue circles).

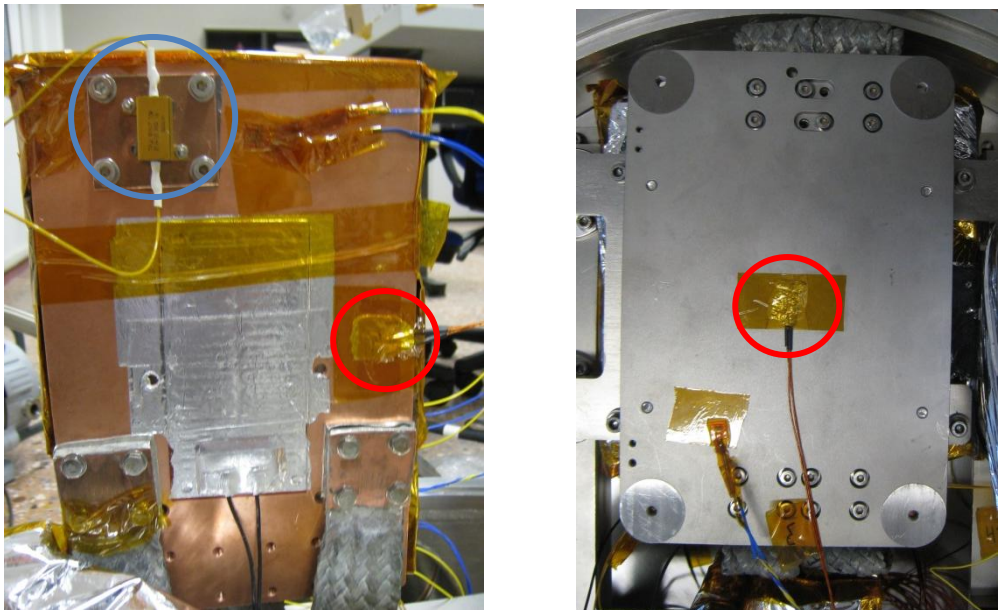

Fig. 7-64 Position of the reference sensors on the PE HPS and on the invar plate

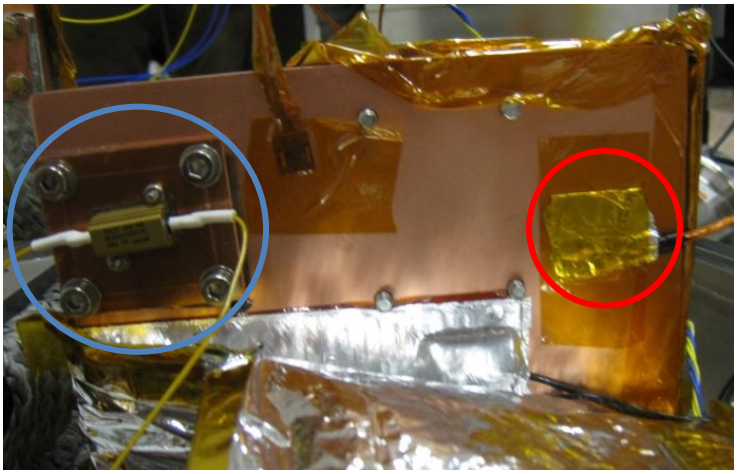

Fig. 7-65 Position of the reference sensor on the detector HPS

7.4.3 Test levels

The following table summarizes the test levels to be reproduced at the different thermal I/Fs:

Thermal case	Temperature [°C]		
	Detector HPS	PE HPS	Invar plate
Hot non operative	65	65	50
Hot operative	24	24	40
Cold non operative	-50	-50	-50
Cold operative	-20	-20	-30

Table 7-33 Test levels to be applied on the thermal I/Fs

During operative cases (cold and hot), heaters which simulate units (PE and detector) heat dissipations have been activated. The following table reports the electrical parameters (resistance, voltage, power) of such heat loads for each thermal case.

Location	R (Ω)	Hot operative		Cold operative	
		V (V)	P (W)	V (V)	P (W)
Detector HPS	28	13	6	9.5	3.2
PE HPS	30	13	5.7	9.5	3.0

Table 7-34 Heat dissipation for the HPSs in the hot and cold operative cases

7.4.4 Test results

All tests have been performed in vacuum conditions: as an example, the following graph shows the pressure profile inside the TVC during the cold case tests (non operative and operative) as a function of time (such values have been provided by the pumps system controller).

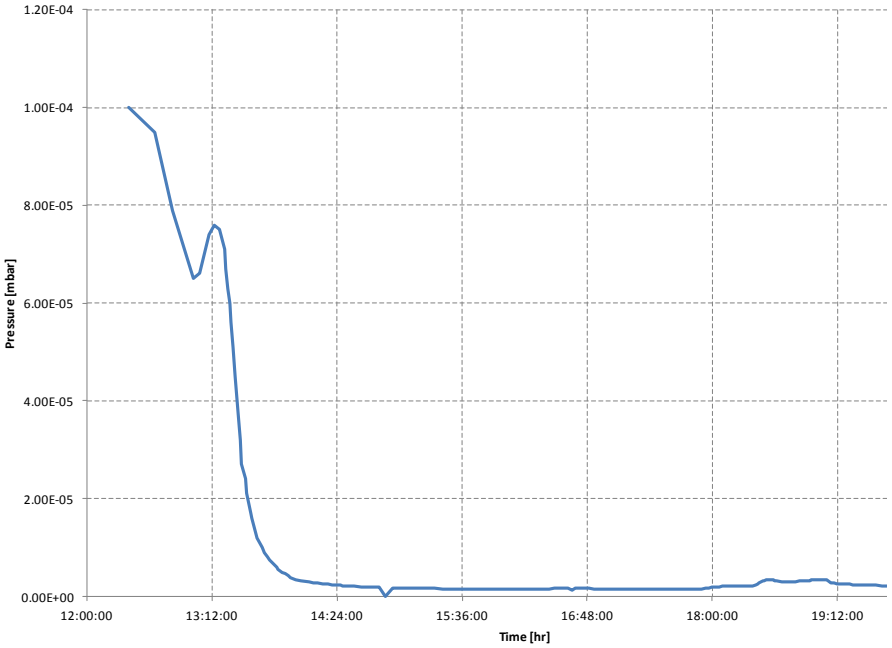

Fig. 7-66 TVC internal pressure as a function of time during the cold test

7.4.4.1 Cold case

The following graph reports the temperature of the PE HPS (red curve), the detector HPS (green curve) the invar plate (blue curve) and the chiller liquid (orange curve) in the cold case. At first cold non – operative case is reproduced (until the dotted line), then temperature of the IFs is increased in order to simulate the cold operative case.

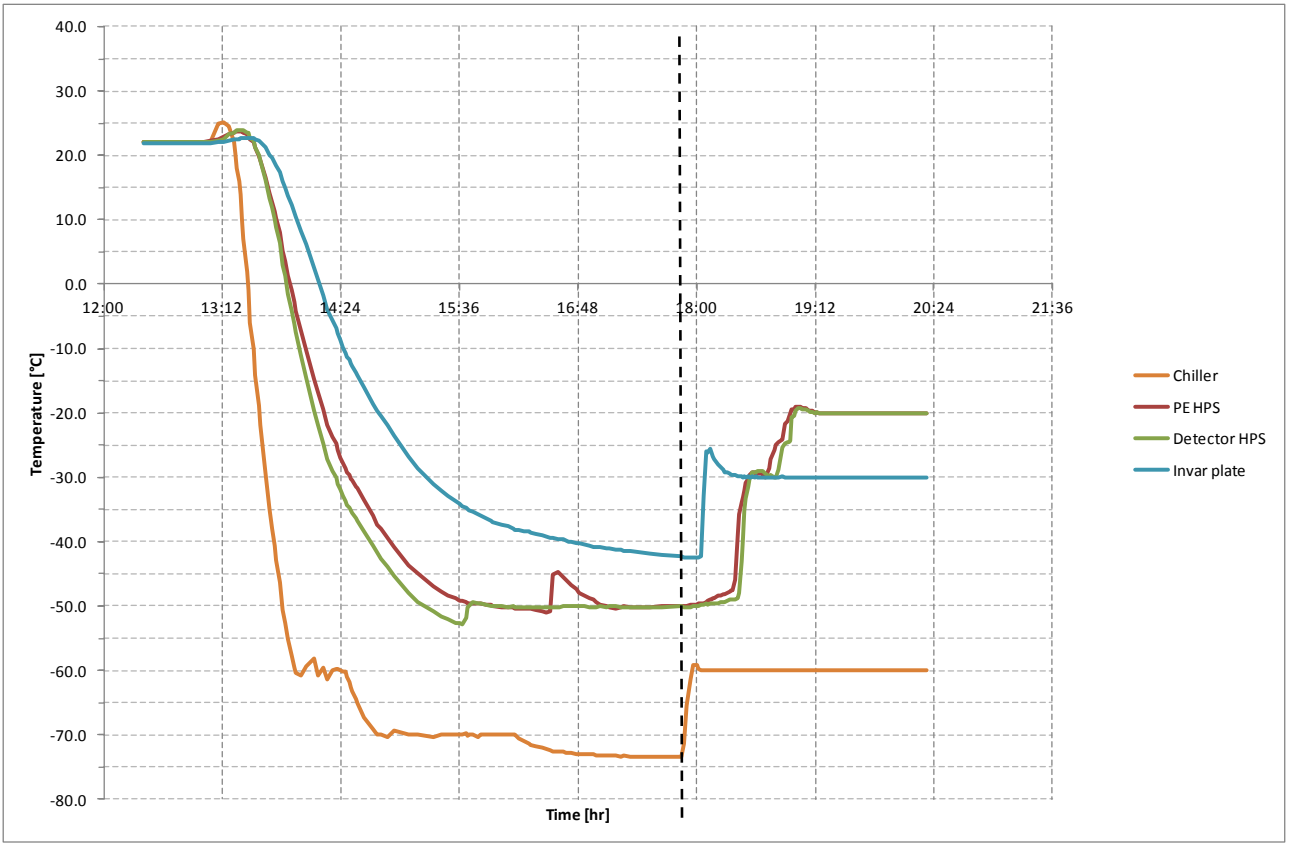

Fig. 7-67 Cold non – operative and operative case results

- In the non – operative case stability has been assured for the detector HPS and the PE HPS (-50°C), whereas invar plate temperature was still decreasing when test has been stopped.
- In the operative case all test levels have been assured at the different interfaces (-20°C for both the PE and detector HPS, -30°C for the invar plate).

7.4.4.2 Hot case

The following graph reports the temperature of the PE HPS (red curve), the detector HPS (green curve) the invar plate (blue curve) and the chiller liquid (orange curve) in the hot case. At first hot non – operative case is reproduced (until the dotted line), then temperature of the I/Fs is decreased in order to simulate the hot operative case.

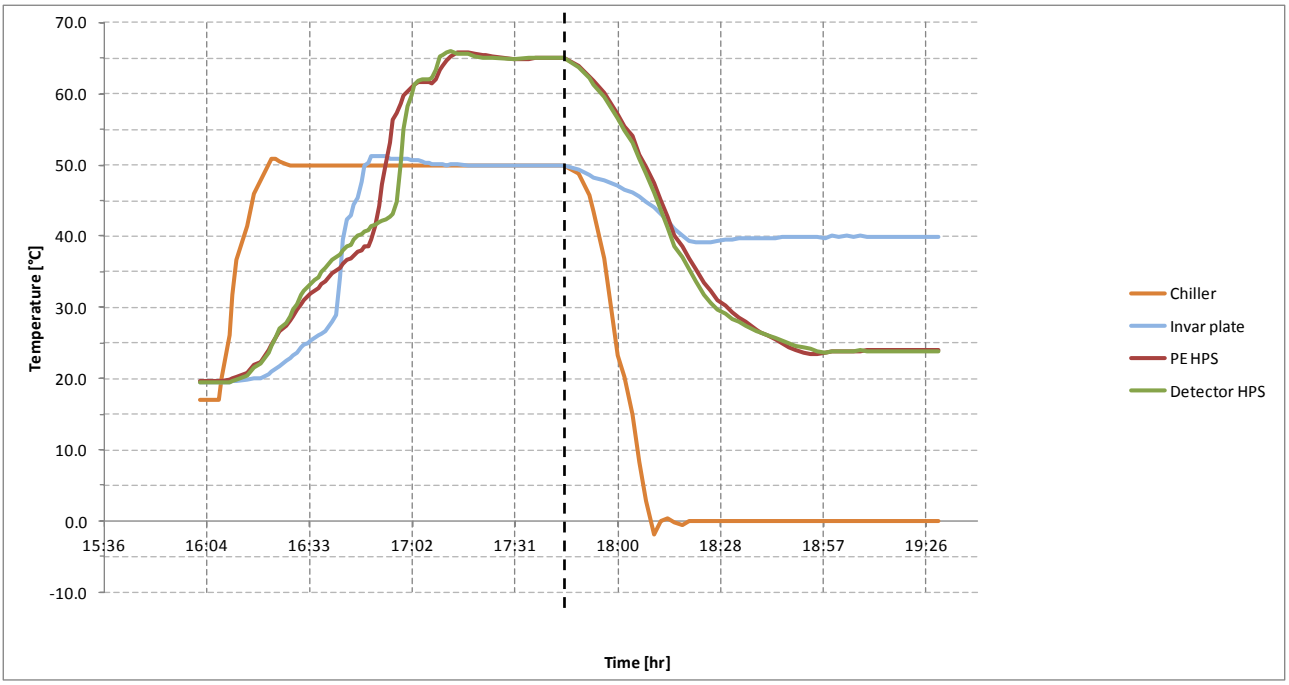

Fig. 7-68 Hot non – operative and operative case results

- In the non – operative case stability has been assured both for detector and PE Heat Pipes Simulators (65°C) and for invar plate (50°C).
- In the operative case all test levels have been assured at the different interfaces (24°C for both PE and detector HPS, 40°C for the invar plate). In the hot operative case, temperature of the chiller liquid has been forced to be equal to 0°C (at a temperature value noticeably lower than test levels which have been assured on the thermal I/Fs) in order to prove the efficiency of the heating system on the thermal I/Fs.

7.4.5 Conclusions

All thermal IFs have been controlled at the desired temperature in the different thermal cases, except for invar plate in the non operative cold case, due to an early stop of the test.
In any case different solutions will be implemented in order to completely fulfill the requirement, such as:

- Increase of the contact area between the thermal straps and the thermal I/Fs;
- Increase of the efficiency of the thermal exchange between of the coil inside the copper plate and the plate itself, interposing conductive material between the two plates which constitute the heat sink;

- Reduction of the heat leaks which take place along the connection between the cryostat and the TVC;
- Reduction of the temperature of the chiller liquid.

Further tests will be performed increasing the number of sensors (as an example some sensors will be placed on the heat sink and near to the thermal straps) in order to have a complete view of the thermal situation inside the TVC and eventually provide some modifications to increase the thermal performance.

Conclusions

In this thesis work several numerical and experimental methods for design and test of units and devices of SIMBIO-SYS suite onboard BepiColombo Mission around Mercury have been implemented.
The treatise is subdivided in three main parts:

1. The first part (chapters one, two and three) is a literature survey on the mission, the instrumentation onboard and the operative thermal scenario (some preliminary analyses results are also summarized to provide an estimation of the orbital thermal fluxes). The concepts reported are essential to deeply understand the objectives and the requirements of the mission, the mechanical, thermal and electrical interfaces of the instrumentation, the constraints on it, the problems related to the thermal environment to cope with, the state-of-art thermal control techniques.
2. Considered the aggressive thermal environment in which SIMBIO-SYS will operate and the consequent need to test the instrumentation and validate the thermal models, two different innovative test-beds have been designed, in order to reproduce indoor the thermal orbital fluxes. The first one, described in chapter four, is devoted to the Structural Thermal Models of the SIMBIO-SYS baffles, which have been subjected to the infrared planetary flux inside a thermal vacuum chamber. Different active and passive thermal control techniques (heaters, thermal straps, liquid nitrogen circuits and so on) have been also applied in order to control the thermal interfaces of the baffles, according to the requirements described in the EID-A. Test campaign did successfully take place in September 2010: after tests the instrumentation has been delivered to Selex ES without any damages or evident modifications.

The results of the test campaign have been compared then with the numerical results obtained by the thermal analyses: the thermal mathematical models of the baffles, provided by Selex ES, have been included into the thermal mathematical models of the thermal vacuum chambers, together with all thermal interfaces inside it. Thanks to the correlation between the experimental results and the numerical results of the new thermal analyses, the numerical models of the baffles have been validated, with a maximum deviation of 5.2°C for STC-VIHI baffles, 2.9°C for HRIC Stavroudis baffle. Thanks to this correlation, described in chapter five, some useful and original information and modifications to the thermal models of the baffles have been provided to Selex ES and ESA (such as the conductance between the frontal ring of the Stavroudis baffle and the first vane of the baffle itself) and these modifications have been implemented in the new TMMs of the baffles Flight Models.

The second test-bed which has been designed will be used for tests on the Qualification Model of the Stavroudis baffle of HRIC unit, whose surfaces are characterized by the final thermal and optical properties. The set-up, described in chapter six, is mainly constituted of two different parts: an innovative solar simulator, which produces a nearly – collimated (divergence < 30') steady beam with a homogeneous flux distribution (uniformity better than 5%) across an aperture of 300 mm diameter and allows to reach up to 6-7 Solar Constant flux intensity (about 8700 W/m^2); a custom thermal vacuum chamber, which hosts the equipment to be tested and thermal interfaces for the simulation of the infrared planetary heat flux (incoming from the illuminated and shadowed surface of the planet) and for the simulation of all conductive thermal interfaces of the test object (plates actively heated and cooled). The main goal of the test campaign is to verify the thermal behavior of the qualification model of the baffle up to the temperature range limits (operative and non-operative) and in the most critical orbital conditions, basing on the temperature measured on a black thin aluminum plate (TIRD simulator) placed behind the baffle.

After tests on the QM of the baffle, it will be possible to provide an estimation of the baffle performance in terms of heat rejection and to validate the thermal numerical models of the baffle, as for the thermal model of the structural mathematical model.

3. The last part of the thesis work is devoted to the description of the design procedure which has been followed to realize two thermal vacuum chambers for the qualification and the calibration of STC-VIHI and HRIC units, with and without baffles. The design process, described in chapter seven, started from the comprehension of the mechanical, thermal, electrical, vacuum, cleanliness and contamination requirements and proceeded with the conceptual design of the chambers, the detailed mechanical, thermal and electrical design (several structural and thermal simulations have been performed for this purpose), the procurement, the assembling operations and the thermal tests to verify the fulfillment of the initial requirements. Thermal vacuum chambers are characterized by similar shapes and dimensions (they are AISI316 stainless steel cylinders, with 510 mm external diameter, height lower than 1 m) but mechanical, thermal and electrical interfaces are different for each chamber. Detailed thermal analyses with the software suite ESATAN-TMS have been performed in order to size the thermal interfaces and the components (e.g. the thermal straps), choose the heaters and the refrigerating system. HRIC thermal vacuum chamber has been successfully assembled and tested in December 2012.

In the near future also thermal STC-VIHI thermal vacuum chamber will be completely assembled and, basing on the results obtained with the previous thermal tests on HRIC thermal vacuum chamber, some modifications and improvements involving the design will be implemented in order to completely fulfill the requirements and increase the performance of the whole system.

References

[1] F. Angrilli, B. Saggin, G. Fanti, M. Zaccariotto, *Corso di misure meccaniche, termiche e collaudi*, CEDAM, 2000

[2] Baffle Team CONTRAVES, *Reflective Baffle for BepiColombo Study, Final Report*, 2005

[3] A. Balogh, G. Giampieri, *Mercury: the planet and its orbit*, Reports on Progress in Physics, 2002

[4] T. Beck et al., *BELA Stavroudis Baffle (Mercury Simulator and Conical Approximations in Thermica)*, 2007

[5] T. Beck et al., *Thermal analysis of a reflective baffle designed for space applications*, Acta Astronautica, vol. 69, p.323-334, 2011

[6] J.Benkhoff et al., *BepiColombo-Comprehensive exploration of mercury: Mission overview and science goals*, Planetary and Space Science, 58, 2010

[7] BepiColombo Project Team, *Experiment Interface Document – Part A, BepiColombo*, BC-EST-RS-01140, issue 1, rev.0, 2008

[8] C. Bonacina, A. Cavallini, L. Mattarolo *Trasmissione del calore*. CLEUP, 1989

[9] A. Cavallini, L. Mattarolo *Termodinamica applicata*. CLEUP, 1992

[10] G.Colombo, *Rotational Period of the Planet Mercury*, Nature, 1965

[11] G. Colombo, I. I. Shapiro, *The rotation of the Planet Mercury*, American Astronomical Society,1965

[12] A. C. M. Correia, J. Laskar, *Mercury's capture into 3/2 spin-orbit resonance as a result of its chaotic dynamics*, Nature, 2004

[13] F. Cucciarrè, C. Bettanini, S. Debei, *Definizione e modellazione termica di un baffle Stavroudis per la missione BepiColombo*, Master Degree Thesis, CISAS, University of Padova, 2007

[14] F. Cucciarrè, S. Debei, *SIMBIO SYS baffles STM Thermal Vacuum Test Procedure*, BC-SIM-CIS-TP-001, Technical Note, CISAS, University of Padova, 2010

[15] F. Cucciarrè, S. Debei, *Simbio – Sys baffle STM Thermal Vacuum Test Report*, BC-SIM-CIS-TR-001, Technical Note, CISAS, University of Padova, 2010

[16] F. Cucciarrè, S. Debei, *STC-VIHI baffles' STM TMM validation*, Technical Note, CISAS, University of Padova, 2011

[17] F. Cucciarrè, S. Debei, *Stavroudis baffle's STM TMM validation*, Technical Note, CISAS, University of Padova, 2011

[18] F. Cucciarrè, E. Friso, S. Debei, *HRIC baffle EQM Thermal Vacuum Test Procedure*, BC-SIM-CIS-TP-006, Technical Note, CISAS, University of Padova, 2012

[19] V. DaDeppo et al., *A Novel Optical Design for the Stereo Channel of the Imaging System Simbiosys for the BepiColombo ESA Mission*, 2008

[20] S. Debei, P. Ramous, C. Bettanini, F. Cucciarrè, E. Friso, M. Pertile, M. Zaccariotto, M. Tordi, *CISAS Solar Simulator for equipment testing in high thermal fluxes environment*, Venezia, AIDAA, CEAS 2011

[21] E. Doebelin, *Measurement Systems*, Mc Graw Hill, 2004

[22] ESA BepiColombo Mission web page: http://www.esa.int/Our_Activities/Space_Science/BepiColombo_overview2

[23] E. Flamini et al., *SIMBIO-SYS: The spectrometer and imagers integrated observatory system for the BepiColombo planetary orbiter*, Planetary and Space Science, 2010

[24] E. Friso, C. Bettanini, F. Cucciarrè, P. Ramous, M. Zaccariotto, S. Debei, I. Ficai Veltroni, M. Rossi, *Thermal modelling and testing of the baffles of SIMBIO-SYS scientific suite of BepiColombo*, Venezia, AIDAA, CEAS 2011

[25] E. Friso, S. Debei, *Simbio-Sys orbital thermal environment: complementary assessment*,

simulations and sun incidence angle evaluations, Technical Note, CISAS, University of Padova, 16 April 2010
[26] R.Gardon, *An instrument for the direct measurement of intense thermal radiation*, The Review of Scientific Instruments, Vol.24, 1953
[27] D. G. Gilmore *Spacecraft thermal control handbook*. The Aerospace press, 1994
[28] Y. Hello et al., *Visible and near infrared detector for BepiColombo's spectrometer VIHI*
[29] ITP Engines, *ESATAN-TMS Thermal Engineering Manual*, UK, 2010
[30] ITP Engines, *ESATAN-TMS Workbench User Manual*, UK, 2011
[31] ITP Engines, *ESATAN-TMS Thermal User Manual*, UK, 2011
[32] G. Naletto, M. Cesaro et al., *Innovative optical setup for testing a stereo camera for space applications*, SPIE, 8442, 2012
[33] G. Pastorini et al., STC & VIHI Thermal Vacuum Chamber Requirement Specification, BC-SIM-GAF-RS-021, 2012
[34] G. Pastorini et al., HRIC Thermal Vacuum Chamber Requirement Specification, BC-SIM-GAF-RS-022, 2012
[35] P. Poinas, *SIMBIO-SYS ISRR Thermal, Mercury Environmental Specification Complementary Information*, 2007
[36] E. F. Robert, T. G. Biljana, *Optical System Design*, McGraw-Hill, 2000
[37] J. Schilke et al., *MPO Instrument MLI Interfaces*, BC-ASD- TN-00052, Technical Note, 2009
[38] J. Schilke et al., Assessment of P/L temperature results, BC-ASD-TN-00232, Technical Note, 2009
[39] R. Siegel, J. R. Howell, *Thermal Radiation Heat Transfer*, McGraw Hill,1992
[40] W. J. Smith, *Modern Optical Engineering, The Design of Optical Systems*, McGraw-Hill, 2000
[41] O. N. Stavroudis, L. D. Foo, *System of reflective telescopes baffles*, Optical Engineering 33(3), 1994
[42] O. N. Stavroudis, *System of reflective telescope baffles using conic sections of revolution*, Patent Number:5 225 931, 1993
[43] D. Stramaccioni, *Mercury Environmental Specification (Part I)*, BC-EST-TN-00112, 2006
[44] D. Stramaccioni, *Mercury orbital heat fluxes assessment*, 2003
[45] N. Thomas et al, *The BepiColombo Laser Altimeter (BELA): Concept and baseline design, Planetary and Space Science*, 55, 2007
[46] N. Thomas et al, *A wide beam continuous solar simulator for simulating the solar flux at the orbit of Mercury*, Measurement Science and Technology, , 22, 2011